MODELING CLIMATE AND LAND USE CHANGE IMPACTS ON WATER RESOURCES AND SOIL EROSION IN THE DANO CATCHMENT (BURKINA FASO, WEST AFRICA)

Dissertation

zur

Erlangung des Doktorgrades (Dr. rer. nat.)

der

Mathematisch-Naturwissenschaftlichen Fakultät

der

Rheinischen Friedrich-Wilhelms-Universität Bonn

vorgelegt von

Felix Op de Hipt

aus

Köln, Deutschland

Bonn, 28.09.2017

Angefertigt mit Genehmigung der Mathematisch-Naturwissenschaftlichen Fakultät

der Rheinischen Friedrich-Wilhelms-Universität Bonn

1. Gutachter: Prof. Dr. Bernd Diekkrüger

2. Gutachter: PD Dr. Thomas Hoffmann

Tag der mündlichen Prüfung: 31.01.2018

Erscheinungsjahr: 2018

This work is dedicated to my parents, Ulrich and Theresa, and my brothers and sisters Alix, Pia Leo and Joseph and to Jenny.

ACKNOWLEDGMENTS

This worked has been funded by the German Federal Ministry of Education and Research (BMBF) (Grant No. 01LG1202E) through the West African Science Service Centre for Climate Change and Adapted Land Use (WASCAL) project. I am very thankful to this financial support.

This work was enabled by the generous contribution of many people and words may not be sufficient to express my appreciation. First and foremost, I am deeply grateful to my supervisor Prof. Dr. Bernd Diekkrüger. He was always there for me and gave wise and thoughtful advices, well balanced between scientific guidance and personal liberty. I enjoyed each talk with him and appreciate very much his great sense of humor. With his pleasant nature he motivated me to the last point.

I owe special thanks to my second supervisor Dr. Thomas Hoffmann and my tutors Gero Steup and Prof. Dr. Michael Rode for their great support. Gero introduced me to the magic of programming and guided me through the highs and lows of field work and instrumentation. I learned a lot from his pursuit of perfection and sense of persuasion. Thomas showed me the wonderful world of R. His valuable comments and his praises always motivated me. With Michael, I spend inspiring days in the field. Thank all of you for your generous support!

What would be this work without helpful colleagues and friends? Particular thanks go to my office mates (Dr. Yacouba Yira, Thomas Poméon, Mouhamed Idrissou) who always grounded me if pressure became high and helped me a lot during each phase of this work. Thank you for your friendship! Furthermore, I owe thanks to Dr. O. Hounkpatin, Dr. A. Bossa, K. Näschen, C. Schepp, W. Somda, I. Rabbel, Dr. H. Webber, Dr. G. Welp, Dr. C. Leemhuis, Dr. T. Cornellissen, G. Gabiri, R. Wolter, L. Yameogo, N. Moret, Dr. I. Danso and J. Sörensen.

My field work in Dano and Tanguieta was enabled by many colleagues and friends. I owe thanks to my friend Hermann Hien with whom I experienced so many days in the field and who always motivated me to literally go the extra mile. Furthermore, organization and administration built an important part of this work. Therefore, I appreciate the help of the WASCAL competence center (especially Dr. J. Tondoh, Dr. W.Fonta, Dr. G. Forkuor, Dr. J. Naab, I. & R. Bado, M. Sessouma, A. Avocah, H. Barro, S. Somé, M. Somande, I.Zongo, O. Doussi, A. Zibrila, K. Yokoue, K. Orchard) and the colleagues from ZEF (Prof. Dr. C. Borgemeister, Dr. M. Denich, Dr. J. Lamers, H. Gregorian, S. Verleysdonk, A. Rogman). I express my gratitude to former students of the WASCAL graduate research program for the time we spent in Bonn and to the inhabitants of Tambiri (especially E. and P. Dabiré) who always welcomed me.

Last but not least I am extremely grateful to Jennifer Schwertfeger for her unconditional support.

ABSTRACT

The study assesses the effect of climate and land use change on water resources and soil erosion in the Dano catchment, Burkina Faso. Field measurements and derived process understanding are complemented by a physically based modeling approach that is also used to simulate the impact of land use and climate change.

Extensive hydro-meteorological (e. g. precipitation, discharge), pedological (e. g. texture, bulk density) and soil erosion measurements (e. g. suspended sediment load) are investigated to gain knowledge on governing hydrological and soil erosion processes. Data from erosion plot measurements suggest statistically significant differences of runoff and soil erosion between differently used plots.

The data and the retrieved understanding are used to setup and drive the physically based spatially distributed hydrological and soil erosion model SHETRAN. Statistical performance measures (R^2, NSE, KGE) range between 0.66 and 0.8 for the calibration and validation of discharge. Achieved quality measures of suspended sediment load are lower than for hydrology but comparable to other SHETRAN studies.

The impact of land use and land cover (LULC) change on water resources and soil erosion is studied by applying observed and modeled land use maps to the period 1990 – 2030. The past LULC change is studied using land use maps of the years 1990, 2000, 2007 and 2013. Based on these maps future LULC scenarios were developed for the years 2019, 2025 and 2030. Observed and modeled climate data cover the period 1990 – 2030. The observed past and modeled future LULC maps are used to feed SHETRAN. The isolated and combined influence of LULC and climate change is investigated. The land use investigation from 1990 to 2013 suggests a decrease of savanna at annual rates of 1.15% while cropland and settlement areas have increased. The simulations that assumed a constant climate and a changing LULC show increasing water yield (3.9% – 77.5%) and mainly increasing specific sediment yield (-1.4% – 115.78%). The simulations that assume constant LULC and climate as changing factor indicate increases in water yield of 24.5% to 46.7% and in sediment yield of 31.1% to 54.7%. The combined application of LULC and climate change signals a clear increase in water yield (20.3% – 73.4%) and specific sediment yield (24.7% to 90.1%). Actual evapotranspiration is estimated to change across all simulations by -6.8% to 3.35%.

The predicted climate change signal is investigated in detail by comparing the future period 2021 – 2050 with the historical period 1971 – 2000. Representative concentration pathways (RCP) 4.5 and 8.5 of six datasets of the CORDEX framework were used to study the future change in tem-

perature and precipitation. Most of the used climate models predict an increase of temperature between 0.9°C and 2.0°C. Large uncertainties among the climate models exist regarding the climate change signal of future precipitation. Some climate models predict an increase (5.9% – 36.5%) others a decreased (6.4% – 10.9%) or a mixed signal. The application of the historical and future climate data to SHETRAN shows that future changes in discharge and specific sediment yield follow the predicted precipitation signal. Simulated future discharge change ranges from -43% to +207%. The future change in sediment yield is in the same order.

ZUSAMMENFASSUNG

Diese Arbeit ermisst den Einfluss von Klima- und Landnutzungswandel auf Wasserressourcen und Bodenerosion im Dano-Einzugsgebiet in Burkina Faso. Messungen im Gelände und davon abgeleitetes Prozessverständnis werden durch einen physikalisch basierten Modelansatz ergänzt, der auch zur Simulation des Einflusses von Landnutzungs- und Klimawandel genutzt wird.

Daten umfangreicher hydro-meteorologische (z.B. Niederschlag, Abfluss) und pedologische (z.B. Textur, Lagerungsdichte) Messungen sowie Messungen von Bodenerosion (z.B. Suspensionsfracht) werden untersucht um Wissen über die herrschenden Prozesse zu gewinnen. Daten von Erosionsparzellen weisen statistisch signifikante Unterschiede von Oberflächenabfluss und Sedimentaustrag zwischen unterschiedlich genutzten Parzellen auf.

Die Daten und das gewonnene Verständnis werden genutzt um das physikalisch basierte und räumlich verteilte Model SHETRAN zur Simulation von Hydrologie und Bodenerosion zu betreiben. Statistische Gütemaße (R^2, NSE, KGE) lieben zwischen 0.8 und 0.66 für Kalibrierung und Validierung von Abfluss. Die erreichten Qualitätsmaße für die Suspensionsfracht sind niedriger als für den Abfluss aber vergleichbar mit anderen Studien, die SHETRAN genutzt haben.

Die Auswirkungen des Landnutzungswandels werden untersucht, indem beobachtete und modellierte Landnutzungskarten auf die Periode 1990 – 2030 angewendet werden. Der vergangene Landnutzungswandel wird anhand von Karten aus den Jahren 1990, 2000, 2007 und 2013 untersucht. Auf Basis dieser Karten werden zukünftige Landnutzungsszenarien für die Jahre 2019, 2025 und 2030 entwickelt. Die beobachteten vergangenen und modellierten zukünftigen Landnutzungskarten werden als Eingangsdaten für das Model SHETRAN genutzt. Der isolierte und kombinierte Einfluss von Landnutzungs- und Klimawandel wird untersucht. Die Untersuchung der Landnutzung von 1990 bis 2013 weist auf eine Abnahme der Savanne mit jährlichen Raten von 1.15% hin während sich Ackerland und Siedlungen ausgedehnt haben. Die Simulationen, die eine konstante Landnutzung und sich ändernde Klimabedingungen annehmen, zeigen eine Zunahme des mittleren jährlichen Abflusses von 24.5% bis 46.7% und des mittleren jährlichen spezifischen Sedimentertrags von 31.1% bis 54.7%. Die kombinierte Anwendung von Landnutzungs- und Klimawandel signalisiert eine klare Zunahme des Abflusses (20.3% – 73.4%) und des spezifischen Sedimentertrags (24.7% – 90.1%).

Das vorausgesagte Signal des Klimawandels wird im Detail untersucht, indem die zukünftige Periode 2021 – 2050 mit der historischen Periode 1971 – 2000 verglichen wird. Repräsentative Emissionspfade (RCP) 4.5 und 8.5 von sechs CORDEX-Datensätzen werden genutzt um die

zukünftige Entwicklung von Temperatur und Niederschlag zu untersuchen. Die meisten der genutzten Klimamodelle sagen einen Anstieg der Temperatur zwischen 0.9°C und 2.0°C vorher. Große Unsicherheiten existieren zwischen den Klimamodellen bezüglich des Signals für zukünftige Niederschläge. Einige Modelle sagen einen Anstieg (5.9% – 36.5%), andere eine Abnahme (6.4% – 10.9%) oder ein gemischtes Signal vorher. Die Anwendung historischer und zukünftiger Klimadaten als Eingabedaten in SHETRAN zeigt, dass zukünftige Änderungen des Abflusses und des spezifischen Sedimentertrags dem Signal der vorhergesagten Niederschläge folgt. Simulierte zukünftige Abflussänderungen reichen von -43% bis +207%. Die zukünftige Änderung des Sedimentertrags hat eine ähnliche Größenordnung.

TABLE OF CONTENTS

LIST OF FIGURES

LIST OF TABLES

ABBREVIATIONS

ANOVA	*Analysis of variance*
CEC	*Cation Exchange Capacity*
DGM	*Direction Générale de la Météorologie du Burkina*
ETa	*Actual evapotranspiration*
ETp	*Potential evapotranspiration*
GCM	*Global Climate Model*
ITCZ	*Innertropical Convergence Zone*
KGE	*Kling-Gupta-Efficiency*
LHS	*Latin Hypercuce Sampling*
LULC	*Land Use and Land Cover*
NSE	*Nash-Sutcliffe-Efficiency*
NSE_m	*modified NSE*
OFAT	*one factor at a time*
PTF	*Pedotransfer function*
R^2	*Coefficient of determination*
RCM	*Regional Climate Model*
RSG	*reference soil group*
SHE	*Système Hydrologique Européen*
SHETRAN	*SHE-TRANsport*
SOC	*Soil Organic Carbon*
SPEI	Standardized Precipitation and Evaporation Index
SPI	*Standardized Precipitation Index*
SRTM	*Shuttle Radar Topography Mission*
SSA	*Sub-Saharan Africa*
SSC	*suspended sediment concentration*
SSL	*Suspended Sediment Load*
WASCAL	*West African Science Service Centre on Climate Change and Adapted Land Use*
WMO	*World Meteorological Organization*
WRB	*World Reference Base for Soil Resources*

1 GENERAL INTRODUCTION

1.1 Problem statement

In recent decades environmental degradation has attracted more and more public attention worldwide. Degradation processes like soil erosion and water pollution are directly or indirectly related to the vast population growth that mostly takes place in Asia and Africa (UNDP, 2016). The African population is predicted to increase by almost 50% till 2050 (UN DESA, 2015). The high population growth in Africa poses already a challenge to environmental resources such as soil and water and consequently increases the necessity for future planning and protection programs (UNEP, 2012). As most African societies are dependent on rain-fed agriculture, soil quality and a stable climate is the fundamental base for their livelihood. Accordingly, the African population is highly vulnerable to environmental changes (Niang et al., 2014).

One problem of the fast population growth is the extension of agricultural areas at the expense of natural vegetation. As agricultural investments in Sub-Saharan Africa (SSA) are low an increase in crop production is rather achieved by extension instead of intensification (Nkonya et al., 2012). The conversion of natural vegetation to cropland has adverse effects on water and soil resources (CILSS, 2016; Yira et al., 2016). Especially in countries with fragile ecosystems as well as with limited water and soil resources, changes in the hydrological cycle through land use and land cover (LULC) changes may lead to an increased flood and drought risk as well as accelerated erosion rates. Understanding the effect of LULC change on water and soil resources is paramount especially in countries whose societies are highly dependent on rain-fed agriculture (UNEP, 2012; WWAP, 2015).

Additional pressure on African ecosystems and societies is expected from climate change (UNEP, 2012). Hydrological and soil erosion processes are substantially driven by the atmosphere through rainfall and evapotranspiration. Rising temperatures are frequently predicted by regional (RCM) and global (GCM) climate models and are considered to intensify atmospheric processes which may change among others the rainfall pattern. Changing rainfall patterns and temperature have distinct effects on water resources and soil erosion (Field and Barros, 2014; Mullan et al., 2012; Nearing et al., 2004; Yira et al., 2017).

Different studies have already contributed to the understanding of hydrological and soil erosion processes and investigated the impact of land use and climate change on water and soil resources (e.g. Bossa et al., 2014; Giertz et al., 2005; Giertz and Diekkrüger, 2003; Hiepe, 2008; Mahé et al., 2005; Schmengler, 2010; Yira et al., 2017, 2016). Among these studies Schmengler

(2010) investigated soil erosion and reservoir sedimentation in three headwater catchments in the same area. She used Cs-137 measurements, bathymetric surveys and the erosion models WEPP and WATEM/SEDEM to investigate soil erosion and deposition at hillslope and catchment scale. From her hillslope study she concluded that soil erosion is highly variable at smaller scales (slope length 240 – 380 m) and that it depends among others on the slope gradients and the land use. In general, she concluded, most of the study area is characterized by low erosion rates (< 1 t/ha/year). However, the number of samples did not allow a clear and representative validation of the model outcome and the disagreement between modeled sediment yield and measurements are possibly related to shortcomings of both methods. Furthermore, she focused on the past and present state of soil erosion and the impact of future LULC and climate change has not been investigated. Consequently, a clear knowledge gap regarding the influence of LULC and climate change on soil erosion for past and future periods exists and this study aims to provide new knowledge to fill this gap.

From the studies conducted in the region two principle outcomes can be summarized:

- Surface runoff and soil erosion rates are controlled by LULC change and both are increased if natural vegetation is converted to cropland or settlement areas (e.g. Giertz et al., 2005; Schmengler, 2010; Yira et al., 2016).
- The impact of climate change on discharge and soil erosion is unclear because large differences in future climate are projected by the GCMs although they were driven by the same scenarios. The climate change signal is reflected by discharge and soil erosion change (e.g. Bossa et al., 2014; Yira et al., 2017).

Studying the effect of LULC and climate change on water and soil resources requires the use of hydrological and soil erosion models as measurements on the required spatial and temporal scale are not possible. However, physically based and spatially distributed models such as SHETRAN (Ewen et al., 2000), which is used in the present study, require information that is mostly not available in data scarce region such as West Africa. Therefore, the collection of primary data in the field was necessary. The analyses of the collected data and observations from the field considerably improved the understanding of hydrological and erosion processes. This knowledge is a prerequisite for the application of environmental models as it allows to adequately represent the environmental conditions. An entire understanding of the catchment sediment system is hampered by the complexity of the interacting processes and factors and therefore requires a multi-method approach combining advantages of several research methods. The novelty of this study includes therefore the combination of different measurement methods on

multiple scales with the application of a physically based spatially distributed hydrological and soil erosion model that has not been used so far in Africa.

1.2 Research questions

According to the problems stated in the previous section, this study aims to find answers to the following research questions:

1. **How do different land use types affect surface runoff and soil erosion on the plot scale?** This research question is treated using data derived from erosion plots with different land use covers (cotton, sorghum, fallow) that were installed during 2013 - 2015. The effect of different land use types on surface runoff and soil erosion as well as on rainfall-runoff and runoff-erosion relations is studied.
2. **Is the hydrological and soil erosion model SHETRAN able to simulate discharge and soil erosion on the catchment scale?** SHETRAN is calibrated and validated in the study area using turbidity derived suspended sediment loads and erosion plot measurements. The retrieved outputs are subject to uncertainty that is related to the simplification of the model, the uncertainty of the model parameter and the measurement uncertainty. A quantification of the measurement and parameter uncertainty is necessary to contextualize the quality of the modeled output.
3. **How does the predicted precipitation and temperature trend of the future period 2021 – 2050 affect water resources and soil erosion compared to the historical period (1971 – 2000)?** Increasing temperatures over West Africa are frequently predicted by Regional and Global Climate Models (RCM-GCM) while the climate change signal of precipitation is unclear for the mid 21st century. This unclear trend has implications for climate change adaption strategies as it is reflected by future discharge and soil erosion predictions.
4. **How does LULC and climate change affects hydrology and soil erosion on the catchment scale?** The extension of cropland due to population growth is frequently observed in West Africa with adverse effects on hydrology and soil erosion. Isolated and combined impacts of LULC and climate change on water and soil resources are investigated to answer the third research question.

1.3 Objectives

The principle aim of the study is to improve knowledge on the impact of LULC and climate change on water resources and soil erosion in the West African region in order to enable decision makers to plan future adaption strategies. The geographical focus is set to the Dano catchment in Burkina Faso which is one of 3 focal research catchments of the West African Science Service Centre on Climate Change and Adapted Land Use (WASCAL). According to the stated problems and the corresponding research questions this study aims to:

1. **use measured data to complement existing knowledge on the effect of different land use types on soil erosion on the plot scale,**
2. **calibrate and validate the hydrological and soil erosion model SHETRAN for the Dano catchment and assess the related uncertainties,**
3. **investigate the impact of climate change on the development of water resources and soil erosion for the period 2021 – 2050,**
4. **study the effect of LULC and climate change on hydrology and soil erosion on the catchment scale.**

1.4 Structure of the thesis

The thesis starts with a general introduction. The remaining chapters can be structured in two principle parts: Part 1 (chapters 2, and 3) treat the applied methods, the collected data and their analyses. In part 2 (chapters 4, 5, 6, and 7) the modeling approach and the simulated impact of LULC and climate change on hydrology and soil erosion is discussed.

2 STUDY AREA

2.1 Location

The field study was conducted in the south-western region of Burkina Faso within a catchment (126 km²) surrounding the city of Dano, the capital city of Ioba province. The study area is a sub-catchment of the Dano-catchment (195 km²) which is one of three catchments operated by the research project WASCAL (West African Science Service Centre on Climate Change and Adapted Land Use, www.wascal.org). Figure 2-1 shows the location of the study area.

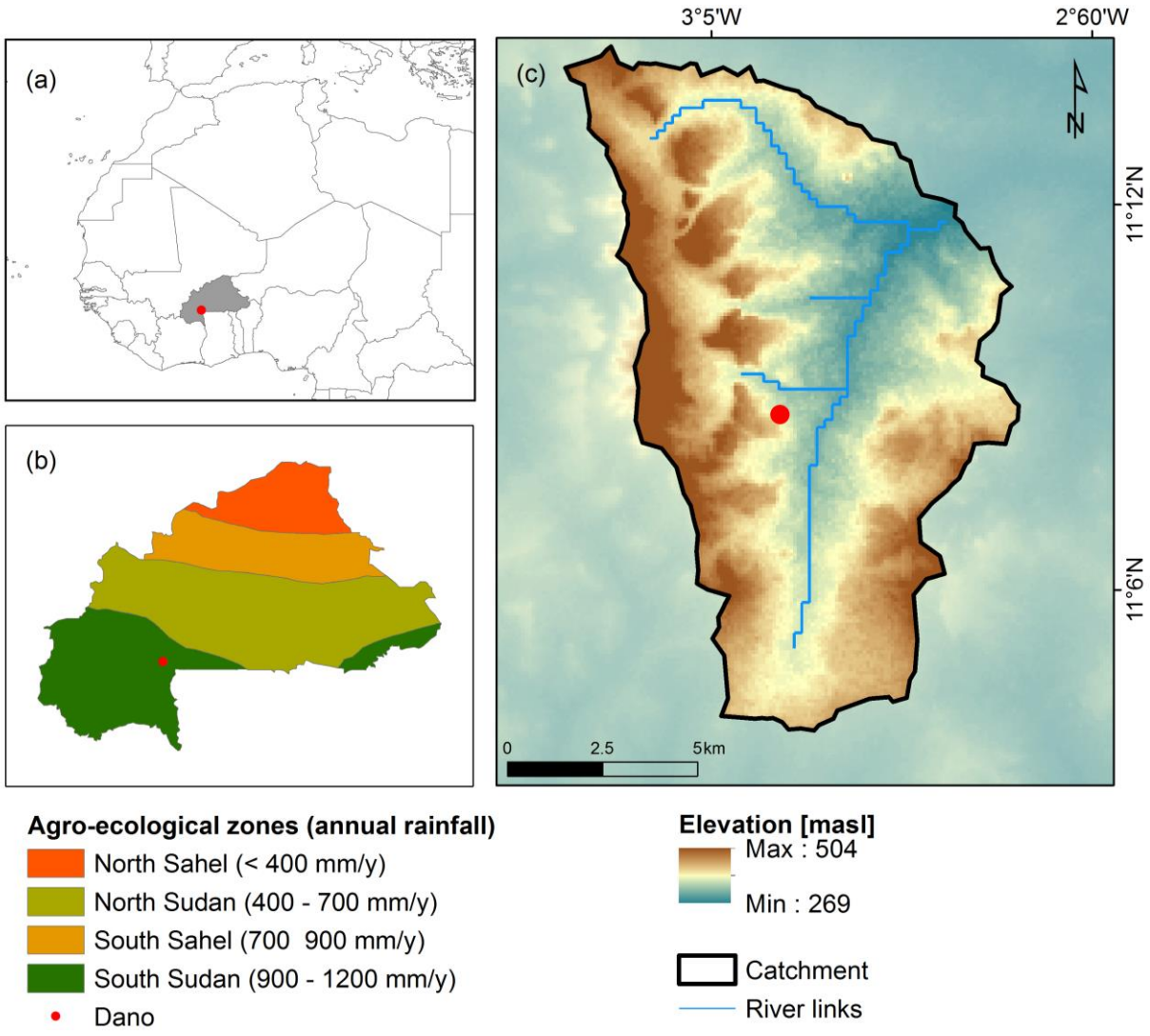

Figure 2-1: Location map of the Dano catchment: **(a)** location of the catchment and Burkina Faso in West Africa; **(b)** location of the catchment in the agro-ecological zones; **(c)** model catchment.

2.2 Climate

The climate in Burkina Faso is influenced by the Hadley cell, a model explaining the atmospheric circulation pattern between the Sahara and the Equator. High solar radiation along the Equator leads to the warming and lifting of moist air masses generating a permanent low pressure zone called the Innertropical Convergence Zone (ITCZ). The ITCZ follows the annual position of the sun. It moves northward in the northern summer and brings monsoonal rainfall to the northern countries of West Africa (Lauer and Bendix, 2006). The unimodal rainy season starts in May and ends in October in southern Burkina Faso. After the rainy season, the ITCZ moves towards the south leaving West African countries under the influence of the northeast trade winds locally known as *Harmattan.* It brings hot and dusty air from the Sahara to the south. The dry season in Burkina lasts from November to May (Badini et al., 1997; Sivakumar and Gnoumou, 1987; Yahmed, 2005).

The atmospheric circulation results in a distinct agro-ecological north-south gradient in West Africa. Four different agro-ecological zones are specified based on climatic criteria (see Figure 2-1b)). The southern part of Burkina Faso is situated in the southern Sudano zone with annual rainfall between 900 and 1200 mm. Figure 2-2a shows the average monthly rainfall and temperatures in Dano. The mean annual precipitation in Dano (1990 – 2015) amounts to 899 mm with a mono-modal distribution and a mean of about 226 mm in August. The onset of the rainy season is variable and starts between mid to end of May and ends in October. The remaining months are dry (Schmengler, 2010). The region is characterized by a remarkable interannual variability of the rainfall as shown by the Standardized Precipitation (SPI) and Standardized Precipitation-Evaporation Index (SPEI) in Figure 2-2b. Climate variability is considered to be an important factor influencing the food security. This became evident in the 1970s and 1980s when the African continent experienced a pronounced period of drought which resulted in famines and migration (Callo-Concha et al., 2012).

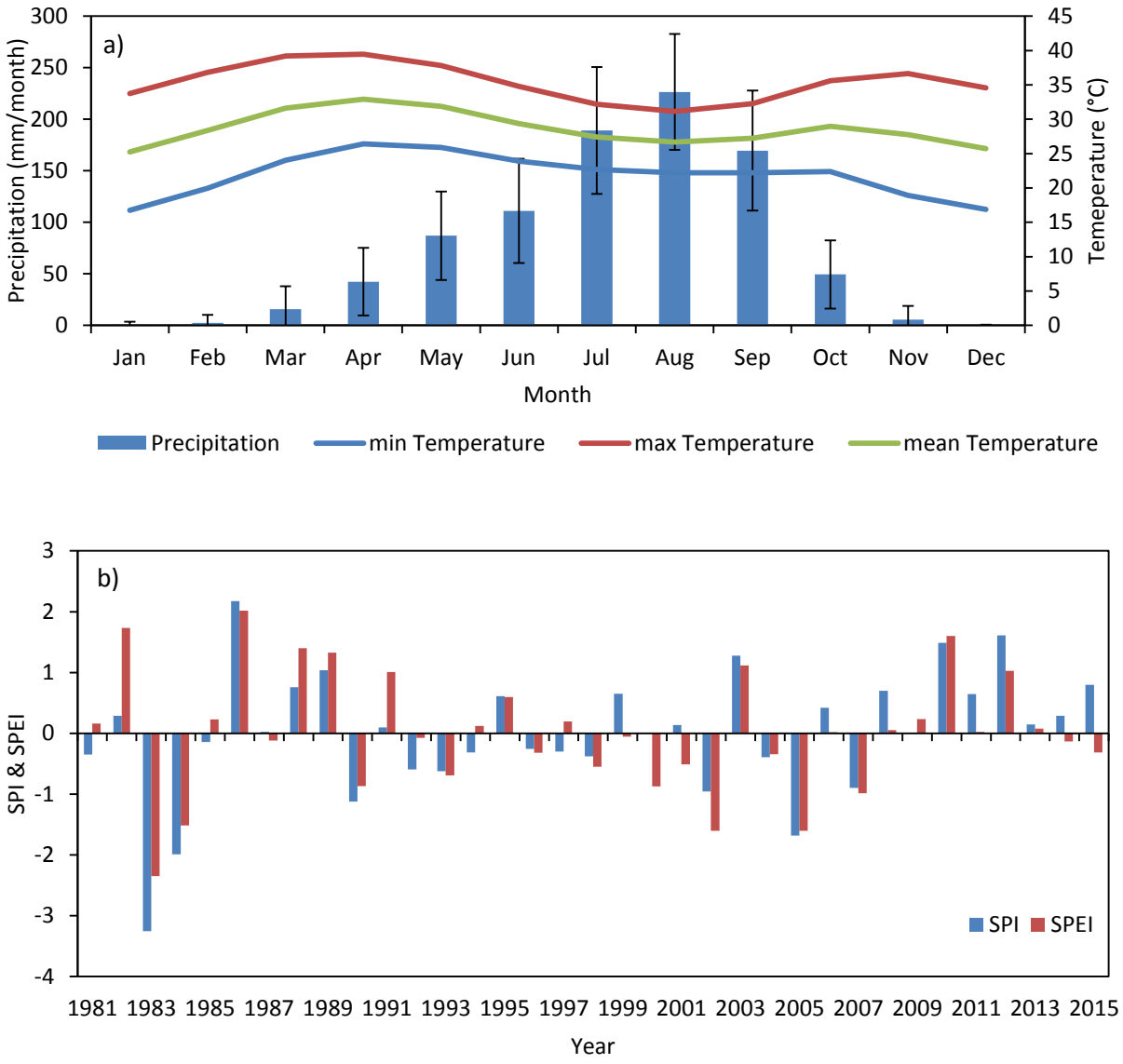

Figure 2-2: **a)** Monthly rainfall and temperature time series in the Dano catchment for the period 1981 – 2015. Error bars refer to the standard deviation. **b)** Standardized precipitation Index (SPI) (McKee et al., 1993) and Standardized Precipitation and Evaporation Index (SPEI) (Vicente-Serrano et al., 2010). Data sources: WASCAL, DGM (Direction Générale de la Météorologie du Burkina).

2.3 Vegetation and land use

The general appearance of the vegetation in the Sudano savanna is dominated by open forests and scrubby grassland areas (CILSS, 2016). Common tree species are the Karité tree (*Vitellaria paradoxa*), the Néré tree (*Parkia biglobosa*), the Baobab (*Adansonia digitata*) and *Anogeissus*

leiocarpus. Perennial grass species, for instance *Adropogon gayamus* and *Cymbopogon ssp.* form a more or less continuous vegetation cover during the rainy season. Gallery forests located along the rivers are composed of for instance *Berlinia grandiflora* (Yahmed, 2005). The natural vegetation in this region is threatened since the growing population cultivates the former untouched areas and uses the trees for firewood production (Schmengler, 2010; Yira et al., 2016).

Agricultural land use is the most important land use category in the region (Forkuor, 2014; Gleisberg-Gerber, 2012; Yira et al., 2016). The farming system has been changing since decades because of the growing demographic pressure. The former shifting cultivation system has gradually been replaced by permanent cultivation. This process is accompanied by reduced fallow periods and the expansion of agriculture to marginal land areas with adverse effects on the soil fertility (Bationo et al., 2007; Callo-Concha et al., 2012). Farming takes place on a small scale and is mostly rain-fed and subsistence-oriented (Callo-Concha et al., 2012; Gleisberg-Gerber, 2012). Furthermore, it is characterized by low investments with regards to fertilizer and machines. Animal power is sometimes used for cultivation as shown in Figure 2-3a). The main staple food crops cultivated in the region are sorghum, millet, maize and rice. Vegetables like tomato and aubergine are cultivated in smaller areas close to rivers and are sold on the local market as are legumes like groundnut and cowpea which are often intercropped. Cotton represents the most important cash crop for the local farmers.

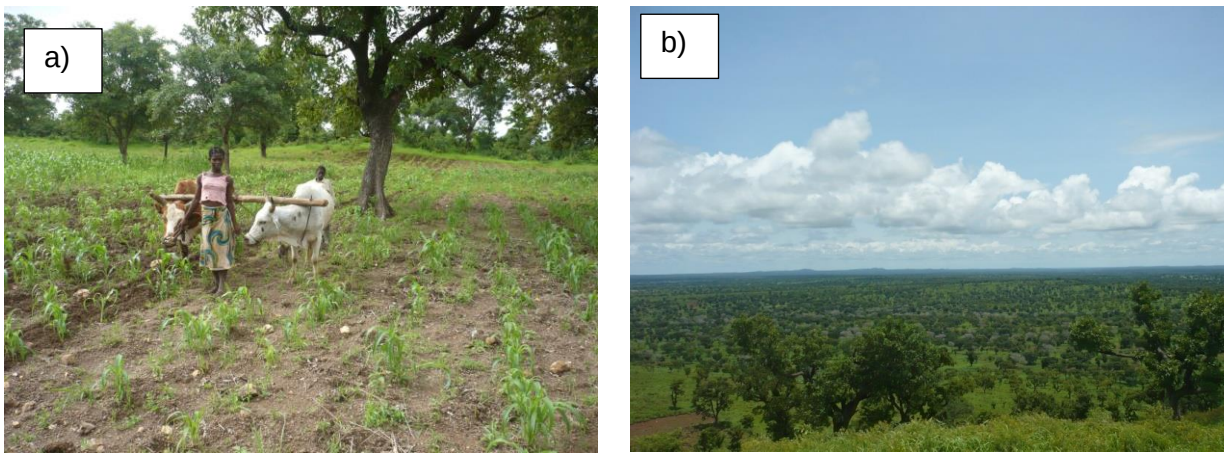

Figure 2-3: **a)** Animal drawn cultivation and **b)** view from the western border of the catchment

2.4 Geology and geomorphology

The geology of Burkina Faso is dominated by the African craton which consists of mostly crystalline (plutonic and methamorphic) basement rocks formed during the Precambrium (Kaloga, 1966). The geology of the research area is composed of rocks from the Birimian. Kaloga (1966)

distinguishes three principal Birimian rock formations: schists of different composition, neutral (metamorphosed diorites and andesites) and basic (gabbros, dolerites, amphibolites) orthometamorphites. In the course of the geologic history, the basement rocks have been subject to erosion and intensive chemical weathering. Although this long lasting exposure has led to a flat and rolling landscape (Figure 2-3b)) with an altitude between 269 and 504 m above sea level, the relief is interrupted by inselbergs and mountain chains often protected from erosion by stable petroplinthitic crusts or by the intrinsic resilience of the forming rock type (Boulet, 1970; Ker, 1995).

The major part of the underground of the study area is formed by Birimian metavolcanites. These basement rocks cut the surface in the hilly terrain in the western part of the catchment. However, geologic formations were rarely seen in the field since they are covered by (often several meters) thick petroplinthite that is often mined (see Figure 3-4). Figure 2-3b) shows a photograph taken from the summit of the hills forming the western boarder of the catchment. It underlines the flat to slightly undulating character of the landscape. The average slope gradient is 1.6° but some slopes, especially in the western part, exhibit inclinations of more than 10°.

2.5 Population

As in many other African countries the population in Burkina Faso is growing at comparatively high rates. Since 1980 the population has almost tripled from 7 Mio to 18 Mio in 2015. The annual population growth rate of Burkina Faso increased from 2.8% (1997) to 3% (2015) (The World Bank, 2017). A distinct urbanization takes place (The World Bank, 2017). The agricultural sector dominates the employment structure as 85% of the citizens are employed here (FAOSTAT, 2017). In 2006 the total population of the Dano district amounted to 46 469 inhabitants (Ministere de l'Economie et des Finances, 2008).

3 INSTRUMENTATION AND DATA AVAILABILITY

Environmental process understanding is achieved by field observations, the analyses of environmental data and the application of physically based models. Consequently, data are needed for analyses, to run, calibrate and validate the model. Environmental data sets are rare in the study area and had to be complemented by measurements of climate, discharge soil and erosion data. Measuring environmental variables is frequently hampered by the scale (temporal and spatial) on which the measurement is possible. The measurement scales are often very small in time and space (Beven, 2008). Therefore, most probes are measuring on the point scale (e.g. precipitation, temperature, radiation, soil data). However, the collected data are assumed to be representative for a larger area. In the present study the differentiation between measurements conducted on the catchment and the plot scale is based on the scale on which these data were used and analyzed. One major aim of this study is to observe hydrological and soil erosion processes on different scales. Hydro-meteorological measurements, the soil survey and the collection of SSL data were mainly conducted on the catchment scale and are presented in chapter 3.1. Measured data from the plot scale are used to estimate the effect of land use change on surface runoff and soil erosion (chapter 3.2).

Table 3-1 shows the data sets that were available at the start of the work. To complement these data sets, an instrumentation design was developed and implemented consisting of climate stations, discharge and turbidity stations as well as erosion plots. An overview over the instrumentation is given in Figure 3-1. Additionally, measurements of soil physical and chemical properties were conducted at the point scale distributed over the study area.

Table 3-1: Available data sets for the study catchment

Data set	Resolution/scale	Source
Topography	90 m	SRTM (Jarvis et al., 2008)
Soil	1:500 000	Kaloga et al. (1973)
Land use map	5 to 250 m	Forkuor (2014), Landmann et al. (2007)
Climate	Daily	DGM (observed), CORDEX-Africa project (http://www.cordex.org/)

3.1 Catchment scale

3.1.1 Introduction

Hydro-meteorological measurements are needed in an acceptable spatial and temporal resolution to drive hydrological and soil erosion models. However, the instrumentation is a compromise between the available budget and personnel and the required resolutions. The measurement of meteorological variables and water level/water discharge was done on the catchment scale with a sub-daily resolution.

Soil data of high quality are necessary for the simulation of environmental processes. As the soil properties controls principle hydrological and erosion processes the analyses of soil data and the parameterization of the model to reflect these properties is of great importance for the modeling approach. Soil data that meet these requirements are rare in the region of West Africa (Forkuor et al., 2017). Therefore, basic research was necessary to obtain information on soil properties required by the model and to create a soil map.

The measurement of soil hydrological properties was harmonized with the soil survey planned by Hounkpatin (2017). Based on topography, land use, geology and soil information representative transects were chosen along which soil pits were dug to describe the soils according to the WRB (IUSS Working Group, 2006) and to sample the soil regarding soil physical (K_{sat}, bulk density, texture etc.) and chemical properties (SOC, CEC, base saturation etc.). The following sections focus on the soil properties that were most important for the work.

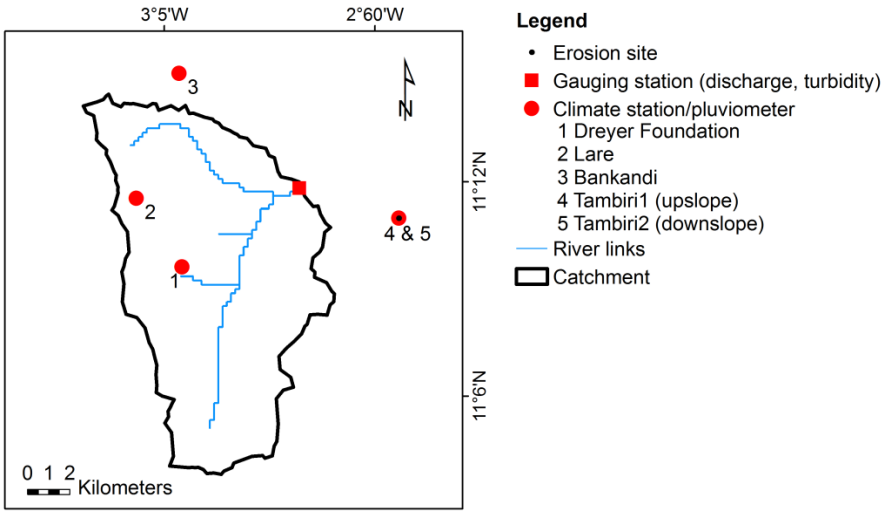

Figure 3-1: Instrumentation of the investigated catchment as used in this study. The erosion plots are outside of the catchment (between station 4 and 5).

3.1.2 Methods

3.1.2.1 Hydro-meteorological measurements

Five automatic climate stations of different types were installed in the study catchment (CR200, CR800 and CR1000, Campbell Scientific INC.). Rainfall, air temperature, relative humidity, solar radiation, wind speed and direction were recorded in 10-minute intervals from which the different time steps required for the different model purposes were calculated. The installation locations were chosen based on elevation, the representativeness of the environment in terms of land use and morphology and the safety and accessibility as recommended by the World Meteorological Organization (WMO, 1993). However, as the land use in the catchment is characterized by a quite patchy structure with mixed and alternating use, topography, spatial coverage, accessibility and safety were the major selection criteria. Climate data from the DGM, the national meteorological service, was available on a daily basis covering the period 1971 – 2011. These data were used for the land use and climate change impact studies.

The location of the discharge gauging station was selected according to guidelines by the WMO (WMO, 2010). Special attention was given to the straightness of the course and the absence of vegetation, the technical requirements for installation and protection and the accessibility. A water level sensor (EcoLog 500, OTT Hydromet GmbH) was installed to record the water pressure (10 minutes interval) which was corrected for the atmospheric pressure. A rating curve was created by pairing the measured water level with several discharge measurements at differing water

levels using a digital acoustic current meter (ADC, OTT Hydromet GmbH). This was done under the consideration of ISO 1100-2:2010 (ISO, 2010).

3.1.2.2 Turbidity and suspended sediment concentration

Turbidity as a surrogate measurement for suspended sediment concentration (SSC) in rivers is frequently used to overcome the disadvantages of conventional sediment measurement techniques regarding temporal resolution and continuity. Water turbidity is the optical property of water that leads to scattering and absorption of light rays. The turbidity of water samples is caused by particles (clay, silt, organic matter) that scatter and absorb the light. Consequently, a relationship between turbidity and suspended solids can be assumed (Gippel, 1995, 1989; Rasmussen et al., 2009). The use of turbidity measurements requires a close correlation between turbidity and SSC. Daily in situ measurements of SSC manually collected close to the turbidity sensor and the corresponding turbidity readings are used to obtain the site-specific calibration curve. A nephelometric turbidity sensor (type 6136, YSI Inc.) was used to measure turbidity at 15 minutes interval. The SSC was measured using filter papers (MN 1640 de ¼, Macherey-Nagel GmbH & Co. KG) following the procedure described in ISO 4365 (ISO 2005).

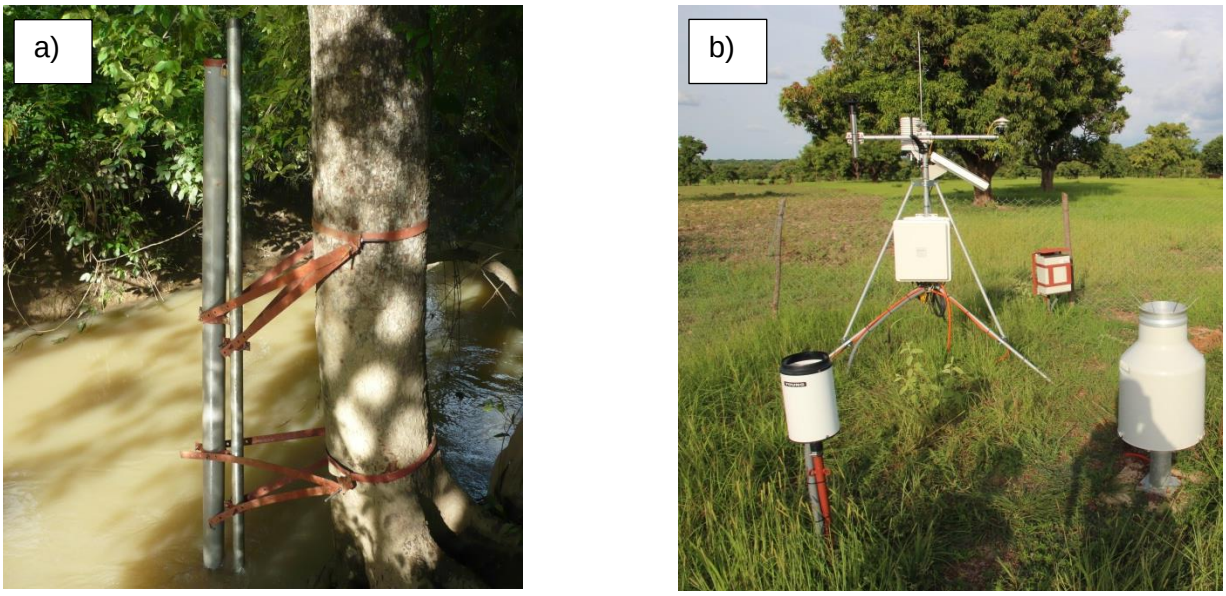

Figure 3-2: **a)** Discharge and turbidity station **b)** and climate station (Nr. 4 in Figure 3-1)

3.1.2.3 Soil texture

The texture analysis was done according to the method proposed by van Reeuwijk (2002). The destruction of sesquioxides prior to analysis as advised in this work was not applied as it was very time consuming.

3.1.2.4 Soil organic carbon

The samples were ground to fine powder and weighted in tin capsules. The determination of elemental C and N was done using an elemental analyser (Fisons NA 2000 elemental analyser, Fisons Instruments, Rodao, Italy).

3.1.2.5 Saturated hydraulic conductivity

Standardized sample rings with known volume (250 cm^3) and a dead blow hammer were used to obtain three undisturbed soil samples (repetitions) of each soil horizon. The surfaces at each end were leveled to guarantee the right soil volume and enable the further processing. The cylinder samples were gradually saturated for 24 hours. Air inclusions were minimized by the progressive filling of the saturation vessel up to the edge of the soil cylinder. The K_{sat} was measured using a constant-head laboratory permeameter (Eijkelkamp Soil & Water). The percolated water volume per time was measured and K_{sat} was calculated using Darcy's equation for saturated conditions (Eq. 3-1):

$$k_{sat} = \frac{Q\ L}{h\ A} \qquad \text{Eq. 3-1}$$

Where K_{sat} is the saturated hydraulic conductivity [cm/d], Q the water volume percolating through the soil per time [cm^3/d], L the length of the soil sample [cm], h the water level differences outside and inside the ringholder [cm] and A the surface area of the sample [cm^2].

The soil properties required by physically based spatially distributed hydrological and soil erosion models are difficult to measure in situ due to temporal, personal and financial efforts necessary to retrieve these information. Pedotransfer functions (PTFs) use basic soil information (texture, SOC, coarse particle content) to obtain principle hydrological soil properties (K_{sat}, θ_{res}, θ_{sat}) (Wösten et al., 2001). A variety of PTFs exists for different regions and they may be tested against measured data to validate their applicability in the study area (Cornelis et al., 2001; Young et al., 1999). Another approach is to obtain parameter ranges from different PTFs and use these ranges to find an optimal parameter setting (Yira et al., 2016). The laboratory measurement of K_{sat} were complemented by estimates derived from several PTFs (Brakensiek and

Rawls, 1994; Cosby et al., 1984; Saxton et al., 1986; Saxton and Rawls, 2006; Schaap et al., 2001; Vereecken et al., 1990).

3.1.2.6 van Genuchten parameters

The saturated water content (θ_{sat}), the residual water content (θ_{sat}), the inverse of the air entry suction (α) and the pore size distribution (n), commonly designated as the van Genuchten parameters after van Genuchten (1980), were calculated based on soil texture and organic matter content following Rawls and Brakensiek (1985).

3.1.2.7 Bulk density

The bulk density was measured using the samples used to determine K_{sat}. The dry bulk density was measured according to ISO 11272 (ISO, 1998).

3.1.2.8 Soil map

The available soil map (Kaloga et al., 1973) covers the entire state territory of Burkina Faso and its scale of 1:500 000 is considered too coarse to reflect the local variability of soils in the study catchments as this map only designates 4 different soils. Therefore, a soil mapping campaign was started in 2012 (Hounkpatin, 2017). Extensive soil augering and the chemical and physical analyses (texture, bulk density, K_{sat}, soil organic carbon, pH, cation exchange capacity) of soil samples from profile pits following van Reeuwijk (2002) were done to capture the spatial heterogeneity of soils. The soils were classified according to the WRB (IUSS Working Group, 2006). The Soil and Terrain Digital Database (SOTER) approach was used to create a soil map for the study area. This approach delineates soil units based on landform units with common terrain characteristics (slope, surface form), geology and soils (Engelen and Ting-Tian, 1995).

3.1.3 Results and discussion

Results of hydro-meteorological measurements are discussed in detail in chapter 5.3. The same chapter also includes a discussion of the measured turbidity and the calculated suspended sediment concentration. To avoid repetitions, these results are not presented here.

3.1.3.1 Soil texture

The textural classes vary between soil types, landscape position and vertically in the different soil reference groups. Vertical translocation of clay from the topsoil to the subsoil is observed in all soil groups. The proportion of sand and silt is higher in the topsoil as they are relatively enriched. The soil texture has distinct effects on hydrological soil parameter as K_{sat} and water con-

tent. K_{sat} is reported to decrease with decreasing grain size as a result of the reduction of pore diameter (Blume et al., 2010). As grains size and pore diameter decrease with depth K_{sat} also decreases. Furthermore, texture affects soil erodibility among others through its inherent properties (density, cohesion etc.) its influence on the formation of aggregates (Le Bissonnais, 1996; Wischmeier and Mannering, 1969).

3.1.3.2 Soil organic carbon

Soil organic carbon (SOC) content is relatively low (≤ 1.5 %) in all soils and decreases with depth. Post et al. (1982) compared the C densities of different life zones and conclude, that C stocks are comparatively lower in regions influenced by a distinct seasonality with repeated wetting and drying. The reason for this is the activity of decomposers at water potentials that are far too low for plant growth. Consequently, microbial decomposition reacts less sensitively to water shortage than plant growth does, which finally leads to equilibrium on a lower level of SOC contents. SOC has effects on hydrological parameters (K_{sat}, porosity, water retention) (Rawls et al., 2004) and erodibility (Guerra, 1994). In general, soils whose SOC content is high are characterized by a better soil structure and increased biological activity which has positive effects on soil water movement and soil resistance against erosion (Blume et al., 2010; Guerra, 1994; Léonard et al., 2004).

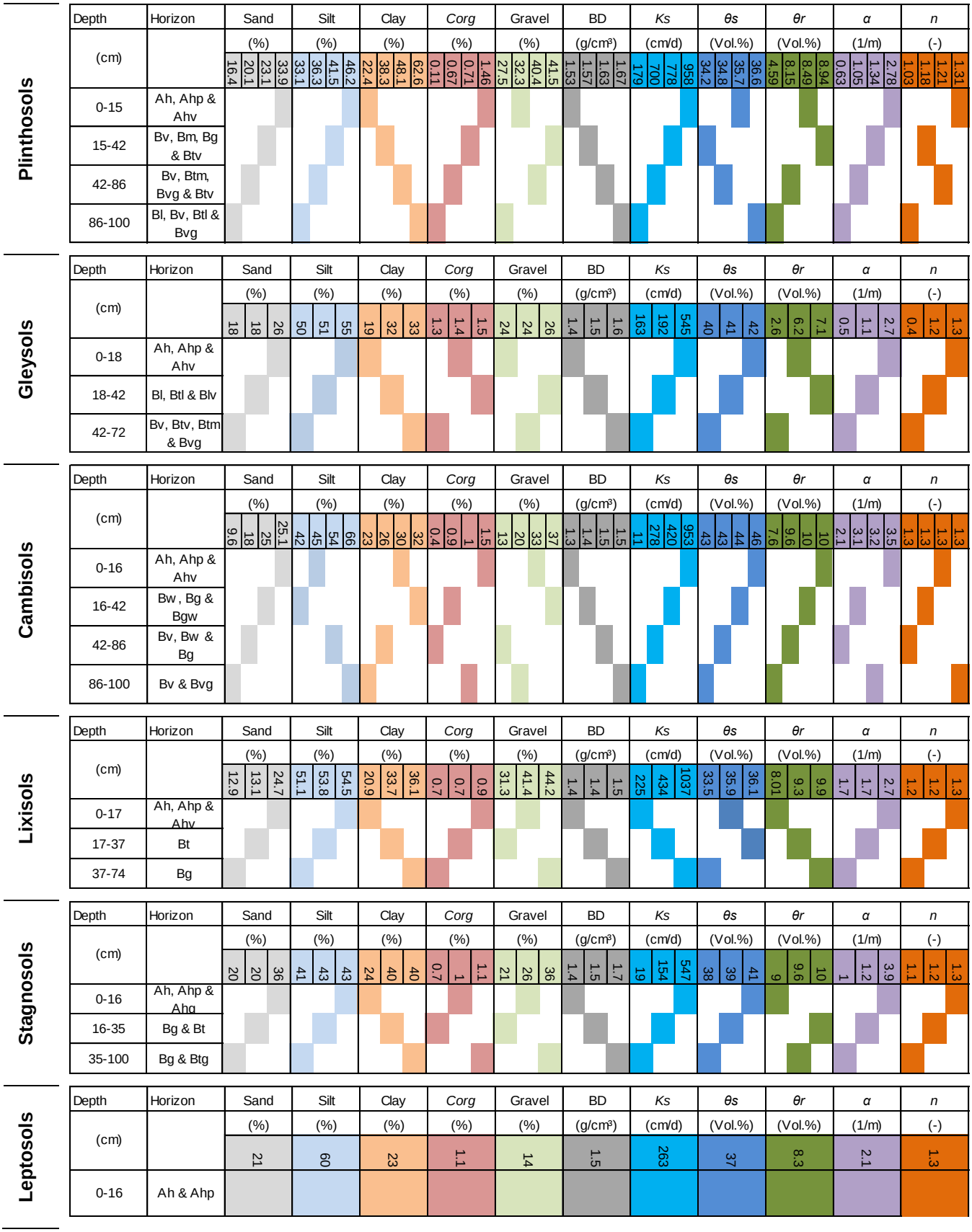

Figure 3-3: Mean soil groups properties. K_{sat} values are measured (adopted from Yira (2016))

Figure 3-4: Active petroplinthite mine in Dano

3.1.3.3 Saturated hydraulic conductivity

As described before (section 3.1.2.5), saturated hydraulic conductivity was measured and estimated based using the PTF of Brakensiek and Rawls (1994). Regardless of the applied method K_{sat} decrease with increasing soil depth as a result of the changing soil properties. Consequently, it is highest in the topsoils ($263 \leq K_{sat} \leq 1037$ cm/d) and decrease in the subsoil ($11 \leq K_{sat} \leq 778$ cm/d) as shown in Figure 3-3. K_{sat} controls water movement in soils. High K_{sat} values throughout the profiles indicate the preference of vertical flow. Nevertheless, the reduction of K_{sat} with soil depth and the occurrence of petroplinthite lead to lateral flow (interflow) which is also confirmed by observations from soil pits.

The widespread occurrence of petroplinthite strongly affects K_{sat} and water movement in the catchment. Hydrological properties of the petroplinthite seem to vary depending on the degree of cementation and the presence of macropores. However, measurements have not been conducted due to the difficulties regarding sampling and measuring (Yira, 2016).

The measured K_{sat} values are high compared to measurements in the same region and for the same soil groups (Giertz et al., 2010; Azuka et al., 2015) and compared to K_{sat} as estimated using the PTF (Brakensiek and Rawls, 1994). K_{sat} derived from the PTF ranges from 2 cm/d to 8 cm/d for topsoils. This large difference is explained by problems regarding the measurement of K_{sat} and the calculation by the chosen PTF. Soils of the study catchment may contain a high

proportion of coarse particles in the form of Fe and Mn concretions which hampers the measurement of K_{sat} by the method described in section 3.1.2.5. Large artificial pores may occur between the cylinder wall and the soil matrix which leads to extremely high measured K_{sat} values, a phenomenon called “sidewall leakage” (Bowders et al., 2002; Mohanty et al., 1994). This effect is difficult to avoid especially regarding soils that are characterized by a high coarse particle content. On the other hand, the PTF derived K_{sat} is calculated mainly based on texture and therefore ignores soil structure and especially biopores which can dominate the hydraulic properties of soils.

Both determination methods were used as input into SHETRAN and the corresponding model responses were compared. The simulations with measured K_{sat} were discarded as the simulated water table rose above the ground surface causing saturated runoff only which does not fit to observed runoff processes. K_{sat} values derived from several PTFs (Brakensiek and Rawls, 1994; Cosby et al., 1984; Saxton et al., 1986; Saxton and Rawls, 2006; Schaap et al., 2001; Vereecken et al., 1990) were also used as input into SHETRAN among which the one by Brakensiek and Rawls (1994) was used. This PTF considers soil texture, coarse particle content and organic matter content. Using the range of estimated K_{sat} values by the different PTFs for the calibration of SHETRAN would be a better approach but the runtime of SHETRAN limits the calibration parameters and focus was put to the calibration of the surface runoff.

3.1.3.4 Soil map and soil reference groups

Figure 3-5a shows the maps of the six reference soil groups (RSG) with qualifiers as derived from the soil map provided by Hounkpatin (2017). The initial soil map was reclassified in order to meet the model requirements concerning the maximum number of soils (9). The reclassified map is shown in Figure 3-5b. The reclassification was done based on the RSG, common physical properties and the spatial dominance. In order to avoid the smoothing and averaging of soil properties and the corresponding creation of artificial soil types, the properties of the major RSG were assigned to the reclassified soils.

A typical transect in the southern part of the catchment and the corresponding soil profiles are given in detail in Figure 3-6. Both figures support the dominance of Plinthosols. Almost 72% of the area is covered by Plinthosols followed by Gleysols (10%), Cambisols (7%), Leptosol (5%) and Lixisols (4%).

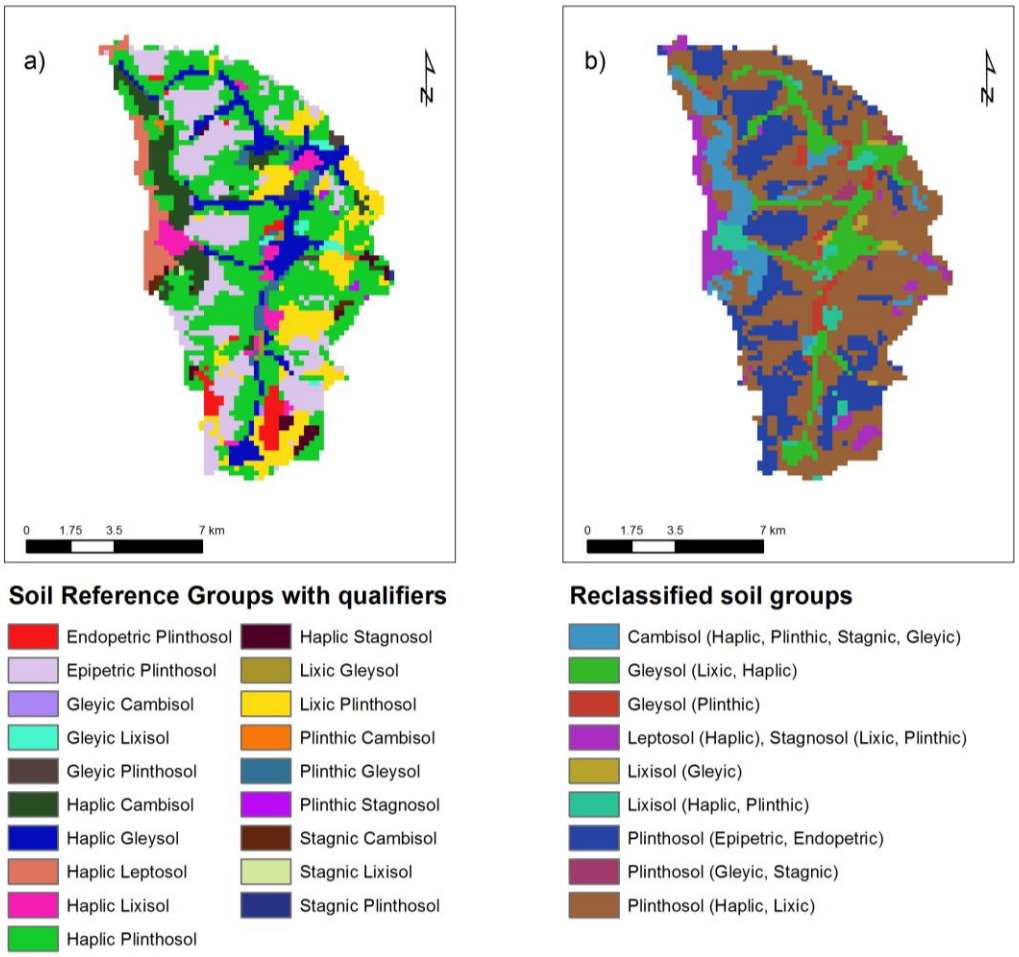

Figure 3-5: **a)** Soil map of the study catchment with the initial 19 soils (Hounkpatin, 2017) and **b)** reclassified soil map with 9 soil groups

Plinthosols

Figure 3-3 shows average values of soil properties calculated using data from all soil groups. Therefore, the data in Figure 3-3 are rather hypothetical and reflect mean soil properties. The transect shown in Figure 3-6 shows shallow Plinthosols at the summit and shoulder positions and limited by the occurrence of a petroplinthitic horizon (Bmv), which is expressed in the WRB by the prefix qualifier (“endo-”, “epi-“) “petric”. The occurrence of shallow petroplinthite is frequently a result of erosion processes that have transported the overlying soil material in the past. The petroplinthite is frequently mined and used as construction material (Figure 3-4).

From Figure 3-3 (Plinthosols) it can be observed that Plinthosols are characterized by a high content of nodules often above 30% by volume in the topsoil. Apart from plinthisation the translocation of clay is an important soil forming process indicated in each soil by a sharp increase in

clay with depth and decreasing sand and silt contents. This has also implications on K_{sat} which decreases with depth as a result of the increasing clay content and the decreasing pore size.

Gleysols

Gleysols are hydromorphic soils and strongly influenced by groundwater. Consequently, they are located along rivers and cover the valley bottom (see Figure 3-5 and Figure 3-6). The long periods of saturation lead to a characteristic gleyic color pattern. Figure 3-3 (Gleysols) shows clay translocation from the topsoil to the subsoil while the content of silt and sand decreases. K_{sat} is markedly lower in all horizons compared with Plinthosols.

Cambisols

Cambisols predominantly occur at the footslope of the Ioba mountain chain as a result of weathering and translocation processes taking place in this area. In contrast to Plinthosols where the parent material is not identifiable anymore, Cambisols are formed through the weathering of the parent material and characterized as moderately developed soils. Because of this and the procedure of exclusion used in the WRB (IUSS Working Group WRB, 2007) a clear identification of horizon boundaries is sometimes challenging as Cambisols are characterized by quite variable properties and soil forming processes. This is also reflected by the properties given in Figure 3-3 (Cambisols) which do not follow the already observed pattern regarding clay and SOC.

Leptosols

Leptosols occur in the western part of the catchment where the basement rocks of the Ioba mountains cut the surface. They are characterized by a shallow depth over continuous rock and have often a high percentage of coarse rock fragments. This is also reflected by the data in Figure 3-3 which are only available for the topsoil.

Lixisols

The occurrence of Lixisols is scattered as shown in Figure 3-5. As a consequence of vertical clay translocation the subsoil is enriched with clay compared to the topsoil (argic horizon). This is also shown by the data in Figure 3-3. Clay content increases with depth whereas K_{sat} decreases.

Stagnosols

Stagnosols are rare in the catchment and do not follow a clear pattern. This hydromorphic soil is influenced by a perched water table leading to seasonal water saturation and the development

of redoximorphic features in the soil matrix. Water stagnation may be a result of low permeable or impermeable soil or rock layers.

3.1.4 Conclusion

Information from field work and laboratory measurements of physical and chemical soil properties and their combination to create the soil map allow the parameterization of the hydrological and soil erosion model SHETRAN (see chapter 5).

The soil map (Hounkpatin, 2017) shows that the soil diversity is higher than the initially available map suggests. Plinthosols, Gleysols, Cambisols, Lixisols, Leptosols and Stagnosols were identified. The analyses of soil properties revealed differences between soil groups and vertical changes. A decrease in grain size and K_{sat} is observed with increasing depth. Measured K_{sat} is extremely high compared to measurements from the same region and compared to K_{sat} derived from PTFs. The large differences can be explained by shortcomings of the measurement method and the ignorance of large biopores by the PTFs. The range of K_{sat} values derived from the different PTFs cannot be used for the model calibration due to the long runtime which limits the number of calibration parameters.

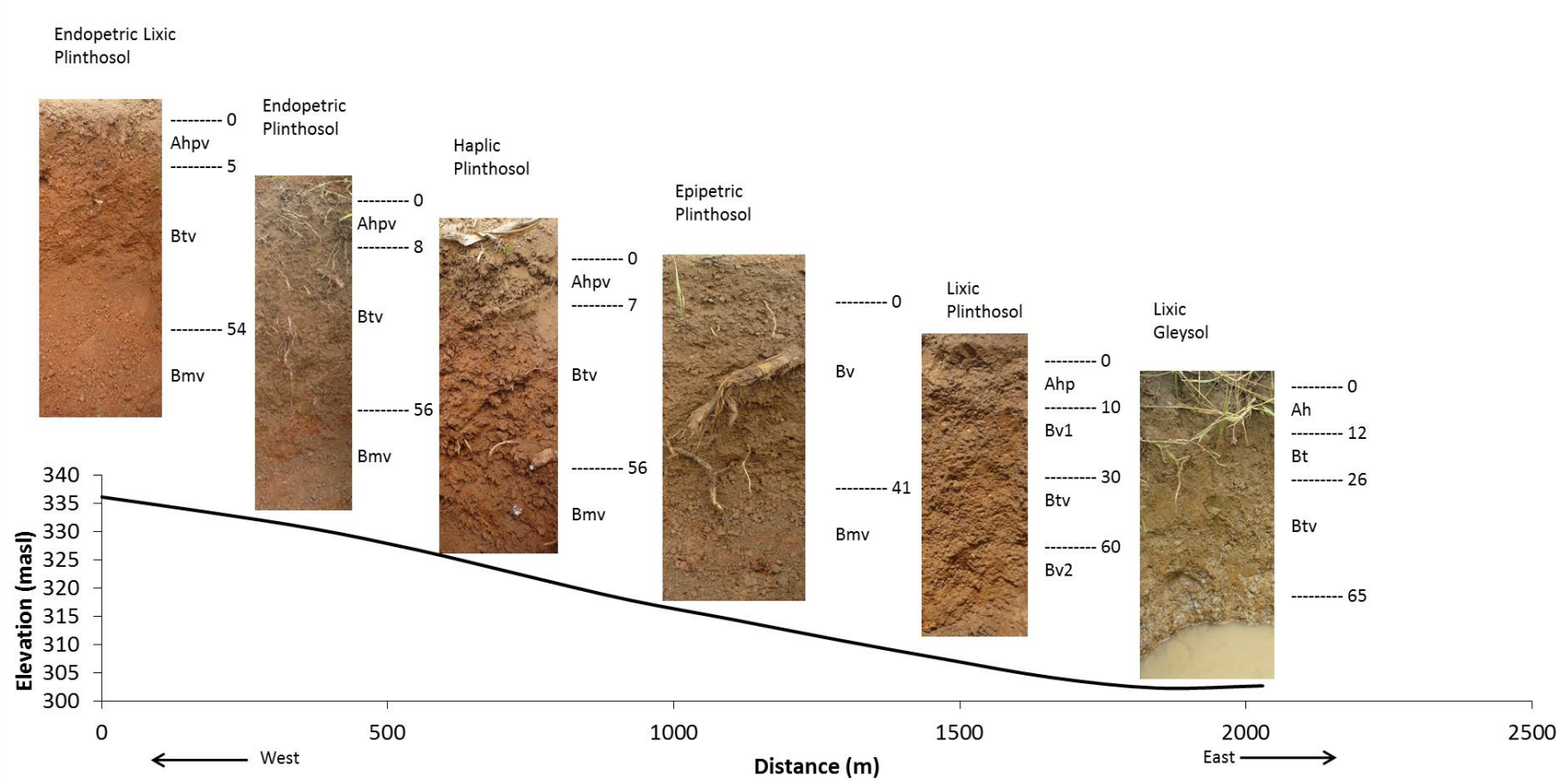

Figure 3-6: Schematic figure of a typical transect in the Dano catchment with horizon description in cm.

3.2 Plot scale: The effect of land use on surface runoff and soil erosion in the sudano savanna of Burkina Faso

3.2.1 Introduction

Population and economic growth are considered to be the most important drivers of land degradation. Human induced land use and land cover (LULC) changes influence the hydrological cycle and intensifies land degradation through soil erosion and nutrient depletion (UNEP, 2012). Especially in countries with fragile ecosystems and limited water and soil resources, changes in the hydrological cycle through LULC may lead to an increased flood and drought risk as well as accelerated erosion rates. Understanding and quantifying the effect of LULC on hydrological processes and soil resources is paramount especially in countries whose societies are highly dependent on agriculture. Water and soil erosion are closely linked and among others controlled by LULC. Therefore, a combined consideration is necessary (Diekkrüger, 2010). Conversion of natural and semi-natural vegetation to cropland presents an important problem in the study area as reported by Yira et al. (2016). They studied LULC maps from different years and found out that the savanna area has decreased since 1990 by a mean annual rate of 2%. This is mostly attributed to an increasing population (3% growth rate) and the resulting demand for food leading to an extension of agricultural fields.

The effect of land use on surface runoff and soil erosion has been investigated by previous experimental studies in this region (e.g. Giertz et al., 2005; Kiepe and de Graaff, 2001; Roose and Sarrailh, 1989; Roose, 1977; Valentin et al., 2004; Yira, 2016). The general conclusion from most studies relates increasing runoff and soil erosion to the conversion of natural/semi-natural to cropland. The present study presents detailed analyses of the mentioned effects of LULC change on runoff and erosion under the consideration of the data variability. It may provide new impulses for the discussion whether data obtained from plot studies can be used to verify hydrological and soil erosion models. Therefore, the objectives of the present study are:

(i) to present and test a new autonomously collecting device designed to measure the full range of surface runoff and soil erosion events from experimental plots;

(ii) to assess the measurement and natural variability of the collected data;

(iii) to present the effect of land use on surface runoff and soil erosion by comparing the data and regression coefficients from different regression models.

3.2.2 Material and methods

3.2.2.1 Measurement of surface runoff and soil erosion

In order to assess the effect of land use on surface runoff and soil erosion, three measurement sites were chosen in comparable topographical positions on a representative slope (2°) and soil type (plithosol). Each site has three erosion plots (replicates) of 40 m² (length 20 m, width 2 m) with the same land use. Following studies on land use conducted in the catchment (Forkuor, 2014; Landmann et al., 2007; Schmengler, 2010) and personal observations from the field cotton, sorghum and fallow were selected as most representative land use types. The experimental design is shown in Figure 3-7. Figure 3-7a) schematically shows the experimental design as implemented in the field. Sediment and surface runoff is measured independently 3 times for each land use type. To allow comparisons between plots of the same treatment and between plots of different treatments, the distance between the plots was kept as small as possible. However, the distance between the fallow plots and the others is slightly larger (70 – 100 m) than between cotton and sorghum (30 m). Figure 3-7b) shows schematic diagram of a measurement unit. A measurement unit is enclosed by a plot border to prevent surface runoff to enter the plot. It is made of corrugated sheets which are 20 cm high (above ground). The sheets are buried in the soil (10 cm) and mounted by pegs. Surface runoff and eroded sediment is collected at the lower end of the plot by a simple collector made of steel. A pipe conveys the water-sediment mixture to the sample splitter. Surface runoff and sediment concentration was measured using six specially designed multi-slot sample splitters and simple plastic barrels of 300l capacity (Figure 3-7d) and e)). The sample splitter was designed in a way that the measurement of the full range of runoff and erosion events is possible through the splitting of collected water by 40 slots. Excess surface runoff that can't be stored in the principle tank (315l) was collected in two additional tanks of different storage volumes (20l, 300l) per splitter.

The data were collected once a day by measuring the water volume and taking sediment samples. The rainfall was measured in 5 minute intervals by a climate station installed nearby. Rainfall characteristics of a measured event were determined from the period since the last data collection (≤ 24 hours). Sediment was measured using filter papers following the procedure described in ISO4365 (ISO, 2005).

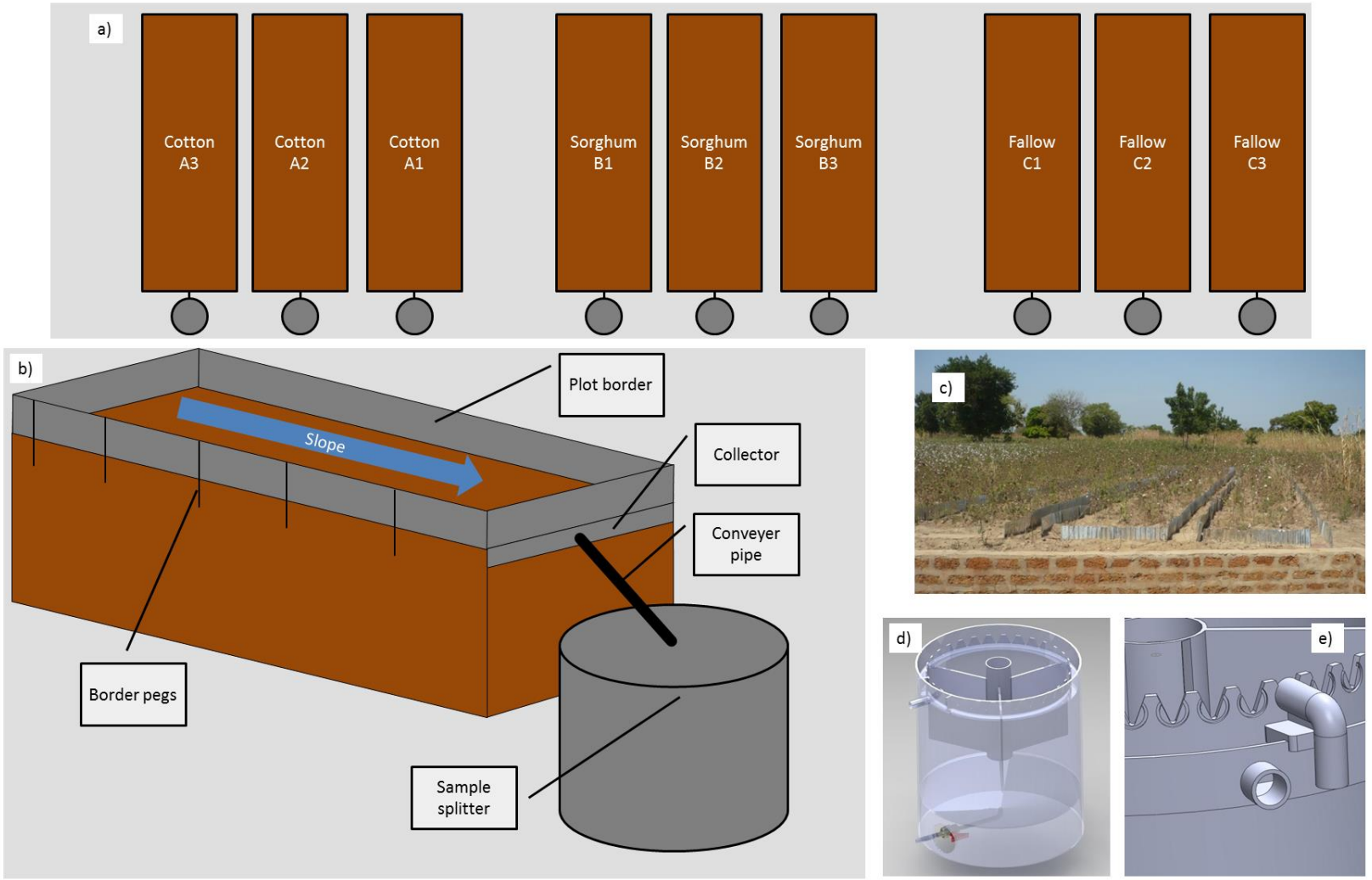

Figure 3-7: **a)** Simplified diagram of the experimental design, **b)** simplified diagram of an erosion plot, **c)** photo of three repetitions draining into the sample splitter in the sampling pit **d)** and **e)** blueprint of the sample splitter.

3.2.2.2 Measurement variability

Measurement variability refers to the errors related to the chain of the measurement processes that starts with the sample collection and ends with the weighing of sediment samples (Hudson, 1993).

The measurement error of the multi-slot sample splitter used here was determined by a number of experiments. Different intensities of water flow (0.06 – 1.46l/s) were applied to the device and the measured total applied water volume was compared to the one calculated by the split samples.

The measurement error related to the filtering and weighing of samples is difficult to quantify. Very small sediment masses are difficult to weigh since air humidity influences the filter weight although a desiccator was used to avoid this problem. The increase of measurement error with decreasing sample volume or mass was also discussed by Rode and Suhr (2007).

The measurement error associated with the collection of water samples to define the eroded sediment was assessed by comparing two samples of 1.5l each.

3.2.2.3 Natural variability

Natural variability can be assessed by comparing plot replicates under the assumption that the measurement errors between repetitions remain equal. In the present study, at each site two different collectors (sample splitter and simple barrels) were used to measure surface runoff and soil erosion from the plots. To achieve comparability, events with a total runoff volume ≤ 300l were used for comparison because below this threshold the sample splitter acts as a simple barrel without sample splitting. For the investigation of the natural variability, complete cases were considered only. Events with incomplete measurement of repetitions were not considered.

3.2.2.4 Statistical analyses

3.2.2.4.1 Land use effects on runoff and erosion

The three erosion sites were compared by using the full number of available samples (n = 225) including replicates. Runoff, erosion and rainfall data were log-transformed to achieve normal distribution and homoscedasticity. Analysis of variance (ANOVA) was performed to test for differences between the three groups. The t-test (Holm adjustment method) was used to do a pairwise comparison.

3.2.2.4.2 Rainfall-runoff-erosion relations

The effect of rainfall and three vegetation types on runoff and soil erosion is studied using simple linear regression equation of log-transformed data:

$$\log y = a \log x + b \qquad \text{Eq. 3-2}$$

Where y is the dependent variable (runoff, soil erosion), x the independent variable (rainfall, runoff), a the slope and b the intercept. A bootstrapping sampling with n=1000 was used to be able to compare regression coefficients of the different land use types. The t-test (Holm adjustment method) was used to prove differences between land use types regarding slope and intercept (Hoffmann et al., 2013).

3.2.3 Results

3.2.3.1 Measurement variability

The accuracy of the sample splitter was assessed by comparing measured and calculated water volumes. Figure 3-8a shows the deviation in % between measured and calculated water volumes as a function of different applied intensities. At higher intensities (> 0.25l/s, green points) measured water volume is underestimated but the deviations are rather low. At lower intensities (< 0.2l/s, red points), the deviation between measured and calculated volume increases drastically. Reasons for this pattern are certainly to be found in effects that are difficult to control as the varying start of water flow through the slots due to water tension effects and wavelets.

Possible errors regarding sediment samples were assessed by comparing replicate samples. Figure 3-7b) shows a scatter plot of the two replicate water samples. The regression line shows a small deviation from the line of equality with a slope of 0.76.

3.2.3.2 Natural variability

The natural variability was assessed by comparing the replicates of each treatment (intra-replicate). Coefficients of variation for runoff range from 8.9% to 98% with a median of 49%. For soil erosion intra-replicate variability is larger and ranges from 16.2% to 127.3% with a median of 61.6%. Factors between minimum and maximum values of three replicates range from 1 to 15 for measured runoff and 1 to 32 for soil erosion.

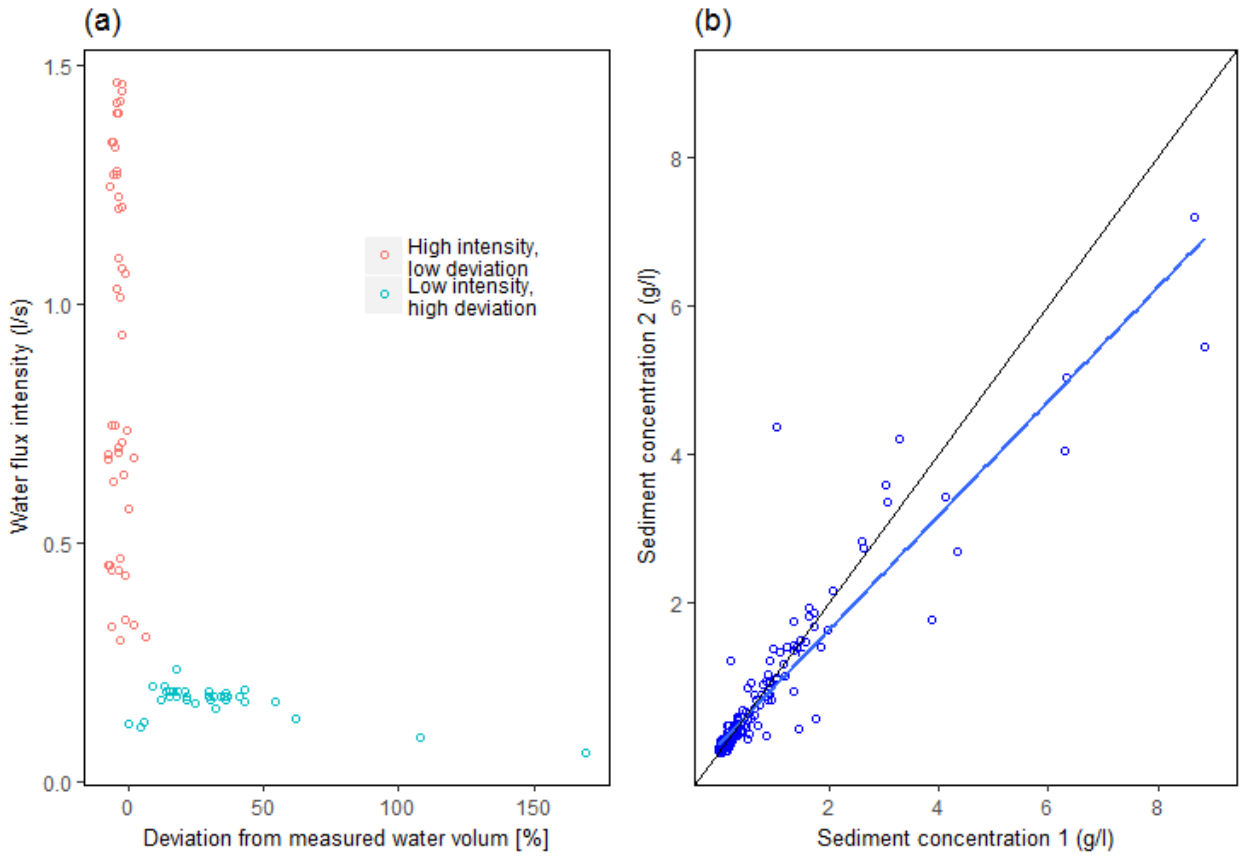

Figure 3-8: Scatter plot showing **(a)** the deviation between measured and calculated water volume as a function of water flux and **(b)** the scatter plot of replicated measured sediment samples and the regression line. n equals 85.

3.2.3.3 Land use effects on runoff

Results obtained from the comparison of the log-transformed runoff coefficients of each site show that there are statistically significant ($p < 0.05$) differences between each of the three land use types (see Figure 3-9a) and b)). The median runoff coefficient of the cotton field is highest (15.7%) followed by the fallow (6.6%) and sorghum plots (4.2%).

3.2.3.4 Land use effects on soil erosion

The statistical analyses of the log-transformed erosion data show significant differences between the pairs cotton-sorghum and cotton-fallow. Median soil erosion on the cotton plots is with 0.98 g/m² almost five times higher than on fallow fields (0.2 g/m²) and 2.8 times higher than observed on the sorghum plots (0.34 g/m²) (Figure 3-9c and d).

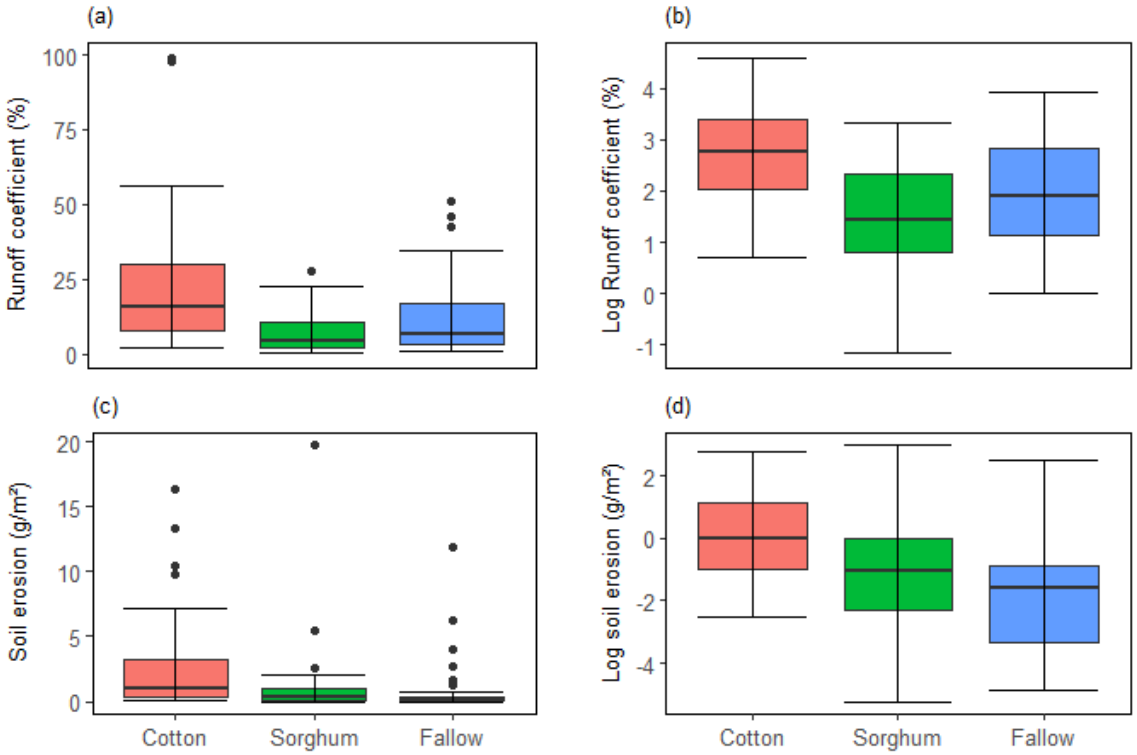

Figure 3-9: **a)** Box plots of untransformed and **b)** log-transformed runoff coefficients and **c)** of untransformed and **d)** log-transformed soil erosion on cotton, sorghum and fallow. n = 225.

3.2.3.5 Land use effects on rainfall-runoff relations

Surface runoff is controlled by soil physical properties, rainfall characteristics and the vegetation. The effect of rainfall and land use on surface runoff is studied in this section. Rainfall runoff relations of each land use type are shown in Figure 3-10a. Runoff is positively correlated with the total event rainfall on all land uses. Slopes of the regression equations (see Table 3-2) indicate that 1% change in the total event rainfall leads to an increase in runoff of 1.5% for sorghum, 1.8% for fallow and 2.1% for cotton. Figure 3-11 shows that bootstrapped coefficients approach a normal distribution. The probability areas are almost congruent for sorghum and fallow for both coefficients. However, the pairwise t test shows significant differences between slopes and intercepts of all land use types.

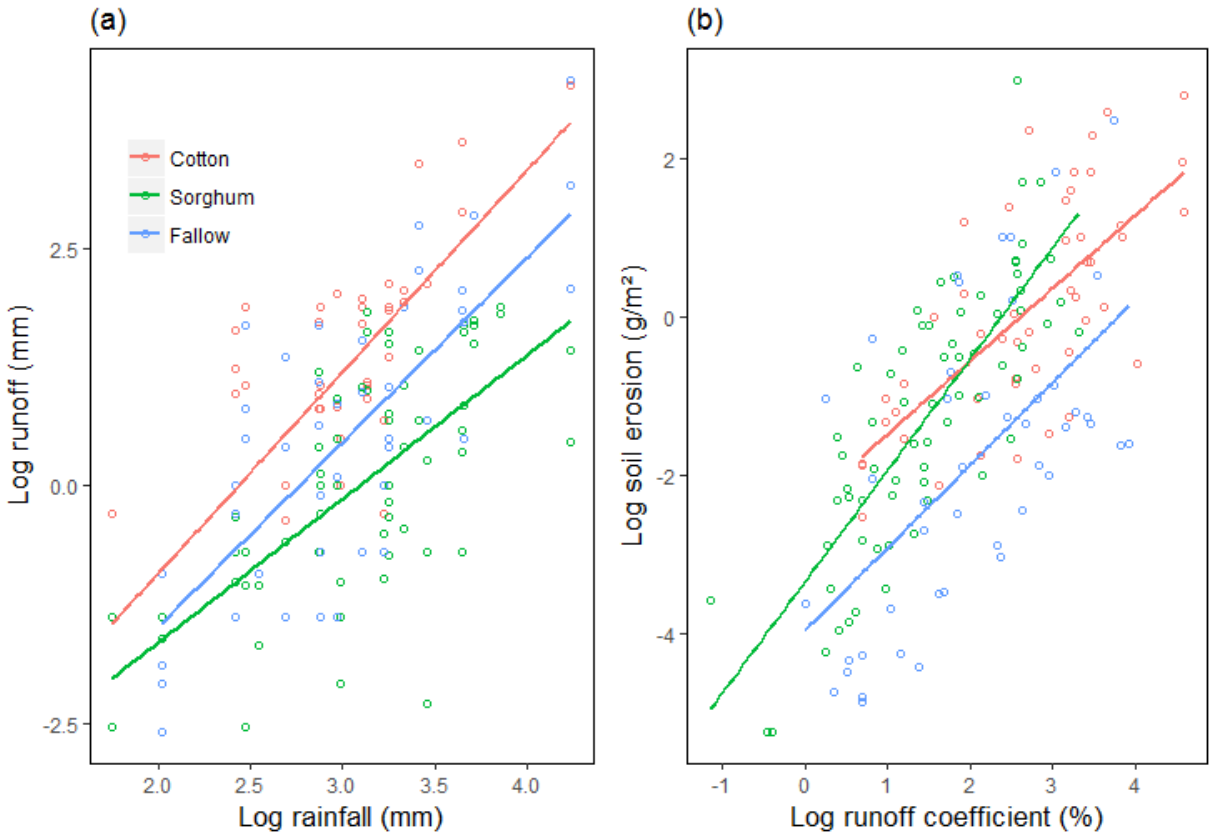

Figure 3-10: **a)** Log-Log regression model of rainfall and runoff and **b)** runoff coefficient and soil erosion for each land use. n = 225.

Table 3-2: Regression coefficients including their standard deviations (SD).

Land use	Slope a	aSD	Intercept b	bSD	R^2
		Rainfall-runoff			
Cotton	2.1	0.26	-5.2	0.79	0.60
Sorghum	1.5	0.15	-4.7	0.44	0.49
Fallow	1.8	0.23	-5.02	0.73	0.52
		Runoff-erosion			
Cotton	0.9	0.1	-2.4	0.3	0.49
Sorghum	1.4	0.14	-3.3	0.25	0.65
Fallow	1.04	0.2	-3.9	0.5	0.36

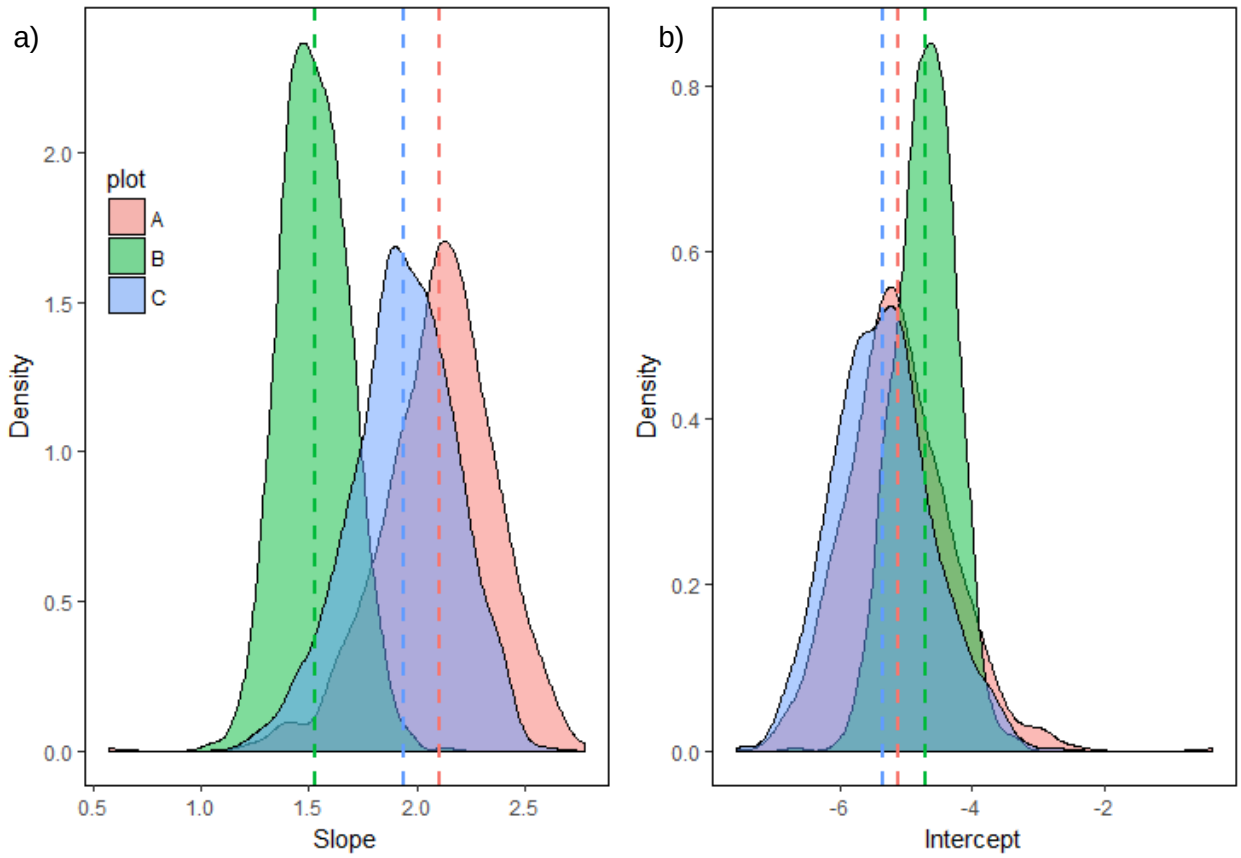

Figure 3-11: Histograms of bootstrapped **a)** slope and **b)** intercept from the rainfall-runoff regression. Dashed vertical lines show location of original regression coefficients. A = Cotton, B = Sorghum, C = Fallow.

3.2.3.6 Land use effects on runoff-erosion relations

Soil erosion is among others influenced by rainfall, runoff, soil and vegetation properties. The effect of land use on the relation between runoff and erosion is studied by comparing three regression models. Figure 3-10b shows that soil erosion is positively correlated with the runoff coefficients in all three cases. An increase of the runoff coefficient of 1% leads to an increase in soil loss of 0.9% for cotton, 1.04% for fallow and 1.4% for sorghum (Table 3-2). Figure 3-12 shows that bootstrapped coefficients approach a normal distribution. The probability areas are rather different for both coefficients. The pairwise t test shows significant differences between slopes and intercepts of all land use types.

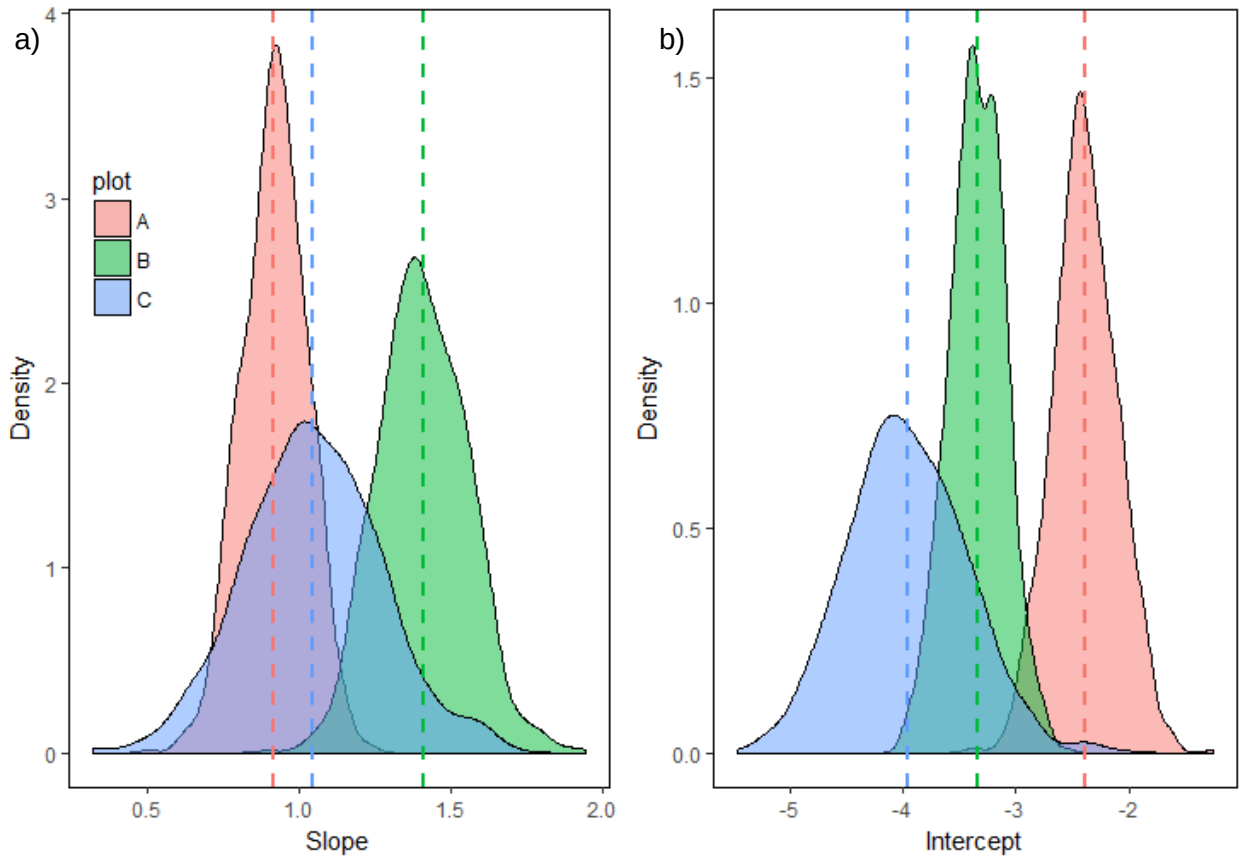

Figure 3-12: Histograms of bootstrapped **a)** slope and **b)** intercept from the runoff coefficient-erosion regression. Dashed vertical lines show location of original regression coefficients. A = Cotton, B = Sorghum, C = Fallow.

3.2.4 Discussion

3.2.4.1 Data variability

The use of runoff and erosion plots has been harshly criticized by Hudson (1993) since they are "expensive and usually ineffective, and usually the vast majority of plots have produced little or no usable or worthwhile information" (Hudson, 1993, p. 25). And in fact, some of the mistakes he lists in his "catalogue of disasters" (Hudson, 1993, p. 26) also happened during this study. One major problem was the flooding of the sampling pits by interflow which results in the floating of the sample splitters and loss of data in 2014. This was solved by draining the sampling pit. Independently of the technical problems encountered, the collected data are valid for the measured area only and can't be transferred to larger areas. However, plot measurement of erosion is inevitable to (i) assess its magnitude and (ii) to study controlling factors as land use (Nearing et

al., 1999). The drawbacks of plot data may be partly overcome by clearly describing the methods used and discussing the encountered problems such as data variability. A number of authors strengthen the high variability related to runoff and soil erosion observations from plots (Bagarello and Ferro, 2004; Boix-Fayos et al., 2007, 2006; Kirkby, 2010; Nearing, 2000; Nearing et al., 1999). Measurement and natural variability can theoretically be distinguished whereby natural variability is much more difficult to quantify and remains often unexplained since it requires a very high number of replicates (Wendt et al., 1986).

The measurement variability was assessed by studying the performance of the newly designed multi-slot sample splitter and by comparing replicate samples of sediment concentration. Samples taken by the sample splitter show low variabilities at high intensities (deviation of -3%) and high variabilities at low intensities (deviation of +30%). This general trend was also observed by Pinson et al. (2003) although they stated less deviation at low intensities. Unfortunately, the experimental design set up to assess the performance of the sample splitter does not allow to transfer uncertainty thresholds to the measured runoff and erosion since the temporal scale used in the experiment (minute-scale) differ substantially from the measured one (event-scale). However, despite the imprecision at low intensities which is difficult to correct, the sample splitter worked well and was able to measure a maximum runoff of 67 mm per event. The comparison of replicated samples of sediment concentration only shows a small deviation. However, to avoid unrealistic high erosion rates, samples with a concentration difference of factor ≥ 2 were removed from the data set.

The natural variability was evaluated by comparing the intra-plot measurement differences per event. The variability differs widely for both runoff and erosion for all events. High intra-replicate variabilities are also reported by other studies (Bagarello and Ferro, 2004; Nearing et al., 1999; Wendt et al., 1986). Reasons may be found in the highly variable hydraulic conductivity as reported by Ajayi (2004) or Giertz et al. (2005). The frequently observed increasing variability with decreasing event magnitude was not observed here. Nearing (1998) states that some reasons for variabilities are theoretically definable and measurable but in practice these measurement are difficult. Some others, he concludes, are unexplainable.

3.2.4.2 The effect of land use change on surface runoff and soil erosion

The frequently reported effect of cultivation on hydrological processes and soil erosion is also observed in this study. Our analyses show that land use has statistically significant effects on runoff and soil erosion. Runoff on cotton plots may be up to 4 times higher than on plots covered by natural/semi-natural vegetation. This effect is also observed regarding soil erosion which may

be up to 5 times higher on cotton plots. The results are partly confirmed by findings from previous studies in the same region (Descroix et al., 2009; Giertz et al., 2005; Hauchart, 2008; Junge, 2004; Kiepe and de Graaff, 2001; Zougmore et al., 2003). An increased surface runoff on cultivated fields is a result of reduced hydraulic conductivities following a reduction of macropores due to disturbed soil biological activity (Giertz et al., 2005; Léonard et al., 2004; Valentin et al., 2004; Yira, 2016). The higher runoff measured on the fallow site may be explained by the soil properties which are dependent on the position in the landscape. As described in section 3.2.2.1 the fallow plots were installed in a larger distance to the others due to practical reasons. Directly upslope of these plots appears a petroplinthic soil layer on the surface and exfiltration of subsurface lateral fluxes was observed. Although the plots are enclosed to prevent surface water from outside to enter the plot, subsurface fluxes may increase subsurface soil moisture within the plots which may lead to faster and higher surface runoff. The cited authors underline the importance of their findings in the context of increasing cropland areas in Africa. Different studies report a substantial land use change from natural/semi-natural vegetation to cropland in different parts of West Africa (Descroix et al., 2009; Gray, 1999; Mahé et al., 2005; Ramankutty, 2004; Yira et al., 2016; Zoungrana et al., 2015). This extension of cropland is driven by socio-economic factors such as population growth and political and private decisions to increase monetary income. Cotton is the most important cash crop in the studied catchment. Its production has been tripled in Burkina Faso in the last 20 years making it to the largest producer and exporter within Africa (Kaminski, 2011). This increase has positive effects for small-scale farmers since it generates monetary income and also higher yields of the subsequent crop due to residual effects of mineral fertilizer applied to the cotton crops. However, negative effects of cotton cultivation on biodiversity (Baudron et al., 2009) and soil erosion (Giertz et al., 2005; Junge, 2004) are the other side of the coin. The adverse effect of cotton on soil erosion is highlighted by previous studies conducted in the region (Giertz et al., 2005; Hauchart, 2008; Junge, 2004). Junge (2004), for example, observed erosion rates between 0.008 g/m² and 9 g/m² on a cotton field and between 0.003 g/m² and 24.6 g/m² on savanna in Benin. The erosion rates measured on the cotton plots (0.08 – 16.3 g/m²) and on the fallow plots (0.007 – 11.8 g/m²) are of the same order. Roose (1977) summarize results from different studies and reports annual erosion rates between 0.6 and 8 g/m² for cropland and from 0.2 to 5 g/m² for natural vegetation. Both studies refer to the higher surface runoff (see section 3.2.3.3) on cultivated areas as one important reason. Furthermore, differences in extent and temporal development of the vegetation covers protecting the soil against splash erosion may explain the differences between the land use types (Morgan, 2005).

3.2.5 Conclusion

This study presented results from surface runoff and soil erosion measurement from experimental plots in southwestern Burkina Faso. Our specific conclusions are as follows:

i) The new multi-slot sample splitter was successfully tested and was able to measure the full range of runoff and soil erosion events.

ii) The measurement variability of the sampling device was acceptable for larger runoff intensities and in line with other devices. Unfortunately, the measured uncertainty caused by the sample splitter could not be transferred to the real runoff measurement. Differences between replicate sediment concentration samples were small. However, a difference with a factor of ≥ 2 was considered to be erroneous and the measurement was removed. Intra-plot variabilities are large for surface runoff and even larger for erosion. This is frequently observed when using experimental plots as shown by the comparison with previous studies.

iii) A statistical significant influence of three representative land use types on surface runoff and soil erosion was confirmed by this study. An unexpected higher surface runoff on the fallow plots in comparison with sorghum could be explained by the local scale differences in soil properties. Measured soil erosion was almost threefold higher on cotton fields as compared to fallow. Regression analyses and comparisons showed that rainfall-runoff relations were statistically different for each land use. The regression of cotton shows a significantly higher slope which results in a quicker runoff response to rainfall. The effect of the runoff coefficients on soil erosion significantly differs for each land use type. The unexpected low slope of the cotton regression equation in comparison with the other land uses remains unexplained.

The construction and maintenance of experimental plots is time-consuming and expensive but inevitable to quantify the influence of land use on runoff and erosion. These investigations may allow us to better assess how the commonly observed LULC change will influence hydrological processes and soil resources. However, to provide data of better quality, measurements should be taken over a sufficient long duration. This will give insights in possible intra-annual variability. Further investigation should also incorporate additional measurement of e.g. vegetation and coarse particle cover.

4 MODELING HYDROLOGICAL AND SOIL EROSION PROCESSES: THE SHETRAN MODELING SYSTEM

The modeling of hydrological and erosion processes was done using the physically based, spatially distributed model SHETRAN (Ewen et al., 2000; Wicks and Bathurst, 1996). SHETRAN is based on SHE (Système Hydrologique Européen) which was jointly developed by the British Institute of Hydrology, the Danish Hydraulic Institute and the French consulting company SOGREAH (Abbott et al., 1986). During the thirty years of successful application, SHETRAN has been continuously improved and equipped with new components as e. g. the sediment component (Wicks, 1988; Wicks and Bathurst, 1996) and a fully 3d subsurface water flow component (Parkin, 1996). The model was already applied with various objectives (Birkinshaw, 2008; Birkinshaw and Bathurst, 2006; Birkinshaw and Webb, 2010; Tripkovic, 2014; Zhang, 2015) and in different regions (Bathurst et al., 2011; Birkinshaw et al., 2010a, 2017; de Figueiredo and Bathurst, 2007; Đukić and Radić, 2014; Lukey et al., 1995).

4.1 Simulation of processes

4.1.1 Hydrology

4.1.1.1 Evapotranspiration

Potential evapotranspiration (ETp) refers to the transpiration and evaporation of a reference surface that is covered by a grass crop and whose water supply is unlimited (Shuttleworth, 1993). Timeseries of ETp were calculated externally based on the Penman-Monteith equation (Monteith, 1975):

$$\lambda E = \frac{\Delta \cdot (H_{net} - G) + p_{air} \cdot C_p \cdot \frac{(e_s - e_a)}{r_a}}{\Delta + \gamma \cdot \left(1 + \frac{r_c}{r_a}\right)} \qquad \text{Eq. 4-1}$$

where

λE	latent heat flux density	[MJ/m²/h]
E	depth rate of evaporation	[mm/h]
Δ	slope of the saturation vapour pressure-temperature curve	[kPa/°C]
H_{net}	net radtion	[MJ/m²/h]
G	soil heat flux	[MJ/m²/h]

p_{air}	air density	[kg/m³]
C_p	the specific heat at constant pressure	[MJ/kg/C°]
e_s	the saturation vapour pressure of air	[kPa]
e_a	The actual saturation vapour pressure of air	[kPa]
γ	psychometric constant	[kPa/°C]
r_c	plant canopy resistance	[s/m]
r_a	aerodynamic resistance	[s/m]

Actual evapotranspiration (ETa) is calculated by the model based on the approach by Feddes et al. (1976) which estimates ETa based on soil moisture tension. In SHETRAN, the ratio of ETa/ETp at field capacity is the parameter that controls the reduction of ETa based on the soil moisture tension (Figure 4-1). In the given example ETa equals ETp at field capacity. If soil moisture tension drops below field capacity ETa is reduced based on the increasing soil moisture tension. The different points (a-g) shown on the blue line are proportionally calculated based on the equations given under Eq. 4-2.

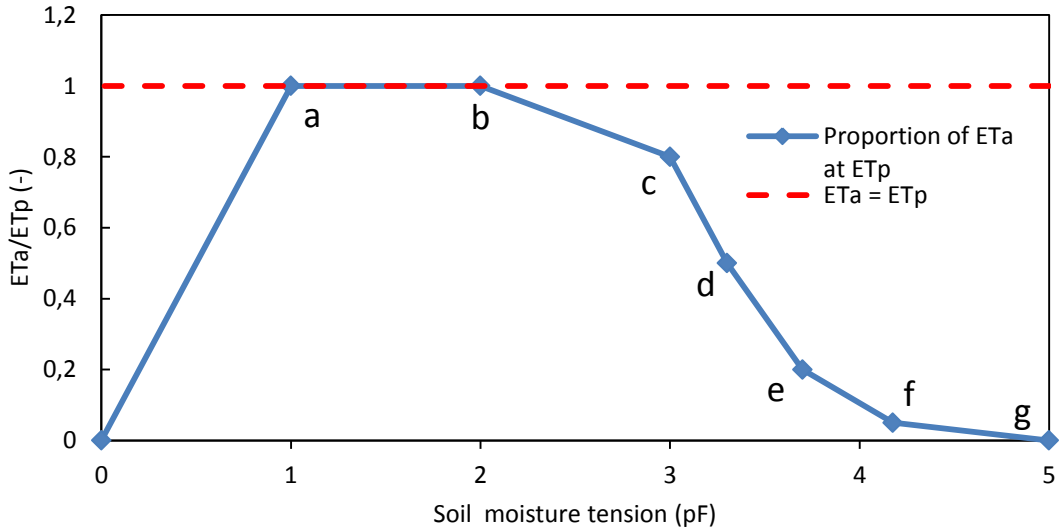

Figure 4-1: Schematic graph showing the reduction of ETa with increasing pF as calculated by SHETRAN with the ratio ETa/ETp at field capacity = 1. Dashed red line indicates maximum ETa.

$$a = \frac{ETa/ETp}{1} \qquad b = \frac{ETa/ETp}{1}$$

$$c = \frac{ETa/ETp}{1.25} \qquad d = \frac{ETa/ETp}{2} \qquad \text{Eq. 4-2}$$

$$e = \frac{ETa/ETp}{5} \qquad f = \frac{ETa/ETp}{20}$$

4.1.1.2 Interception

Interception refers to the temporary storage of precipitation by vegetation (Shuttleworth, 1993). This is implemented in SHETRAN by a bucket approach following Rutter et al. (1975, 1972). The interception storage is filled by precipitation and emptied by evaporation based on equation Eq. 4-3.

$$\frac{\partial C}{\partial t} = Q - ke^{b(C-S)} \qquad \text{Eq. 4-3}$$

where

C	Depth of water on the canopy [mm]
Q	Net rainfall supply to canopy [mm/h]
S	Canopy storage capacity [mm]
k,b	Drainage parameters
t	Time [hour]

4.1.1.3 Infiltration

The infiltration process is calculated using the Richards' equation. The model distinguishes between two conditions:

1. Flux controlled/unsaturated condition: Under conditions when ponded surface water is absent, infiltration is calculated based on Eq. 4-4:

$$k_z(\theta)\left(\frac{\partial \psi}{\partial z} + 1\right) = q_p - E \qquad \text{Eq. 4-4}$$

where

$k_z(\theta)$	Vertical unsaturated hydraulic conductivity [m/d]
θ	Volumetric water content [m^3/m^3]
z	Elevation above datum [m]
ψ	Pressure potential [m]
q_p	Net precipitation at ground surface [mm/h]
E	Evaporation rate at ground surface [mm/h]

2. Soil controlled/saturated conditions: Under conditions when ponded surface water exists, infiltration is calculated based on Eq. 4-5.

$$I=-k_{z,sat}\left(\frac{\partial\psi}{\partial z}+1\right) \qquad \text{Eq. 4-5}$$

where

I	Infiltration rate [m/d]
$k_{z,sat}$	Vertical saturated hydraulic conductivity [m/d]

Based on the two conditions the model is able to simulate infiltration and saturation excess overland flow.

4.1.1.4 Overland flow

Overland flow is represented by the diffusive wave approximations of the Saint-Venant equations and involves the mass and momentum conservation equations and the calculation of friction slopes based on Manning-type law. The equations are given in detail in Zhang (2015). Combining these equations water flow between two grid cells is calculated by Eq. 4-6

$$Q_x=-\frac{K_{st,x}\, w\, h^{5/3}}{L^{1/2}}\,(z_u-z_d)^{1/2} \qquad \text{Eq. 4-6}$$

where

Q_x	Water flow in the x direction [m^3/s]

$K_{st,x}$	Strickler coefficient in the x direction [$m^{1/3}/s$]
w	Cell width [m]
h	Depth of surface water [m]
L	Distance between the centers of neighboring grid cells [m]
z_u	Water surface elevations in the upstream element [m]
z_d	Water surface elevations in the downstream element [m]

4.1.1.5 Variably saturated subsurface

The subsurface flow of water under saturated and unsaturated condition is described by fully 3D Richards' equation (see Eq. 4-7) (Parkin, 1996). A detailed description of the vertical and lateral interactions between grid cells and channel links is given in Parkin (1996). The relationship between soil moisture and pressure potential (θ(ψ)) is called retention curve and is provided as tabulated values.

$$\eta \frac{\partial \psi}{\partial t} = \frac{\partial}{\partial x}\left[k_x(\theta)\frac{\partial \psi}{\partial x}\right] + \frac{\partial}{\partial y}\left[k_y(\theta)\frac{\partial \psi}{\partial y}\right] + \frac{\partial}{\partial z}\left[k_z(\theta)\frac{\partial \psi}{\partial z}\right] + \frac{\partial (k_z(\theta))}{\partial z} - q \qquad \text{Eq. 4-7}$$

where

$\eta = \frac{\theta \cdot S_s}{n} + \frac{d\theta}{d\psi}$	Storage coefficient [m^{-1}]
ψ	Pressure potential [m]
$k_x(\theta)$, $k_y(\theta)$, $k_z(\theta)$	Hydraulic conductivity in x, y, z direction [m/s]
q	Specific volumetric flow rate out of the medium, e.g. root water uptake [s^{-1}]
t	time

4.1.2 Soil erosion

A short summary of erosion processes simulated by SHETRAN is given below:

Soil detachment is accounted for by three separate equations describing detachment by raindrop/leaf drip (Eq. 4-8) (Wicks et al., 1988), by overland flow (Eq. 4-9) (Ariathurai and Arulanandan, 1978) and by channel flow (Eq. 4-10) (Osman and Thorne, 1988):

$$D_r = k_r F_w (1 - C_g - C_r)(M_r + M_d) \qquad \text{Eq. 4-8}$$

where D_r is the rate of soil detachment [kg/m²/s], F_w [-] accounts for the protection against drop detachment by surface water, k_r is the raindrop impact erodibility coefficient [J^{-1}], C_g is the proportion of ground covered by near ground vegetation [%], C_r is the rock cover [-], M_r/M_d is the momentum squared of raindrops/leaf drips reaching the ground per unit time and area [kg²/s³],

$$D_q = \begin{cases} k_f(1-C_r)\left[\frac{\tau}{\tau_{ec}}-1\right] & \text{if } \tau > \tau_{ec} \\ 0 & \text{otherwise} \end{cases} \quad \text{Eq. 4-9}$$

where D_q is the rate of soil detachment per unit area [kg/m²/s], k_f is the overland flow erodibility coefficient [kg/m²/s], C_r is the proportion of ground shielded by rock cover [-], τ is the shear stress exerted by overland flow [N/m²], τ_{ec} is the critical shear stress for the initiation of motion [N/m²],

$$E_b = \begin{cases} BKB\left[\frac{\tau_b}{\tau_{bc}}-1\right] & \text{if } \tau_b > \tau_{bc} \\ 0 & \text{otherwise} \end{cases} \quad \text{Eq. 4-10}$$

where E_b is the detachment rate of bank material per unit area [kg/m²/s], BKB is the bank erodibility coefficient [kg/m²/s], τ_{bc} is the critical shear stress for the initiation of motion of bank material [N/m²] and τ_b is the shear stress acting on the bank [N/m²].

Sediment is transported based on the transport capacity of overland (Eq. 4-11) (Yalin, 1963) and channel flow (Eq. 4-12) (Ackers and White, 1973):

$$G_{tot} = 0.635\sqrt{\frac{\tau}{p}}\, l D_{50}\delta\left[1-\frac{1}{a\delta}\ln(1+a\delta)\right] \quad \text{Eq. 4-11}$$

where G_{tot} is the transport capacity rate for overland flow [m³/s], τ is the shear stress [N/m²], p is the water density [kg/m³], l is the width of flow [m], Q is the water discharge [m³/s], D_{50} is the median sediment diameter, δ and a are parameters,

$$G_i = Q\frac{D_i}{H}\left(\frac{U}{u_*}\right)^{n_i} G_{gr,i} \quad \text{Eq. 4-12}$$

where G_i is the transport capacity rate of particle size in group i [m³/s], D_i is the particle diameter in size group i [m], H is the water flow depth [m], U is the mean water flow velocity [m/s], u_* is the shear velocity [m/s], $G_{gr,i}$ is the dimensionless sediment transport rate for sediment size group i.

Further details are given in Morgan and Nearing (2011) and Wicks (1988).

4.1.2.1 Soil detachment

Eq. 5-1 given in section 5.2.3 describes the detachment rate D_r of soil particles by the impact energy of raindrops and leaf drips (Wicks, 1988). In the following some terms are graphically explained. The values used in the graphical examples below are not necessary reasonable as the examples should only demonstrate how the model internally works.

F_w represents the water correction factor and considers the protective effect of surface water regarding the impact of drops. Figure 4-2a shows how the detachment rate (D_r) is corrected by F_w. The greater the water heights the higher will be the reduction of D_r.

M_r is the squared raindrop momentum and controls basically the impact force of raindrops as a function of drop diameter and rainfall intensity. Figure 4-2b shows that increasing rainfall intensity leads to an increasing Mr.

Similarly to M_r **M_d** is the squared momentum of leaf drops. It depends among others on the amount of water draining from the leaves, the plant heights and the drop diameter. Figure 4-2c shows the effect of increasing drop diameter on the M_d.

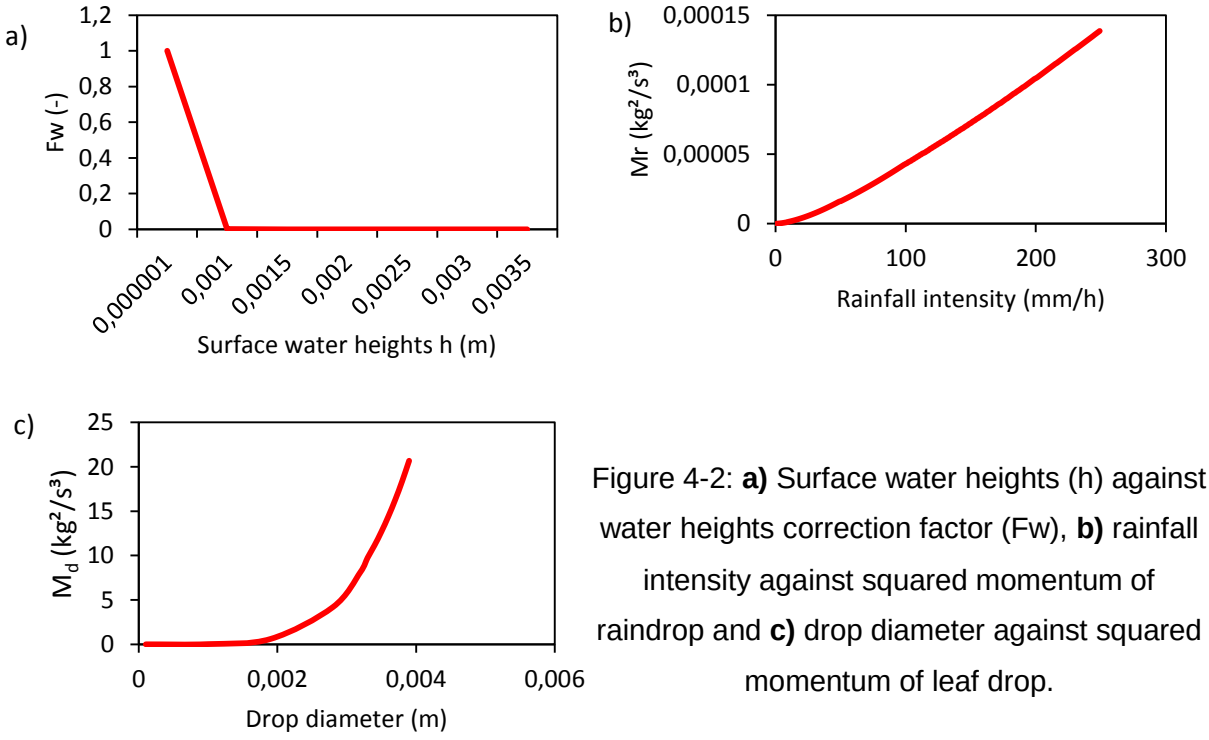

Figure 4-2: **a)** Surface water heights (h) against water heights correction factor (Fw), **b)** rainfall intensity against squared momentum of raindrop and **c)** drop diameter against squared momentum of leaf drop.

4.1.2.2 Overland flow erosion

Eq. 4-9 describes the detachment rate D_q of soil particles by the impact energy of surface runoff on hillslopes (Wicks, 1988). In the following some terms are graphically explained. The values used in the graphical examples below are not necessary reasonable as the examples should only demonstrate how the model internally works.

The shear stress τ reflects the force water flow exerts on the soil mass. It depends on the water density, the acceleration due to gravity, the surface water depth and the slope in the flow direction. Figure 4-3a) shows that the shear stress increases with water heights and surface water slope.

The critical shear stress for particle movement τ_{ec} is calculated based on the approach by Shields (1936) extended by Mantz (1977) for small particles. It depends among others on the particle diameter, its density and Reynolds number and water viscosity. Figure 4-3b) shows how τ_{ec} is affected by the grain size. Sudden changes are explained by the non-continuous shift of equation parameters to account for the reduction of cohesion forces between the particles. In general critical shear stress necessary for the initiation of particle movement increases with grain size. Figure 4-3c) shows the change from stable conditions (no detachment) where the shear stress is less than the critical shear stress to conditions where the shear stress dominates the critical shear stress (detachment) as a result of increasing surface water heights and consecutive flow.

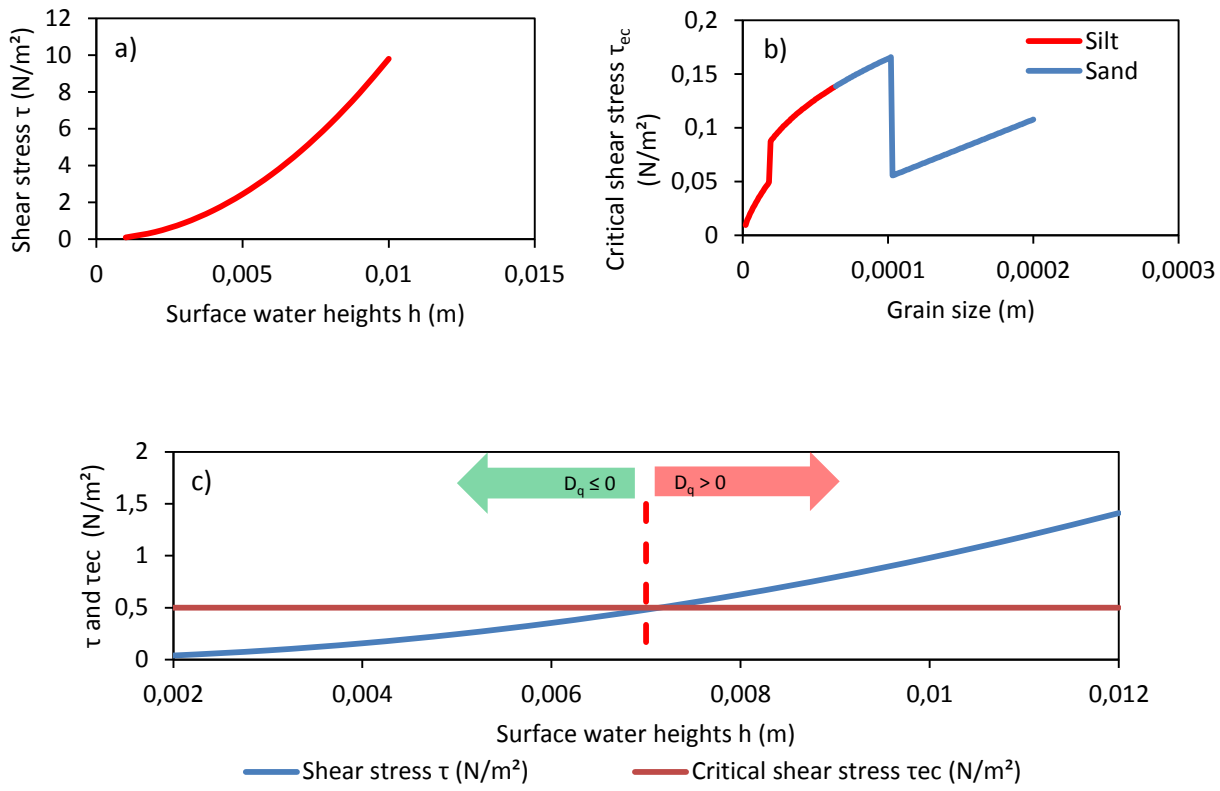

Figure 4-3: **a)** surface water heights (h) against shear stress (τ), **b)** grain size against critical shear stress (τ_{ec}), **c)** change from stable conditions (no detachment, Dq ≤ 0) to unstable conditions (detachment, $D_q > 0$).

4.1.2.3 Channel erosion

Channel bank erosion (Eq. 4-10) is calculated based on the assumption, that the shear stress exerted on the channel bank (τ_b) can be related to the shear stress on the channel bed involving the ratio of channel width (B) to flow depth (H) and some additional coefficients. This is implemented by a proportional constant K by which the shear stress on the channel bed is multiplied to give τ_b. Figure 4-4 shows that the K value increases with increasing ratio B/H suggesting that the larger the higher the water level the higher will be K and τ_b. Bank erosion is also controlled by the bank erodobility coefficient BKB which is usually a calibration parameter.

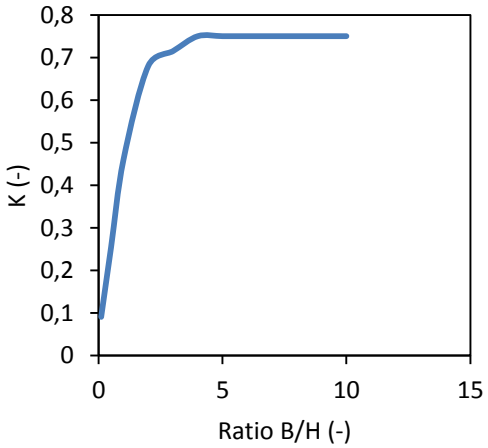

Figure 4-4: The relation between the ratio of channel width (B) to water flow heights (H) and the constant K.

4.1.2.4 Transport capacity

The transport capacity G_{tot} is estimated based on Eq. 4-11 (Yalin, 1963) and depends among others on the width of the flow, the particle size and the shear stress. Figure 4-5 shows the relation between G_{tot}, the shear stress (τ), the critical shear stress (τ_{ec}) and the grain size. G_{tot} decreases as τ_{ec} increases with increasing grain size and becomes 0 as τ_{ec} is higher than τ. At this point the transport capacity of surface water is saturated.

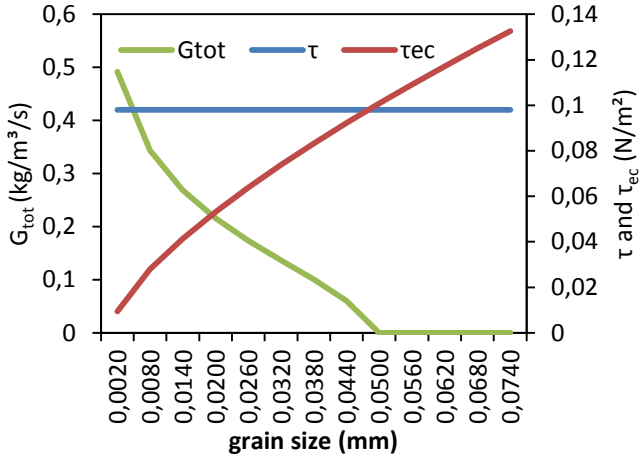

Figure 4-5: Relation between the transport capacity (G_{tot}), the shear stress (τ), the critical shear stress (τ_{ec}) under the consideration of a changing grain size.

4.2 Input

4.2.1 Spatially gridded data

SHETRAN requires spatial information on elevation, soils, vegetation and the spatial assignment of used climate stations in ASCII-format. A pre-processing software (Birkinshaw, 2010; Birkinshaw et al., 2010b) is used to generate the input file formats. This software generates the river

system and geometry and a map of surface roughness. Five climate stations were used and the respective covered area was defined using Thiessen polygons.

4.2.2 Temporal data

SHETRAN accepts time series of precipitation and potential evapotranspiration in different temporal resolutions depending on the study objective and data availability. For calibration and validation, an hourly resolution was used and for long time simulation daily values were applied. Time series data are given in table form were each column contains data of one climate station. Discharge data and suspended sediment loads are required to calibrate and validate the simulated output.

5 APPLYING SHETRAN IN A TROPICAL WEST AFRICAN CATCHMENT (DANO, BURKINA FASO) - CALIBRATION, VALIDATION, UNCERTAINTY ASSESSMENT[1]

Abstract

This study presents the calibration and validation of the physically based spatially distributed hydrological and soil erosion model SHETRAN for the Dano catchment, Burkina Faso. A sensitivity analysis of six model parameters was performed to assess the model response and to reduce the number of parameters for calibration. The hydrological component was calibrated and validated using observed discharge data of two years. Statistical quality measures (R^2, NSE, KGE) ranged from 0.79 to 0.66 during calibration and validation. The calibrated hydrological component was used to feed the erosion modeling. The simulated suspended sediment load (SSL) was compared with turbidity-based measurements of SSL of two years. Achieved quality measures are comparable to other SHETRAN studies. Uncertainties of measured discharge and suspended sediment concentration were determined to assess the propagated uncertainty of SSL. The comparison of measurement uncertainties of discharge and SSL with parameter uncertainty of the corresponding model output showed that simulated discharge and SSL were frequently outside the large measured uncertainty bands. A modified NSE was used to incorporate measurement and parameter uncertainty into the efficiency evaluation of the model. The analyses of simulated erosion sources and spatial patterns showed the importance of river erosion contributing more than 60% to the total simulated sediment loss.

5.1 Introduction

Soil degradation by water-related soil erosion is a major environmental problem threatening food security, income and environmental health especially in tropical and subtropical countries (Bationo et al., 2007; Lal, 2001; Toy et al., 2002; UNEP, 2012). On the one hand, systemic and natural reasons such as unfavorable climatic conditions and the structural instability of soils resulting from low soil organic carbon (SOC) content are responsible for a high erosion risk in these regions (Bationo et al., 2007). On the other hand, socio-economic factors contribute to the problem and are often responsible for the severity of soil erosion. Among those factors, increased pressure on land resources through population growth is highlighted as a major reason for accelerated soil erosion (Morgan, 2005; Okou et al., 2016; Smith et al., 2016; UNEP, 2012).

[1] Published as: Op de Hipt, F., Diekkrüger, B., Steup, G., Yira, Y., Hoffmann, T., Rode, M., 2017. Applying SHETRAN in a Tropical West African Catchment (Dano, Burkina Faso)—Calibration, Validation, Uncertainty Assessment. Water 9, 101. doi:10.3390/w9020101

Soil erosion strongly varies in space and time. Thus measuring soil erosion requires a large personnel and financial effort and despite advances in measurement technology it is often impossible to perform measurements over the required spatial and temporal scales. This especially applies to data scarce regions such as West Africa. To overcome these drawbacks soil erosion models have been frequently used (de Vente et al., 2013; Pandey et al., 2016). Erosion models have also been implemented to predict the effect of land use and climate change on soil erosion and to identify areas where erosion control measures are necessary (Pandey et al., 2016). In general, three types of erosion models are differentiated: Empirical erosion models, conceptual models and physically based erosion models. Physically based erosion models are based on physical principles such as the conservation of mass and momentum (Lal, 1994). After an evaluation of the available erosion models the physically based spatially distributed soil erosion model SHETRAN (Ewen et al., 2000) was chosen to simulate hydrological and soil erosion processes in a tropical West African catchment. The two main reasons for using SHETRAN in this study are its ability to simulate the dominant erosion processes (Birkinshaw and Bathurst, 2006; Wicks and Bathurst, 1996) and the continuity in simulation necessary for the prediction of land use and climate change. The study considers soil erosion by surface runoff.

Physically based models, such as SHETRAN, need to be calibrated and validated. Although parameters of physically based models theoretically do not need calibration, adjustments are necessary to account for an unrealistic representation of environmental properties such as grid size or channel geometry. In the present context, calibration is therefore considered as the adjustment of parameter values to overcome the unrealistic representation of environmental properties. The calibration process requires knowledge on the sensitivity of results to model parameters i) to better assess the model response, ii) to reduce the number of parameters for calibration and iii) to define the parameter uncertainty (Đukić and Radić, 2016; Ewen et al., 2006). Outputs of environmental models are subject to uncertainty that is related to the simplification of the model, the uncertainty of the model parameter and the measurement uncertainty (Beven and Freer, 2001; de Vente et al., 2013; Rompaey and Govers, 2002). Measurement uncertainty refers to the uncertainty of measured data used as input (e.g. precipitation) and to calibrate and validate the model. Studying the uncertainty associated with the modeling output is important since decision making is often based on the output of environmental models (Harmel and Smith, 2007). The present study focuses on the assessment of two sources of uncertainty in environmental modeling, the parameter and the measurement uncertainty. Information on and measurements of the required model parameters are difficult if possible at all and often not available for the study area or on the required spatial or temporal scale. Quantifying parameter uncertainty

is necessary for the interpretation of model outcomes and its application in environmental planning (Ewen et al., 2006; Pandey et al., 2016).

Measured variables, such as water discharge and suspended sediment concentration (SSC), are subject to uncertainties. These uncertainties are propagated if different measurements are combined to calculate variables that are used to calibrate and validate the model (Harmel and Smith, 2007; Navratil et al., 2011; Rasmussen et al., 2009; Rode and Suhr, 2007). For instance, the suspended sediment load (SSL), which is frequently used to validate erosion models, is calculated using the SSC and water discharge. Defining ranges of measured uncertainties is important to contextualize the simulated output.

Studies on soil erosion in West Africa often use USLE-based modelling approaches since data required to run and validate complex, physically based and spatially distributed hydrological soil erosion models are rarely available (see Table 5-1). Empirically based erosion models are relatively easy to use and only a few input data sets are required to run these models. However, their process representation and applicability to complex conditions of land use and climate change is limited (Pandey et al., 2016). Most of the studies listed in Table 5-1 are not comparable with the present study since they use different modeling approaches regarding catchment size, continuity and considered output. Despite numerous studies that applied SHETRAN in different regions and with multiple objectives (see Table 5-2) the model hasn't been tested in the West African environment. The environmental properties of the study catchment such as the low slope angles and the peculiar rainfall pattern may provide a new challenge to SHETRAN. Therefore, the present study may also serve as a model test of the particular environmental conditions found in the study region. Furthermore, the present study can also be considered as an independent check on the ease of use of the model as most of the studies that used SHETRAN before were conducted by members of the team that developed the model. Thus, this study aims to:

1. assess the uncertainty of measured discharge and SSL used to calibrate and validate the hydrological and erosion components of SHETRAN;
2. perform a detailed sensitivity analysis to define parameter ranges and to reduce the number of calibration parameters;
3. use a Latin Hypercube Sampling approach to calibrate the model and to define uncertainty bounds of simulated discharge and SSL;
4. evaluate model performance considering the uncertainty of measured data used to compare the model output and parameter uncertainty.

Table 5-1: Selected studies on soil erosion modelling in West Africa. NSE is the Nash-Sutcliff efficiency.

Study	Model	Location	Spatial/ temporal resolution	Catchment/plot size	Performance	
					Discharge	Sediment yield
Kusimi et al. (2016)	RUSLE	Ghana	30 m/annual	23,188 km²	-	-
Bossa et al. (2014)	SWAT	Benin	90 m, 250 m/daily (continuous)	6,980 km²	0.6 ≤ NSE ≤ 0.9	0.6 ≤ NSE ≤ 0.64
Obeta and Adewumi (2013)	WEPP/ EUROSEM	Nigeria	-	24 m²	-	-
Schmengler (2010)	WEPP	Burkina Faso	-	-	-	-
Schmengler (2010)	WATEM	Burkina Faso	20 m/annual	7.9 - 23.6 km²	-	-
Hiepe (2008)	SWAT	Benin	90 m/daily, weekly (continuous)	586 - 2324 km²	0.81 ≤ NSE ≤ 0.85	0.68 ≤ NSE ≤ 0.7
Visser et al. (2005)	EUROSEM	Burkina Faso	-	1 m², 20 m²	0.7 ≤ R^2 ≤ 0.9	-
Karambiri and Ribolzi (2005)	KINEROS2	Burkina Faso	-	0.014 km²	-	-
Mati and Veihe (2001)	USLE	Ghana	-	900 km²	-	-
Igwe and Mbagwu (1999)	SLEMSA	Nigeria	13 km²	17,500 km²	-	-
Roose (1977)	USLE	West Africa	-	100 – 500 m²	-	-

Table 5-2: Selected studies using SHETRAN for water flow and/or sediment flow simulations

Study	Location	Spatial/ temporal resolution	Catchment/plot size	Performance	
				Discharge	Sediment yield
Present study	Burkina Faso	200m/hourly (continuous)	126 km²	0.65 ≤ NSE ≤ 0.7	0.2 ≤ NSE ≤ 0.4
Đukic and Radic (2016, 2014)	Serbia	25 m/hourly (event)	114 km²	0.8 ≤ R^2 ≤ 0.9	
Zhang (2015)	Portugal	2 km/hourly (event)	705 km²	0.7 ≤ NSE ≤0.8	NSE = 0.56
Mourato et al. (2015)	Portugal	- /daily (continuous)	61 - 834 km²	0.5 ≤ NSE ≤0.7	-
Naseela et al. (2015)	India	- /daily (continuous)	69,425 km²	0.8 ≤ R^2 ≤0.9	-
Birkinshaw (2014)	UK	50 m/hourly (continuous)	1.5 km²	0.8 ≤ NSE ≤ 0.9	-
Tripkovic (2014)	UK	10 m,100 m/hourly (continuous, event)	0.09km², 9.2 km²	0.5 ≤ NSE ≤ 0.9	-
Elliott et al. (2011)	New Zealand	20 m/15 minutes (event)	1.46 - 167 km²	0.6 ≤ NSE ≤ 0.9	-2.1 ≤ NSE ≤ 0.8
Bathurst et al. (2011)	Middle/ South America	50 - 500 m/hourly, daily (continuous)	0.35 - 131 km²	0.8 ≤ NSE ≤ 0.9	-
Birkinshaw et al. (2010a)	Chile	50 m/hourly (continuous)	0.35 km²	0.8 ≤ NSE ≤ 0.9	
de Figueiredo and Bathurst (2007)	Brazil	5 m - 2 km/daily - monthly (continuous)	100 m² - 137 km²	0.3 ≤ R^2 ≤ 0.9	0.34 ≤ R^2 ≤ 0.98

5.2 Materials and Methods

5.2.1 Study area

The investigated Dano catchment in the Ioba province covers an area of 126 km² and is located in the Southwest of Burkina Faso (Figure 5-1). The study area is in a focal catchment of the WASCAL program (West African Science Service Centre on Climate Change and Adapted Land

Use, www.wascal.org). The multidisciplinary program is designed to study the influence of climate and land use / land cover change on human and environmental systems and to enhance their resilience.

Agricultural land use is the most important land use category in the region (Figure 5-1d)). The agricultural area has expanded in recent decades due to a growing demographic pressure indicated by an annual population growth of 3%. It has gradually been intensified accompanied by reduced fallow periods and expansion to marginal land areas with adverse effects on soil fertility (Callo-Concha et al., 2012; 2016; Gleisberg-Gerber, 2012; 2012; Yira et al., 2016). Since 1990 each year on average 2% of the savanna in the study area was converted to agricultural land (Yira et al., 2016). The general appearance of the vegetation in the Sudano savannah is dominated by open forests and wide arborous and shrubby areas. The main staple food crops cultivated in the region are sorghum (Sorghum bicolor), millet (Pennisetum glaucum), maize (Zea mays), cowpeas (Vigna unguiculata) and groundnut (Arachidis hypogaea). Cotton (Gossypium hirsutum) is the most important cash crop. During the rainy season between 40% and 70% of the soil is covered by vegetation.

The catchment is dominated by a flat and slightly undulating landscape characterized by low slope gradients (average and maximum gradients are 3.1% and 38%, respectively, Figure 5-1b)) and an elevation ranging from 236 to 565 m above sea level (masl). The annual mean temperature is 28.6°C and annual precipitation ranges from 800 to 1200 mm/a for the period 1951-2005 (Schmengler and Vlek, 2015). The rainfall pattern is uni-modal and characterized by a distinct rainy season from May to October and a dry season from November to April. 80% of the rain falls between July and September with high rainfall intensities. As an example from the Dano catchment, 60 mm/h were measured as maximum in 2014. The flow regime is ephemeral and the channel geometry is divers ranging from strongly incised (3 – 4m) clearly defined channels to broader inland valleys. Information on the ranges of measured parameters is given in Table 5-3.

Most of the soils (73%) are plinthosols according to the World Reference Base for soil resources (WRB) (IUSS Working Group, 2006) characterized by a high content of coarse particles and a plinthitic subsurface layer in the first meter of the profile. Other soils that were formed in the region are gleysols, cambisols, lixisols, leptosols and stagnosols (Figure 5-1e)).

5.2.2 Data sources

In order to calibrate and validate SHETRAN, multiple data sets are required (Table 5-4). Existing data were complemented by a measurement network consisting of 5 automatic climate stations and pluviometers (tipping bucket type) and one discharge and turbidity station. Additionally,

physical and chemical analyses of soil samples were done to retrieve necessary soil parameters for the erosion model (Table 5-4).

Table 5-3: Range of the measured parameters for the years 2014 and 2015. SSC refers to suspended sediment concentration and SSL to suspended sediment load.

Parameter	**Station number**	**Measured range**	
		2014	**2015**
Rainfall (mm/h)	1	0 – 25	0 – 48.6
	2	0 – 40.4	0 – 51.5
	3	0 – 60.1	0 – 46
	4	0 – 42.8	0 – 37.7
	5	0 – 43.1	0 – 35.2
Average daily discharge (m^3/s)		0 – 16.8	0 – 26.2
Average daily SSC (kg/m^3)		0.01 – 0.3	0.009 – 0.47
Average daily SSL (kg/s)		0.001 – 1.9	0.001 – 4.7

Table 5-4: Applied datasets and required inputs for SHETRAN

Data set	**Resolution/time scale**	**Source**	**Required parameters**
Topography	90 m	SRTM (Jarvis et al., 2008)	
Soil	1:25 000	Soil survey	Soil hydrological parameters (α, n[1)], K_{sat}[2)], θ_{sat}[3)], θ_{res}[4)])texture etc.
Land use map	5 to 250 m	Forkuor (2014)	Land use type distribution
Land use characteristic		Literature	LAI[5)], Strickler coefficient, ETa/ETp ratio[6)]
Climate	Hourly, Daily	Instrumentation WASCAL	Rainfall, temperature, humidity, solar radiation, wind speed
Discharge	Hourly	Instrumentation WASCAL	Discharge
Erosion	Hourly, Event	Instrumentation WASCAL	Suspended sediment load, soil erosion rate

[1)] α and n are van Genuchten empirical parameters, [2)] K_{sat} refers to the saturated hydraulic conductivity, [3)] θ_{sat} to the saturated water content, [4)] θ_{res} to the residual water content, [5)] LAI to the leaf area index and [6)] ETp/ETa ratio to the ratio of potential evapotranspiration to actual evapotranspiration.

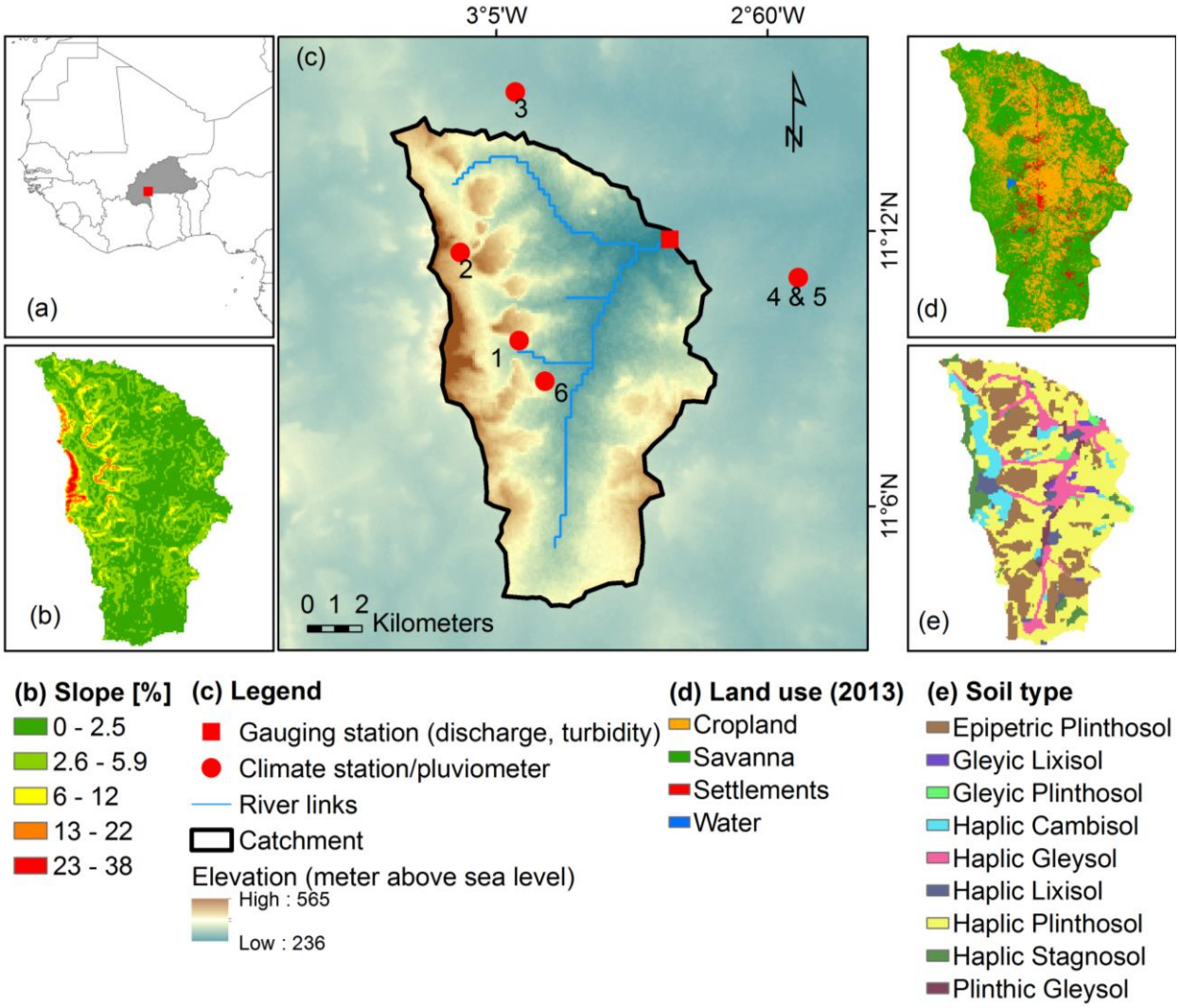

Figure 5-1: Location map of the Dano catchment: (**a**) location of the catchment and Burkina Faso in West Africa; (**b**) slope of the catchment; (**c**) model catchment; (**d**) land use map (Forkuor, 2014); (**e**) soil map (data base: soil survey done by Ozias Hounkpatin, University of Bonn, Institute of Crop Science and Resource Conservation, Soil Science and Soil Ecology).

5.2.3 Model description

Modeling of hydrological and erosion processes was performed using the physically based, spatially distributed and raster-based model SHETRAN (Ewen et al., 2000; Wicks and Bathurst, 1996). SHETRAN is based on SHE (Système Hydrologique Europeen) which was jointly developed by the British Institute of Hydrology, the Danish Hydraulic Institute and the French consulting company SOGREAH (Abbott et al., 1986). During the last thirty years SHETRAN has been continuously improved and equipped with new components that include e.g. the sediment com-

ponent (Wicks, 1988; Wicks and Bathurst, 1996) and a fully 3D subsurface water flow component (Parkin, 1996). A summary of SHETRAN applications with various objectives and in different regions is given in Table 5-2.

Detailed information about the model is given in Bathurst [86]. A short overview of the most important hydrological process descriptions of the model is summarized in the following list:

- Fully 3D subsurface flow simulation based on Richards´ equation.
- Infiltration is calculated using Richards´ equation.
- Overland and channel flow is calculated using the diffusive wave approximations of the full Saint-Venant equation.
- Potential evapotranspiration (ETp): Potential plant transpiration, evaporation from intercepting surfaces and from bare soil as well as water bodies was calculated externally based on the Penman-Monteith equation (Monteith, 1975) and added as input into SHETRAN.
- Actual evapotranspiration (ETa) is estimated based on the approach introduced by Feddes et al. (1976) where the ratio ETa/ETp is a function of soil moisture tension. The ratio ETa/ETp at field capacity is the input parameter and the reduction of ETa with decreasing soil moisture tension is calculated based on this parameter.
- Interception is calculated based on the approach by Rutter et al. (1975, 1972) who relates interception to the leaf area index, the vegetation cover and the maximum depth of water on leaves.

The parameterization and calibration of land use and soil properties was done based on data obtained from literature and measurements (see Table 5-4 and Table 5-5). The parameters (θ_{sat}, θ_{res}, α, n) used to describe the soil water retention curve after van Genuchten (1980) were determined from soil texture and organic matter content following Rawls and Brakensiek (1985). Measured saturated hydraulic conductivity (K_{sat}) was used for the top soil horizon. For the remaining horizons K_{sat} was calculated using soil texture and organic matter content following Brakensiek and Rawls (1994).

SHETRAN requires different types of input data. Spatially distributed data, including digital elevation model (DEM), the soil and land use map, were used in a raster format with a grid resolution of 200 m x 200 m. The applied resolution is relatively coarse compared with other applications of SHETRAN with resolutions typically below 100 m (Table 5-2). Nevertheless, the topography of the study area is characterized by long straight slopes which are well represented in

this resolution. Zhang (2015) applied a resolution of 2 km to a larger catchment (705 km²) and compared it with resolutions of 0.5 and 1 km. The performance measure using the Nash-Sutcliff-Efficiency (NSE) decreased by 3.7% with decreasing resolution (from 1 to 2km) as a result of information loss as land use and soil type maps become coarser.

Precipitation and potential evapotranspiration (ETp) are given as time series over two years for each of the five stations considered in the modeled catchment. The area that is represented by each station is determined by Thiessen polygons. A pre-processing software uses the DEM to determine the river geometry and produces the input files (Birkinshaw, 2010). The temporal resolution of 1 hour used here is the standard timestep of SHETRAN and commonly used in other studies (see Table 5-2). The precipitation input has an hourly timestep.

A short summary of erosion processes simulated by SHETRAN is given below:

Soil detachment is accounted for by three separate equations describing detachment by raindrop/leaf drip (Eq. 5-1) (Wicks et al., 1988), by overland flow (Eq. 5-2) (Ariathurai and Arulanandan, 1978) and by channel flow (Eq. 5-3) (Osman and Thorne, 1988):

$$D_r = k_r F_w (1 - C_g - C_r)(M_r + M_d) \qquad \text{Eq. 5-1}$$

where D_r is the rate of soil detachment [kg/m²/s], F_w [-] accounts for the protection against drop detachment by surface water, k_r is the raindrop impact erodibility coefficient [J^{-1}], C_g is the proportion of ground covered by near ground vegetation [%], C_r is the rock cover [-], M_r/M_d is the momentum squared of raindrops/leaf drips reaching the ground per unit time and area [kg²/s³],

$$D_q = \begin{cases} k_f (1 - C_r) \left[\frac{\tau}{\tau_{ec}} - 1 \right] & \text{if } \tau > \tau_{ec} \\ 0 & \text{otherwise} \end{cases} \qquad \text{Eq. 5-2}$$

where D_q is the rate of soil detachment per unit area [kg/m²/s], k_f is the overland flow erodibility coefficient [kg/m²/s], C_r is the proportion of ground shielded by rock cover [-], τ is the shear stress exerted by overland flow [N/m²], τ_{ec} is the critical shear stress for the initiation of motion [N/m²],

$$E_b = \begin{cases} BKB \left[\frac{\tau_b}{\tau_{bc}} - 1 \right] & \text{if } \tau_b > \tau_{bc} \\ 0 & \text{otherwise} \end{cases} \qquad \text{Eq. 5-3}$$

where E_b is the detachment rate of bank material per unit area [kg/m²/s], BKB is the bank erodibility coefficient [kg/m²/s], τ_{bc} is the critical shear stress for the initiation of motion of bank material [N/m²] and τ_b is the shear stress acting on the bank [N/m²].

Sediment is transported based on the transport capacity of overland (Eq. 5-4) (Engelund and Hansen, 1967) and channel flow (Eq. 5-5) (Ackers and White, 1973):

$$G_{tot}=0.635\sqrt{\frac{\tau}{p}}\,lD_{50}\delta\left[1-\frac{1}{a\delta}\ln(1+a\delta)\right] \qquad \text{Eq. 5-4}$$

where G_{tot} is the transport capacity rate for overland flow [m³/s], τ is the shear stress [N/m²], p is the water density [kg/m³], l is the width of flow [m], Q is the water discharge [m³/s], D_{50} is the median sediment diameter, δ and a are parameters,

$$G_i=Q\frac{D_i}{H}\left(\frac{U}{u_*}\right)^{n_i}G_{gr,i} \qquad \text{Eq. 5-5}$$

where G_i is the transport capacity rate of particle size in group i [m³/s], D_i is the particle diameter in size group i [m], H is the water flow depth [m], U is the mean water flow velocity [m/s], u_* is the shear velocity [m/s], $G_{gr,i}$ is the dimensionless sediment transport rate for sediment size group i.

Further details are given in Morgan and Nearing (2011) and Wicks (1988).

5.2.4 Model sensitivity, calibration and validation

Several parameters of SHETRAN need to be calibrated by comparing simulated and observed variables. Prior to the calibration parameters to which the model output is most sensitive and the corresponding initial values were identified based on previous studies that used SHETRAN and based on sensitivity analyses. The sensitivity analyses were done based on the "one factor at a time" (OFAT) method using Eq. 5-6 (de Roo, 1993):

$$SI_{90}=\frac{|O_{90}-O_{-90}|}{O_0} \qquad \text{Eq. 5-6}$$

where SI_{90} is the sensitivity index, O_{90} and O_{-90} the model output resulting from a parameter value increased or decreased by 90% and O_0 the model output from the base run.

A list of parameters to which the model output responds sensitively and the corresponding calibration ranges used in this study is given in Table 5-5. The parameter range of k_f is quite low compared with what has been indicated in literature. However, as this parameter is considered to be a calibration parameter (Wicks, 1988), we assume that the range is representative for the soil properties in the study area.

The Latin Hypercube Sampling (LHS) (McKay et al., 1979) was used to generate 300 parameter sets within the defined value ranges. This is considered as a reasonable compromise between

the necessary model executions which is dependent on the number of parameters used and the run time. The hydrological component of SHETRAN was calibrated based on the observed hydrograph in 2014. The soil erosion component was calibrated based on the observed SSL in 2014. The model performance was statistically evaluated by the coefficient of determination (R^2), the Nash-Sutcliff efficiency (NSE) (Nash and Sutcliffe, 1970) and the Kling-Gupta efficiency (KGE) (Gupta et al., 2009; Kling et al., 2012). The model was validated using data from the year 2015.

Table 5-5: Soil, land use and erosion parameters in SHETRAN

Parameter	Description	Unit	Parameter range	Source
		Hydrology		
ETa/ETp at field capacity (varies with land use type)	Ratio of actual evapotranspiration to potential evapotranspiration at field capacity	-	0.01 – 1.99	Shuttleworth (1993)
KSTR (varies with land use type)	Strickler roughness coefficient	$m^{1/3}$ s^{-1}	0.3 – 9.9	Mohamoud (1992), Shen and Julien (1993)
		Soil erosion		
k_f (soil invariant)	Overland flow soil erodibility	kg m^{-2} s^{-1}	2.54 x 10^{-11} –4.68 x 10^{-10}	Calibration
k_r (varies with texture)	Raindrop soil erodibility coefficient	J^{-1}	0.19 – 7.9	Adams and Elliott (2006), Birkinshaw et al. (2010a), de Figueiredo and Bathurst (2007), Elliott et al. (2011), Lukey et al. (2000, 1995), Norouzi Banis et al. (2004), Wicks and Bathurst (1996)
BKB (soil invariant)	Channel bank erodibility coefficient	kg m^{-2} s^{-1}	1 x 10^{-6} – 3 x 10^{-6}	Calibration
DLSMAX	Threshold depth of loose sediment	mm	1 x 10^{-6} – 9.9 x 10^{-6}	Calibration

5.2.5 Uncertainty analyses

5.2.5.1 Measurement uncertainty

A power regression model was used to describe the relation between measured water level and water discharge. The relation between measured suspended sediment concentration (SSC) and turbidity was defined by a linear regression model. Polynomial and power regression equations of confidence intervals calculated by Eq. 5-7 (Helsel and Hirsch, 2002) were used to express the measured uncertainty of both regression models.

$$\Delta X_i = Y_i \pm t_\alpha \, SE \sqrt{\frac{1}{DF} + \frac{(X_i - X_m)^2}{SS_{xx}}} \qquad \text{Eq. 5-7}$$

where ΔX_i is the confidence interval of the predictor, Y_i is the response variable, t_α is the t-value at $\alpha = 0.05$ significance level, SE is the standard error, DF are the degrees of freedom, X_m is the mean of X and SS_{xx} is the sum of squared differences.

The uncertainty of water discharge and the combined uncertainty of SSL were compared with the simulated discharge and SSL through visual inspection and the calculation of R- and P-factors. The P-factor gives the proportion of the variable in question which is within the corresponding uncertainty bands in percent. The R-factor is defined as the mean width of the uncertainty band divided by the standard deviation of the variable in question (Abbaspour et al., 2009).

Uncertainties related to field measurements of discharge and SSC sampling as well as laboratory work were not explicitly accounted for in this study.

5.2.5.2 Parameter uncertainty

The ten best simulations were chosen out of the 300 parameter sets based on the sum of NSE, R^2 and KGE calculated separately for discharge and SSL. The ten best hydrological simulations were combined with the ten best sediment simulations to define the parameter uncertainty bounds. Among these, the parameter set with the highest sum of performance measures and reasonable parameter values is considered to give the best representation of measured discharge and SSL.

5.2.5.3 Uncertainty based modification of the NSE

Based on the work by Harmel and Smith (2007) and Harmel et al. (2010) a modified error term e_i ($O_i - P_i$) was incorporated into the traditional calculation of the NSE that considers the uncertainty of both measured and parameter uncertainty at each observation. A correction factor (CF_i) is calculated based on the degree of overlap of the assumed distributions of the observed and predicted values (see Eq. 5-8). In the present study measured and predicted values are assumed to be normally distributed.

CF_i ranges from 0 (total overlap) to 1 (no overlap):

$$CF_i = 1 - \{[prob(o_i < P_{imax}) - prob(o_i < P_{imin})] \times [prob(p_i < O_{imax}) - prob(p_i < O_{imin})]\} \qquad \text{Eq. 5-8}$$

where $prob(o_i < P_{imax})$ and $prob(o_i < P_{imin})$ are the probability distributions of the observed value o_i limited by the maximum (P_{imax}) and minimum (P_{imin}) predicted value and $prob(p_i < O_{imax})$ and

prob($p_i < O_{imin}$) are the probability distributions of the predicted value p_i limited by the maximum (O_{imax}) and minimum (O_{imin}) observed 95%-uncertainty bounds.

The error term e_i ($O_i - P_i$) is then multiplied by CF_i and substituted into the NSE to get the modified NSE_m (Eq. 5-9).

$$NSE_m = 1 - \left(\frac{\sum_{t=1}^{T} CF_i (O_i - P_i)^2}{\sum_{t=1}^{T} (O_i - \bar{O})} \right) \qquad \text{Eq. 5-9}$$

5.3 Results and Discussion

5.3.1 Measurement uncertainty

Figure 5-2a and Figure 5-2b show the stage-discharge regression line and the corresponding uncertainty ranges of the years 2014 and 2015. Two different rating curves were used in order to consider the changes of channel morphology and the human intervention in the channel system. However, data collection in the focus area is challenging and the limited number of observations is also reflected in the uncertainty bands. Uncertainties increase with increasing water level and discharge due to the chosen power regression equation and the sample properties. Overbank flow was observed following intense rainfall events but could not be measured due to inaccessibility. Therefore, extrapolation beyond the measured range was done despite the increasing uncertainties during peak flows.

Figure 5-2c shows the linear regression line and the uncertainty band of suspended sediment concentration (SSC) and turbidity. The uncertainty ranges are almost parallel due to the linear regression equation. As a result from the error propagation the combined uncertainty of SSL is quite large.

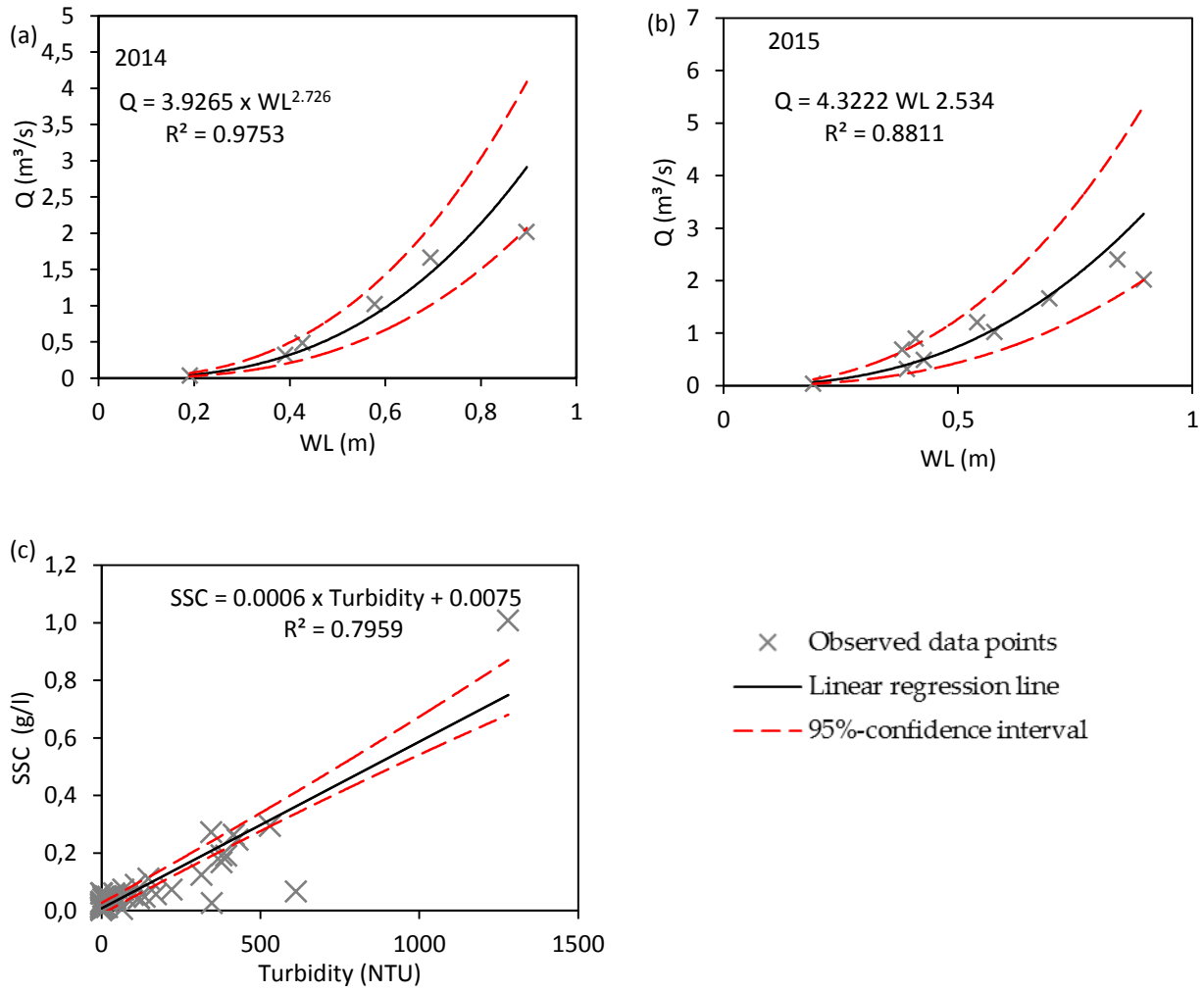

Figure 5-2: Scatter plots of recorded water level and measured water discharge for **a)** 2014 (n = 6) and **b)** 2015 (n = 10) and of **c)** the recorded turbidity and measured suspended sediment concentration (SSC) (n = 57).

5.3.2 Model sensitivity

Figure 5-3 shows the model sensitivity to the investigated soil, land use and erosion parameters (Table 5-5) following the OFAT method. Total and maximum water discharge as well as suspended sediment load is used for comparison.

Changing parameter values of the ratio ETa/ETp (Figure 5-3a) specified for each land use strongly influence total runoff which is indicated by a relatively high SI_{90} of 1.8. As this parameter directly affects the actual evapotranspiration (ETa), an increase of e.g. 90% leads to 60% less surface runoff due to higher ETa.

The roughness coefficient KSTR (Figure 5-3b) is given for each land use type and controls the surface roughness. Larger KSTR results in faster surface runoff and therefore especially influences the maximum runoff. However, interactions between surface roughness, infiltration and evapotranspiration also lead to a change of total catchment runoff. The total runoff responds less sensitively (SI_{90} = 0.4). An increase of 90% results in 6% higher total runoff but increases the maximum runoff by 52%. The higher sensitivity of the maximum discharge is also shown by SI_{90max} of 1.2.

Figure 5-3c and Figure 5-3d show the effect of the changing erodibility coefficients k_f and k_r on the sediment yield respectively. An increase leads to higher erosion in both cases. However, the results are more sensitive to k_r in comparison with k_f as indicated by the higher SI_{90}. An increase of k_r by 90% leads to 10% higher total sediment yield while an increase of k_f by 90% results in only 2.8% higher sediment yield.

Figure 5-3e shows the model's response to a changing river bank erodibility coefficient (BKB). The SI_{90} is the highest in comparison with the other parameter indicating the importance of bank erosion for the catchment sediment yield. An increase of 90% leads to a 40% higher sediment yield.

DLSMAX can be considered as maximum sediment storage depth above which the soil is protected against erosion (Zhang, 2015). In other words, the soil material that can't be transported due to an insufficient transport capacity is considered to be available and stored as loose sediment till it reaches DLSMAX. Figure 5-3f shows that a 90% increase of DLSMAX leads to a 14.5% higher SSL since more soil material can be stored as available sediment.

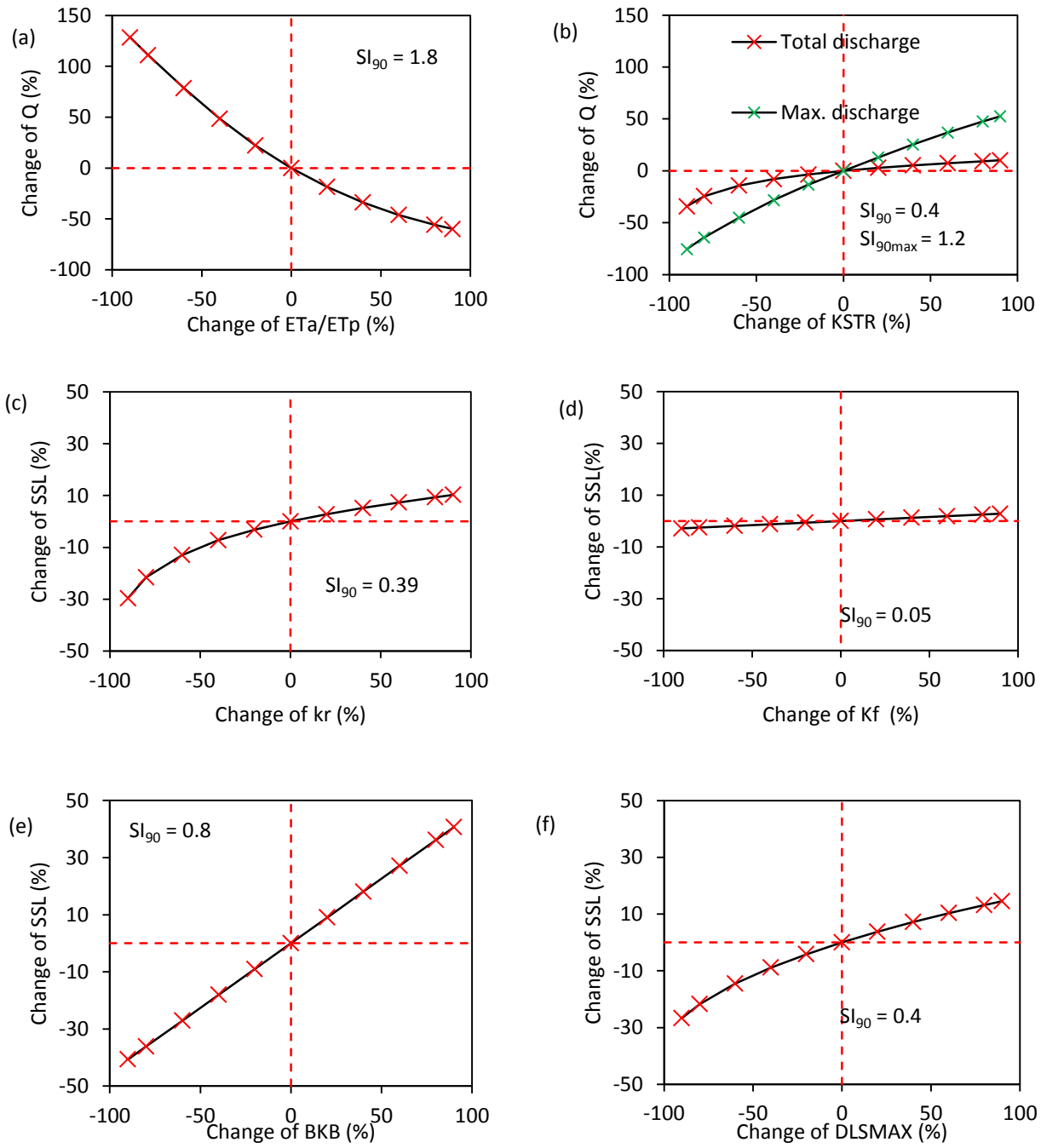

Figure 5-3: Scatter plots showing the sensitivity of water discharge Q to the ratio of actual to potential evapotranspiration (ETa/ETp) **(a)** and surface roughness (KSTR) **(b)** and the sensitivity of the catchment suspended sediment load (SSL) to the raindrop erodibility coefficient (k_r) **(c)**, the overland flow erodibility (k_f) **(d)**, the bank erodibility (BKB) (e) and the depth of loose sediment (DLSMAX) **(f)**. Red dashed lines indicate the base run used for comparison. SI_{90max} indicates the SI_{90} for the maximum discharge.

5.3.3 Calibration and validation

5.3.3.1 Hydrological modelling

Two parameters (ETa/ETp, KSTR) of SHETRAN to which the results are sensitive were used to calibrate the hydrological component. Although other parameters such as K_{sat} or soil hydrological parameters are reported to be important, a choice was made based on previous studies (Bathurst et al., 2011, 2004; Birkinshaw et al., 2010a; Mourato et al., 2015; Parkin et al., 1996) in order to limit run time. Based on the sum of R^2, KGE and NSE, several parameter sets gave satisfactory to good quality measures according to the equifinality concept introduced by Beven and Freer (2001). The hydrograph of the simulation having the highest sum of the performance indices and a reasonable parameter setting is shown in Figure 5-4. For the calibration period the parameter uncertainty is based on the ten best parameter sets.

The calculated NSE for the best hydrological simulation is 0.7 and 0.66, the KGE 0.79 and 0.76 and the R^2 0.72 and 0.7 for calibration (2014) and validation (2015) respectively. The model performance is good and in the range of other studies that used SHETRAN (see Table 5-2). Among these studies R^2 and NSE values above 0.5 are frequently reported.

Measurement uncertainty, as presented by the 95%-confidence interval, is large for discharge especially during peak flows. The maximum uncertainty ranges from 17.3 to 40.3 m^3/s. However, P-factors show that the model is often not able to simulate discharge within the measured uncertainty bounds even if the bounds are wide (Figure 5-4). This is supported by the small difference between NSE and NSE_m. A higher NSE_m would signify a greater overlap between the simulated and observed distributions. However, overlapping areas are observed only during peak flows and that does not change the NSE_m substantially. Figure 5-4c shows in more detail that the rising base flow during the rainy season is not well represented by the model. The simulated low flow is frequently below the measured uncertainty band. During base flow conditions even the parameter uncertainty range does not overlap with the measured uncertainty range. This is not surprising since low flow was not in the focus of this study and therefore parameters that control low flow were not considered in the calibration process. The comparison of the hyetographs from all climate stations suggests that overestimated peaks during the rainy season are attributed to the spatial assignment of climate stations which was done using Thiessen polygons. As the polygon sizes are unevenly distributed (range from 0.3 to 82 km^2) this method may not be appropriate to account for localized precipitation events. Hence, local precipitation events may result in errors if this method is applied. Other interpolation methods as inverse distance are not implemented in the model code.

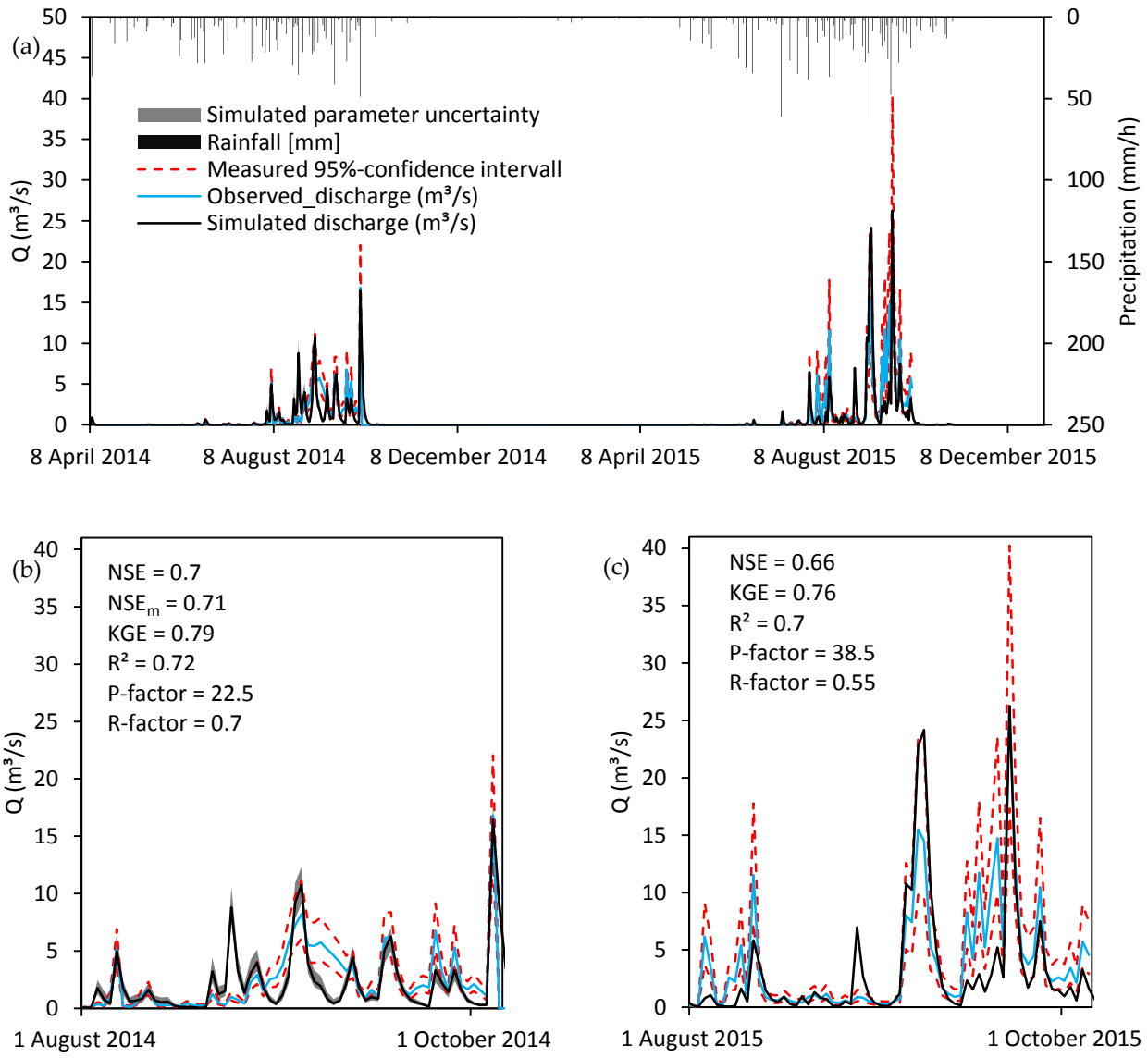

Figure 5-4: Observed and simulated daily discharge (Q) over the calibration and validation period **(a)** and over a selected period for the calibration **(b)** and validation **(c)** period. The measured 95%-confidence interval is given for both periods, simulated parameter uncertainty only for the calibration year.

5.3.3.2 Erosion modelling

The total simulated suspended sediment load responds sensitively to four model parameters (k_f, k_r, BKB and DLSMAX) that were included in the LHS.

Figure 5-5 shows the simulated SSL having the highest sum of the performance indices for the calibration and validation period. The NSE is 0.4 and 0.2, the KGE 0.3 and 0.01 and the R^2 is

0.47 and 0.37 for calibration and validation respectively. The NSE is in the range of other SHETRAN studies (see Table 5-2). However, few studies used the erosion component and if so performance indices are sometimes not reported. Other physically based erosion models may perform worse or better ($-0.75 \leq NSE \leq 0.94$) as shown by model comparison studies of de Vente et al. (2013) and Pandey et al. (2016) but a comparison with other models is difficult due to differences regarding the model setup (spatial/temporal scale) and the chosen output variable (de Vente et al., 2013). Given the various sources of measurement uncertainty a NSE of larger than 0.7 can not be expected (de Vente et al., 2013). Nevertheless, it has to be noted that especially for the validation period, quality measures are not satisfactory. This may be related to the large differences between 2014 and 2015 regarding the observed SSL. The measured annual erosion rate in 2015 is almost three times higher than in 2014 whereas the simulated erosion rate is only 1.6 times higher in 2015. The simulated and measured annual sediment yield is 700 t and 970 t for 2014 and 1045 t and 2725 t for 2015. Reasons for the differences between simulated and observed SSL may be the setting of the erosion parameters as some values are markedly different from what has been found in literature. However, an adjustment of erosion parameters to different conditions as discussed by Bathurst (2010) is not possible during continuous simulations. Another reason may be the hourly timestep of the precipitation input which may be too long since erosion often occurs on sub-hourly periods.

Parameter and measurement uncertainty are shown in Figure 5-5b. The assessment of the measured uncertainties of discharge and SSC results in relatively large combined uncertainty bands of SSL especially during peak flow periods. Possible measurement errors may be attributed to the discharge rating curve that does not cover the full range of recorded water levels and the calibration of the turbidity sensor that is also subject to uncertainty as shown in section 5.3.1 (Minella et al., 2008; Rode and Suhr, 2007). The large measured uncertainty is also reflected in higher R-factors and results in higher P-factors since simulated SSL and its uncertainty band are more often within the large measured uncertainty. This is also supported by the NSE_m which is higher than the classical version.

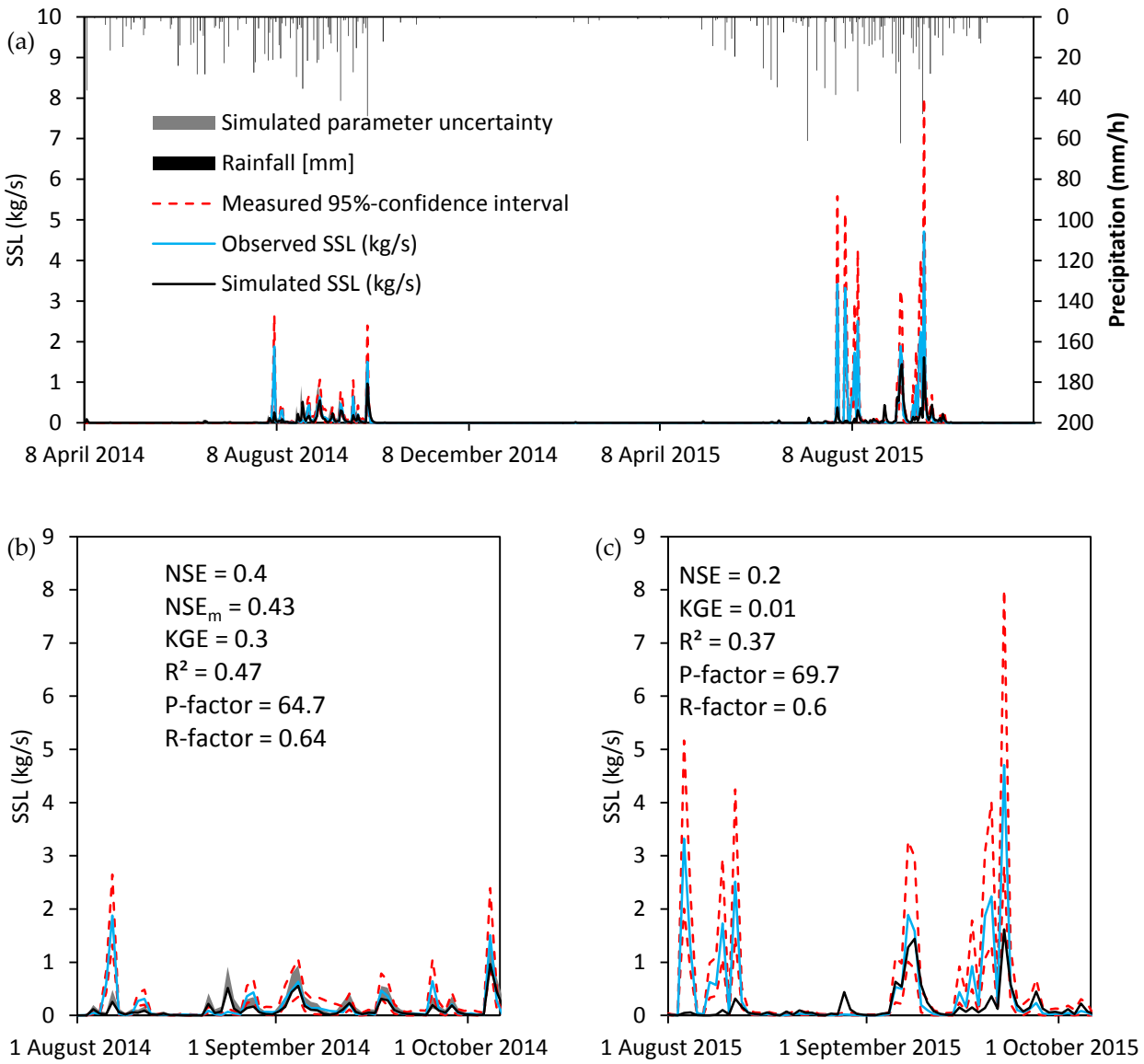

Figure 5-5: Observed and simulated daily suspended sediment load (SSL) over the calibration and validation period **(a)** and a selected period for the calibration **(b)** and validation **(c)** period. Measurement uncertainty is given for both periods, parameter uncertainty only for the calibration.

Simulated erosion sources

Table 5-6 shows the relative contribution and the sediment yield of each source as simulated by SHETRAN. The interpretation of the results is associated with large uncertainties since results from fingerprinting analyses necessary to validate the simulated results are not yet available. Furthermore, knowledge on the erosion parameters is limited but the model output is strongly

controlled by the parameterization. Among the sediment sources listed in Table 5-6 water contributes up to 1% to the sediment yield of the catchment. As the erosion parameters in SHETRAN are linked to the soil types an additional soil type would have been necessary to account for the conditions of areas covered by water. The number of soil types is limited in SHETRAN. Therefore, an additional soil type could not be implemented.

The simulated range of river erosion (including bank erosion and incision) dominates contributions from hillslope erosion. Between 68% and 89% of the simulated sediment loss are supplied from river erosion whereas 11% to 32% is eroded on the hillslopes. Simulated erosion rates for the calibration period range from 0.008 to 0.081 t/ha/year for the entire catchment. The simulated values are low but in the range of the measured SSL (0.04 – 0.13 t/ha for 2014). However, the parameterization of a model to well simulate very small erosion rates is also challenging as discussed by Nearing (1998). Hillslope erosion rates derived from ^{137}Cs measurement on hillslopes in the same area (Schmengler, 2010) are three orders of magnitude higher compared with the simulated hillslope erosion rates (0.005 – 0.022 t/ha). In the study by Roose (1977) soil erosion rates measured under different experimental conditions in West Africa range from 0.01 to 90 t/ha/year. Walling et al. (2001) assessed the sediment budget of a catchment in Zambia and measured 0.2 t/ha/year. The same study assessed the channel bank and gully contribution by using the fingerprint method to be in the order of 17%. Data collected in 2015 from plot measurements close to the study site indicate a range between 0.05 and 0.6 t/ha/year. Based on the comparison with measured ranges, hillslope erosion seems to be underestimated whereas the contribution of river bank and bed erosion is overestimated by the model. Knowledge on the relative contribution of hillslopes and rivers to the total catchment erosion is limited. The link between the sediment mobilization in the source area and the sediment yield measured at the outlet is difficult to study due to a lack of knowledge regarding the magnitude and residence time of sediment in storage (Hoffmann, 2015; Walling et al., 2001). Additionally, information on the erodibility parameters of SHETRAN is often obtained from previous studies and has rarely been validated against measured plot data. Hence, setting the parameter range in order to reflect the catchment conditions is difficult and mainly based on the modelers' perception of the main erosion processes taking place in the catchment.

Table 5-6: Relative contribution and specific sediment yield of the different erosion sources as simulated by the best SHETRAN run for the year 2014 (calibration) and 2015 (validation). Min. and max. indicate the ranges of the ten considered simulations.

Erosion source		Relative contribution [%]		Specific sediment yield [t/ha/year]	
		2014 (Min – Max)	2015	2014 (Min – Max)	2015
Catchment			100	0.056 (0.008 – 0.081)	0.08
Hillslope		32 (11 – 32)	27	0.018 (0.005 – 0.022)	0.023
	Cropland	15 (3 – 15)	12	0.023 (0.003 – 0.025)	0.03
	Settlement	14 (2 – 14)	11	0.155 (0.015 – 0.155)	0.004
	Savanna	2 (2 – 12)	3	0.002 (0.002 – 0.016)	0.181
	Water	1 (0 – 1)	1	0.14 (0.012 – 0.14)	0.196
River		68 (68 – 89)	73	0.038 (0.034 – 0.065)[1)]	0.063

[1)] River bank and bed erosion rates are calculated in reference to the total catchment size.

Catchment distributed erosion

Figure 5-6 shows the spatial pattern of soil erosion and deposition on hillslopes as simulated by the best SHETRAN simulation for the calibration period. Erosion ranges from 1.6 to almost 0 t/ha/year and deposition from 0 to 1.8 t/ha/year. Regarding erosion 55% of the grid cells are within the range of -0.03 to < 0 t/ha/year. However, given the spatial heterogeneity of the controlling factors that are considered (slope, land use, soil properties, hydrological conditions) and the complex model approach it is difficult to clearly identify erosion hot spots and to explicitly attribute these hot spots to a single factor or reason. One example in this context is the hilly area in the western part of the catchment: We assumed the highest erosion rates would be found here due to the steep slopes and the partly practised agriculture but simulated erosion is not especially high compared with other parts of the catchment. The small erosion rates are attributed to the low simulated surface runoff due to a small drainage area of these cells. Hence, rain drop detachment may be high but surface runoff is insufficient to transport the available sediment. High erosion rates simulated close to the river channel are a result of higher surface runoff simulated in cells close to the valley bottoms as a result of larger drainage areas and overbank flow. Field observations confirm overbank flow during large events but the areas are rather characterized by deposition of fine material and not necessarily by erosion as simulated. To get a more realistic representation of the vegetation close to the rivers (gallery forests), a fifth land use type with the same properties as savannah vegetation was introduced around the river links. Though this

led to lower erosion rates, it negatively affected the performance of the simulated hydrograph and was therefore discarded.

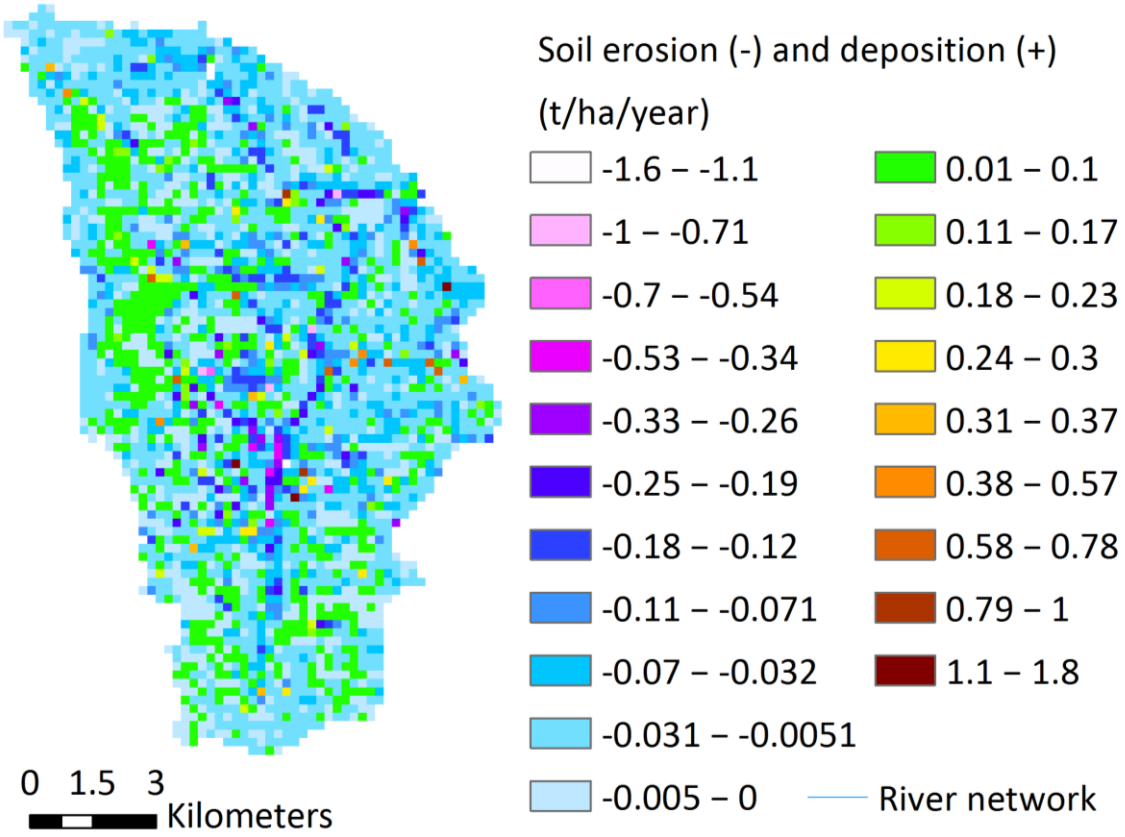

Figure 5-6: Annual soil erosion (-) and deposition rate (+) on hillslopes as simulated for the calibration period.

5.4 Conclusions

This study applied the hydrological soil erosion model SHETRAN in a tropical West African catchment and investigates measurement and parameter uncertainty. From the investigations we draw the following conclusions:

1. The performed uncertainty analyses of observed discharge reveals large uncertainty bands especially during peak flows (max. uncertainty from 17.3 (-34.1% of measured value) to 40.3 m³/s (+53.1% of measured value)) which was attributed on the one hand to the power law chosen for the rating curves and on the other hand to the sample properties. As a result of the intrinsic measurement errors and the error propagation the combined uncertainty of SSL is quite large (max. uncertainty from 2.8 to 8 kg/s).

2. Two hydrological parameters were tested regarding the sensitivity of the model response. Whereas the ratio ETa/ETp affects total catchment runoff, the roughness coefficient KSTR has greater effect on the maximum runoff. Among the four tested erosion related model parameters the river bank erodibility coefficient BKR had the largest impact on the model response. Parameter ranges of the overland flow erodibility coefficient k_f and DLSMAX were quite low which was explained by the higher soil erodibility of the soils found in the study area.

3. The performance indices of simulated discharge are good (≥ 0.66) and comparable with other studies that used SHETRAN. Among these studies R^2 and NSE values above 0.5 are frequently reported. However, SHETRAN often underestimates base flow which could be explained by the missing calibration of hydrological subsurface parameters. Some peaks were not well represented due to the differences between real and model spatial representation of rainfall. The performance indices of the simulated SSL are comparable with the few studies that used SHETRAN to simulate soil erosion and that indicated model performance. As the calculation of SSC is based on the relation between turbidity and sediment concentration, input of organic material into the river following the burning of crop residues and grassland may lead to high turbidity readings although the measured weight is low (Gippel, 1989, 1995). Thus, the mismatch between observed and simulated SSL at the start of the rainy season may also be explained by the method used to obtain the sedigraph.

4. The combined uncertainty assessment of measured and simulated discharge showed that SHETRAN frequently underestimates base flow despite large measured uncertainty bounds. The modified NSE_m used to include both uncertainties in the quality assessment showed that the overlapping areas of distributions are rarely observed and small. As a result of the large uncertainty of observed SSL the model uncertainty is almost always within the range of measured uncertainty bounds. This is also reflected by a slightly higher NSE_m in comparison with the traditional NSE. The erosion sources simulated by SHETRAN do not correspond with the sources reported in the literature. The contribution of river bank and bed erosion may be too high and the erosion on hillslopes too low. However, knowledge on this point is limited. Results from fingerprint analyses may help to validate the simulated output.

We showed that the physically based spatially distributed erosion model SHETRAN offers chances and challenges. SHETRAN provides a better representation of erosion processes, especially in environments that are characterized by low frequency and high magnitude erosion

events, than low-complexity models that focuses on mean annual erosion rates (such as the USLE). So far, the application to larger river catchments is limited due to the incomplete knowledge on the model parameters and the limited availability of model input data at large scales and with appropriate resolution. Yet, the modeling results obtained here help to improve the parameterization of large-scale, low-complexity erosion models and to improve the representation of the strong temporal variability of erosion rates in the Sudano savanna zone of Africa. Consequently, modeling erosion on small scales is needed to optimize parameter estimation and process understanding which in turn helps to improve large scale modeling (2016). Erosion modeling with SHETRAN should therefore focus on better and broader knowledge on the erosion parameters, including the definition of parameter ranges for different environmental conditions. The application of SHETRAN to erosion plots may be an opportunity to better assess these parameter values.

6 MODELING THE IMPACT OF CLIMATE CHANGE ON WATER RESOURCES AND SOIL EROSION IN A TROPICAL CATCHMENT IN BURKINA FASO, WEST AFRICA

Abstract

Soil erosion is recognized as one main reason for soil degradation in West Africa. However, predictions on the impact of climate change on soil erosion are rare for most West African countries including Burkina Faso.

This study assesses the impact of climate change on water resources and soil erosion in a small catchment (126 km²) in southwestern Burkina Faso. Climate data from an ensemble of six regional (RCM) and global (GCM) climate models were used to run the physically based spatially distributed hydrological and soil erosion model SHETRAN. The Representative Concentration Pathways (RCPs) 4.5 and 8.5 were selected as future climate scenarios.

Bias corrected precipitation and temperature required for the calculation of potential evapotranspiration were used as input for the SHETRAN model to simulate total discharge and specific suspended sediment yield (SSY). Discharge and SSY from simulations run with climate data were able to reproduce discharge and SSY from a simulation that used observed precipitation and temperature from the historical period (1971 – 2000).

The impact of climate change on hydrology and soil erosion was assessed by comparing the historical period with the future climate scenarios (2021 – 2050). Most of the used climate models predict an increase of temperature between 0.9°C and 2.0°C. The bias correction did not alter the climate change signal of temperature. Large uncertainties among the RCMs-GCMs exist regarding the climate change signal of future precipitation. Some climate models predict an increased (5.9% – 36.5%) others a decreased (6.4% – 10.9%) or mixed signal. The applied bias correction did not reverse the climate change signal in most cases but it influenced magnitude and timing of precipitation. The ensemble mean suggests an increased discharge between 27.1% and 59.8% and an increased SSY of the same order. In general, the climate change signal and the corresponding discharge and SSY predictions are afflicted with large uncertainties. These uncertainties impede direct conclusions regarding future development of discharge and erosion. As a consequence of the mixed signals, potential increase and decrease of future discharge and soil erosion have to be incorporated in climate change adaption strategies.

6.1 Introduction

Hydrological and soil erosion processes are substantially driven by the atmosphere through rainfall and evapotranspiration. Rising temperatures are frequently predicted by regional (RCM) and

global (GCM) climate models and are considered to change spatial and temporal rainfall pattern. Changing rainfall patterns and temperature have distinct effects on water resources and soil erosion (Field and Barros, 2014; Mullan et al., 2012; Nearing et al., 2004). The West African region is severely exposed to the effect of climate change due to the high vulnerability of the predominantly agricultural societies (Serdeczny et al., 2016). Analyzing the impact of climate change on hydrological and soil erosion processes is hampered by the lack of adequate data in terms of spatial and temporal resolution especially in a data scarce region as West Africa. Hydrological and soil erosion models are necessary to estimate past, present, and future development of water and soil resources. The modeled output can be used to provide guidance to decision makers regarding the implementation of climate change adaptation strategies (Beven, 2008; de Vente et al., 2013; Pandey et al., 2016). However, adaptation strategies necessary to mitigate the possible effects of climate change on hydrology, soil erosion and accordingly agriculture are challenging in the context of uncertain future climate change signals (Muerth et al., 2013).

The impact of climate change on the rainfall pattern and temperature in West Africa is difficult to assess due to differences between climate models regarding amplitude and direction of changing temperature and precipitation (Kasei et al., 2010; Niang et al., 2014). This is mainly attributed to the difficulties of simulating convective rainfalls and the rainfalls generated by the West African Monsoon (WAM) which is attributed to the incomplete knowledge of the involved processes, a lack of observations and the natural climate variability in the region (Cook, 2008; Druyan et al., 2010; Field and Barros, 2014; Klein et al., 2015; Niang et al., 2014). Consequently, climate model comparison studies report a large spread of rainfall projections (Table 6-1). A trend towards the increase of frequency and magnitude of extreme precipitation events is debated and differs from region to region (Aguilar et al., 2009; Hounkpè et al., 2016; Mouhamed et al., 2013; New et al., 2006; Sylla et al., 2016b).

The effect of climate change on hydrology and soil erosion is difficult to assess using RCMs and GCMs due to their large uncertainty and biases regarding predicted rainfall patterns (Ehret et al., 2012; Hagemann et al., 2011; Muerth et al., 2013). Therefore, precipitation is frequently bias corrected to avoid unrealistic simulations and to enable correct impact assessment (Johnson and Sharma, 2015; Teutschbein and Seibert, 2012). Nevertheless, the application of bias correction is criticized because some assumptions of climate models are violated and the climate change signal may be changed (Ehret et al., 2012; Muerth et al., 2013). Because of this, a clear presentation and discussion of used data, differences between bias corrected and uncorrected results are necessary (Ehret et al., 2012). To account for the uncertainty in climate model predic-

tions it is recommended to perform a multi-model assessment (Field and Barros, 2014). Therefore, in this study an ensemble of six RCMs-GCMs from the Coordinated Regional climate Downscaling Experiment project (CORDEX-Africa, http://www.cordex.org/) were used to evaluate the impact of climate change on hydrology and soil erosion in the Dano catchment.

Most of the available studies that used climate predictions for environmental models are focused on hydrological simulations. Studies that used climate change predictions of a multi-model ensemble as input to simulate the impact on hydrology and soil erosion are rare for the West African region (Li and Fang, 2016; Walling, 2009) but necessary as the effect of climate change on hydrology and soil erosion in this region is quite unclear (Niang et al., 2014). Mixed signals of discharge change are frequently reported by different studies in the region and may be attributed to the high uncertainty of precipitation projections for West Africa (Niang et al., 2014; Yira et al., 2017). A negative signal is reported to range from -80% to -11% (Table 6-1) for different climate models. Hiepe (2008) and Bossa (2014) report negative signals for discharge in the Ouémé catchment in Benin as well as Ruelland et al. (2012) for the Bani catchment in Mali. Further negative discharge trends were found out by Mbaye et al. (2015) and Cornelissen et al. (2013). A positive trend is indicated by Ardoin-Bardin et al. (2009) for the discharge of the Sassandra catchment in Ivory Coast.

Among the listed studies only two deal with the impact of climate change on soil erosion. Both studies used the SWAT modeling system which is semi distributed and whose erosion module is based on the empirical MUSLE approach which does not consider gully and river bank erosion (Neitsch et al., 2011). Furthermore, the cited studies were conducted on a much larger scale (≥ 2344 km²).

Table 6-1: Selected studies on the impact of climate change on water resources in West Africa (changed after Yira (2016))

Study	Location/seize	GCM/RCM	Scenario	Reference period	Future period	Precipitation change (%)	Discharge change (%)	SSY change (%)
Hiepe (2008)	Upper Oueme/ 14500 km²	REMO-ECHAM5/MPI-OM	A1B, B1	1960 - 2000	2001 - 2050	-3 to -8	-6 to -23	-5 to -27
Itiveh and Bigg (2008)	Niger/1471 000 km²	HadCM3, PCM, CGCM, CSIRO	A1, A2, B1, B2	1950 - 2000	2070s	Mixed trend	-15 to +20	-
Kunstmann et al. (2008)	Volta Basin/94 000 km²	ECHAM4	IS92a	1991 - 2000	2030 - 2039	-20 to +50	-10< to >+20	-
Ardoin-Bardin et al. (2009)	Sassandra, Ivory Coast/ 62173 Km²	HadCM3-A2	-	1971-1995	2036-2065	11.4	38	-
Kasei (2010)	Volta Basin/400000 km²	MM5WRF and REMO-ECHAM5/MPI-OM	B1	1991-2000 and 1961-2000	2030-2039 and 2001-2050	+12 and -6	+40 and -5	-
Ruelland et al. (2012)	Bani catchment, Mali/100 000 km²	MadCM3 and MPI-M	A2	1961-1990	2041-2070	-2 to -10	-30 to -46	-
Oguntunde and Abiodun (2013)	Niger/2.27 Mio km²	RegCM3	A1B	1980 - 2000	2030 - 2050	-13 to +32.6	-33 to +35	-
Cornelissen et al. (2013)	Térou Catchment, Benin/2344 km²	REMO-ECHAM5/MPI-OM	B1	2001-2010	2031-2049	-11	-11	-
Aich et al. (2014)	Niger Basin/ 2156000 Km²	HadGEM2-ES, IPSL-5 CM5A-LR, MIROC-ESM-CHEM, GFDL-ESM2M, NorESM1-M	RCP8.5	1970-1999	2070-2099	mixed trend	-50 to +50	-
Bossa et al. (2014)	Ouémé catchment, Benin/ 49256 Km²	REMO-ECHAM5/MPI-OM	A1B	2000-2009	2010-2029	-10	-18	0
Mbaye et al. (2015)	Upper Senegal Basin, Senegal-Mali-Mauritania/218000 km²	REMO-MPI-ESM-LR	RCP4.5 and RCP8.5	1971-2000	2071-2100	negative trend	up to -80	-

Based on the described challenges, we aim to provide additional knowledge on the future impact of climate change on water and soil resources in West Africa with a focus on the Dano catchment in Burkina Faso. In this study we use the physically based spatially distributed hydrological and soil erosion model SHETRAN for the simulation of catchment discharge and soil erosion. SHETRAN was already tested in the Dano catchment (Op de Hipt et al., 2017) and was used to study the climate change impact on hydrology and soil erosion in other regions (e.g. Bathurst, 2010; Birkinshaw et al., 2017; Zhang, 2015).

Based on the importance of knowledge on the future impact of climate change on water and soil resources for a society, which is highly dependent on rain-fed agriculture, the present study has the following objectives:

1) Compare bias corrected and uncorrected precipitation and temperature data of six climate models with measured data;
2) Analyze the climate change signal of temperature, mean and extreme precipitation;
3) Use observed and modeled historical precipitation and temperature as input to run SHETRAN and compare the corresponding simulated discharge and specific suspended sediment yield;
4) Assess the impact of climate change on discharge and specific suspended sediment yield by comparing the reference period (1971 – 2000) with the future period (2021 – 2050) and discuss the uncertainty related to the output of the different climate models.

6.2 Material and methods

6.2.1 Study area

The study catchment is located in the southern part of Burkina Faso, West Africa (Figure 6-1a). The biggest settlement in the catchment is Dano after which it is named. The catchment covers an area of 126 km² and is one of three focal watersheds of the West African Science Service Center on Climate Change and Adapted land use (WASCAL, www.wascal.org).

The catchment lies in the sudano savanna zone of West Africa whose natural vegetation is characterized by wooded and shrubby plant associations and abundant annual grasses. The natural vegetation is extensively converted to cropland and settlement as shown by Yira et al. (2016) for the Dano catchment and by CILSS (2016) on the national level. The cropland is used to produce food crops such as sorghum (*Sorghum bicolor*), millet (*Pennisetum glaucum*), maize

(*Zea mays*), cowpeas (*Vigna unguiculata*) and groundnut (*Arachidis hypogaea*). The most important cash crop in the area is cotton (*Gossypium hirsutum*).

Large parts of the study catchment are characterized by a flat topography with gentle slope gradients (average and maximum gradients are 1.8° and 20°, respectively). The flat landscape is interrupted by the Ioba mountain chain that covers the western part of the catchment (Figure 6-1b). The elevation ranges from 269 m to 504 m above sea level.

The annual rainfall ranged from 800 – 1200 mm for the period 1951 – 2005 (Schmengler, 2010). The rainfall pattern is characterized by a distinct seasonality through the West African monsoon. The rainy season starts in July and ends in September. 65% of the mean annual precipitation falls in these months. The dry season ranges from October to June.

Soils are dominated by plinthosols (73%) which are characterized by high content of coarse particles and a plinthic subsurface layer. Soils of the valley bottoms are mainly gleysols. Other soils formed in the region are cambisols, lixisols, leptosols and stagnosols (Figure 6-1e).

6.2.2 Climate data

Daily precipitation and mean daily temperature were available from a station operated by the national meteorological service (Direction Générale de la Météorologie du Burkina, DGM) for the period from 1971 to 2000 (see Figure 6-1c).

Historical precipitation and temperature data for the same period (1971 – 2000) were retrieved from an ensemble of six RCM-GCMs (see Table 6-2). The RCM-GCM simulations were run in the framework of the Coordinated Regional climate Downscaling Experiment (CORDEX-Africa, www.cordex.org). The three RCMs (CCLM4-8: Climate Limited-area Modelling Community, Germany; HIRHAM5: Alfred Wegener Institute, Germany; RACMO22: Royal Netherlands Meteorological Institute, Netherlands) use the atmospheric boundary condition of four GCMs (CNRM-CM5: National Centre for Meteorological Research, France; EC-EARTH: consortium of 27 European members; ESM-LR: Max-Planck-Institute for Meteorology, Germany; NorESM1-M: Research Council of Norway, Norway).

Future temperature and precipitation projections for the period 2021 – 2050 were retrieved from the same RCM-GCM combinations. The Representative Concentration Pathways RCP 4.5 and RCP 8.5 (Moss et al., 2010) were used as future scenarios.

Datasets of the extent of 3 x 3 nodes surrounding the catchment were compared to investigate the rainfall variability in the region. However, due to the run time of SHETRAN and the small differences between the nodes as revealed in section 6.3.1.1, the closest node was used only

(see Figure 6-1c) although different studies recommend the use of more nodes to account for climate variability (e.g. Villani et al., 2014).

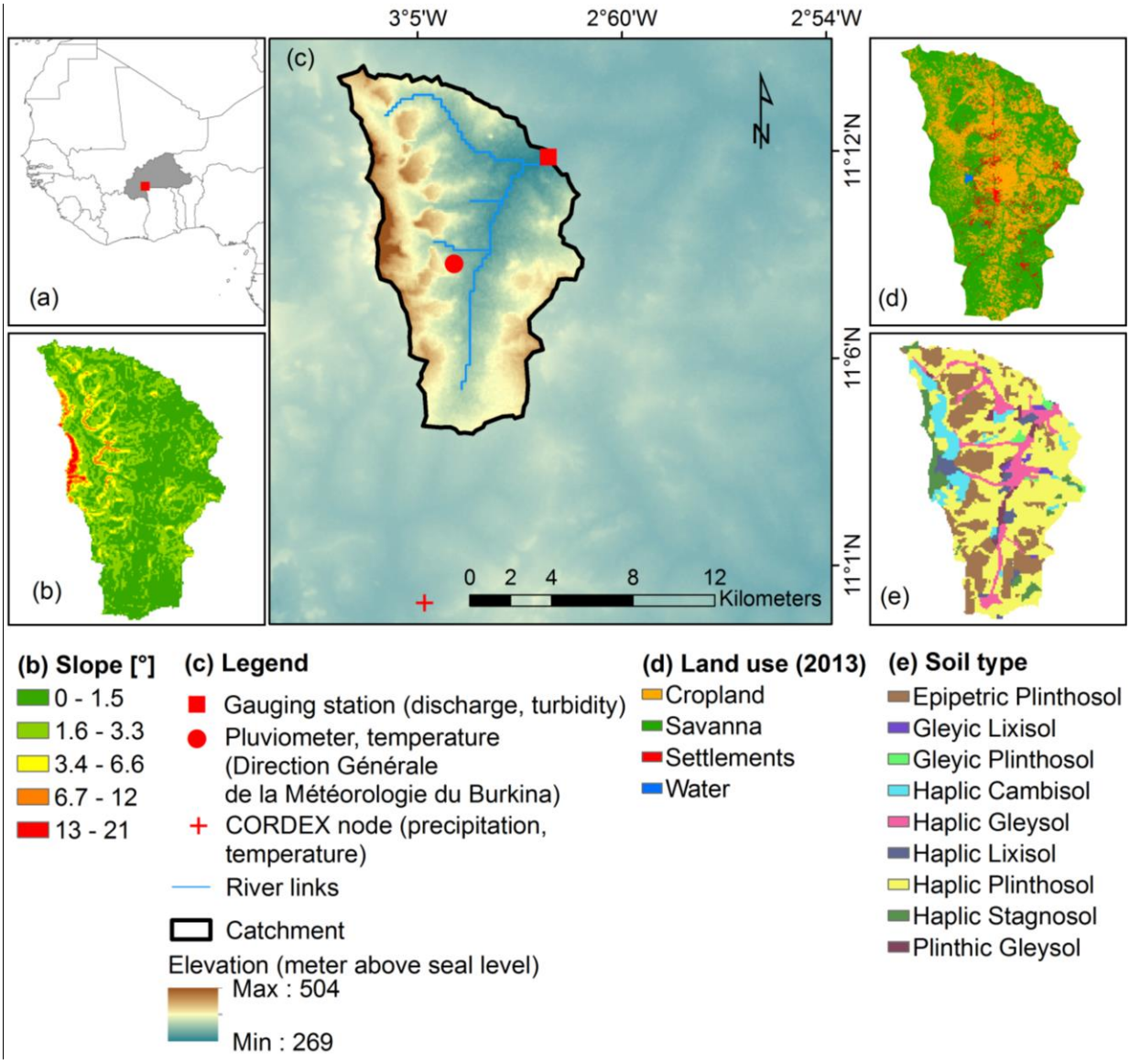

Figure 6-1: Location map of the Dano catchment: **(a)** location of the catchment and Burkina Faso in West Africa, **(b)** slope of the catchment, **(c)** model catchment, **(d)** land use map (Forkuor, 2014), **(e)** soil map (data base: soil survey done by Ozias Hounkpatin, Institute of Crop Science and Resource Conservation, University Bonn).

Table 6-2: RCM-GCM products and labels

Regional Climate Model	Driving Global Climate model	RCM Centre/Institute	Labels
CCLM4-8	CNRM-CM5	CCLMcom	CCLM-CNRM
CCLM4-8	EC-EARTH	CCLMcom	CCLM-EARTH
CCLM4-8	ESM-LR	CCLMcom	CCLM-ESM
HIRHAM5	NorESM1-M	DMI	HIRHAM-NorESM
HIRHAM5	EC-EARTH	DMI	HIRHAM-EARTH
RACMO22	EC-EARTH	KNMI	RACMO-EARTH

6.2.2.1 Bias correction of precipitation and temperature data

Historical precipitation and temperature data from six climate models were compared with their observed counterparts for the period 1971 – 2000 to control if the modeled output is in agreement with the observation. The modeled temperature shows a negative deviation for most models (see section 6.3.1.1). As temperature is used to calculate potential evapotranspiration and has therefore strong effects on catchment hydrology, it was bias corrected using the delta change approach described in Haddeland et al. (2012).

A bias correction method was used to correct the historical and future rainfall data derived from the six climate models. The non-parametric quantile mapping approach introduced by Gudmundsson et al. (2012) was applied. This approach derives monthly transfer functions from cumulative distribution functions of observed and modeled historical precipitation data and applies this transfer function to past and future modeled precipitation. Further details are given in Boé et al. (2007).

6.2.2.2 Analysis of extreme rainfall events

The determination of extreme values is done using the annual maxima series (AMS) method. AMS uses the annual precipitation maxima and is consequently limited to the number of years used for the study. Generalized Extreme Value (GEV) distributions were used to fit the empirical precipitation distributions. Monthly precipitation data of the reference period 1971 – 2000 were separated in two groups reflecting the characteristics of the seasons: Group 1 comprises the starting and the ending rainy season (April, May, October) and group 2 the rainy season (June, July, August, September). The GEV was fitted to the data of each group separately and the distribution parameters were estimated using the Generalized Maximum Likelihood Estimator (Gilleland and Katz, 2016). The fitted distribution was used to retrieve precipitation magnitude with return periods of 2-, 5-, 10-, 20-, 25- and 50-years for each group. Bias corrected rainfall data from the projected scenarios (RCP 4.5 and RCP 8.5) of each RCM-GCM were analyzed based

on the same approach. Finally, the percentage change D_i of the rainfall intensity (I_i) at the chosen return period (i) was calculated between the modeled historical data (A) and the future scenarios (B) by using equation Eq. 6-1 (Hounkpè et al., 2016):

$$D_i = \frac{\left(I_i(B) - I_i(A)\right)}{I_i(B)} \qquad \text{Eq. 6-1}$$

where I_i (A) is the i-th intensity computed for the historical data and I_i (B) is the i-th intensity calculated for the future scenario data. The paired sample t-test and the Wilcoxon test were used to test for significant differences between the historical and future return levels. A change is considered as significant if both tests agree (Hounkpè et al., 2016).

6.2.3 Hydrological and soil erosion modeling

Observed and modeled precipitation and temperature data were used as climate input into the hydrological and soil erosion model SHETRAN (Birkinshaw, 2010; Ewen et al., 2000). SHETRAN is a physically based spatially distributed hydrological soil erosion model. It is a derivative of SHE (Système Hydrologique Européen), which was jointly developed by the British Institute of Hydrology, the Danish Hydraulic Institute and the French consulting company SOGREAH (Abbott et al., 1986). SHETRAN has been refined and complemented by new components as e.g. the fully 3D simulation of subsurface water flow (Parkin, 1996) and sediment transport (Wicks, 1988; Wicks and Bathurst, 1996). Detailed information is available online (http://research.ncl.ac.uk/shetran/). The model was already calibrated and validated in the Dano catchment. Detailed information on the parameterization can be found in Op de Hipt et al. (2017). The model was set up based on a 200 m x 200 m horizontal resolution and by using climate, discharge and suspended sediment load (SSL) data from the years 2013 and 2014 for calibration and validation respectively. Different performance measures (Nash Sutcliffe Efficiency (Nash and Sutcliffe, 1970), Kling-Gupta efficiency (Gupta et al., 2009; Kling et al., 2012) and R^2) for discharge are in the range of 0.7 and 0.79 for calibration and between 0.66 and 0.76 for validation. These measures are in the range of other studies that used SHETRAN (e.g. Birkinshaw et al., 2014; Đukić and Radić, 2016, 2014; Mourato et al., 2015; Naseela et al., 2015; Tripkovic, 2014; Zhang, 2015). Among these studies R^2 and NSE values above 0.5 are frequently observed. The calibration and validation of the erosion component showed NSE of 0.4 and 0.2 and R^2 of 0.47 and 0.37 for calibration and validation of SSL, respectively. These performance measures are in agreement with results of other studies (de Figueiredo and Bathurst, 2007; Elliott et al., 2011; Zhang, 2015) and comparable with other erosion models (de Vente et al., 2013; Jetten et al., 1999).

As hydrological and soil erosion data do not exist for the reference period the expected climate change impact on hydrology and soil erosion is estimated by studying the differences between the simulated hydrological and soil erosion variables of the reference period (1971 – 2000) and the future period (2021 – 2050).

The present study differentiates between suspended sediment load (SSL in kg/s) and suspended specific sediment yield (SSY in t/ha/year).

6.2.4 Time step sensitivity

The long term historical and future climate data was only available on a daily basis. This is critical since results of dynamic models such as SHETRAN respond sensitively to the chosen simulation time step (Bruneau et al., 1995; Hessel, 2005; Yira, 2016; Zhang, 2015) and consequently the discussion of time and spatial scales is fundamental in hydrological modeling (Blöschl and Sivapalan, 1995). Yira (2016) reports a decreasing modeled discharge with longer time step. This can be explained by the information loss during aggregation of rainfall data from sub-daily to daily resolution: It reduces the maximum precipitation intensities and therefore leads to an underestimation of overland flow due to infiltration excess. Consequently, simulated discharge and hence sediment yield may be underestimated by the model. Figure 6-2a shows that exceedance probabilities for both hourly and daily suspended sediment loads are rather small. Figure 6-2b shows that there exists a statistically significant positive relation between hourly and daily suspended sediment loads. Interestingly, highest differences occur at both extremes of the data. The Wilcoxon signed rank test was applied to prove that the hourly and daily values are identical populations (H0: hourly and daily suspended sediment loads come from an identical population). To satisfy the assumption of the test that the paired values observations are randomly and independently drawn it was applied to a random set of paired values (Hogg et al., 2015). The test indicated that hourly and daily suspended sediment loads have similar populations (p-value = 0.2467). The limitations related to a daily timestep cannot be avoided for the long-term simulations as no hourly data are available. Furthermore, our results are comparable to other SHETRAN studies that also used a daily timestep (Birkinshaw et al., 2017; de Figueiredo and Bathurst, 2007; Mourato et al., 2015).

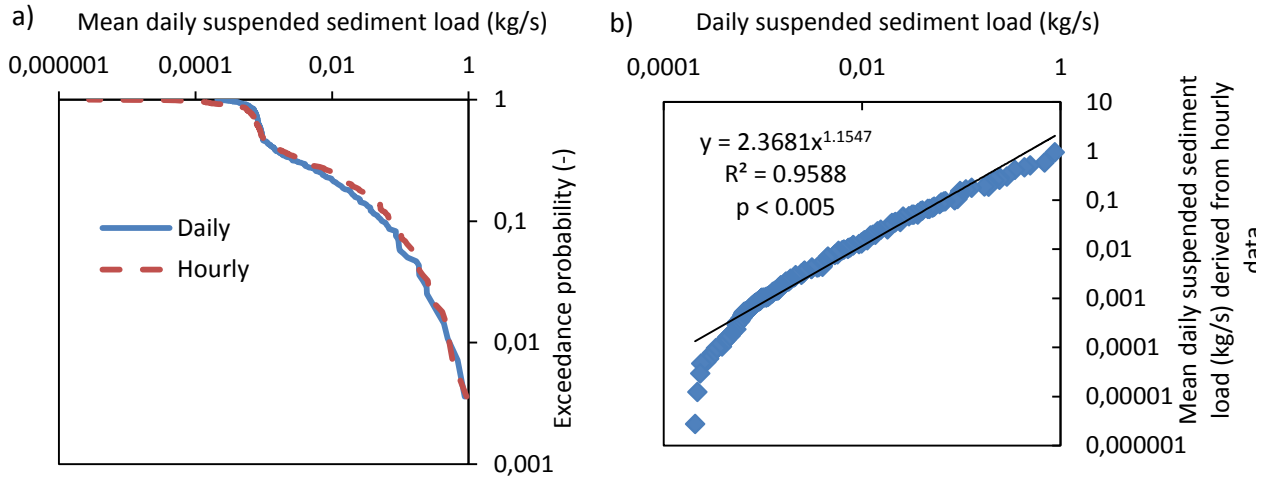

Figure 6-2: **a)** Exceedance probability of hourly and daily suspended sediment load, **b)** scatter plot of hourly and daily suspended sediment load. LOG10 scale is used.

6.2.5 Assessment criteria

Different performance measures were used to investigate the RCM-GCM driven historical simulations and to compare observed and modeled climate data.

i. P-factor: It measures the proportion of observed climate data that is covered by the range of RCM-GCM derived climate data.

ii. R-factor: It expresses ratio between the range of minimum and maximum RCM-GCM for precipitation and temperature and the standard deviation of observed counterparts. Consequently, the R-factor indicates how wide the range of the modeled variable is, compared to the observed standard deviation:

$$R - factor\ (Var) = \frac{1}{n\sigma_{Var_{obs}}} \sum_{l=1}^{n} (Var_{Si_{max}} - Var_{Si_{min}}) \qquad \text{Eq. 6-2}$$

W

where Var is the climate variable, n the observation data points, Si_{min} and Si_{max} the minimum and maximum value of the RCM-GCM ensemble and σ the standard deviation.

iii. The normalized root mean square deviation (NRMSD), NSE (Nash and Sutcliffe, 1970), KGE (Gupta et al., 2009; Kling et al., 2012) and R^2 assess if the RCM-GCM

based discharge and SSY simulations agree with the simulations run based on observed climate data.

6.3 Results and Discussion

6.3.1 Climate data

6.3.1.1 Bias correction

The output of climate models necessary for hydrological and soil erosion modeling is frequently biased over the scale it is needed (Haddeland et al., 2012; Hagemann et al., 2011; Maraun et al., 2010; Randall et al., 2007). Therefore, the use of bias correction methods is frequently considered as inevitable although it is also debatable (Ehret et al., 2012). The lack of a physical justification and the possible violation of climate model assumptions by bias correction are criticized. Furthermore, bias correction may have a large influence on the climate change signal in terms of magnitude (Ehret et al., 2012). However, these disadvantages are often neglected due to the advantages of bias correction. The assessment of climate change impact on hydrology and hydrologically driven processes such as soil erosion is only useful for environmental planning, if the input data (especially precipitation) are realistic in term of magnitude and distribution (Muerth et al., 2013; Piani et al., 2010; Sharma et al., 2007; Teutschbein and Seibert, 2012).

The ability of uncorrected precipitation and temperature from the RCM-GCM ensemble to reflect observed data is expressed by the coefficient of determination and the normalized root mean square deviation (NRMSD). All climate models clearly differ from the observed data. The observed temperature is better represented by the modeled data as shown by correlation coefficients between 0.57 and 0.78 compared to precipitation with values between 0.4 and 0.68. The best correlation coefficients are achieved by HIRHAM-EARTH for precipitation (0.68) and temperature (0.78). Especially precipitation data show a high deviation with NRMSD values of higher than 0.73. The deviation of temperature is smaller with a minimum NRMSD of 0.2 (CCLM-ESM).

Figure 6-3a shows that the observed mean monthly temperature is within the temperature range as simulated by the ensemble of climate models. However, mean monthly observed temperature is frequently higher than temperature derived from the climate models. Temperature is used to calculate potential evapotranspiration (ETp) using the Hamon equation (Oudin et al., 2005a). Therefore, temperature indirectly influences discharge and soil erosion by controlling ETp (Chaplot, 2007; Li and Fang, 2016). To avoid inconsistencies between observed and modeled potential evapotranspiration, temperature was bias corrected. The bias correction led to an

overall agreement between observed and modeled temperature as shown in Figure 6-3b. Due to the small differences data from climate models are masked by the observed temperature.

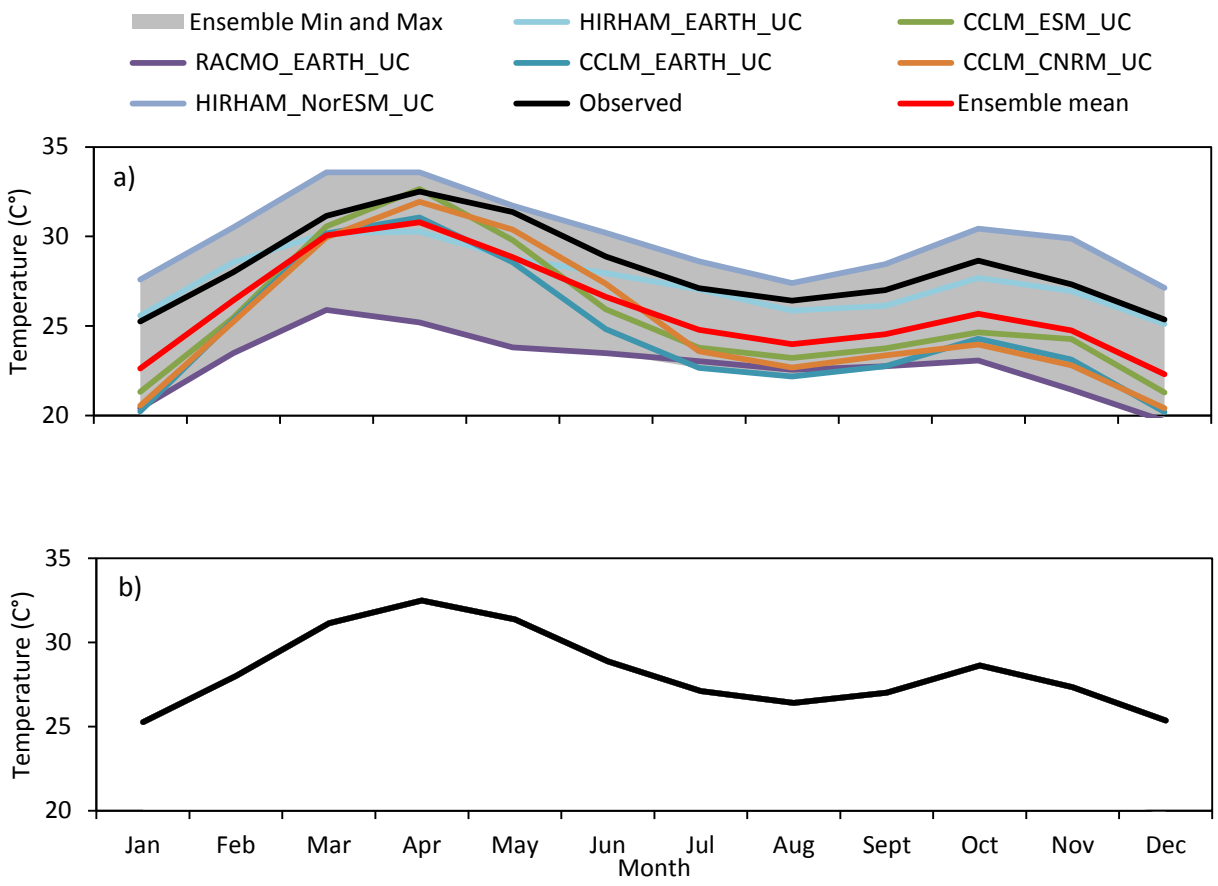

Figure 6-3: Observed, uncorrected **(a)** and bias corrected **(b)** mean monthly temperature data for the reference period 1971-2000. Due to the small differences data from climate models are graphically masked by the observed temperature.

The question of how many nodes to include in climate change studies to account for the spatial climatic variability is frequently discussed (e.g. Villani et al., 2014). Yira et al. (2017) for example used 9 nodes for a larger watershed of the same river system and did the hydrological modeling for each of these nodes. We compared uncorrected and bias corrected rainfall data of each climate model from a rectangular grid of 3 x 3 nodes surrounding the catchment. Figure 6-4 shows the exceedance probability of the modeled rainfall from 9 nodes from HIRHAM-EARTH and the observed rainfall data. The inter-node deviation and the deviation between the uncorrected data and the observed are quite large as shown in Figure 6-4a and Figure 6-4c. After the bias correction (Figure 6-4b and d) the deviation between modeled and observed as well as the inter-node deviation is negligible. A similar pattern was also observed for the remaining five climate models

(data not shown). Based on the small difference between the nodes data from the closest node were used only.

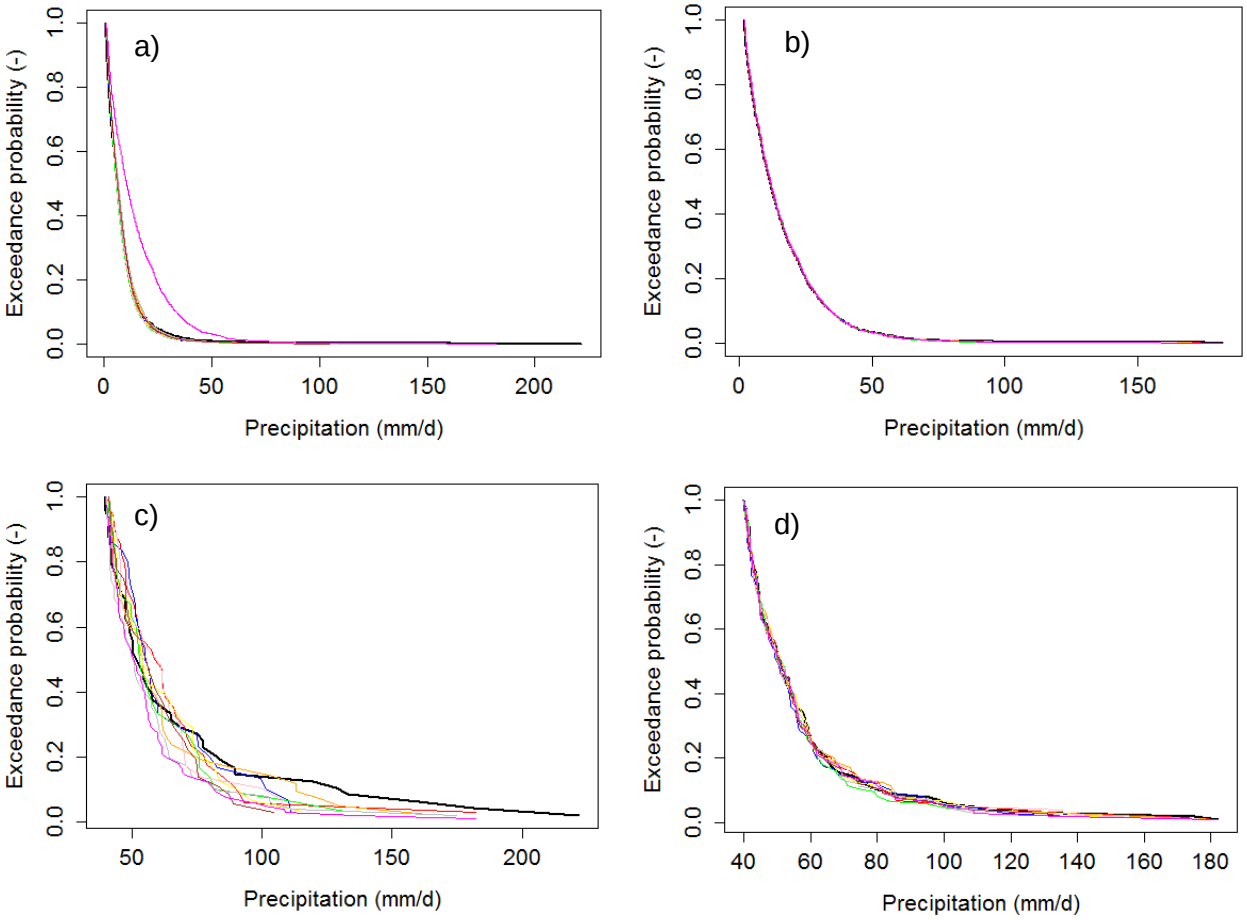

Figure 6-4: **(a)** Exceedance probability of uncorrected modeled rainfall data and the observed rainfall data (magenta line) from each node (9) for the reference period 1971-2000, **(b)** exceedance probability of bias corrected modeled rainfall data and the observed rainfall data from each node (9), **(c)** exceedance probability of uncorrected modeled rainfall data and the observed rainfall data from each node (9) with a threshold of >40 mm/d, **(d)** exceedance probability of bias corrected modeled rainfall data and the observed rainfall data from each node (9) with a threshold of >40 mm/d. All data are from HIRHAM-EARTH.

Figure 6-5a shows that uncorrected precipitation of most RCMs-GCMs overestimate magnitude of mean monthly precipitation compared to the observed rainfall. Furthermore, the timing of the rainy season partly disagrees with the observed pattern. The differences between mean monthly precipitation from all climate models and the observed precipitation are considerably reduced after bias correction (Figure 6-5b). Bias corrected mean monthly precipitation reflects well timing and magnitude of the rainy season. Figure 6-5c shows that annual precipitation is frequently

overestimated by uncorrected data from all climate models. Despite the large spread (R-factor = 4.8) only 60% of observed rainfall falls within the modeled precipitation range. As result of the applied bias correction (Figure 6-5c) the P-factor increases (P-factor = 86%) while the R-factor decreases (R-factor = 3.6). The modeled precipitation range captures the observed precipitation.

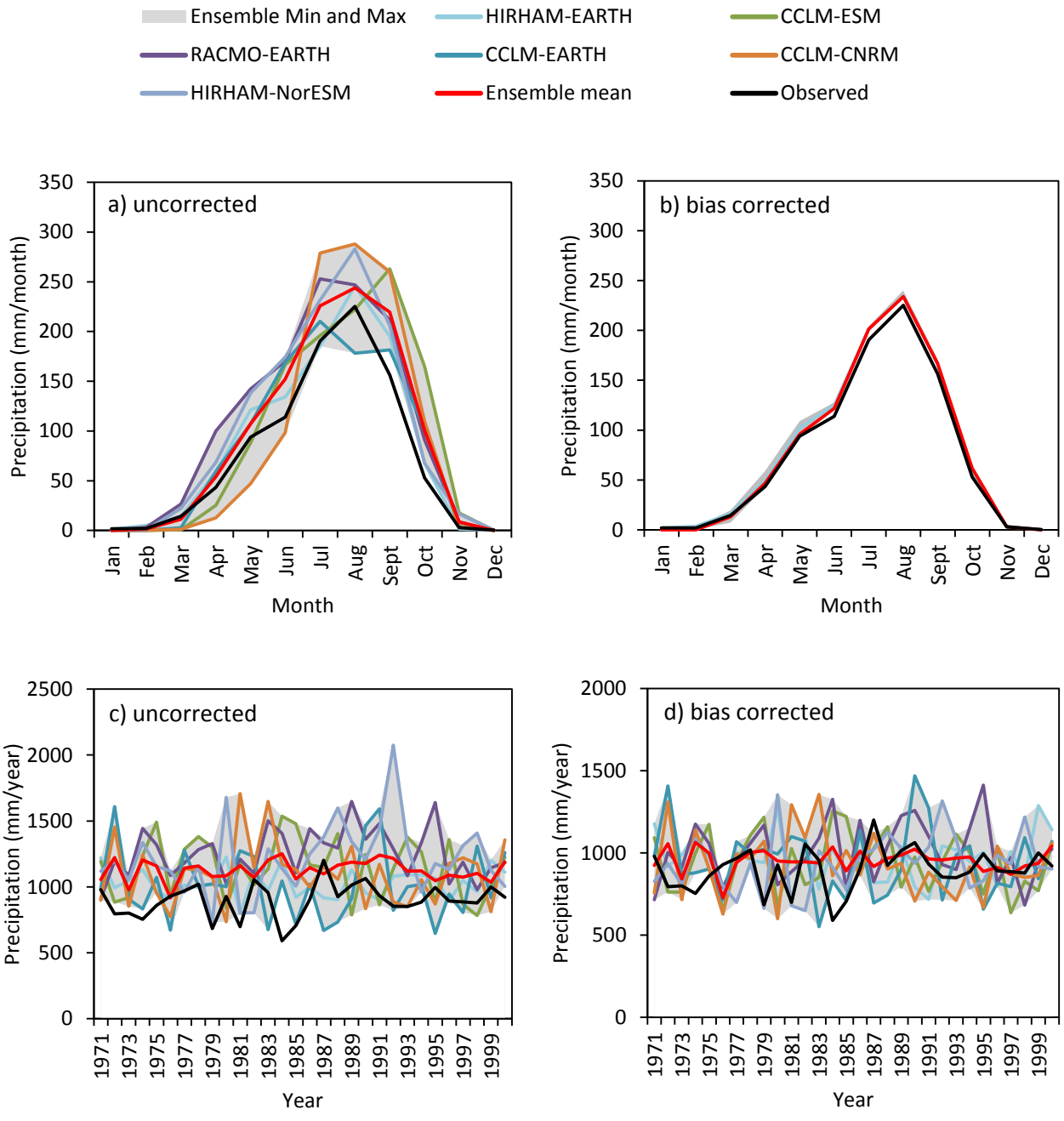

Figure 6-5: Historical mean monthly **(a,b)** and mean annual **(c,d)** precipitation for the reference period 1971-2000.

The ability of the six selected RCMs-GCMs to reproduce the West African climate has already been proven in previous studies (Cook and Vizy, 2006; Dosio et al., 2015; Gbobaniyi et al., 2014; Paeth et al., 2011; Yira et al., 2017). Furthermore, as already shown by Yira et al. (2017), the selected RCM-GCM give a quite large range of the possible impact of climate change on hydrology in this region. The overestimation and misrepresentation of the timing of the rainy season, that rectifies the bias correction of precipitation, is also reported by other authors for sub-Saharan Africa (Nikulin et al., 2012; N'Tcha M'Po et al., 2016; Oyerinde et al., 2017; Paeth et al., 2011).

6.3.1.2 Climate change signal

A comparison of the uncorrected and bias corrected historical temperature with the future temperature shows a clear increase for most climate models and scenarios. An exception is RCP4.5 of HIRHAM-EARTH which projects a decrease in temperature (Table 6-3). The bias corrected ensembles show a mean increase of 3.4% (RCP4.5) and 5.4% (RCP8.5), which is slightly lower than the uncorrected temperature increase. The bias correction did not change the climate signal of the uncorrected data. Increasing temperatures over West Africa were already observed for the last 50 years and different studies suggest that this trend will continue in the future (Niang et al., 2014; Waongo, 2015). Rising temperatures are observed by all multi-model ensemble studies conducted in the region (Field and Barros, 2014).

Table 6-3: Relative temperature change of RCP4.5 and RCP8.5 (2021 – 2050) compared to the reference period (1971 – 2000).

	Uncorrected			Bias corrected		
RCM-GCM	**Mean historical temperature (°C)**	**Temperature change RCP 4.5 (%)**	**Temperature change RCP 8.5 (%)**	**Historical temperature (mm)**	**Temperature change RCP 4.5 (%)**	**Temperature change RCP 8.5 (%)**
HIRHAM_EARTH	27.5	-2.8	5.6	28.2	-2.7	5.5
CCLM_ESM	25.5	6.6	7.7	28.2	5.9	6.9
RACMO_EARTH	22.9	6.2	6.5	28.2	5.0	5.3
CCLM_EARTH	24.6	6.0	6.8	28.2	5.3	5.9
CCLM_CNRM	25.2	4.0	5.3	28.2	3.6	4.7
HIRHAM_NorESM	29.9	3.2	3.6	28.2	3.3	3.8
Ensemble mean	25.9	3.9	5.9	28.2	3.4	5.4

Table 6-4 shows the relative change of predicted precipitation (2021 – 2050) from all climate models and scenarios compared to the historical period (1971 – 2000). It is important to notice

that the climate models do not agree on one common signal. Increased precipitation (5.9% – 36.5%) is predicted by RCP4.5 of HIRHAM-EARTH and by RACMO-EARTH, CCLM-CNRM and HIRHAM-NorESM while a decrease (0.2% – 10.9%) is projected by RCP8.5 of HIRHAM-EARTH and by CCLM-ESM and CCLM-EARTH. HIRHAM-EARTH is characterized by a mixed precipitation signal. The disagreeing signals between models may be attributed to data scarcity and limited knowledge of the regional climatology (Niang et al., 2014). The Coupled Model Intercomparison Project Phase 5 (CMIP5) showed different precipitation changes till 2050 (Field and Barros, 2014).

The trend suggested by the uncorrected data seems to be maintained after bias correction. The only exception is RCP4.5 of CCLM-ESM whose signal is changed from 0% to -4.2%. This can be explained by the bias correction method. If the difference between historical and uncorrected precipitation is very small or not existent, bias correction may lead to an inversion of the signal. As Hagemann (2011) points out, "the impact of bias correction on the climate change signal may be larger than the signal itself" (Hagemann et al., 2011, p. 575) if the signal is small.

Table 6-4: Relative change of mean annual precipitation between reference period (1971 – 2000) and future period (2021 – 2050). Uncorrected and bias corrected mean values are used for calculation. Bias correction was performed using observed data with mean annual precipitation of 897 mm.

	Uncorrected			Bias corrected		
RCM-GCM	**Mean historical precipitation (mm)**	**Precipitation change RCP 4.5 (%)**	**Precipitation change RCP 8.5 (%)**	**Historical precipitation (mm)**	**Precipitation change RCP 4.5 (%)**	**Precipitation change RCP 8.5 (%)**
HIRHAM-EARTH	1029.6	23.7	-1.8	961.7	36.5	-0.2
CCLM-ESM	1143.9	0.0	-7.0	942.2	-4.2	-6.4
RACMO-EARTH	1253.4	7.2	16.1	1005.2	9.0	18.1
CCLM-EARTH	1014.7	-14.1	-8.1	944.2	-10.9	-6.4
CCLM-CNRM	1099.0	16.2	25.7	929.9	10.8	19.3
HIRHAM-NorESM	1209.1	4.5	17.1	941.2	5.9	12.0
Ensemble mean	1125.0	6.3	7.0	954.1	7.8	6.1

Figure 6-6 shows the mean relative change of bias corrected precipitation return levels of six return periods for each model and RCP. For RCP4.5 (Figure 6-6a) it is observable that return levels of most models (HIRHAM-EARTH, RACMO-EARTH, CCLM-CNRM, HIRHAM-NorESM) are predicted to increase. For example, the 50-year return level of RCP4.5 of HIRHAM-EARTH

is predicted to increase by 193%. In agreement with the overall negative precipitation signal of CCLM-EARTH (see Table 6-4), return levels of this model decrease over all return periods. For RCP8.5 all models except CCLM-ESM are characterized by increased return levels (0.4% - 226.8%). The change in return levels for bias corrected data from most models and RCPs is statistically significant as tested by the paired t-test and the Wilcoxon test. A similar trend also applies to the data from April, May and October (not shown here). RCP4.5 of HIRHAM-EARTH and both RCPs of HIRHAM-NorESM show larger increases in return levels. This is attributed to very high precipitation extremes of > 500 mm/d which remain improbable even after bias correction. However, the inclusion of extremely high precipitation rates may substantially influence the fitted extreme value distribution and the predicted return levels accordingly.

The change in magnitude and frequency of extreme precipitation due to climate change is frequently attributed to the increase of atmospheric moisture content (Emori and Brown, 2005; O'Gorman and Schneider, 2009). Global studies report mixed signals depending among other on the chosen climate model and the scenario (Field et al., 2012; Field and Barros, 2014). Studies that focused on the investigation of climate change impact on extreme precipitation are rare in the West African region. Some of the available studies work with historical precipitation (Aguilar et al., 2009; New et al., 2006; Hounkpè et al., 2016) and do not use future scenarios from climate models. Sylla et al. (2016b) compared different climate models available in the CORDEX framework and report a precipitation change between -10% and +10% with greater amplitudes. They further notice an increase of very wet days between +5% and +10%. Druyan (2011) reviews several studies on precipitation trends and reports a mixed signal. Other studies that used climate model derived precipitation data consistently report increased magnitude of high intensity precipitation events for the West African Region. (Abiodun et al., 2013; Giorgi et al., 2014; Lintner et al., 2012; Scoccimarro et al., 2013; Vizy and Cook, 2012).

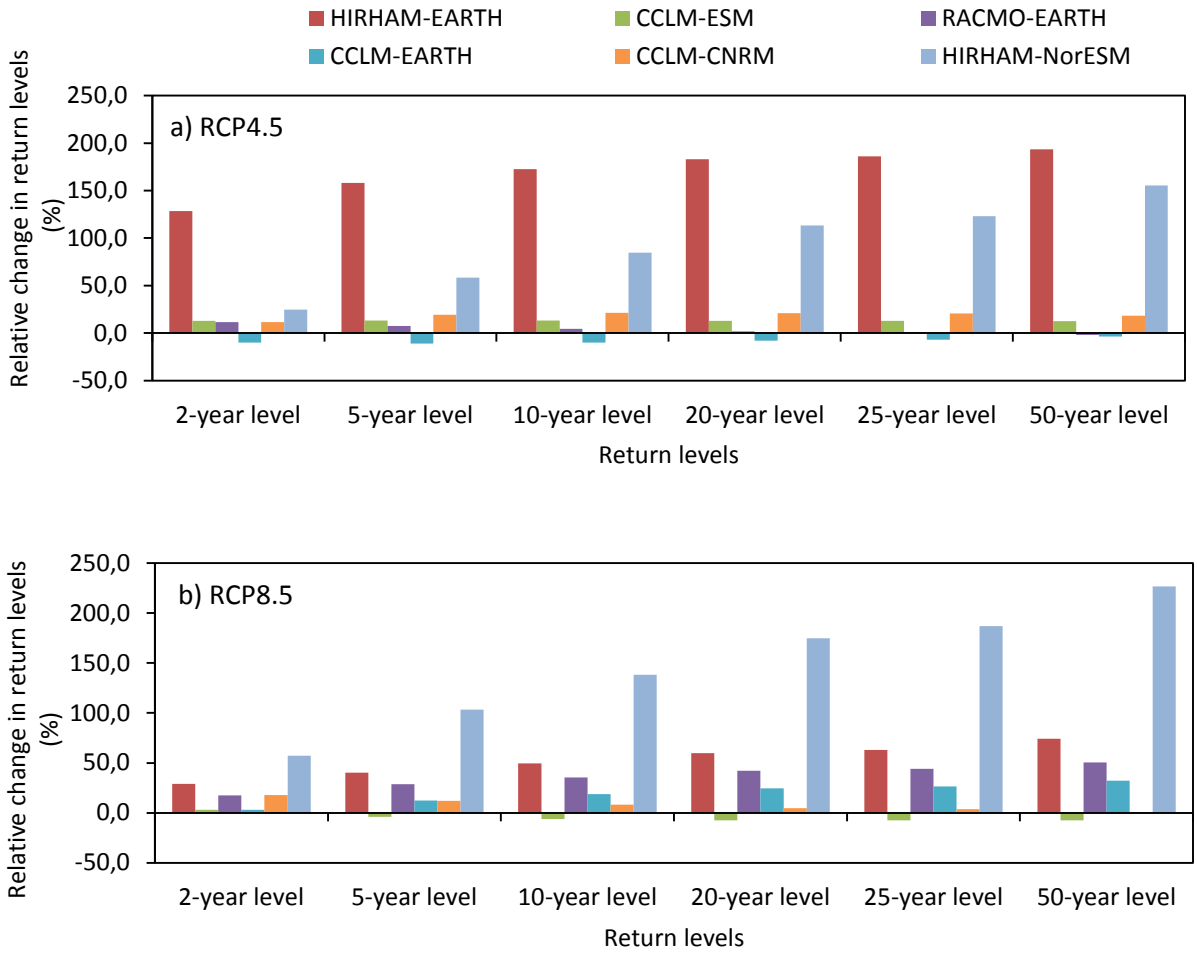

Figure 6-6: Relative change (%) of rainfall return levels (2021 – 2050) for **(a)** RCP4.5 and **(b)** RCP8.5 compared to the reference period (1971 – 2000). The change was calculated based on the bias corrected data.

6.3.2 Modeling

6.3.2.1 Hydrology

6.3.2.1.1 Historical simulated discharge

SHETRAN was run with observed and modeled climate data. The discharge and SSY simulated using observed climate variables is denoted as observed discharge/SSY and the discharge and SSY simulated using modeled climate data is indicated by modeled discharge/SSY. To test the ability of modeled discharge to reproduce the observed discharge, modeled mean monthly dis-

charge was compared to observed mean monthly discharge over the reference period (1971 – 2000). Figure 6-7 shows that modeled discharges are mostly overestimated compared to observed discharge. The use of uncorrected precipitation data from CCLM-ESM additionally leads to a shift of the peak discharge to September.

Performance measures (NSE, R^2, KGE) are used to quantify the ability of the RCMs-GCMs to reproduce the historical discharge simulated based on measured precipitation and temperature. Table 6-5 shows that all climate models reproduce timing and magnitude of discharge well. Differences between observed and modeled discharges may be explained by varying temporal patterns of precipitation and potential evapotranspiration. Precipitation of RACMO-EARTH, for example, is frequently higher than observed precipitation despite bias correction. The use of uncorrected precipitation and temperature data (CCLM-ESM-UC) leads to an overestimation and wrong timing of the discharge. Yira et al. (2017) used the same data base and also state a trend towards discharge overestimation by most models. They argue that shortcomings regarding the bias correction approach, which was run using a monthly correction, may be responsible for the overestimation of precipitation and consequently also for the simulated discharge.

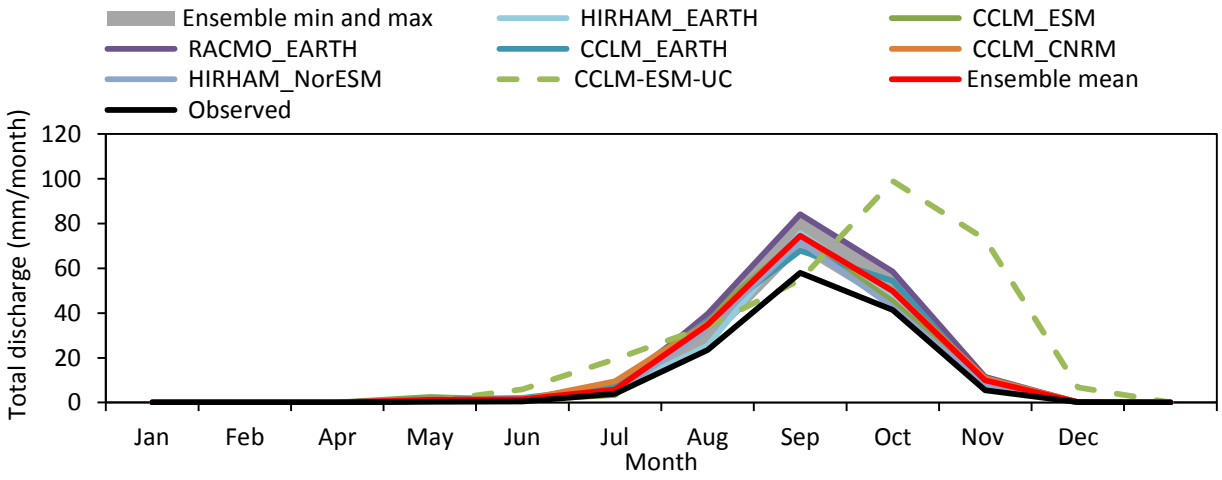

Figure 6-7: Modeled discharge using observed and modeled precipitation for the reference period (1971 – 2000). CCLM-ESM-UC refers to the uncorrected data.

Table 6-5: Performance measures of discharge and SSY simulated based on climate models and observed precipitation. Calculation basis are mean monthly discharges/SSY for the reference period. NSE refers to the Nash-Sutcliffe-Efficiency, R^2 to the coefficient of determination and KGE to the Kling-Gupta-Efficiency.

Model	**discharge**			**soil erosion**		
RCM-GCM	**NSE**	**R^2**	**KGE**	**NSE**	**R^2**	**KGE**
HIRHAM-EARTH	0.9	1.0	0.7	0.8	1.0	0.7
CCLM-ESM	0.9	1.0	0.7	0.8	1.0	0.7
RACMO-EARTH	0.7	1.0	0.5	0.6	1.0	0.4
CCLM-EARTH	0.9	1.0	0.7	0.9	1.0	0.6
CCLM-CNRM	0.9	1.0	0.6	0.8	1.0	0.6
HIRHAM-NorESM	0.9	1.0	0.8	0.9	1.0	0.8
CCLM-ESM-UC	-1.0	0.5	-0.2	-2.0	0.5	-0.5

6.3.2.1.2 Future simulated discharge change

The impact of climate change on discharge is assessed by comparing the historical discharge as simulated using precipitation and temperature from climate models to the future discharge (both simulated using data from climate model scenarios). Table 6-6 shows that only HIRHAM-EARTH shows different signals for RCP4.5 and RCP8.5 with a strong increase in discharge for RCP4.5 and decrease for RCP8.5. Three climate models (RACMO-EARTH, CCLM-CNRM, HIRHAM-NorESM) project an increase of discharge between 15.2% and 67.7% whereas two models (CCLM-ESM, CCLM-EARTH) indicate a decrease between 21.8% and 42.9%. The precipitation signal is reflected by the discharge change across all models. The ensemble mean suggest an increase of discharge for both emission scenarios. High future discharge gains correspond to increasing return levels as observed in section 6.3.1.2. For example, RCP4.5 of HIRHAM-EARTH shows a very large discharge increase and high positive changes of return levels whereas discharge and return levels of CCLM-EARTH are predicted to decrease (see Figure 6-6). Table 6-1 gives an overview over selected studies that investigate the impact climate change on hydrology. The range of future discharge change reported by these studies roughly corresponds to the ranges presented in Table 6-6 with the exception of RCP4.5 of HIRHAM-EARTH.

Table 6-6: Mean relative change of mean annual discharge/suspended sediment yield (SSY) as projected by the climate model ensemble for the future period (2021 – 2050) compared to the historical period (1971 – 2000). CCLM-ESM-UC refers to the uncorrected data. The mean annual discharge simulated using observed climate data is 133.6 mm.

RCM-GCM	Historical discharge (mm)	Discharge change RCP 4.5 (%)	Discharge change RCP 8.5 (%)	Historical SSY (t/ha/year)	SSY change RCP 4.5 (%)	SSY change RCP 8.5 (%)
HIRHAM-EARTH	167.8	207.5	-5.8	0.0911	217.3	-4.8
CCLM-ESM	173.8	-21.8	-24.7	0.0969	-21.2	-24.8
RACMO-EARTH	202.1	15.2	43.4	0.1121	14.1	44.4
CCLM-EARTH	178.9	-42.9	-27.4	0.0980	-45.0	-26.6
CCLM-CNRM	183.3	31.6	63.8	0.1014	30.4	64.4
HIRHAM-NorESM	162.6	29.4	67.7	0.0898	23.4	59.5
CCLM-ESM-UC	167.8	-8.5	-30.1	0.1760	-7.1	-29.6
Ensemble mean	173.8	36.5	19.5	0.1093	36.5	18.7

In general, changes in discharge can be explained by the combination of the climate model predictions regarding precipitation, temperature and accordingly potential evapotranspiration. Increased temperature will amplify evapotranspiration, which results in decreased runoff assuming stable or decreasing precipitation while increased rainfall leads to increased discharge assuming temperature/evapotranspiration stagnates or is reduced. In addition to the direct effects through changed rainfall and temperature characteristics, feedbacks with soil and vegetation properties as well as land use change may have an even stronger impact on change in water discharge (Mullan et al., 2012; Slaymaker, 2001) but are not considered in the present study due to limited knowledge and model restrictions. The sensitivity of discharge simulated by SHETRAN to changes in precipitation and potential evapotranspiration (ETp) is shown in Figure 6-8. The correlation between precipitation and simulated discharge (Figure 6-8a) is positive while the relationship between ETp and discharge (Figure 6-8b) is negative. Both relations are statistically significant. For RCP4.5 an increase of precipitation by 20% leads to an increase in discharge of 100% while an increase of ETp by 20% results in a negative discharge change of 161%. For RCP8.5 the same increase in precipitation would lead to an increase of discharge of 68% and an increase in ETP of 20% would result in a discharge change of -156%. These numbers and the comparison of the regression slopes between precipitation and ETp suggest that a changing

ETp has a stronger impact on discharge then precipitation. This is not always the case as shown by Yira et al. (2017) who identified precipitation as major factor whereas ETp is reported to have no significant influence on discharge as the environmental system is water limited and not energy limited. Differences between the models (SHETRAN, WaSiM) and their paramterisation (Op de Hipt et al., 2017; Yira et al., 2016).

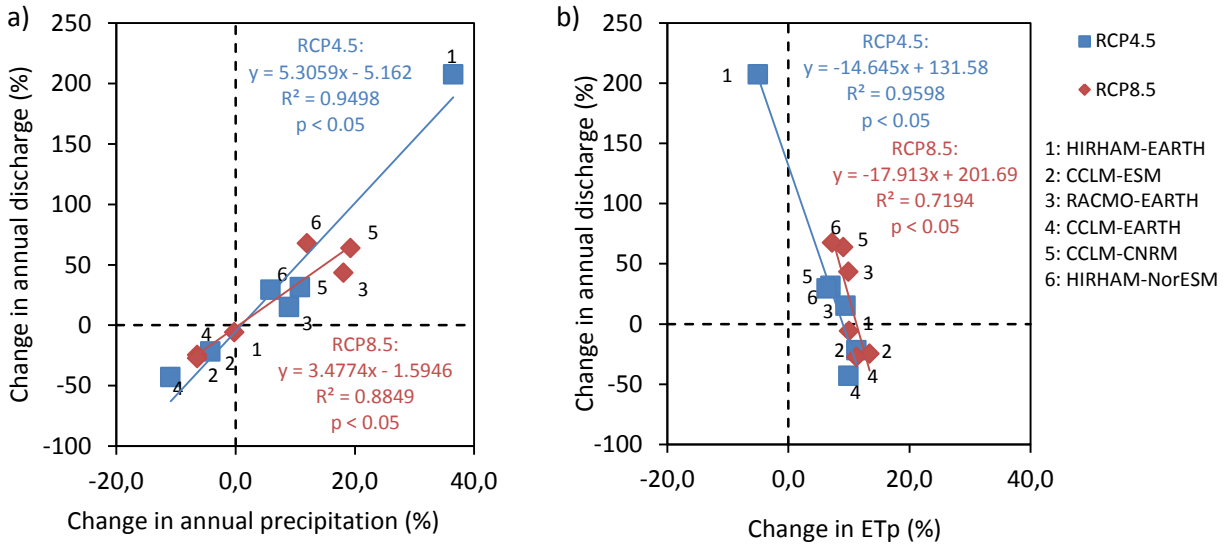

Figure 6-8: Simulated future discharge change vs. bias corrected annual precipitation change **(a)** and potential evapotranspiration (ETp) change **(b)** under emission scenarios RCP4.5 and RCP8.5. Relative changes are calculated by comparing the reference period (1971 – 2000) with the future period (2021 – 2050).

The mixed discharge signals result from uncertain precipitation predictions for the West African region due to the described difficulties in modeling the West African climate (Field and Barros, 2014). As a consequence, this uncertainty will be propagated as these data are required input to environmental models. Figure 6-9 shows the uncertainties of discharge simulations, which are attributed to the different climate model outputs. The large inter-annual and inter-model variability becomes evident and underlines the need to include several climate models in climate change studies in order to cover the range of possible developments (Sylla et al., 2016a; Zhang et al., 2011).

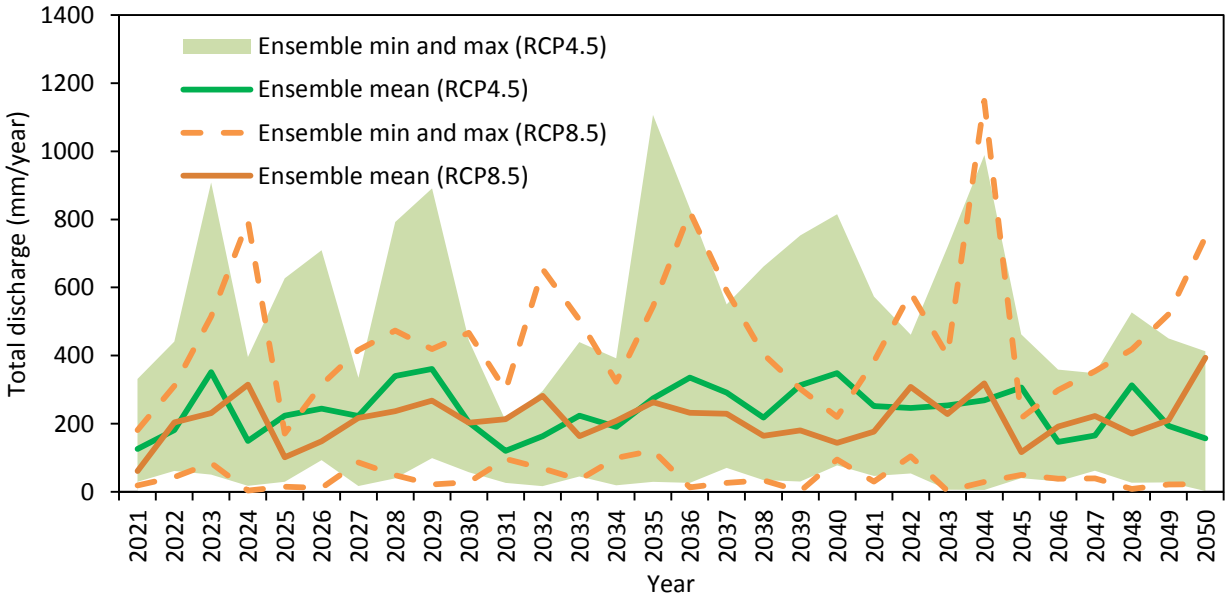

Figure 6-9: Annual total simulated discharge as projected by bias corrected data from the climate model ensembles for RCP4.5 and RCP8.5.

6.3.2.2 Soil erosion

6.3.2.2.1 Historical simulated soil erosion

The specific suspended sediment yield (SSY) simulated with observed precipitation and temperature data (observed SSY) is compared to the SSY simulations fed with bias corrected precipitation and temperature data of the six RCMs-GCMs (modeled SSY). Figure 6-10 shows that all climate models lead to a higher modeled SSY compared to observed SSY. Since soil erosion is mainly driven by surface runoff, the described pattern is similar to what has been discussed before (see section 6.3.2.1.1). The use of uncorrected precipitation data leads to an extreme overestimation and to a temporal shift of peak SSY and is not recommended to assess the future impact of climate changes on soil erosion.

Performance measures (NSE, R^2, KGE) are used to express the capability of climate models to provide input data for SSY models. Data of all models are able to reproduce magnitude and timing of SSY derived from observed precipitation. The performance values range from 0.4 to 1. Further details are given in Table 6-5.

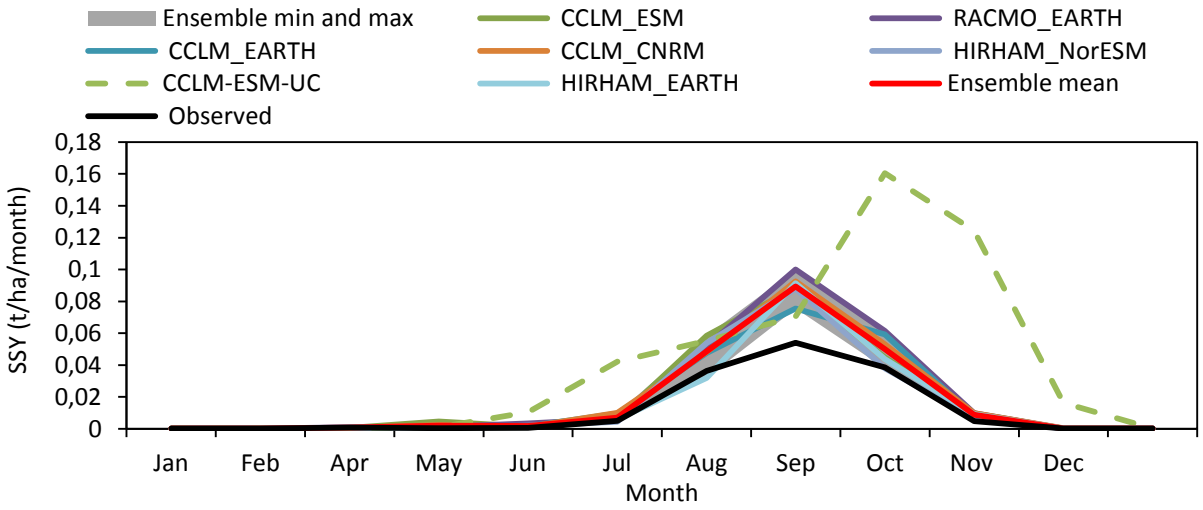

Figure 6-10: Observed and modeled precipitation based specific suspended sediment yield (SSY) as simulated for the reference period (1971 – 2000). CCLM-ESM-UC refers to the uncorrected data.

6.3.2.2.2 Future simulated soil erosion

The impact of climate change on soil erosion is investigated by comparing the relative differences between climate model driven historical simulations (1971 – 2000) and the future scenarios (2021 – 2050). Table 6-6 shows that three models predict an increase (14.1% – 64.4%) of soil erosion (RACMO-EARTH, CCLM-CNRM, HIRHAM-NorESM) while two models (CCLM-ESM, CCLM-EARTH) forecast a decreasing trend (21.2% – 45%) of soil erosion. The RCPs of HIRHAM-EARTH give a mixed signal. The erosion predictions follow the same trend as the precipitation and discharge predictions. The signal based on uncorrected precipitation data (CCLM-ESM-UC) correspond to the bias corrected counterpart. The unclear climate change signal is also stated by Li and Fang (2016) who reviewed more than 200 climate impact studies indicating increasing and decreasing future erosion trends. They underline that future uncertainty in erosion is above all a result from uncertainty in precipitation predictions.

The described change of future erosion rates can be explained by direct and indirect, positive and negative climatic impacts on soil erosion. Changing spatiotemporal patterns and magnitudes of precipitation are expected to directly influence hydrological processes like runoff (Figure 6-8) and consequently soil erosion rates through altered conditions of soil/sediment entrainment and transport. Increased soil erosion rates are sometimes reported even if the precipitation sum is expected to decrease (Nunes et al., 2013). This can be explained by increased rainfall intensi-

ties as also predicted by some RCMs-GCMs for the present study catchment (see Figure 6-6). Especially semi-arid environments, in which Hortonian runoff dominates, are susceptible to increased rainfall intensities. The importance of extreme precipitation events for annual specific suspended sediment yield is also reflected by our data. In average around 25% of the predicted annual SSY across all models originates from maximum daily SSY. The analyses of predicted return levels (see section 6.3.1.2) and the comparison of historical with future monthly maximum precipitation (data not shown) show that the contrasting combination of decreasing precipitation sums and increasing erosion rates as a result of increasing precipitation intensities are not observed in this study.

Indirect impacts are expected from changing temperatures which may lead to altered vegetation zones, plant properties and changed vegetation phases. Agricultural adaption strategies like revised planting and harvesting dates and new crops may also lead to increase or decrease of soil erosion rates. However, the impact of climate change does not need to be negative as increased precipitation, temperature and CO_2 concentrations may increase plant biomass, vegetation canopy and the growing season (Li and Fang, 2016). As already stated above the relationships and complex feedback mechanisms between hydrology and consequently soil erosion and climate as well as land use change are very complex. A combined analysis of the impact of land use and climate change may lead to increased erosion rates as human induced land use change is expected to negatively affect discharge and accordingly soil erosion (Yira et al., 2016). Furthermore, cultivated soils are considered to be more susceptible to climate change than the uncultivated counterparts (Nunes et al., 2013). The indirect impacts like human or climate induced land use change may be even stronger than the direct effect of climate change (Latocha et al., 2016; Li and Fang, 2016).

Figure 6-11 shows the mean monthly SSY of all climate models and scenarios. The distinct differences between models reflect the large uncertainties of future climate and erosion predictions. The largest erosion rates are predicted by RCP4.5 of HIRHAM-EARTH for the rainy season (Figure 6-11a). A substantial amount of uncertainty is also added by RCP4.5 of HIRHAM-EARTH which predicts monthly erosion rates to be up to 5.7 times higher than the model mean. Except for HIRHAM-EARTH predicted erosion rates are similar for RCP8.5.

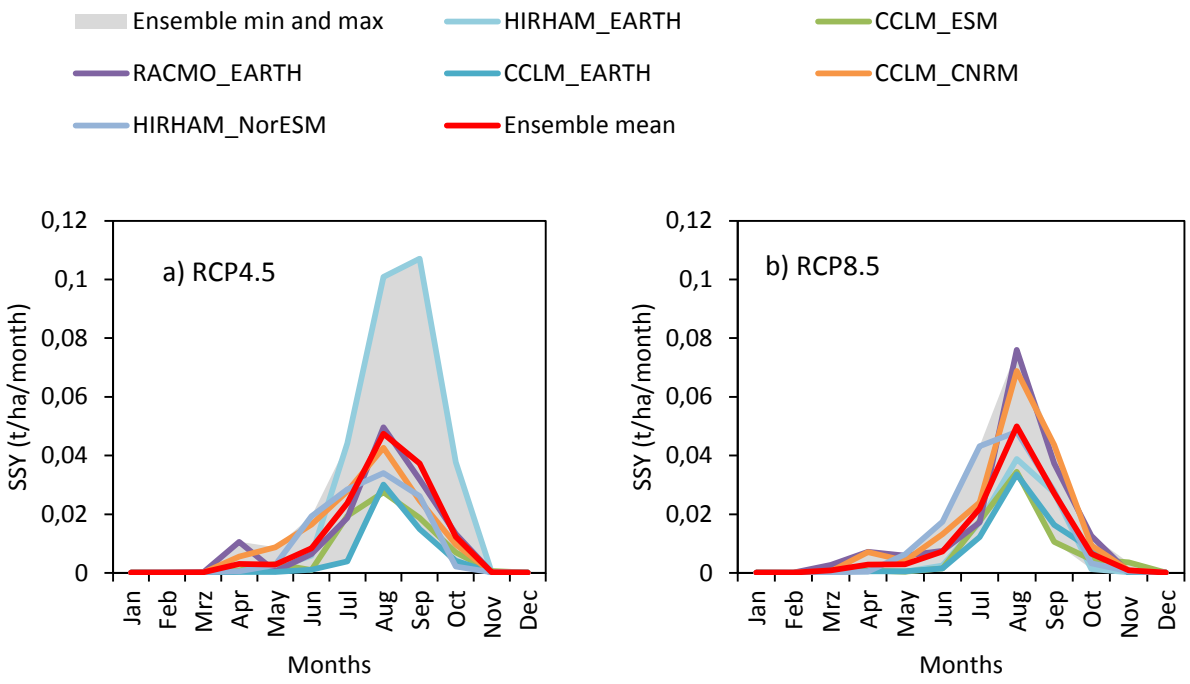

Figure 6-11: Mean monthly specific suspended sediment yield (SSY) as simulated using bias corrected data from the climate model ensembles for RCP4.5 **(a)** and RCP8.5 **(b)** (2021 – 2050).

Predicted annual SSY (0.11 t/ha/year – 0.13 t/ha/year for all models and RCPs) are considerably lower than current global erosion rates which are estimated to be 10.2 t/ha/year (Li and Fang, 2016). Schmengler (2010) investigates current soil erosion in the same area using the WATEM/SEDEM modeling approach and reports simulated SSY between 0.4 t/ha/year and 3.4 t/ha/year. It is worth to underline that SHETRAN was calibrated and validated using turbidity derived suspended sediment loads (SSL) as these data were available (Op de Hipt et al., 2017). Consequently, SSY of the suspended sediment fraction are lower than sums across all fractions. However, as the model was calibrated using SSL, only the suspended sediment fraction is considered. This explains why the simulated erosion rates are substantially lower. Despite the high vulnerability of savannas to soil degradation caused by water erosion, the low erosion rates in the Dano watershed are also caused by the gentle hillslope gradients.

Comparable analyses of future impact of climate change on soil erosion are rare for West Africa in general and especially on a watershed scale as used in this study (Li and Fang, 2016; Walling, 2009). Yang et al. (2003) assessed the impact of future climate change on soil erosion on the global scale and reports an increase for the African continent. Studies conducted on a small-

er scale suggest a mixed signal ranging from a decrease in soil erosion by 5% to 27% (Hiepe, 2008) to no change (Bossa et al., 2014) (see Table 6-1). However, given the small number of studies, different climate models, different spatial scales, varying environmental conditions and modeling approaches a direct comparison between the studies is challenging.

6.4 Conclusion

The present study assessed the impact of climate change on hydrological and soil erosion processes by the mid-21st century by using data from the CORDEX-Africa project to feed the hydrological and soil erosion model SHETRAN.

1) We showed by the comparison of uncorrected and bias corrected precipitation data with observed data, that the application of bias correction - although frequently criticized - is necessary to enable realistic simulations of discharge and soil erosion. Uncorrected data overestimate precipitation and result in wrong temporal pattern compared to observed data. Although the overestimation was reduced and the timing improved, bias correction was not able to completely remove the biases. The six climate models fairly agree with observed temperature. A negative deviation of up to -3° C and the importance of temperature for the calculation of ETp motivated the bias correction of temperature.

2) All climate models except RCP4.5 of HIRHAM-EARTH predict an increase in uncorrected and bias corrected temperature between 0.9° C and 2° C. The future precipitation signal is not consistent. Some climate models (RACMO-EARTH, CCLM-CNRM, HIRHAM-NorESM) predict an increase, others a decreased or mixed signal (HIRHAM-EARTH, CCLM-ESM, CCLM-EARTH. Bias correction mostly did not alter the climate change signal of precipitation and if so (RCP4.5 of CCLM-ESM) it was attributed to a small climate change signal (0.0%) that was manipulated by the bias correction. The impact of climate change on return levels differs between models, return periods and emission scenarios. Most models predict small changes of return levels ranging from -11% to +21%. However, RCP4.5 of HIRHAM-EARTH and both RCPs of HIRHAM-NorESM show high increases in return levels which can be explained by improbably high precipitation rates which remain despite bias correction.

3) The comparison of simulated discharge and SSY derived from observed precipitation and temperature with simulated discharge and SSY derived from climate model data reveals that discharge and SSY simulated with input data from climate models is higher. This is attributed to an overestimation of modeled precipitation, which persists even after bias correction. However, the performance measures were good when bias corrected

precipitation and temperature were used supporting the application of bias correction. Furthermore, the example of CCLM-ESM, which was run with and without bias corrected data, showed that neither the discharge nor the SSY signal were changed after bias correction. However, testing all climate models in the same way would be interesting but not possible due to the runtime of SHETRAN.

4) The impact of climate change on discharge and soil erosion was evaluated by comparing the historical period (1971 – 2000) with the future period (2021 – 2050). Three out of six climate models predict an increase of discharge and SSY (RACMO-EARTH, CCLM-CNRM, HIRHAM-NorESM) while the signals of two models are negative (CCLM-ESM, CCLM-EARTH). HIRHAM-EARTH predicts a mixed signal. The bias corrected precipitation signals are maintained by discharge and SSY. The ensemble mean suggests an increased discharge between 27.1% and 59.8% and an increased SSY of the same order. However, uncertainties resulting from the RCM-GCM outputs are large.

The bias correction, the model timestep, the model assumptions of SHETRAN and the measured precipitation data may play also an important role regarding the overall uncertainty but couldn't be explicitly addressed in the present work. In this context, we have to stress the large uncertainty of how the discharge in this catchment will develop by 2050. This is in agreement with other climate change studies in the region and has implications for possible climate change adaption strategies as potential discharge increase and decrease need to be considered.

This study supports the need for an improved climate observation network and climate projections for the region as they play a key role for the assessment of climate change impact on hydrology and soil erosion. Predicted soil erosion changes, ranging from -45% up to +217.3%, may strongly be increased or decreased if feedbacks between climate driven land cover changes as well as possible agricultural adaption strategies are included in a more complex model environment. Much progress has to be done, before reliable predictions of future soil erosion in West Africa are achieved.

7 MODELING THE EFFECT OF LAND USE AND CLIMATE CHANGE ON WATER RESOURCES AND SOIL EROSION IN A TROPICAL WEST AFRICAN CATCHMENT (DANO, BURKINA FASO) USING SHETRAN

Abstract

This study investigates the effect of land use and land cover (LULC) change on catchment hydrology (mean annual water yield, actual evapotranspiration) and soil erosion (suspended specific sediment yield) in the Dano catchment in south-western Burkina Faso based on hydrological and soil erosion modeling. The past LULC change is studied using land use maps of the years 1990, 2000, 2007 and 2013. Based on these maps future LULC scenarios were developed for the years 2019, 2025 and 2030. The observed past and modeled future LULC are used to feed SHETRAN, a hydrological and soil erosion model. Observed and modeled climate data cover the period 1990 – 2030.

The isolated influence of LULC change assuming a constant climate is simulated by applying the seven LULC maps under observed climate data of the period 1990 – 2015. The isolated effect of climate scenarios (RCP4.5 and 8.5) derived from the CCLM4-8 climate model is studied by applying the LULC map of 1990 to the period 1990 – 2032. Two chronological and continuous simulations were used to estimate the impact of LULC in the past (observed LULC and climate data) and in the future (modeled LULC and climate data) by gradually applying the LULC maps. These simulations consider the combined impact of LULC and climate change.

The land use assessment of the past suggests a decrease of savanna at annual rates of 1.15% while cropland and settlement areas have increased since 1990. The extension of cropland and settlements may be caused by a high population growth rate of 3%. The trend of cropland and settlement extension is maintained by the future land use scenarios.

The simulations that assumed a constant climate and a changing LULC show increasing water yield (3.9% – 77.5%) and mainly increasing specific sediment yield (-1.4% – 115.78%). The simulations that assume constant LULC and climate as changing factor indicate increases in water yield of 24.5% to 46.7% and in sediment yield of 31.1% to 54.7%. The continuous simulations signal a clear increase in water yield (20.3% – 73.4%) and specific sediment yield (24.7% to 90.1%). Actual evapotranspiration is estimated to change across all simulations by -6.8% to +3.3%.

7.1 Introduction

Population and economic growth are considered to be the most important drivers of land degradation. Human-driven land use and land cover (LULC) changes influence water resources and may intensify land degradation by water-related soil erosion and nutrient depletion (CILSS, 2016; UNEP, 2012). Especially in countries with fragile ecosystems, limited water and soil resources, changes in the hydrological cycle through LULC changes may lead to an increased flood and drought risk as well as accelerated erosion rates. Understanding the effect of LULC change on water and soil resources is paramount especially in countries whose societies are highly dependent on rain-fed agriculture. The population in Burkina Faso is growing at annual rates of about 3% in the last decade (The World Bank, 2017). The growing food demand and the expansion of settlement areas lead to LULC change through the conversion of savanna vegetation to cropland and settlement area. The increased pressure on natural resources such as soils may reduce the agricultural production through nutrient depletion and loss of fertile soil through soil erosion (CILSS, 2016). Assessing the long term impact of LULC change on runoff generation and soil erosion is therefore important for decision makers to plan environmental protection measures. However, the number of studies that investigate the feedback mechanisms between LULC change, runoff generation and soil erosion is limited in West Africa. This study aims to analyze the hypothesis of accelerating soil loss by a LULC conversion from savanna to cropland or settlement.

Hydrological processes and soil erosion are closely linked and strongly controlled by LULC. Sustainable management of water and soil resources require a combined consideration of water and sediment fluxes (Diekkrüger, 2010). LULC change impacts can be studied by comparing field measurements of hydrological and soil erosion variables from different LULC classes (Braimoh and Vlek, 2004; Giertz et al., 2010, 2005; Hiepe, 2008). Field measurements show that a change from savanna or forest vegetation to cropland can reduce soil hydraulic conductivity and increased surface runoff and soil erosion. This can be explained by the reduction of macroporosity as result of decreased biological activity following the disturbance of the soil by agricultural activities (Giertz et al., 2005). However, measurement of soil erosion is often not possible over the required temporal and spatial scale. Field studies have therefore to be complemented by hydrological and soil erosion modeling studies. Hydrological and soil erosion models have been used to predict the effect of land use and climate change on soil erosion and to identify hot spots of soil erosion that require erosion control measures (Bossa et al., 2014; Hiepe, 2008; Pandey et al., 2016). If available, LULC maps from different years may be used as input into hydrological and soil erosion models to simulate the effect on runoff and soil erosion. Increased runoff and

soil erosion rates are often predicted by hydrological and soil erosion models if the natural vegetation is converted to arable land (Bossa, 2012; Hiepe, 2008; Yira et al., 2016).

Different model concepts exist (empirical, conceptual and physically based models) among which physically based spatially distributed models are considered suitable for the analyses of LULC impacts on erosion at smaller scales as a certain complexity is necessary for the predictions of the changing LULC conditions (Pandey et al., 2016). The parameter values of these model types have a physical meaning and therefore can be better estimated which increases the quality of the simulated output (de Vente et al., 2013; Merritt et al., 2003; Pandey et al., 2016). The capabilities of different models (USPED, KINEROS2, EROSION3D, LISEM, WATEM-SEDEM) were compared to a list of predefined criteria in order to decide which model meets the requirements. Conceptual and empirical models were discarded as they may not differentiate between the processes (e.g. USPED) or they may not allow an identification of the sources and sinks (e.g. KINEROS2). The hydrological and soil erosion model SHETRAN (Birkinshaw et al., 2010b; Ewen et al., 2000) has been successfully applied to simulate effects of changing LULC (Bathurst et al., 2011; Lukey et al., 2000, 1995). SHETRAN studies used several approaches to investigate the impacts of a changing LULC. On the one hand, hypothetical scenarios derived from a simple change of vegetation properties (Bathurst et al., 2011; Birkinshaw et al., 2010a; Lukey et al., 2000, 1995) are used and on the other hand the analyses of observed land use in different catchments were compared to reflect changed LULC (Elliott et al., 2011). One novelty of the present study is therefore the combined investigation of observed and future LULC change in the same catchment over more than 20 years using SHETRAN.

The LULC change in the catchment is driven by a high population growth rate (3% per year) leading to the expansion of cropland at the expense of savanna as it is frequently observed in West Africa (CILSS, 2016; Codjoe, 2004; Yira et al., 2016). The principle motivation of the present study is to fill the knowledge gap regarding the impact of LULC change on runoff generation and soil erosion. Studies on these topics are rather limited in West Africa but work on the impact of LULC change on hydrological processes (Yira et al., 2016) and on the general modeling of soil erosion without changing LULC influences (Op de Hipt et al., 2017; Schmengler, 2010) in the present study catchment exist. Despite these studies a clear knowledge gap was identified regarding the assessment of past and future impacts of LULC change on soil erosion. Furthermore, the combined consideration of LULC and climate change is frequently identified as future research objective (Yira, 2016). We aim to fill this gap by a combined assessment of LULC and climate change over a period of 40 years (1990 – 2030). The SHETRAN model was set up to

simulate and to evaluate the impacts of these changes. SHETRAN was already calibrated and validated in the present study catchment (Op de Hipt et al., 2017).

Based on the above described research gaps, the present study aims to:

1. Investigate the observed past and the modeled future LULC change using seven land use maps.
2. Assess the isolated and combined impact of LULC and climate change on simulated mean annual water yield and mean annual actual evapotranspiration.
3. Examine the isolated and combined effect of LULC and climate change on mean annual suspended sediment yield and compare the contribution of different sediment sources (land use, channel, hillslope).

7.2 Methods

7.2.1 Study area

The studied catchment has a size of 126 km² and is located in the south-west of Burkina Faso, West Africa (Figure 7-1). The study site is part of three focal watersheds of the WASCAL program (West African Science Service Center on Climate Change and Adapted Land Use, www.wascal.org). WASCAL is a multidisciplinary program investigating the influence of climate and land use / land cover change on human and environmental systems.

The natural vegetation is characterized by the Sudanian region with wood, shrub and arboraceous savanna and abundant annual grasses. A growing population (growth rate of 3%) and the resulting demand for cropland and settlements lead to a reduction of the areas covered by savanna vegetation (Yira et al., 2016). The dominant cultivated crops are sorghum (*Sorghum bicolor*), millet (*Pennisetum glaucum*), maize (*Zea mays*), cowpeas (*Vigna unguiculata*) and groundnut (*Arachidis hypogaea*). Cotton (*Gossypium hirsutum*) is the main cash crop.

The watershed is characterized by a slightly undulating landscape with low slope gradients (average and maximum gradients are 1.8° and 21°, respectively, Figure 7-1b) and an elevation (Figure 7-1c) ranging from 269 to 504 m above sea level (masl). Annual precipitation range from 800 to 1200 mm/a for the period 1951 – 2005 (Schmengler, 2010). The annual rainfall dynamic is characterized by a distinct rainy season (May to October) and a dry season from November to April.

Soils are dominated by plinthosols (73%) according to the World Reference Base (WRB) for soil resources (IUSS Working Group, 2006). Plinthosols are characterized by high content of coarse

particles and a plinthic subsurface layer. Soils of the valley bottoms are mainly gleysols. Other soils formed in the region are cambisols, lixisols, leptosols and stagnosols (Figure 7-1e).

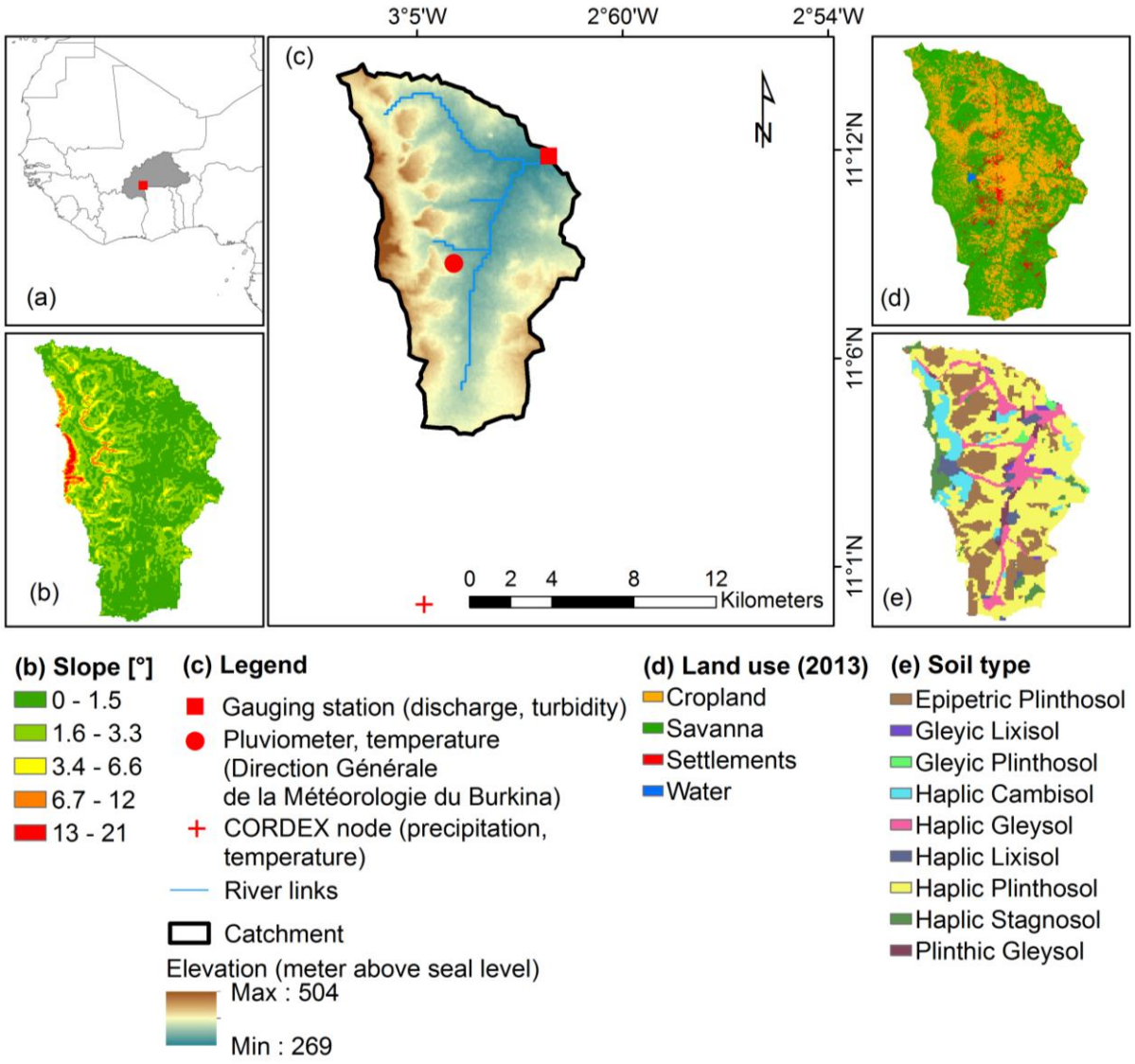

Figure 7-1: Location map of the Dano catchment: **(a)** location of the catchment and Burkina Faso in West Africa, **(b)** slope of the catchment, **(c)** model catchment, **(d)** land use map (Forkuor, 2014), **(e)** soil map (data base: soil survey done by Ozias Hounkpatin, Soil Science of Institute of Crop Science and Resource Conservation, University Bonn). DGM refers to the Direction Générale de la Météorologie du Burkina.

7.2.2 Data sources

SHETRAN requires various input data to simulate hydrological and soil erosion processes (Table 7-1). Some of the listed data sets are already available from previous studies and from

literature. However, the existing data were complemented by a hydrological and meteorological measurement network that was installed during the years 2012 to 2015. Among others, five automatic weather stations including pluviometers (stations 1 to 5 in Figure 7-1c), one water level and one turbidity probe were installed. Furthermore, an extensive soil survey was conducted to analyze physical and chemical soil properties and to retrieve the necessary soil and hydrological parameters required by the model. Meteorological data used to simulate the period before the installation in 2012 were collected from the climate station (station 6 in Figure 7-1c) operated by the national meteorological service (Direction Général de la Météorologie du Burkina, DGM). Precipitation and temperature for the period 1990 – 2032 were derived from CCLM4-8 climate model in the framework of the Coordinated Regional climate Downscaling Experiment (CORDEX) project. The Representative Concentration Pathways (RCP) 4.5 and 8.5 were used.

Table 7-1: Applied datasets and required inputs for SHETRAN

Data set	Resolution/time scale	Source	Required parameters
Topography	90 m	SRTM (Jarvis et al., 2008)	
Soil	1:25 000	Soil survey	Soil hydrological parameters (α, n[1)], K_{sat}[2)], θ_{sat}[3)], θ_{res}[4)]) texture etc.
Land use maps	5 to 250 m	Forkuor (2014), Landmann et al. (2007)	Land use type distribution
Land use characteristic		Literature	LAI[5)], Strickler coefficient, ETa/ETp ratio[6)]
Meteorological data	Hourly, Daily	Instrumentation WASCAL, DGM, CORDEX[7)]	Rainfall, temperature, humidity, solar radiation, wind speed
Discharge	Hourly	Instrumentation WASCAL	Discharge
Erosion	Hourly, Event	Instrumentation WASCAL	Suspended sediment load, soil erosion rate

[1)] α and n are van Genuchten empirical parameters, [2)] K_{sat} refers to the saturated hydraulic conductivity, [3)] θ_{sat} to the saturated water content, [4)] θ_{res} to the residual water content, [5)] LAI to the leaf area index and [6)] ETp/ETa ratio to the ratio of potential evapotranspiration to actual evapotranspiration, 7) Coordinated Regional climate Downscaling Experiment project

7.2.3 Modeling approach

7.2.3.1 Land use change

Observed LULC maps from four different years (LULC_1990, LULC_2000, LULC_2007, LULC_2013) and modeled future LULC maps (LULC_2019, LULC_2025, LULC_2030) were available to assess past and future impact of LULC change on hydrology and soil erosion. The

three maps that show the status from 1990 to 2007 were derived from Landsat TM (http://glovis.usgs.gov/) and MODIS (https://mrtweb.cr.usgs.gov/) images by Landmann et al. (2007). The map of 2013 created by Forkuor (2014) is based on Landsat TM and RapidEye images (https://www.planet.com/products/#satellite-imagery). As the maps are available at different resolutions, they were resampled based on majority to match the resolution of 200 m. Both authors used the Land Cover Classification System (LCCS) legend from the Food and Agricultural Organization (FAO). For the model warm-up climate data from 1990 to 1996 and the land use map LULC_1990 is applied.

- **The observed LULC maps (simulations M1_1990 – M5_90/13):** In order to homogenize the LULC classes for each of the four maps, the initial LULC classes of the years 1990 to 2007 were reclassified. The four classes of the year 2013 were the basis for the reclassification process. The reclassification was done based on the approach described in Yira et al. (2016): Classes with similar characteristics regarding seasonality of vegetation cover and hydrological properties were grouped (Table 7-2). The resulting land use maps (LULC_1990– LULC_2013) were used to simulate the effect LULC change on water and soil resources in the past.

  The simulation M1_1990 is considered as the reference and applies the land use map LULC_1990 over the entire simulation period (1990 – 2015). Simulations M2_2000 – M4_2013 apply the land use maps LULC_2000, LULC_2007 and LULC_2013 to the period 1997 – 2015. During these simulations climate is held constant in order to study the effect of LULC change only. The simulation M5_90/13 encompasses the chronological land use development as it has occurred in the catchment. The four land use maps (LULC_1990, LULC_2000, LULC_2007, LULC_2013) are gradually applied to the periods 1990 – 1996, 1997 – 2003, 2004 – 2010 and 2011 – 2015. An overview of the different simulations is given in Table 7-3.

- Based on the changes between the observed maps LULC_2000 and LULC_2013, future LULC maps were developed for the years 2019, 2025 and 2030 by using the Land Change Modeler (Clark Labs, Clark University, Worcester, USA). The approach used by the Land Change Modeler is based on transition potentials which are calculated using a Multi-Layer Perceptron (MLP) neural network (Chan et al., 2001). The transition potentials for the future depend on the transitions that have already occurred in the past. As explanatory variables several distance maps were used (distance to roads, fields and settlements) as well as spatially autocorrelated maps of the digital elevation model (DEM) and observed disturbances (transitions from savanna to crop or settlements). Finally a stochastic Markov chain tech-

nique (Wilson and Weng, 2011) is applied to simulate the probability of LULCC and generate the future land use maps.

- **The modeled scenarios (simulations M6_2019 – M12_90/30_RCP8.5):** Simulations M6_2019 – M8_2030 apply the land use maps LULC_2019, LULC_2025 and LULC_2030 to the period 1997 – 2015 using observed climate data. Climate is held constant in order to study the isolated effect of LULC change. The simulations M9_1990_RCP4.5 and M10_1990_RCP8.5 use modeled climate data (see section 7.2.3.2) of the period 1990 – 2032 assuming a constant LULC since 1990. These simulations enable the assessment of climate change as single factor. A chronological and continuous application of all LULC maps (M11_90/30_RCP4.5, M12_90/30_RCP8.5) was only possible through the use of precipitation and temperature from a climate model. Modeled precipitation and temperature (1990 - 2032) were used to drive the simulations M11_90/30_RCP4.5, M12_90/30_RCP8.5). Details of the modeled climate data are discussed in section 7.2.3.2.

  As the prediction of the development of areas covered by water is difficult based on a very small proportion of grid cells, the change of water areas was considered as stable after 2013. An overview of the different simulations is given in Table 7-3.

Table 7-2: Initial LULC classes as given by Landmann et al. (2007) and Forkour (2014) and reclassified classes used in this study

Initial LULC classes	Proportional area [%] per year							Reclassified LULC classes
	1990	2000	2007	2013	2019	2025	2030	
Regularly flooded, woody, closed to open	1.03	29.2	-	-	-	-	-	Tree and shrub savannah
Broadleaved forest, closed, evergreen (>=65%)	1.77	-	-	-	-	-	-	Tree and shrub savannah
Woodland, closed (40 – 65%)	5.22	-	-	-	-	-	-	Tree and shrub savannah
Woodland closed/forest closed	59.3	-	8.80	-	-	-	-	Tree and shrub savannah
reg. flooded, high confidence	1.16	-	-	-	-	-	-	Tree and shrub savannah
Burned area	4.03	2.64	-	-	-	-	-	Cropland
Bare soil scattered vegetation	1.00	-	-	-	-	-	-	Urban area
Regularly flooded wetland	0.84	-	-	-	-	-	-	Tree and shrub savannah
Herbaceous crops	8.28	-	-	-	-	-	-	Cropland
Herbaceous vegetation, closed (>=65%)	17.28	-	-	-	-	-	-	Tree and shrub savannah
Forest	-	3.45	15.5	-	-	-	-	Tree and shrub savannah
Grassland	-	35.1	46.7	-	-	-	-	Tree and shrub savannah
Cropland	-	16.1	20.4	36.3	42.3	48.3	54.5	Cropland
Wetland	-	13.2	1.52	-				Tree and shrub savannah
Urban area	-	0.16	6.54	5.19	7.19	9.19	11.1	Urban area
Water	-	-	0.42	0.39	0.39	0.39	0.39	Water
Natural/-semi-natural Vegetation	-	-	-	58.1	50.0	42.0	33.9	Tree and shrub savannah

The model has already been calibrated and validated using measured discharge and SSL from 2014 and 2015 (see sections 7.2.3.4 and 7.3.2 and for more detail Op de Hipt et al. (2017)). The model parameters and boundary conditions remain unchanged for the simulations. Therefore, LULC change is not reflected by changing parameters but the changing spatial patterns of the land cover classes. As the years 1990 – 1996 of each scenario were used as the warm-up phase to reach hydrological equilibrium conditions, the period 1997 – 2032 (evaluation period) was used to evaluate the effect of LULC change on average annual water components and on the average annual specific sediment yield. Statistical differences between the selected model outputs (water yield, actual evapotranspiration, specific sediment yield) between each model run was investigated on a daily basis using the Kruskal-Wallis test. Pairwise comparisons were studied by applying the Bonfferoni correction to results of Mann-Whitney U tests.

Table 7-3: LULC simulations, model periods and applied land use maps.

Data	Simulation	Simulation period						
		Warm-up period	Evaluation period					
		1990 – 1996	1997 – 2003	2004 – 2010	2011 – 2015	-	-	-
Observed climate and LULC maps	M1_1990	LULC_1990		LULC_1990		-	-	-
	M2_2000	LULC_1990		LULC_2000		-	-	-
	M3_2007	LULC_1990		LULC_2007		-	-	-
	M4_2013	LULC_1990		LULC_2013		-	-	-
	M5_90/13	LULC_1990	LULC_2000	LULC_2007	LULC_2013	-	-	-
Observed climate and modeled LULC maps	M6_2019	LULC_1990		LULC_2019		-	-	-
	M7_2025	LULC_1990		LULC_2025		-	-	-
	M8_2030	LULC_1990		LULC_2030		-	-	-
	Simulation	**Warm-up period**	**1997 – 2005**	**2006 – 2010**	**2011 – 2016**	**2017-2022**	**2023-2027**	**2028-2032**
Modeled climate and observed LULC map	M9_1990_RCP4.5	LULC_1990	LULC_1990					
	M10_1990_RCP8.5	LULC_1990	LULC_1990					
Modeled climate and modeled LULC maps	M11_90/30_RCP4.5	LULC_1990	LULC_2000	LULC_2007	LULC_2013	LULC_2019	LULC_2025	LULC_2030
	M12_90/30_RCP8.5	LULC_1990	LULC_2000	LULC_2007	LULC_2013	LULC_2019	LULC_2025	LULC_2030

7.2.3.2 Climate data

Two climate datasets were used in this study. Observed climate data for the period 1990 – 2015 were used to assess the influence of LULC change on hydrology and soil erosion. These data were collected by the national meteorological service. Historical (1990 – 2005) and future (2006 – 2032) precipitation and temperature data were retrieved from the regional climate model (RCM) CCLM4-8 (Climate Limited-area Modelling Community, Germany) driven by the global climate model (GCM) ESM-LR (Max-Planck-Institute for Meteorology, Germany). The Representative Concentration Pathways RCP 4.5 and RCP 8.5 (Moss et al., 2010) were used as future scenarios. The RCM-GCM simulation was run in the framework of the Coordinated Regional climate Downscaling Experiment (CORDEX-Africa, www.cordex.org). Due to the run time of SHETRAN and the small differences between the nodes the closest node was used only.

Historical precipitation and temperature data from CCLM-ESM model were compared with their observed counterparts for the period 1971 – 2000 to control if the modeled variables are in agreement with the observed. The modeled temperature shows a negative deviation compared to the observed temperature (Figure 7-2a). As temperature is used to calculate potential evapotranspiration (Oudin et al., 2005b) and has therefore strong effects on catchment hydrology, it

was bias corrected using the delta change approach described in Haddeland et al. (2012) (Figure 7-2b).

The comparison of modeled and observed precipitation indicates an obvious bias. Modeled precipitation is often higher than measured and a shift between the observed and the simulated timing of the rainy season can be observed (Figure 7-2c). Therefore, a bias correction method was used to correct the historical and future rainfall data derived from CCLM-ESM. The non-parametric quantile mapping approach introduced by Gudmundsson et al. (2012) was applied. The observed data were used to establish a transfer function which was applied to the historical and the future rainfall data. The differences between mean monthly precipitation from all climate models and the observed precipitation are considerably reduced after bias correction (Figure 7-2d).

The comparison of bias corrected precipitation and potential evapotranspiration between the periods 1990 – 2016 and 2017 – 2032 shows an increase of precipitation by 5.4% to 7.8% and an increase of ETp by 4.7% to 6%.

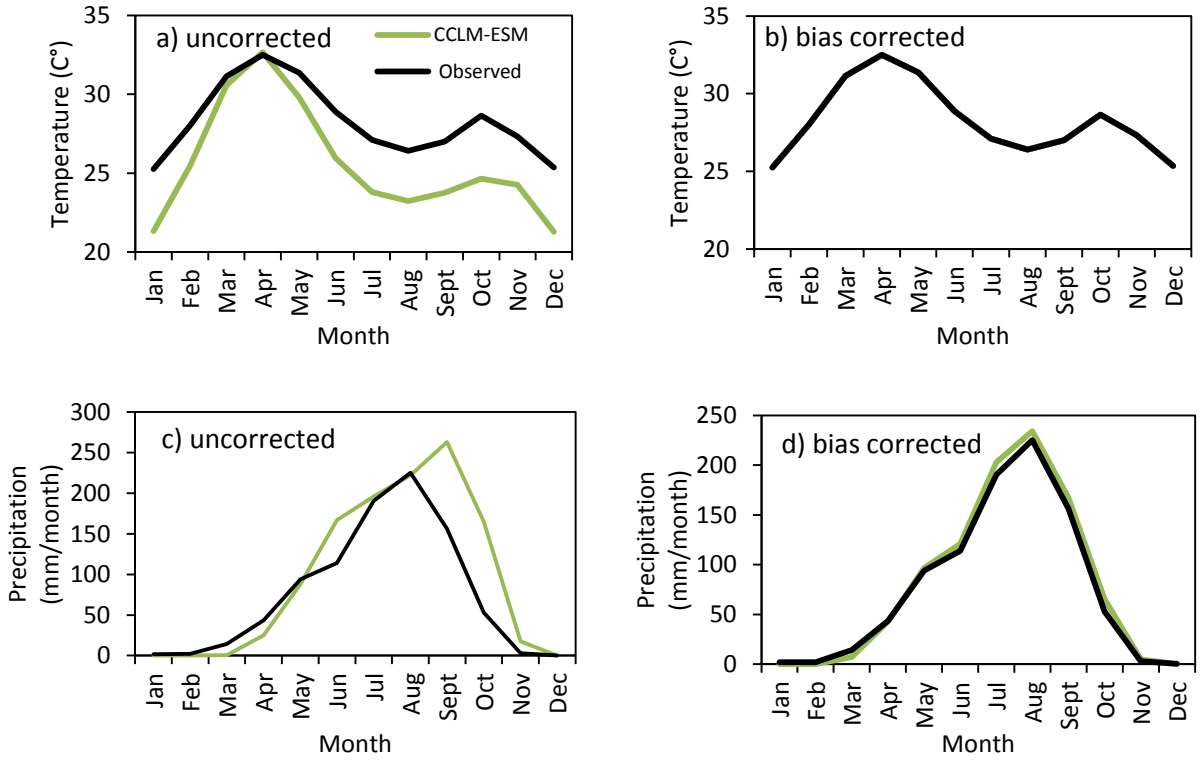

Figure 7-2: Uncorrected and bias corrected temperature **(a, b)** and precipitation **(c, d)**.

7.2.3.3 Model description

SHETRAN was selected in this study due to two main reasons. First, SHETRAN is able to simulate erosion on hillslopes as well as in the river which are both considered as important processes in the catchment. Second, it simulates continuously, which is necessary for land use comparisons over a given period. SHETRAN is a physically based spatially distributed hydrological soil erosion model. It is a derivative of SHE (Système Hydrologique Européen) which was jointly developed by the British Institute of Hydrology, the Danish Hydraulic Institute and the French consulting company SOGREAH (Abbott et al., 1986). SHETRAN has been refined and complemented by new components as e.g. the fully 3D simulation of subsurface water flow (Parkin, 1996) and sediment transport (Wicks, 1988; Wicks and Bathurst, 1996). Detailed information is available online (http://research.ncl.ac.uk/shetran/).

7.2.3.4 Model parameterization, calibration and validation

The model parameterization, calibration and validation are given in detail in Op de Hipt et al. (2017) and are briefly summarized here. The parameterization of soil properties was done based on data obtained from field measurements and additional literature analysis (Table 7-1, Table 7-4). Land use parameters were taken from literature. Although SHETRAN comprises numerous parameters that reflect the influence of the vegetation on hydrology we focused on two parameters: i) the ratio of actual evapotranspiration (ETa) to potential evapotranspiration (ETp) and ii) the Strickler coefficient (KSTR) that were reported to be sensitive regarding surface runoff (Bathurst et al., 2004; Birkinshaw et al., 2010a; Đukić and Radić, 2016; Zhang, 2015). Changes in the spatial distribution of LULC classes are considered using the different land use maps (see section 7.2.3.1 and 7.3.1). Erosion was described using four parameters (overland flow and rain drop soil erodibility coefficients, channel bank erodibility coefficient, threshold depth of loose sediment) that were adjusted based on literature (Adams and Elliott, 2006; Birkinshaw et al., 2010a; de Figueiredo and Bathurst, 2007; Elliott et al., 2011; Lukey et al., 2000, 1995; Norouzi Banis et al., 2004; Wicks and Bathurst, 1996) and calibration (Table 7-4).

Precipitation and potential evapotranspiration (ETp) are given as hourly time series for each of the five climate stations located in the studied catchment. Spatially distributed data, including digital elevation model (DEM), the soil and land use map, were used in a raster format with a grid resolution of 200 x 200 m. The long term meteorological data from station 6 (see Figure 7-1c) operated by the national meteorological service was only available on daily basis. This is critical since results of dynamic models such as SHETRAN respond sensitively to the chosen simulation time step (Bruneau et al., 1995; Hessel, 2005; Yira, 2016; Zhang, 2015) and conse-

quently the consideration of time and spatial scales is fundamental in hydrological modeling (Blöschl and Sivapalan, 1995). Yira (2016) reports a decreasing modeled discharge with increasing time step. This can be explained by the information loss during aggregation of rainfall data from sub-daily to daily resolution: It reduces the maximum intensities and therefore leads to an underestimation of overland flow due to infiltration excess as this depends on rainfall intensity and soil infiltration rate. Consequently, simulated discharge and hence sediment yield may be underestimated by the model. However, some SHETRAN studies also use a daily timestep (de Figueiredo and Bathurst, 2007; Mourato et al., 2015). Figure 7-3 shows that the exceedance probability do not change substantially between two simulations with different timesteps. Although an increase in timestep reduces surface runoff and sediment yield, this limitation cannot be avoided for the long-term simulations as no hourly data are available. Because all scenarios are influenced by the same effect, conclusions drawn from the analysis are not biased by the temporal resolution of the model runs.

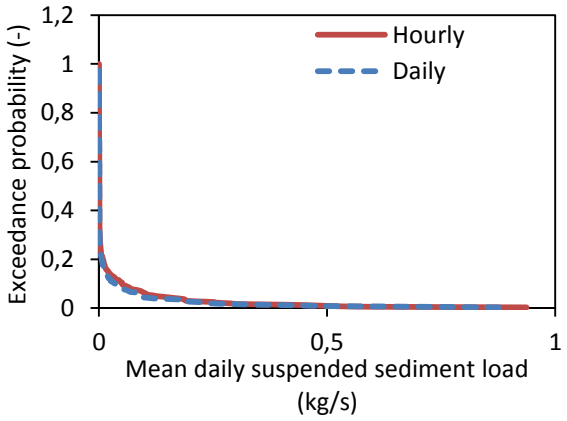

Figure 7-3: Exceedance probability of hourly and daily suspended sediment load

Although SHETRAN is physically based, land use and soil erosion related parameters were calibrated to adjust for model approximations and the spatial or temporal resolution of the input data. In the present study six selected parameters (Table 7-4) were calibrated based on the Latin Hypercube Sampling (LHS) methodology (McKay et al., 1979). Briefly, using LHS the possible multi-dimensional parameter space is sampled n times (usually n>100) in a stratified manner and the parameters are used in the simulation model to determine behavioral simulations (simulations which show an acceptable comparison with observed data). The hydrological component of SHETRAN was calibrated based on the observed hydrograph from 2014 to 2015. The soil erosion component was calibrated based on the observed suspended sediment load (SSL). The model performance was statistically evaluated by the coefficient of determination (R^2), the Nash-Sutcliff efficiency (NSE) (Nash and Sutcliffe, 1970) and the Kling-Gupta efficiency (KGE) (Gupta

et al., 2009; Kling et al., 2012) because a single quality measure is not sufficient for model evaluation. The model was validated using data from the year 2015.

Table 7-4: Soil, land use and erosion parameters in SHETRAN

Parameter	Description	Unit	Parameter range	Source
		Hydrology		
ETa/ETp at field capacity (varies with land use type)	Ratio of actual evapotranspiration to potential evapotranspiration at field capacity	-	0.01 – 1.99	Shuttleworth (1993)
KSTR (varies with land use type)	Strickler roughness coefficient	$m^{1/3}\ s^{-1}$	0.3 – 9.9	Mohamoud (1992), Shuttleworth (1993)
		Soil erosion		
k_f (soil invariant)	Overland flow soil erodibility	$kg\ m^{-2}\ s^{-1}$	2.54×10^{-11} – 4.68×10^{-10}	Calibration
k_r (varies with texture)	Raindrop soil erodibility coefficient	J^{-1}	0.19 – 7.9	Adams and Elliott (2006), Birkinshaw et al. (2010a), de Figueiredo and Bathurst (2007), Elliott et al. (2011), Lukey et al. (2000, 1995), Norouzi Banis et al. (2004), Wicks and Bathurst (1996)
BKB (soil invariant)	Channel bank erodibility coefficient	$kg\ m^{-2}\ s^{-1}$	1×10^{-6} – 3×10^{-6}	Calibration
DLSMAX	Threshold depth of loose sediment	mm	1×10^{-6} – 9.9×10^{-6}	Calibration

7.3 Results and discussion

7.3.1 Land use and land cover change

The LULC maps and changes of the period 1990 – 2030 are shown in Figure 7-4. The observed LULC maps (LULC_1990 – LULC_2013) show an increase of mainly cropland and settlement area at the expense of savanna areas, which have decreased by almost 30% between 1990 (86.69%) and 2013 (58.12%) whereas cropland has increased by almost 24% in the same period. An urbanization trend has occurred between 1990 and 2013 as shown by an increase in settlement areas by 4.1%. The area covered by surface water increases between 2000 and 2007 as the Moutouri reservoir was built in 2002. The future LULC change (LULC_2019 – LULC_2030) mainly follows the trend of the past. An increase of cropland (42.2%) and settlement areas (10.19%) between 1990 and 2030 is opposed to a decrease in savanna by 52.7%.

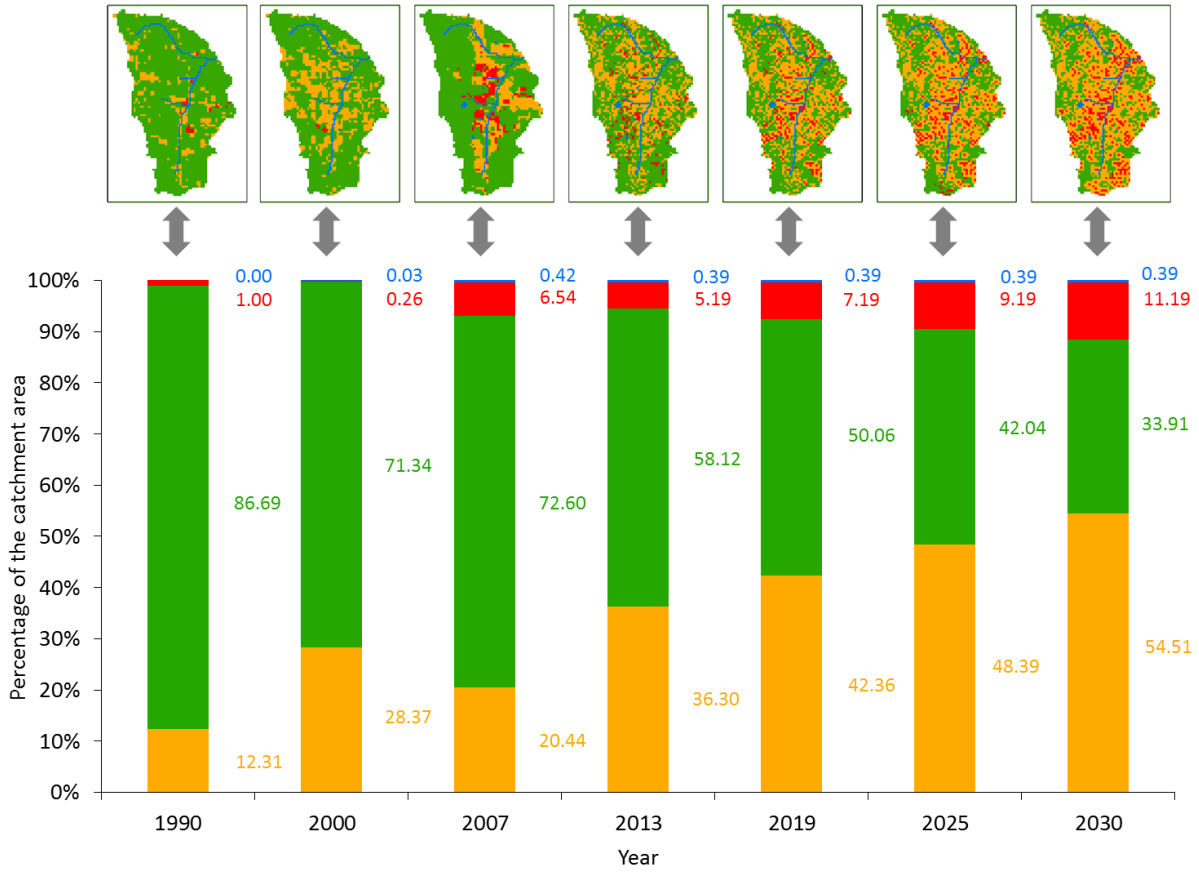

Figure 7-4: Observed (1990 – 2013) and modeled (2019 – 2030) LULC maps and the corresponding relative proportion of each land use.

Some inconsistencies are observed between the past LULC maps. This applies above all to the spatial distribution of settlements and the way how these areas are converted. It is especially observable between the maps LULC_1990 and LULC_2000 where settlement areas are reduced due to the unlikely conversion of settlements to savanna, water and cropland. Further unlike LULC changes are noticed between the other maps as for example between LULC_2000 and LULC_2007 where the settlement area is 25 fold increased over 7 years. The inconsistencies are of relatively low importance as the maximum proportion of cells characterized by an improbable change is < 7%. The LULC mapping of savanna areas is impeded due to the seasonality and the scattered LULC pattern (Cord et al., 2010; Forkuor, 2014). Therefore, the observed inconsistencies can be explained by a misclassification related to the difficulties of the LULC mapping of areas characterized by a distinct seasonality (Wagner et al., 2013). Another reason may be the resampling of the maps needed to attain the same grid resolution which discriminates the scattered land use classes (Yira et al., 2016).

The large visual and numerical differences between LULC_2007 and the other maps rectified the use LULC_2000 and LULC_2013 for the derivation of the future LULC maps. Two important issues have to be discusses in this context: First, the future LULC development only depends on the change that occurred between LULC_2000 and LULC_2013. Second, the future LULC may be afflicted with large uncertainties because important variables as population growth and agronomical developments are not available to improve the predictions. However, based on observations from the field and personal communication with local farmers, the distance to the farm house and the accessibility play an important role for cultivation.

An expansion of cropland at the expense of natural vegetation mainly due to increasing demand for agricultural areas as a result of the population growth and national migration is also reported by others (CILSS, 2016; Gray, 1999; Mahé et al., 2005; Ouedraogo et al., 2010; Paré et al., 2008; Stephenne and Lambin, 2001; Thiombiano and Kampmann, 2010). The present study assesses the increase of cropland by 0.95% per year while savanna is reduced by 1.14% per year for the observed period (1990 – 2013). Paré et al. (2008) studied the influence of population growth on land use change and reports conversion rates of 3.75% per year in the Sissili and Ziro provinces which are located in approximately 100 km distance to the study area. Although the exact number differ the major driver controlling LULC change in the study area is population growth and urbanization trends, which is also reported on the national level (CILLS, 2016). Future LULC maps suggest an increase of cropland of 42.2% till 2030. This corresponds to the scenarios used by Hiepe (2008) who reports increases between 56% – 119%. The deforestation in the catchment is directly related to the growing demand in firewood used among others for the production of local beer and remote areas are increasingly affected as the number of unprotected trees close to the main settlements diminishes. The logging of shea trees (*Vitellaria paradoxa*) used to produce shea butter for export may pose a problem in the future as it is an important financial income for small scale farmers. Another important cash crop is cotton whose production has increased by 350% since 1990 (FAOSTAT, 2017).

7.3.2 Hydrological and erosion modeling

The performance of SHETRAN regarding the hydrological and erosion modeling is discussed in Op de Hipt et al. (2017) and therefore only briefly summarized here. Based on the various performance measures (sum of R^2, KGE and NSE), several parameter sets gave satisfactory to good quality measures according to the equifinality concept introduced by Beven and Freer (2001). The given performance measures for discharge are in the range of 0.7 and 0.79 for calibration and between 0.66 and 0.76 for validation which is comparable to other studies that used SHETRAN (e.g. Birkinshaw et al., 2014; Đukić and Radić, 2016, 2014; Mourato et al., 2015;

Naseela et al., 2015; Tripkovic, 2014; Zhang, 2015). Among these studies R^2 and NSE values above 0.5 are frequently reported. Larger differences between simulated and observed discharge occur during low flow conditions where the observed discharge is frequently underestimated by the model. This is not surprising since low flow was not in the focus and consequently parameters controlling low flow such as K_{sat} in sub-surface soils were not considered during the calibration. Overestimated peaks during the rainy season can be attributed to the spatial assignment of climate stations, which was done using Thiessen polygons. This method may not be appropriate to account for localized precipitation events. Nevertheless, alternative interpolations methods like inverse distance weighting and Kriging may also be inadequate to reflect local storms as they smooth rainfall intensities over larger spatial extends.

In terms of erosion rates the NSE is 0.4 and 0.2 and the R^2 is 0.47 and 0.37 for calibration and validation of SSL respectively. These results are in the range of other studies (de Figueiredo and Bathurst, 2007; Elliott et al., 2011; Zhang, 2015) and comparable with other erosion models (de Vente et al., 2013; Jetten et al., 1999). Given the various sources of measurement uncertainty a NSE of larger than 0.7 can't be expected (de Vente et al., 2013).

7.3.3 Land use and climate change effects

7.3.3.1 Hydrology

Figure 7-5a) and Table 7-5 show the influence of land use on simulated mean annual water yield over the considered period (1997 – 2030). The simulations that were driven by the past observed climate and LULC maps (M1_1990 – M5_2015) indicate an increased water yield by 3.9% (M2_2000) to 36.7% (M3_2007). The water yield of the continuous simulation M5_90/13 is 20.3% higher compared to M1_1990. It shows that LULC change over almost 20 years has affected the water balance of the studied catchment.

Simulations driven by future modeled LULC maps and observed climate data (M6_2019 – M8_2030) show highest increases in discharge between 45.9% – 77.5% compared to M1_1990. Consequently, the predicted LULC change will lead to an increased discharge assuming a similar climate development as observed between 1990 and 2016.

Simulations M9_1990_RCP4.5 and M10_1990_RCP8.5 are driven by modeled climate data and the map LULC_1990 only, assuming no change of LULC since 1990. Consequently, the increased water yield of 24.5% (M10_1990_RCP8.5) and 46.7% (M9_1990_RCP4.5) is attributed to climate change only. In case of M9 and M10, the period 2006 – 2032 is compared to the period 1990 – 2005.

Simulations M11_90/30_RCP4.5 and M12_90/30_RCP8.5 are driven by a combined LULC and climate change. These simulations show high increases (50.2% – 73.4%) of discharge compared to the period 1990 – 2005. Consequently, the combined development of climate and LULC may intensify the future change of hydrological conditions in the catchment. The comparison between the groups M9/M10 and M11/M12 suggest that LULC change may have a larger impact on hydrology than climate change as the differences regarding the increase between M9/M10 (no LULC change) and M11/M12 (LULC and climate change) are relatively large.

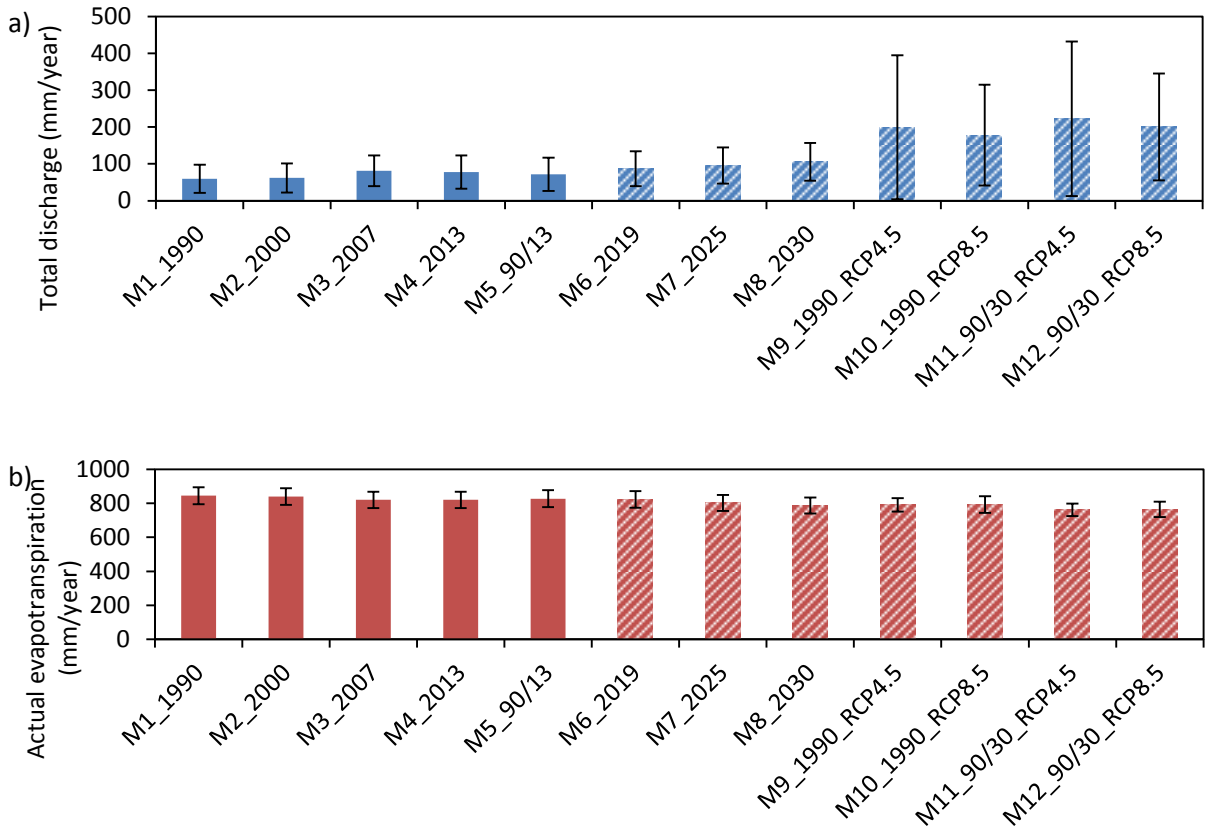

Figure 7-5: **a)** Mean annual total water yield for M1_1990 – M6_2030 and **b)** mean annual actual evapotranspiration for simulations M1_1990 – M6_2030. Error bars indicate the standard deviation. Dashed bars indicate the use of modeled LULC and/or climate.

Statistically significant ($p < 0.0007$) differences exist between almost all pairs. Exceptions are the M1_1990/M5_2013, M3_2007/M4_2013, M4_2013/M10_1990_RCP8.5 and M11_90/30_RCP4.5/M12_90/30_RCP8.5.

The effect of LULC and climate change on ETa is shown in Figure 7-5b. The simulations driven by observed data indicate that ETa decreases by between 0.5% and 2.88%. Simulations that

used modeled LULC maps and observed climate data (M6_2019 – M8_2030) show decreasing ETa (2.5% – 6.6%) compared to M1_1990. The simulations that use climatic predictions assuming constant LULC since 1990 (M9, M10) show an increasing ETa by about 3%. The largest change is predicted by the combined consideration of LULC and climate change as shown by simulations M11 (-1.5%) and M12 (-0.9%). Significant ($p < 0.0007$) differences compared to the reference the simulation M1_1990 exist for the majority of considered pairs.

The presented figures for simulations M1_1990 – M5_90/13 are similar to the results of Yira et al. (2016) who studied the influence of a changing LULC on the hydrology in the same area based on similar data using WASiM (Water Balance Simulation Model). He observed an increase in discharge of 20% between M1_1990 and M5_90/13. The general trend of increasing discharge and decreasing ETa is reported by others and LULC change was frequently responsible for this development (Bossa et al., 2014; Cornelissen et al., 2013; Mahé et al., 2005; Roudier et al., 2014; Yira et al., 2016). Bossa et al. (2014) studied the impact of climate and LULC change on hydrology in the Ouémé catchment in Benin. They assess the effect of different LULC scenarios on water yield to be between +3% and +8%. For the combined consideration of climate and LULC change they report a decreasing water yield over the period 2015 – 2019 according to the negative future precipitation signal. The influence of the future precipitation signal on water yield is also confirmed by Yira et al. (2017) and by the present study as CCLM-ESM shows a positive future signal for the considered period (2006 – 2032). However, conclusions drawn from simulations that use data from climate models have to be considered carefully as uncertainties of future precipitation predictions are large (Yira et al., 2017). Simulations M9 and M10 are afflicted with large inter-annual variabilities as indicated by the high standard deviation. These variabilities are a result from the precipitation as predicted by CCLM-ESM.

Regarding the consideration of LULC change only, the presented results are confirmed by experiments conducted on smaller scales. These experiments suggest that the increase of water yield due to land use change is attributed to a change of soil properties such as an decreasing K_{sat} leading to Hortonian surface runoff (Giertz et al., 2005; Yira, 2016). However, in SHETRAN K_{sat} varies with soil type and not with land use. Consequently, it remained unchanged over all applied scenarios and cannot explain the differences between the scenarios. Among the land use specific model parameters LAI, the vegetation cover fraction, the Strickler roughness coefficient (KSTR), and the ratio ETa/ETp were adjusted to the corresponding land use types to reflect their differences regarding the hydrological effects. In SHETRAN the roughness coefficient and the ratio ETa/ETp have distinct effects on discharge as shown by Op de Hipt et al. (2017) and Đukić and Radić (2016). Decreased surface roughness as observed on agricultural fields

(Engman, 1986) results in higher surface runoff velocities and therefore especially influences the runoff peaks. However, interactions between surface roughness, infiltration and evapotranspiration also lead to a change of water yield. The ratio ETa/ETp, which depends on the vegetation type and varies with soil water tension, has strong effects on the water balance components. A higher actual evapotranspiration on natural land use types is frequently reported (e.g. Compaoré, 2006). Other vegetation properties such as LAI or vegetation cover also influence the discharge. Decreasing LAI and vegetation cover leads to more throughfall, which may increase surface runoff.

Table 7-5: Average annual water balance and specific suspended sediment yield. Annual means of the modeled past (1990 – 2005) and the modeled future (2006 – 2032) are indicated for simulations M9 – M12.

Base scenario	M1_1990	M2_2000	M3_2007	M4_2013	M5_90/13	M6_2019	M7_2025	M8_2030	M9_1990_RCP4.5	M10_1990_RCP8.5	M11_90/30_RCP4.5	M12_90/30_RCP8.5
Mean annual observed rainfall (mm)	903	903	903	903	903	903	903	903.4	951 – 1026	951 – 1002	951 – 1002	951 – 1002
ETp (mm)	1809	1809	1809	1809	1809	1809	1809	1809	1578 – 1653	1578 – 1674	1578 – 1653	1578 – 1674
ETa (mm)	844	839	820	820	827	822	802	786	775 – 799	775 – 801	768 – 756	768 – 761
Water yield(mm)	59.4	61.7	81.2	77.6	71.4	86.7	95.5	105.4	154 – 226	154 – 192	152 – 264	152 – 229
Specific suspended sediment yield (t/ha)	0.032	0.031	0.045	0.044	0.039	0.053	0.059	0.068	0.084 – 0.13	0.084 – 0.11	0.082 – 0.15	0.082 – 0.13

7.3.3.2 Soil erosion

Figure 7-6 and Table 7-5 show the effect of LULC and climate change on the mean annual specific suspended sediment yield (SSY). Simulations driven by observed data (M1_1990 – M5_90/13) show a change of SSY between -1.4% (M2_2000) and +41.8% (M3_2007). The relative contribution of each land use type to the catchment erosion varies between M1_1990 to M5_90/13: The relative contribution of cropland increases by 12% whereas the contribution of savanna decreases by 11% as a result of the changing proportion of each land use type. The channel contribution varies between 42% (M4_2013) and 51% (M1_1990) suggesting that if the contribution of hillslope erosion increases the channel contribution decreases. Among the sediment sources water also contributes to the sediment yield of the catchment. The model structure only allows a limited number of soil types and an additional soil type reflecting the conditions of areas covered by water could not be implemented. The continuous simulation M5_90/13 exhibits

an increase of 24.7% compared to the reference scenario M1_1990 suggesting that LULC change has already a pronounced impact on soil erosion.

Simulations driven by future modeled LULC maps and observed climate data (M6_2019 – M8_2030) show highest increases in SSY between 67.7% (M6_2019) and 115.7% (M8_2030) compared to M1_1990. Consequently, the predicted LULC change will lead to an increased SSY assuming a similar climate development as observed between 1990 and 2016. The proportion of the different sources remains roughly similar between M6 – M8 except for savanna whose contribution decreases by 6%.

The simulation M9_1990_RCP4.5 and M10_1990_RCP8.5 reflect a changing climate assuming stable LULC since 1990. The periods 2006 – 2032 is compared to the period 1990 – 2005. Both show that the predicted change in precipitation (+5.4% to +7.8%), ETp (+4.7% to +6%) and accordingly water yield (+24.5% to +73.4%) strongly influence SSY. Overall SSY is predicted to increase by 31.1% (M10_1990_RCP8.5) to 54.7% (M9_1990_RCP4.5). Table 7-5 shows that these increases are especially attributed to the future predictions (2006 – 2030). Furthermore, the source distribution indicates that these increases are especially caused by a substantial increase of channel contribution (25% – 27%) compared to M1_1990.

The continuous simulations M11_90/30_RCP4.5 and M12_90/30_RCP8.5 reflect the combined impact of LULC and climate change on SSY. The period 2006 – 2032 is compared to the period 1990 – 2006. Overall SSY is predicted to increase by 67.7% (M12_90/30_RCP8.5) to 90.1% (M11_90/30_RCP4.5) compared to the period 1990 – 2005. The comparison between the groups M9/M10 and M11/M12 suggest that LULC change may have a larger impact on SSY than climate change as the differences regarding the increase between M9/M10 (no LULC change) and M11/M12 (LULC and climate change) are relatively large. However, uncertainties of LULC and climate predictions have to be discussed. Simulations M9 to M12 are characterized by high inter-annual variabilities. This is mostly related to large uncertainties of predicted precipitation. The impact of climate change on the rainfall pattern and temperature in West Africa is difficult to assess and differences between climate models regarding amplitude and direction exists (Kasei et al., 2010; Niang et al., 2014). This uncertainty is among others attributed to the difficulties of simulating convective rainfalls and the rainfalls generated by the West African Monsoon (WAM) which is attributed to the incomplete knowledge of the WAM, lack of observations and the natural climate variability in the region (Cook, 2008; Druyan et al., 2010; Field and Barros, 2014; Klein et al., 2015; Niang et al., 2014).

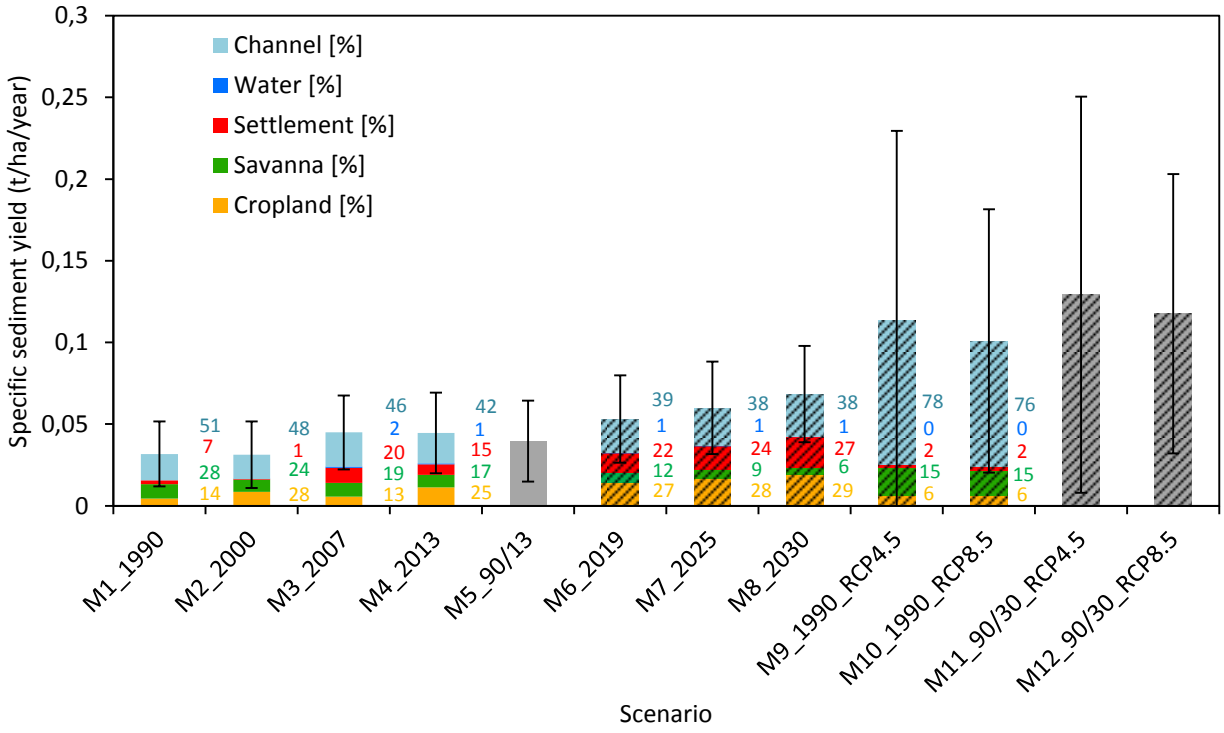

Figure 7-6: Mean annual specific suspended sediment yield for the simulations M1_1990 – M12_90/30_RCP8.5. The contribution of each source is given in % for all simulations except for the continuous simulations (M5, M11, M12). Error bars indicate the standard deviation calculated based on annual sums. Dashed bars indicate the use of modeled LULC maps and/or modeled climate data.

From Figure 7-6 and the described results it can be concluded that LULC and climate change are important drivers that control the catchment sediment yield and the corresponding erosion sources. Increased erosion rates following a conversion from natural vegetation to cropland are frequently confirmed by measurements and simulations in the region (e.g. Bossa et al., 2014; Giertz et al., 2005; Hiepe, 2008). Giertz et al. (2005) compared the influence of different crops and natural vegetation on soil erosion and concluded that increased surface runoff on cropland resulted in increased soil loss on agricultural fields compared to the savanna environment. The increased surface runoff can be explained by the reduction of macroporosity as result of decreased biological activity following the disturbance of the soil by agricultural activities. Furthermore, farming leads to a decreased soil quality parameters (Braimoh and Vlek, 2004) as e.g. a loss of soil organic matter which destabilizes soil aggregates and facilitates surface crusting resulting in a decreased infiltration rate (Descroix et al., 2009; Valentin et al., 2004). However, this process chain is not simulated by SHETRAN. Bossa et al. (2014) investigated the effect of LULC

and climate change on sediment yield in the Ouémé catchment in Benin. Their modeling approach included the SWAT model, climate data from REMO and five LULC maps from 2003 to 2029. The combined application of LULC and climate change suggests an increase of SSY by 6% to 41% (Bossa et al., 2014). This lower increase compared to our results can be explained by the substantial increase of precipitation as predicted by CCLM-ESM which is opposed to the decrease of precipitation as predicted by REMO.

The simulated specific sediment yields are quite low for all simulations (< 0.12 t/ha). In this context it is important to notice, that we consider the suspended fraction only. Furthermore, the term soil erosion is differentiated from sediment yield. Soil erosion refers to soil detachment and not necessarily soil loss from a specific area. Sediment yield refers to the amount of eroded soil that is transported to a certain point in the catchment. However, the simulated suspended sediment yields are comparable with specific suspended sediment yields measured in 2014 (0.04 – 0.13 t/ha/year) especially if the large simulated inter-annual variability is considered. The problem of low simulated SSY is already discussed in Op de Hipt (2017) and may also be attributed to the parameterization of the erosion component and the insufficient representation of space and time in the model approach. However, the adjustment of the erosion parameters in a way that they reflect the natural conditions is quite challenging due to limited knowledge of the parameter ranges and of the erosion processes and source distribution especially in West Africa. Schmengler (Schmengler, 2010; Schmengler and Vlek, 2015) studied soil erosion in the same catchment by comparing sedimentation rates in 3 headwater sub-catchments (7.9 – 23.6 km²). Two of her studied headwater catchments show lower SSY (0.3 t/ha/year – 0.8 t/ha/year). They are representative of the typical flat terrain (2° – 3°). The third headwater catchment is located in the western part and is characterized by steeper slope gradients (up to 20°) which leads to substantially higher SSY (4.4 t/ha/year). The mean slope of our study catchment is 1.8 and therefore comparable to the two catchments showing a low annual SSY. The differences compared to our results can be explained by the different fractions considered and the topographical position. Schmengler (2015) investigated reservoirs located in the headwater areas. Consequently, her measured SSY is only valid for these topographical positions and possible sedimentation downslope is not considered.

The contribution of channels to the mean annual SSY seems to be quite high (51 – 76%) for all simulations. However, recent results from fingerprinting analyses which were conducted in 2013 and 2014 support the modeling result for the past. The contribution of subsurface sources ranges 44% and 47% (Michael Rode, personal communication, 14th July 2017).

7.4 Conclusion

The present study investigated the LULC and climate change in the Dano catchment and its effects on catchment hydrology and soil erosion using a modeling approach. This approach includes the use of SHETRAN which was driven by past (observed) and future (modeled) LULC maps and modeled and observed climate data.

1. The most important land use change in the catchment is the conversion from savanna to cropland. The study of the observed LULC maps (1990 – 2013) shows an annual conversion rate of savanna of 1.14% since 1990. The future LULC maps (2019 – 2030) predict an increase of cropland by 42.2% compared to 1990. The observed and predicted rates are comparable with studies conducted in the region.

2. The analysis of the isolated impact of the LULC change on catchment hydrology clearly suggests an increase of mean annual water yield (3.9% – 77.5%) and a decrease of mean annual ETa (0.5 – 6.8%) while the proportion of cropland increases. Measurements and simulation studies conducted in the region confirm this trend. The comparison between simulations run under constant LULC and changing climate conditions and under LULC and climate change suggests that climate change dominates the future hydrological changes. However, uncertainties of climate model outputs have to be considered. The combined effect of LULC and climate change leads to the high change of water yield (+50.5% – +73.4%) and of ETa (-0.9% – -1.5%).

3. The investigation of the isolated effect of LULC changes on specific suspended sediment yield (SSY) over the period 1990 – 2030 mostly shows a clear increasing trend (-1.4% - 115.7%) which is confirmed by measurements and modeling studies. The increase of SSY is mostly attributed to the enlarging cropland which also forms an important and growing contribution source to total catchment erosion. The comparison of isolated impact of climate change and the combined effect of climate and LULC change suggest climate to be the most important future factor. The combined impact of LULC and climate change results in high change of SSY (+67.7% – +90.1%).

The obtained modeling results confirm the general hypothesis that the conversion of natural vegetation to cropland or settlements has negative effects on catchment hydrology and soil loss. It results in less infiltration, higher surface runoff and soil loss and lower groundwater recharge. However, the present findings are based on results of hydrological and soil erosion modeling driven by LULC and climate data which are subject to uncertainties. The observed LULC maps were produced based on different satellite products and needed to be reclassified. The afflicted

uncertainties are propagated as these maps are the basis for the development of future LULC scenarios. The precipitation as modeled by climate models is frequently considered as uncertain as shown by comparison studies. Furthermore, the modeling approach is based on the changing spatial proportion of the different land use types only and does not consider the complex processes and feedback loops between land use changes, soil properties, hydrology and soil erosion. Consequently, the results must be carefully interpreted even if the model was validated in terms of discharge and SSL. However, focus should be put to relative and not the absolute comparisons between the simulations. This relative comparison signals a clear effect of LULC and climate change on hydrology and soil erosion.

8 GENERAL CONCLUSION

The main goal of the present study is to improve knowledge on the effect of land use and land cover (LULC) as well as climate change on hydrology and soil erosion in the Dano catchment. In order to answer the related research questions the methodological approach combines field investigation on different scales, modeling of hydrological and soil erosion processes and the application of LULC and climate scenarios. Therefore, the combination of measurement methods which are rarely used in a data scarce environment, the use of a physically based spatially distributed hydrological and soil erosion model and the application of LULC and climate change scenarios on a local scale represent a novelty.

To tackle the issue of data scarcity, an observation network is established that consists of climate, discharge and erosion measurements. Furthermore, in situ measurements of different physical and chemical soil properties are conducted. These measurements are used in the following to answer the four research questions that have been formulated.

1. **How do different land use types affect surface runoff and soil erosion?**

   Erosion plots with three different land use types are installed to assess the effect of cotton, sorghum and fallow on surface runoff and soil erosion. The frequently reported effect of cultivation on hydrological processes and soil erosion is also observed in this study. The analyses show that land use has statistically significant effects on runoff and soil erosion. This is mostly explained by hydraulic conductivities that differ depending on the land use type. The conversion of savanna to cropland leads to reduced hydraulic conductivities and increases the exposure to infiltration excess overland flow especially during high intensity rainfalls. However, the natural variability that is evaluated by comparing the intra-plot measurement differences per event was quite large.

2. **Is the hydrological and soil erosion model SHETRAN able to simulate discharge and soil erosion on the catchment scale?**

   The physically based spatially distributed hydrological and soil erosion model SHETRAN is calibrated for discharge and suspended sediment load (SSL). The performance indices of simulated discharge are good (≥ 0.66) and comparable with other studies that used SHETRAN. The performance indices of the simulated SSL are comparable with those few studies that used SHETRAN to simulate soil erosion and provided model performance. One of the major advantages that justify the use of a rather complex model is the sophisticated output that allows to differentiate between erosion sources and to create

soil erosion maps. Results suggest that river incision and bank erosion are the major sources of SSL in the catchment.

3. **How does the predicted precipitation and temperature trend of the future period 2021 – 2050 affect water resources and soil erosion compared to the historical period (1971 – 2000)?**

   Observed historical precipitation and temperature is compared to the data of the same period derived from six Regional and Global Climate Models (RCMs-GCMs) for the period 1971 – 2000. This comparison shows that observed temperature is better reflected by the climate models than observed precipitation. Timing and magnitude of precipitation is considerably biased across all climate models. Therefore, modeled precipitation is bias corrected what increases the agreement between observed and modeled precipitation. Observed temperature is frequently higher than the modeled data. As it controls the calculation of potential evapotranspiration (ETp) and has therefore large implications for the simulation of discharge and soil erosion, temperature is also bias corrected.

   The comparison between historical temperature (1971 – 2000) and future predictions (2021 – 2050) of all climate models simulating the Representative Concentration Pathways (RCP) 4.5 and 8.5 shows a temperature change ranging from -0.8° C to +2° C. Except RCP4.5 of HIRHAM-EARTH all models suggest an increase of temperature. The climate change signal of precipitation is rather unclear and depends on the climate model. The predicted change ranges from -11% to +36.5%. This confirms the necessity of using an ensemble of climate models to assess the possible range of future climate predictions. Observed and modeled precipitation and temperature derived ETp is used as input into SHETRAN in order to test the climate models ability to reproduce the historical discharge and specific sediment yield (SSY). A good agreement between discharge and SSY simulated using observed climate data and climate data from climate models increases the confidence in the model results.

   Precipitation and temperature predictions of each RCM-GCM and both RCPs are used as input for SHETRAN. The relative differences between the historical and the future period concerning discharge and SSY reflect the differences between the precipitation signals. Consequently, no clear signal can be identified as discharge and SSY are predicted to increase or decrease depending on the climate model. This has implications for the planning of adaptions strategies as both, an increase and a decrease of discharge and soil erosion have to be considered.

4. **How does LULC change affects hydrology and soil erosion on the catchment scale?**

   Land use change is dominated by the conversion of savanna to cropland. This was shown by observed LULC maps from 1990 to 2013 and projected by future LULC scenarios. The comparison between the future LULC development (2019 – 2030) and the status of 1990 indicated an increase of cropland by 42.2%.

   The isolated impact of LULC change on catchment hydrology suggested an increase of mean annual water yield (3.9 % – 77.5%) and a decrease of mean annual ETa (0.5 – 6.8%) while the proportion of cropland increases. This trend is confirmed by other studies conducted in the region. The comparison between simulations run under constant LULC and changing climate conditions and under LULC and climate change suggests that climate change dominates the future hydrological changes. However, uncertainties of climate model outputs have to be considered. The combined effect of LULC and climate change leads to the high change of mean annual water yield (+50.5% – +73.4%) and of ETa (-0.9% – -1.5%).

   The isolated effect of LULC changes on specific suspended sediment yield (SSY) over the period 1990 – 2030 mostly shows increasing trend (-1.4% – 115.7%) which is confirmed by measurements and modeling studies. The enlargement of cropland is mainly responsible for the increase in mean annual SSY. The comparison of isolated impact of climate change and the combined effect of climate and LULC change suggest LULC to be the most important future factor. The combined impact of LULC and climate change results in high change of SSY (+67.7 – +90.1%).

Without considering the diverse signal of climate change the observed LULC changes alone suggests that water resources and soil erosion are subject to substantial changes in the Dano catchment mainly due to current and future cropland expansion necessary to feed the growing population. A clear link could be established between cultivation and increased runoff and soil erosion. One major factor that influences surface runoff and consequently erosion is the infiltration rate that is significantly lower on croplands. Therefore, the expansion of cropland will increase surface runoff and soil erosion. Traditional soil and water conservation techniques such as the Zaï system which comprises soil restoration through the use of organic matter, termites and water harvesting (Roose et al., 1999) are essential to cope with the challenges of climate and land use change. Creating incentives for farmers to apply such soil and water conservation techniques may be an opportunity to strengthen the resilience (Lybbert and Sumner, 2012). However, under a sustainable approach to mitigate the impact of future LULC and climate

change education must play a major role as it controls population growth (Crist et al., 2017) and political participation (Persson, 2015). Both factors are most important for the future socio-economic and environmental development in the region.

Although this study contributes to the understanding of possible effect of climate and LULC change several aspects have not been addressed and remain for future studies:

1. In this study, two drivers (climate and LULC change) of changes in hydrology and soil erosion were investigated separately and combined. LULC and climate change occur simultaneously and therefore a combined analysis was necessary. However, feedback loops among the drivers itself are probable but not well understood (UNEP, 2012).
2. This study uses the latest data that were available in 2013. Nevertheless, limitations regarding the spatial and temporal resolution exist. A finer spatial resolution would have been possible for calibration and validation but increased substantially the run time of the model. Temporal and spatial resolution of historical and future data was imperfect but only available as used here. Progress in climate change modeling may provide a better temporal resolution and quality of future data sets.
3. Surface runoff and soil erosion are substantially influenced by the crop species. Specific crop types were not considered in the modeling part of present study. Runoff and erosion from plot measurements was highest on cotton plots whose area has been tripled during the last 20 years making Burkina Faso to the largest producer and exporter within Africa. Including specific crops in the modeling approach may allow detailed conclusions.

A crucial problem of the present study was the lack of adequate data. Therefore, a major heritage of this study are the numerous devices and the staff training for measuring discharge, turbidity, soil erosion, groundwater and climate that have been installed since 2012. However, sufficiently long time series are dependent on a save financial support.

9 REFERENCES

Abbaspour, K.C., Faramarzi, M., Ghasemi, S.S., Yang, H., 2009. Assessing the impact of climate change on water resources in Iran. Water Resources Research 45. https://doi.org/10.1029/2008WR007615

Abbott, M.B., Bathurst, J.C., Cunge, J.A., O'Connell, P.E., Rasmussen, J., 1986. An introduction to the European Hydrological System — Systeme Hydrologique Europeen, "SHE", 1: History and philosophy of a physically-based, distributed modelling system. Journal of Hydrology 87, 45–59. https://doi.org/10.1016/0022-1694(86)90114-9

Abiodun, B.J., Lawal, K.A., Salami, A.T., Abatan, A.A., 2013. Potential influences of global warming on future climate and extreme events in Nigeria. Regional Environmental Change 13, 477–491. https://doi.org/10.1007/s10113-012-0381-7

Ackers, P., White, W.R., 1973. Sediment transport: new approach and analysis. Journal of the Hydraulics Division 99.

Adams, R., Elliott, S., 2006. Physically based modelling of sediment generation and transport under a large rainfall simulator. Hydrological Processes 20, 2253–2270. https://doi.org/10.1002/hyp.6050

Aguilar, E., Aziz Barry, A., Brunet, M., Ekang, L., Fernandes, A., Massoukina, M., Mbah, J., Mhanda, A., do Nascimento, D.J., Peterson, T.C., Thamba Umba, O., Tomou, M., Zhang, X., 2009. Changes in temperature and precipitation extremes in western central Africa, Guinea Conakry, and Zimbabwe, 1955–2006. Journal of Geophysical Research 114. https://doi.org/10.1029/2008JD011010

Aich, V., Liersch, S., Vetter, T., Huang, S., Tecklenburg, J., Hoffmann, P., Koch, H., Fournet, S., Krysanova, V., Müller, E.N., Hattermann, F.F., 2014. Comparing impacts of climate change on streamflow in four large African river basins. Hydrology and Earth System Sciences 18, 1305–1321. https://doi.org/10.5194/hess-18-1305-2014

Ajayi, A.E., 2004. Surface runoff and infiltration processes in the Volta Basin, West Africa: Observation and Modeling. Cuvillier.

Ardoin-Bardin, S., Dezetter, A., Servat, E., Paturel, J.E., Mahé, G., Niel, H., Dieulin, C., 2009. Using general circulation model outputs to assess impacts of climate change on runoff for large hydrological catchments in West Africa. Hydrological Sciences Journal 54, 77–89. https://doi.org/10.1623/hysj.54.1.77

Ariathurai, R., Arulanandan, K., 1978. Erosion rates of cohesive soils. Journal of Hydraulic Division 104, 279–283.

Azuka, C.V., Igué, A.M., Diekkrüger, B., Igwe, C.A., 2015. Soil survey and soil classification of the Koupendri catchment in Benin, West Africa. African Journal of Agricultural Research 10, 3938–3951. https://doi.org/10.5897/AJAR2015.9904

Badini, O., Stöckle, C.O., Franz, E.H., 1997. Application of crop simulation modeling and GIS to agroclimatic assessment in Burkina Faso. Agric., Ecosyst. Environ. 64, 233–244. https://doi.org/10.1016/S0167-8809(97)00041-8

Bagarello, V., Ferro, V., 2004. Plot-scale measurement of soil erosion at the experimental area of Sparacia (southern Italy). Hydrological Processes 18, 141–157. https://doi.org/10.1002/hyp.1318

Bathurst, J.C., 2010. Predicting Impacts of Land Use and Climate Change on Erosion and Sediment Yield in River Basins Using SHETRAN, in: Morgan, R.P.C., Nearing, M.A. (Eds.), Handbook of Erosion Modelling. John Wiley & Sons, Ltd, pp. 263–288.

Bathurst, J.C., Birkinshaw, S.J., Cisneros, F., Fallas, J., Iroumé, A., Iturraspe, R., Novillo, M.G., Urciuolo, A., Alvarado, A., Coello, C., Huber, A., Miranda, M., Ramirez, M., Sarandón, R., 2011. Forest impact on floods due to extreme rainfall and snowmelt in four Latin American environments 2: Model analysis. Journal of Hydrology 400, 292–304. https://doi.org/10.1016/j.jhydrol.2010.09.001

Bathurst, J.C., Ewen, J., Parkin, G., O'Connell, P.E., Cooper, J.D., 2004. Validation of catchment models for predicting land-use and climate change impacts. 3. Blind validation for internal and outlet responses. Journal of Hydrology 287, 74–94. https://doi.org/10.1016/j.jhydrol.2003.09.021

Bationo, A., Kihara, J., Vanlauwe, B., Waswa, B., Kimetu, J., 2007. Soil organic carbon dynamics, functions and management in West African agro-ecosystems. Agricultural Systems 94, 13–25. https://doi.org/10.1016/j.agsy.2005.08.011

Baudron, F., Corbeels, M., Monicat, F., Giller, K.E., 2009. Cotton expansion and biodiversity loss in African savannahs, opportunities and challenges for conservation agriculture: a review paper based on two case studies. Biodiversity and Conservation 18, 2625–2644. https://doi.org/10.1007/s10531-009-9663-x

Beven, K., Freer, J., 2001. Equifinality, data assimilation, and uncertainty estimation in mechanistic modelling of complex environmental systems using the GLUE methodology. Journal of Hydrology 249, 11–29. https://doi.org/10.1016/S0022-1694(01)00421-8

Beven, K.J., 2008. Rainfall-runoff modelling: the primer, Reprinted. ed. Wiley, Chichester.

Birkinshaw, S.J., 2010. Technical Note: Automatic river network generation for a physically-based river catchment model. Hydrology and Earth System Sciences 14, 1767–1771. https://doi.org/10.5194/hess-14-1767-2010

Birkinshaw, S.J., 2008. Physically-based modelling of double-peak discharge responses at Slapton Wood catchment. Hydrological Processes 22, 1419–1430. https://doi.org/10.1002/hyp.6694

Birkinshaw, S.J., Bathurst, J.C., 2006. Model study of the relationship between sediment yield and river basin area. Earth Surface Processes and Landforms 31, 750–761. https://doi.org/10.1002/esp.1291

Birkinshaw, S.J., Bathurst, J.C., Iroumé, A., Palacios, H., 2010a. The effect of forest cover on peak flow and sediment discharge — an integrated field and modelling study in central–southern Chile. Hydrological processes 25, 1284–1297. https://doi.org/10.1002/hyp.7900

Birkinshaw, S.J., Bathurst, J.C., Robinson, M., 2014. 45 years of non-stationary hydrology over a forest plantation growth cycle, Coalburn catchment, Northern England. Journal of Hydrology 519, Part A, 559–573. https://doi.org/10.1016/j.jhydrol.2014.07.050

Birkinshaw, S.J., Guerreiro, S.B., Nicholson, A., Liang, Q., Quinn, P., Zhang, L., He, B., Yin, J., Fowler, H.J., 2017. Climate change impacts on Yangtze River discharge at the Three Gorges Dam. Hydrology and Earth System Sciences 21, 1911–1927. https://doi.org/10.5194/hess-21-1911-2017

Birkinshaw, S.J., James, P., Ewen, J., 2010b. Graphical user interface for rapid set-up of SHETRAN physically-based river catchment model. Environmental Modelling & Software 25, 609–610. https://doi.org/10.1016/j.envsoft.2009.11.011

Birkinshaw, S.J., Webb, B., 2010. Using temperature as a tracer to understand flow pathways in the Slapton Wood and Dunsop catchments, in: Role of Hydrology in Managing Consequences of a Changing Global Environment. Presented at the BHS 3rd International Symposium Managing Consequences of a Changing Global Environment, Newcastle upon Tyne.

Blöschl, G., Sivapalan, M., 1995. Scale issues in hydrological modelling: A review. Hydrological Processes 9, 251–290. https://doi.org/10.1002/hyp.3360090305

Blume, H.-P., Brümmer, G.W., Horn, R., Kandeler, E., Kögel-Knabner, I., Kretzschmar, R., Stahr, K., Wilke, B.M., 2010. Scheffer/Schachtschabel: Lehrbuch der Bodenkunde, 16th ed. Spektrum Akademischer Verlag, Heidelberg.

Boé, J., Terray, L., Habets, F., Martin, E., 2007. Statistical and dynamical downscaling of the Seine basin climate for hydro-meteorological studies. International Journal of Climatology 27, 1643–1655. https://doi.org/10.1002/joc.1602

Boix-Fayos, C., Martinez-Mena, M., Arnau-Rosalen, E., Calvo-Cases, A., Castillo, V., Albaladejo, J., 2006. Measuring soil erosion by field plots: Understanding the sources of variation. Earth-Sci. Rev. 78, 267–285. https://doi.org/10.1016/j.earscirev.2006.05.005

Boix-Fayos, C., Martínez-Mena, M., Calvo-Cases, A., Arnau-Rosalén, E., Albaladejo, J., Castillo, V., 2007. Causes and underlying processes of measurement variability in field erosion plots in Mediterranean conditions. Earth Surface Processes and Landforms 32, 85–101. https://doi.org/10.1002/esp.1382

Bossa, A., 2012. Multi-scale modeling of sediment and nutrient flow dynamics in the Ouémé catchment (Benin) - towards an assessment of global change effects on soil degradation and water quality (Phd thesis). Rheinische Friedrich-Wilhelms-Universität Bonn, Bonn <http://hss.ulb.uni-bonn.de/2012/2983/2983.htm>.

Bossa, A., Diekkrüger, B., Agbossou, E., 2014. Scenario-Based Impacts of Land Use and Climate Change on Land and Water Degradation from the Meso to Regional Scale. Water 6, 3152–3181. https://doi.org/10.3390/w6103152

Boulet, R., 1970. La géomorphologie et les principaux types de sols en Haute-Volta septentrionale. Cahiers ORSTOM, Série Pédologie 8, 245–271.

Bowders, J., Neupane, D., Erik Loehr, J., 2002. Sidewall Leakage in Hydraulic Conductivity Testing of Asphalt Concrete Specimens. Geotechnical Testing Journal 25, 210. https://doi.org/10.1520/GTJ11364J

Braimoh, A.K., Vlek, P.L.G., 2004. The impact of land-cover change on soil properties in northern Ghana. Land Degradation & Development 15, 65–74. https://doi.org/10.1002/ldr.590

Brakensiek, D.L., Rawls, W.J., 1994. Soil containing rock fragments: effects on infiltration. Catena 23, 99–110. https://doi.org/10.1016/0341-8162(94)90056-6

Bruneau, P., Gascuel-Odoux, C., Robin, P., Merot, P., Beven, K., 1995. Sensitivity to space and time resolution of a hydrological model using digital elevation data. Hydrological Processes 9, 69–81. https://doi.org/10.1002/hyp.3360090107

Callo-Concha, D., Gaiser, T., Ewert, F., 2012. Farming and cropping systems in the West African Sudanian Savanna. WASCAL research area: Northern Ghana, Southwest Burkina Faso and Northern Benin (Working Paper No. 100), ZEF Working Paper Series. Center for Development Research, Bonn, Germany <http://www.zef.de/uploads/tx_zefportal/Publications/wp100.pdf>.

Chan, J.C., Chan, K., Yeh, A.G., 2001. Detecting the Nature of Change in an Urban Environment : A Comparison of Machine Learning Algorithms. Photogrammetric Engineering & Remote Sensing 67, 213–225.

Chaplot, V., 2007. Water and soil resources response to rising levels of atmospheric CO2 concentration and to changes in precipitation and air temperature. Journal of Hydrology 337, 159–171. https://doi.org/10.1016/j.jhydrol.2007.01.026

CILSS (Comité Inter-états de Lutte contre la Sécheresse dans le Sahel), 2016. Landscapes of West Africa - A Window on a Changing World. U.S. Geological Survey EROS, Garretson, United States.

Codjoe, S.N.A., 2004. Population and Land Use, Cover Dynamics in the Volta River Basin of Ghana: 1960-2010. Cuvillier Verlag.

Compaoré, H., 2006. The impact of savannah vegetation on the spatial and temporal variation of the actual evapotranspiration in the Volta Basin, Navrongo, Upper East Ghana. Cuvillier.

Cook, K.H., 2008. Climate science: The mysteries of Sahel droughts. Nature Geoscience 1, 647–648. https://doi.org/10.1038/ngeo320

Cook, K.H., Vizy, E.K., 2006. Coupled Model Simulations of the West African Monsoon System: Twentieth- and Twenty-First-Century Simulations. Journal of Climate 19, 3681–3703. https://doi.org/10.1175/JCLI3814.1

Cord, A., Conrad, C., Schmidt, M., Dech, S., 2010. Standardized FAO-LCCS land cover mapping in heterogeneous tree savannas of West Africa. Journal of Arid Environments 74, 1083–1091. https://doi.org/10.1016/j.jaridenv.2010.03.012

Cornelis, W.M., Ronsyn, J., Van Meirvenne, M., Hartmann, R., 2001. Evaluation of Pedotransfer Functions for Predicting the Soil Moisture Retention Curve. Soil Science Society of America Journal 65, 638–648. https://doi.org/10.2136/sssaj2001.653638x

Cornelissen, T., Diekkrüger, B., Giertz, S., 2013. A comparison of hydrological models for assessing the impact of land use and climate change on discharge in a tropical catchment. Journal of Hydrology 498, 221–236. https://doi.org/10.1016/j.jhydrol.2013.06.016

Cosby, B.J., Hornberger, G.M., Clapp, R.B., Ginn, T.R., 1984. A Statistical Exploration of the Relationships of Soil Moisture Characteristics to the Physical Properties of Soils. Water Resources Research 20, 682–690. https://doi.org/10.1029/WR020i006p00682

Crist, E., Mora, C., Engelman, R., 2017. The interaction of human population, food production, and biodiversity protection. Science 356, 260. https://doi.org/10.1126/science.aal2011

de Figueiredo, E.E., Bathurst, J.C., 2007. Runoff and sediment yield predictions in a semiarid region of Brazil using SHETRAN, in: Proceedings of the PUB Kick-off Meeting. Presented at the PUB Kick-off meeting, IAHS, Brasilia, Brazil.

de Roo, A.P.J., 1993. Modelling Surface Runoff and Soil Erosion in Catchments Using Geographical Information Systems: Validity and Applicability of the “answers” Model in Two Catchments in the Loess Area of South Limburg (The Netherlands) and one in Devon (UK) (Phd thesis). Rijksuniversiteit Utrecht, the Netherlands.

de Vente, J., Poesen, J., Verstraeten, G., Govers, G., Vanmaercke, M., Van Rompaey, A., Arabkhedri, M., Boix-Fayos, C., 2013. Predicting soil erosion and sediment yield at regional scales: Where do we stand? Earth-Science Reviews 127, 16–29. https://doi.org/10.1016/j.earscirev.2013.08.014

Descroix, L., Mahé, G., Lebel, T., Favreau, G., Galle, S., Gautier, E., Olivry, J.C., Albergel, J., Amogu, O., Cappelaere, B., 2009. Spatio-temporal variability of hydrological regimes around the boundaries between Sahelian and Sudanian areas of West Africa: A synthesis. Journal of Hydrology 375, 90–102, 10.1016/j.jhydrol.2008.12.012.

Diekkrüger, B., 2010. Hydrological processes and soil degradation in Benin, in: Speth, P., Christoph, M., Diekkrüger, B. (Eds.), Impacts of Global Change on the Hydrological Cycle in West and Northwest Africa. Springer, Berlin.

Dosio, A., Panitz, H.-J., Schubert-Frisius, M., Lüthi, D., 2015. Dynamical downscaling of CMIP5 global circulation models over CORDEX-Africa with COSMO-CLM: evaluation over the present climate and analysis of the added value. Climate Dynamics 44, 2637–2661. https://doi.org/10.1007/s00382-014-2262-x

Druyan, L.M., 2011. Studies of 21st-century precipitation trends over West Africa. International Journal of Climatology 31, 1415–1424. https://doi.org/10.1002/joc.2180

Druyan, L.M., Feng, J., Cook, K.H., Xue, Y., Fulakeza, M., Hagos, S.M., Konaré, A., Moufouma-Okia, W., Rowell, D.P., Vizy, E.K., Ibrah, S.S., 2010. The WAMME regional model intercomparison study. Climate Dynamics 35, 175–192. https://doi.org/10.1007/s00382-009-0676-7

Đukić, V., Radić, Z., 2016. Sensitivity Analysis of a Physically Based Distributed Model. Water Resources Management 30, 1669–1684. https://doi.org/10.1007/s11269-016-1243-8

Đukić, V., Radić, Z., 2014. GIS Based Estimation of Sediment Discharge and Areas of Soil Erosion and Deposition for the Torrential Lukovska River Catchment in Serbia. Water Resources Management 28, 4567–4581. https://doi.org/10.1007/s11269-014-0751-7

Ehret, U., Zehe, E., Wulfmeyer, V., Warrach-Sagi, K., Liebert, J., 2012. Should we apply bias correction to global and regional climate model data? Hydrology and Earth System Sciences 16, 3391–3404. https://doi.org/10.5194/hess-16-3391-2012

Elliott, A.H., Oehler, F., Schmidt, J., Ekanayake, J.C., 2011. Sediment modelling with fine temporal and spatial resolution for a hilly catchment. Hydrological Processes 26, 3645–3660. https://doi.org/10.1002/hyp.8445

Emori, S., Brown, S.J., 2005. Dynamic and thermodynamic changes in mean and extreme precipitation under changed climate. Geophysical Research Letters 32. https://doi.org/10.1029/2005GL023272

Engelen, V. van, Ting-Tian, W., 1995. Global and national soils and terrain digital databases (SOTER): Procedures manual. International Soil Reference and Information Centre.

Engelund, F., Hansen, E., 1967. A monograph on sediment transport in alluvial streams.

Engman, E.T., 1986. Roughness coefficients for routing surface runoff. Journal of Irrigation and Drainage Engineering 112, 39–53. https://doi.org/10.1061/(ASCE)0733-9437(1986)112:1(39)

Ewen, J., O'Donnell, G., Burton, A., O'Connell, E., 2006. Errors and uncertainty in physically-based rainfall-runoff modelling of catchment change effects. Journal of Hydrology 330, 641–650. https://doi.org/10.1016/j.jhydrol.2006.04.024

Ewen, J., Parkin, G., O'Connell, P.E., 2000. SHETRAN: distributed river basin flow and transport modeling system. Journal of Hydrologic Engineering 5, 250–258. https://doi.org/10.1061/(ASCE)1084-0699(2000)5:3(250)

FAOSTAT, 2017. Burkina Faso [WWW Document]. URL http://www.fao.org/faostat/en/#country/233 (accessed 2.16.17).

Feddes, R.A., Kowalik, P., Neuman, S.P., Bresler, E., 1976. Finite Difference and Finite Element Simulation of Field Water Uptake by Plants. Hydrological Sciences Journal 21, 81–98. https://doi.org/10.1080/02626667609491607

Field, C.B., Barros, V., Stocker, T.F., Dahe, Q. (Eds.), 2012. Managing the risks of extreme events and disasters to advance climate change adaptation. Cambridge University Press.

Field, C.B., Barros, V.R. (Eds.), 2014. Climate change 2014: impacts, adaptation, and vulnerability. Cambridge University Press, New York, NY.

Forkuor, G., 2014. Agricultural Land Use Mapping in West Africa Using Multi-sensor Satellite Imagery (Phd thesis). Julius-Maximilians-Universität, Würzburg, Germany <https://opus.bibliothek.uni-wuerzburg.de/frontdoor/index/index/docId/10868>.

Forkuor, G., Hounkpatin, O.K.L., Welp, G., Thiel, M., 2017. High Resolution Mapping of Soil Properties Using Remote Sensing Variables in South-Western Burkina Faso: A Comparison of Machine Learning and Multiple Linear Regression Models. PLOS ONE 12, e0170478. https://doi.org/10.1371/journal.pone.0170478

Gbobaniyi, E., Sarr, A., Sylla, M.B., Diallo, I., Lennard, C., Dosio, A., Dhiédiou, A., Kamga, A., Klutse, N.A.B., Hewitson, B., Nikulin, G., Lamptey, B., 2014. Climatology, annual cycle and interannual variability of precipitation and temperature in CORDEX simulations over West Africa. International Journal of Climatology 34, 2241–2257. https://doi.org/10.1002/joc.3834

Giertz, S., Diekkrüger, B., 2003. Analysis of the hydrological processes in a small headwater catchment in Benin (West Africa). Physics and Chemistry of the Earth, Parts A/B/C 28, 1333–1341. https://doi.org/10.1016/j.pce.2003.09.009

Giertz, S., Hiepe, C., Steup, G., Sintondji, L., Diekkrüger, B., 2010. Hydrological processes and soil degradation in Benin, in: Speth, P., Christoph, M., Diekkrüger, B. (Eds.), Impacts of Global Change on the Hydrological Cycle in West and Northwest Africa. Springer, Berlin.

Giertz, S., Junge, B., Diekkrüger, B., 2005. Assessing the effects of land use change on soil physical properties and hydrological processes in the sub-humid tropical environment of West Africa. Physics and Chemistry of the Earth, Parts A/B/C 30, 485–496. https://doi.org/10.1016/j.pce.2005.07.003

Gilleland, E., Katz, R., 2016. in2extRemes: Into the R Package extRemes. Extreme Value Analysis for Weather and Climate Applications. https://doi.org/10.5065/D65T3HP2

Giorgi, F., Coppola, E., Raffaele, F., Diro, G.T., Fuentes-Franco, R., Giuliani, G., Mamgain, A., Llopart, M.P., Mariotti, L., Torma, C., 2014. Changes in extremes and hydroclimatic re-

gimes in the CREMA ensemble projections. Climatic Change 125, 39–51. https://doi.org/10.1007/s10584-014-1117-0

Gippel, C., 1989. The use of turbidimeters in suspended sediment research. Hydrobiologia 176–177, 465–480. https://doi.org/10.1007/BF00026582

Gippel, C.J., 1995. Potential of turbidity monitoring for measuring the transport of suspended solids in streams. Hydrological Processes 9, 83–97. https://doi.org/10.1002/hyp.3360090108

Gleisberg-Gerber, K., 2012. Livelihoods and land management in the Ioba Province in south-western Burkina Faso (Working Paper No. 91), ZEF Working Paper Series. Center for Development Research, Bonn, Germany <http://www.zef.de/uploads/tx_zefportal/Publications/wp91.pdf>.

Gray, L.C., 1999. Is land being degraded? A multi-scale investigation of landscape change in southwestern Burkina Faso. Land Degradation & Development 10, 329–343. https://doi.org/10.1002/(SICI)1099-145X(199907/08)10:4<329::AID-LDR361>3.0.CO;2-I

Gudmundsson, L., Bremnes, J.B., Haugen, J.E., Engen-Skaugen, T., 2012. Technical Note: Downscaling RCM precipitation to the station scale using statistical transformations - a comparison of methods. Hydrology and Earth System Sciences 16, 3383–3390. https://doi.org/10.5194/hess-16-3383-2012

Guerra, A., 1994. The effect of organic matter content on soil erosion in simulated rainfall experiments in W. Sussex, UK. Soil Use and Management 10, 60–64. https://doi.org/10.1111/j.1475-2743.1994.tb00460.x

Gupta, H.V., Kling, H., Yilmaz, K.K., Martinez, G.F., 2009. Decomposition of the mean squared error and NSE performance criteria: Implications for improving hydrological modelling. Journal of Hydrology 377, 80–91. https://doi.org/10.1016/j.jhydrol.2009.08.003

Haddeland, I., Heinke, J., Voß, F., Eisner, S., Chen, C., Hagemann, S., Ludwig, F., 2012. Effects of climate model radiation, humidity and wind estimates on hydrological simulations. Hydrology and Earth System Sciences 16, 305–318. https://doi.org/10.5194/hess-16-305-2012

Hagemann, S., Chen, C., Haerter, J.O., Heinke, J., Gerten, D., Piani, C., 2011. Impact of a Statistical Bias Correction on the Projected Hydrological Changes Obtained from Three GCMs and Two Hydrology Models. Journal of Hydrometeorology 12, 556–578. https://doi.org/10.1175/2011JHM1336.1

Harmel, R.D., Smith, P.K., 2007. Consideration of measurement uncertainty in the evaluation of goodness-of-fit in hydrologic and water quality modeling. Journal of Hydrology 337, 326–336. https://doi.org/10.1016/j.jhydrol.2007.01.043

Harmel, R.D., Smith, P.K., Migliaccio, K.W., 2010. Modifying goodness-of-fit indicators to incorporate both measurement and model uncertainty in model calibration and validation. Transactions of the ASABE 53, 55–63. https://doi.org/10.13031/2013.29502

Hauchart, V., 2008. Culture du coton, pluviosité et dégradation des sols dans le Mouhoun (Burkina Faso). Science et changements planétaires/Sécheresse 19, 95–102.

Helsel, D.R., Hirsch, R.M., 2002. Statistical methods in water resources, in: Hydrologic Analysis and Interpretation. US Geological survey, Reston, United States.

Hessel, R., 2005. Effects of grid cell size and time step length on simulation results of the Limburg soil erosion model (LISEM). Hydrological Processes 19, 3037–3049. https://doi.org/10.1002/hyp.5815

Hiepe, C., 2008. Soil degradation by water erosion in a sub-humid West-African catchment - a modelling approach considering land use and climate change in Benin (Phd thesis). Rheinische Friedrich-Wilhelms-Universität Bonn, Bonn, <http://hss.ulb.uni-bonn.de/2008/1628/1628.htm>.

Hoffmann, T., 2015. Sediment residence time and connectivity in non-equilibrium and transient geomorphic systems. Earth-Science Reviews 150, 609–627. https://doi.org/10.1016/j.earscirev.2015.07.008

Hoffmann, T., Schlummer, M., Notebaert, B., Verstraeten, G., Korup, O., 2013. Carbon burial in soil sediments from Holocene agricultural erosion, Central Europe. Global Biogeochemical Cycles 27, 828–835. https://doi.org/10.1002/gbc.20071

Hogg, R.V., Tanis, E.A., Zimmerman, D.L., 2015. Probability and statistical inference, Ninth edition. ed. Pearson, Boston.

Hounkpatin, O.K.L., 2017. Digital soil mapping using survey data and soil organic carbon dynamics in semi-arid Burkina Faso (Phd thesis (submitted 06/2017)). Rheinische Friedrich-Wilhelms-Universität Bonn, Bonn.

Hounkpè, J., Diekkrüger, B., Badou, D., Afouda, A., 2016. Change in Heavy Rainfall Characteristics over the Ouémé River Basin, Benin Republic, West Africa. Climate 4, 15. https://doi.org/10.3390/cli4010015

Hudson, N.W., 1993. Field Measurement of Soil Erosion and Runoff (No. 68), FAO SOILS BULLETIN. Food & Agriculture Organization of the United Nations (FAO), Rome Italy.

Igwe, C.A., Mbagwu, J.S.C., 1999. Application of SLEMSA and USLE models for potential erosion hazard mapping in South-Eastern Nigeria. International agrophysics 13, 41–48.

ISO (International Standard Orgainzation), 2010. Hydrometry -- Measurement of liquid flow in open channels -- Part 2: Determination of the stage-discharge relationship (No. 1100–2:2010). Internation Standard Organization.

ISO (International Standard Orgainzation), 2005. ISO 4365:2005 Liquid flow in open channels — Sediment in streams and canals — Determination of concentration, particle size distribution and relative density.

ISO (International Standard Orgainzation), 1998. ISO 11272:1998 Soil quality -- Determination of dry bulk density.

Itiveh, K.O., Bigg, G.R., 2008. The variation of discharge entering the Niger Delta system, 1951–2000, and estimates of change under global warming. International Journal of Climatology 28, 659–666. https://doi.org/10.1002/joc.1568

IUSS Working Group, 2006. World reference base for soil resources 2006, 2nd ed, World Soil Resources Reports. FAO, Rome, Italy.

IUSS Working Group WRB, 2007. World Reference Base for Soil Resources 2006, first update 2007. (World Soil Resources Reports). FAO, Rome.

Jarvis, A., Reuter, H.I., Nelson, A., Guevara, E., 2008. Hole-filled SRTM for the globe Version 4. available from the CGIAR-CSI SRTM 90m Database (http://srtm. csi. cgiar. org).

Jetten, V., de Roo, A., Favis-Mortlock, D., 1999. Evaluation of field-scale and catchment-scale soil erosion models. CATENA 37, 521–541. https://doi.org/10.1016/S0341-8162(99)00037-5

Johnson, F., Sharma, A., 2015. What are the impacts of bias correction on future drought projections? Journal of Hydrology 525, 472–485. https://doi.org/10.1016/j.jhydrol.2015.04.002

Junge, B., 2004. Die Böden des oberen Ouémé-Einzugsgebietes in Benin/Westafrika - Pedologie, Klassifizierung, Nutzung und Degradierung (Phd thesis). Rheinische Friedrich-Wilhelms-Universität Bonn, Bonn <http://hss.ulb.uni-bonn.de/2004/0401/0401.pdf>.

Kaloga, B., 1966. Étude pédologique des bassins versants des Volta blanche et rouge en Haute-Volta. Cah. ORSTOM, Sér. Pédol. 4, 23–61.

Kaloga, B., Boulet, R., Leprun, J.C., Pottier, J.C., Alboucq, G., 1973. Carte pédologique de reconnaissance de la Haute-Volta. Office de la Recherche Scientifique et Technique Outre-Mer, Centre ORSTOM de Dakar.

Kaminski, J., 2011. Cotton dependence in Burkina Faso: Constraints and opportunities for balanced growth, in: Chuhan-Pole, P., Angwafo, M. (Eds.), Yes Africa Can: Success Stories from a Dynamic Continent. Washington DC, pp. 107–124.

Karambiri, H., Ribolzi, O., 2005. Identification of sediment sources in a small grazed Sahelian catchment, Burkina Faso, in: Walling, D.E., Horowitz, A. (Eds.), Sediment Budgets 1. Presented at the Assembly of the International Association of Hydrological Sciences, IAHS, Brazil, p. 291.

Kasei, R., Diekkrüger, B., Leemhuis, C., 2010. Drought frequency in the Volta Basin of West Africa. Sustainability Science 5, 89–97. https://doi.org/10.1007/s11625-009-0101-5

Ker, A., 1995. Farming systems of the African savanna: a continent in crisis. International Development Research Center, Ottawa, Canada.

Kiepe, P., de Graaff, J., 2001. Soil and water conservation in Sahelian villages, in: Stroosnijder, L., Rheene, T. van (Eds.), Agro-Silvo-Pastoral Land Use in Sahelian Villages, Advances on Geoecology. Catena Verlag.

Kirkby, M.I., 2010. Distance, time and scale in soil erosion processes. Earth Surf. Process. Landf. 35, 1621–1623. https://doi.org/10.1002/esp.2063

Klein, C., Heinzeller, D., Bliefernicht, J., Kunstmann, H., 2015. Variability of West African monsoon patterns generated by a WRF multi-physics ensemble. Climate Dynamics 45, 2733–2755. https://doi.org/10.1007/s00382-015-2505-5

Kling, H., Fuchs, M., Paulin, M., 2012. Runoff conditions in the upper Danube basin under an ensemble of climate change scenarios. Journal of Hydrology 424–425, 264–277. https://doi.org/10.1016/j.jhydrol.2012.01.011

Kunstmann, H., Jung, G., Wagner, S., Clottey, H., 2008. Integration of atmospheric sciences and hydrology for the development of decision support systems in sustainable water management. Physics and Chemistry of the Earth, Parts A/B/C 33, 165–174. https://doi.org/10.1016/j.pce.2007.04.010

Kusimi, J.M., Yiran, G.A., Attua, E.M., 2016. Soil Erosion and Sediment Yield Modelling in the Pra River Basin of Ghana using the Revised Universal Soil Loss Equation (RUSLE). Ghana Journal of Geography 7, 38–57.

Lal, R., 2001. Soil degradation by erosion. Land Degradation & Development 12, 519–539. https://doi.org/10.1002/ldr.472

Lal, R., 1994. Soil erosion research methods. CRC Press.

Landmann, T., Herty, C., Dech, S., Schmidt, M., Dech, S., Schmidt, M., Vlek, P., 2007. Land cover change analysis within the GLOWA Volta basin in West Africa using 30-meter Landsat data snapshots, in: 2007 IEEE International Geoscience and Remote Sensing Symposium. Presented at the International Geoscience and Remote Sensing Symposium, Barcelona, pp. 5298–5301. https://doi.org/10.1109/IGARSS.2007.4424058

Latocha, A., Szymanowski, M., Jeziorska, J., Stec, M., Roszczewska, M., 2016. Effects of land abandonment and climate change on soil erosion—An example from depopulated agricultural lands in the Sudetes Mts., SW Poland. CATENA 145, 128–141. https://doi.org/10.1016/j.catena.2016.05.027

Lauer, W., Bendix, J., 2006. Klimatologie, 2nd ed. Westermann, Braunschweig.

Le Bissonnais, Y., 1996. Aggregate stability and assessment of soil crustability and erodibility: I. Theory and methodology. European Journal of Soil Science 47, 425–437. https://doi.org/10.1111/j.1365-2389.1996.tb01843.x

Léonard, J., Perrier, E., Rajot, J.L., 2004. Biological macropores effect on runoff and infiltration: a combined experimental and modelling approach. Agriculture, Ecosystems & Environment 104, 277–285. https://doi.org/10.1016/j.agee.2003.11.015

Li, Z., Fang, H., 2016. Impacts of climate change on water erosion: A review. Earth-Science Reviews 163, 94–117. https://doi.org/10.1016/j.earscirev.2016.10.004

Lintner, B.R., Biasutti, M., Diffenbaugh, N.S., Lee, J.-E., Niznik, M.J., Findell, K.L., 2012. Amplification of wet and dry month occurrence over tropical land regions in response to global warming. Journal of Geophysical Research 117. https://doi.org/10.1029/2012JD017499

Lukey, B.., Sheffield, J., Bathurst, J.., Hiley, R.., Mathys, N., 2000. Test of the SHETRAN technology for modelling the impact of reforestation on badlands runoff and sediment yield at Draix, France. Journal of Hydrology 235, 44–62. https://doi.org/10.1016/S0022-1694(00)00260-2

Lukey, B.T., Sheffield, J., Bathurst, J.C., Lavabre, J., Mathys, N., Martin, C., 1995. Simulating the effect of vegetation cover on the sediment yield of mediterranean catchments using

SHETRAN. Physics and Chemistry of the Earth 20, 427–432. https://doi.org/10.1016/0079-1946(95)00056-9

Lybbert, T.J., Sumner, D.A., 2012. Agricultural technologies for climate change in developing countries: Policy options for innovation and technology diffusion. Food Policy 37, 114–123. https://doi.org/10.1016/j.foodpol.2011.11.001

Mahé, G., Paturel, J.-E., Servat, E., Conway, D., Dezetter, A., 2005. The impact of land use change on soil water holding capacity and river flow modelling in the Nakambe River, Burkina-Faso. Journal of Hydrology 300, 33–43. https://doi.org/10.1016/j.jhydrol.2004.04.028

Mantz, P.A., 1977. Incipient transport of fine grains and flakes by fluids-extended shield diagram. Journal of the Hydraulics division 103.

Maraun, D., Wetterhall, F., Ireson, A.M., Chandler, R.E., Kendon, E.J., Widmann, M., Brienen, S., Rust, H.W., Sauter, T., Themeßl, M., Venema, V.K.C., Chun, K.P., Goodess, C.M., Jones, R.G., Onof, C., Vrac, M., Thiele-Eich, I., 2010. Precipitation downscaling under climate change: Recent developments to bridge the gap between dynamical models and the end user. Reviews of Geophysics 48. https://doi.org/10.1029/2009RG000314

Mati, B.M., Veihe, A., 2001. Application of the USLE in a Savannah Environment: Comparative Experiences from East and West Africa. Singapore Journal of Tropical Geography 22, 138–155. https://doi.org/10.1111/1467-9493.00099

Mbaye, M.L., Hagemann, S., Haensler, A., Stacke, T., Gaye, A.T., Afouda, A., 2015. Assessment of Climate Change Impact on Water Resources in the Upper Senegal Basin (West Africa). American Journal of Climate Change 04, 77–93. https://doi.org/10.4236/ajcc.2015.41008

McKay, M.D., Beckman, R.J., Conover, W.J., 1979. A Comparison of Three Methods for Selecting Values of Input Variables in the Analysis of Output from a Computer Code. Technometrics 21, 239–245. https://doi.org/10.2307/1268522

McKee, T.B., Doesken, N.J., Kleist, J., 1993. The relationship of drought frequency and duration to time scales, in: Proceedings of the 8th Conference on Applied Climatology. American Meteorological Society Boston, MA, pp. 179–183.

Merritt, W.S., Letcher, R.A., Jakeman, A.J., 2003. A review of erosion and sediment transport models. Environ. Modell. Softw. 18, 761–799. https://doi.org/10.1016/S1364-8152(03)00078-1

Minella, J.P.G., Merten, G.H., Reichert, J.M., Clarke, R.T., 2008. Estimating suspended sediment concentrations from turbidity measurements and the calibration problem. Hydrological Processes 22, 1819–1830. https://doi.org/10.1002/hyp.6763

Ministere de l'Economie et des Finances, 2008. RECENSEMENT GENERAL DE LA POPULATION ET DE L'HABITATION DE 2006. Ouagadougou, Burkina Faso.

Mohamoud, Y.M., 1992. Evaluating Manning's roughness coefficients for tilled soils. Journal of Hydrology 135, 143–156. https://doi.org/10.1016/0022-1694(92)90086-B

Mohanty, B.P., Kanwar, R.S., Everts, C.J., 1994. Comparison of saturated hydraulic conductivity measurement methods for a glacial-till soil. Soil Science Society of America Journal 58, 672–677.

Monteith, J.L., 1975. Vegetation and the Atmosphere, vol. 1: Principles, vol. 2. Case studies. Academic Press, New York.

Morgan, R.P.C., 2005. Soil Erosion and Conservation. Blackwell Publishing, Oxford, U.K.

Morgan, R.P.C., Nearing, M.A., 2011. Handbook of erosion modelling. Wiley Online Library.

Moss, R.H., Edmonds, J.A., Hibbard, K.A., Manning, M.R., Rose, S.K., van Vuuren, D.P., Carter, T.R., Emori, S., Kainuma, M., Kram, T., Meehl, G.A., Mitchell, J.F.B., Nakicenovic, N., Riahi, K., Smith, S.J., Stouffer, R.J., Thomson, A.M., Weyant, J.P., Wilbanks, T.J., 2010. The next generation of scenarios for climate change research and assessment. Nature 463, 747–756. https://doi.org/10.1038/nature08823

Mouhamed, L., Traore, S.B., Alhassane, A., Sarr, B., 2013. Evolution of some observed climate extremes in the West African Sahel. Weather and Climate Extremes 1, 19–25. https://doi.org/10.1016/j.wace.2013.07.005

Mourato, S., Moreira, M., Corte-Real, J., 2015. Water Resources Impact Assessment Under Climate Change Scenarios in Mediterranean Watersheds. Water Resources Management 29, 2377–2391. https://doi.org/10.1007/s11269-015-0947-5

Muerth, M.J., Gauvin St-Denis, B., Ricard, S., Velázquez, J.A., Schmid, J., Minville, M., Caya, D., Chaumont, D., Ludwig, R., Turcotte, R., 2013. On the need for bias correction in regional climate scenarios to assess climate change impacts on river runoff. Hydrol. Earth Syst. Sci. 17, 1189–1204. https://doi.org/10.5194/hess-17-1189-2013

Mullan, D., Favis-Mortlock, D., Fealy, R., 2012. Addressing key limitations associated with modelling soil erosion under the impacts of future climate change. Agricultural and Forest Meteorology 156, 18–30. https://doi.org/10.1016/j.agrformet.2011.12.004

Naseela, E.K., Dodamani, B.M., Chandran, C., 2015. Estimation of Runoff Using NRCS-CN Method and SHETRAN Model. International Advanced Research Journal in Science, Engineering and Technology 2, 23–28. https://doi.org/10.17148 /IARJSET.2015.2807

Nash, J.E., Sutcliffe, J.V., 1970. River flow forecasting through conceptual models part I — A discussion of principles. Journal of Hydrology 10, 282–290. https://doi.org/10.1016/0022-1694(70)90255-6

Navratil, O., Esteves, M., Legout, C., Gratiot, N., Nemery, J., Willmore, S., Grangeon, T., 2011. Global uncertainty analysis of suspended sediment monitoring using turbidimeter in a small mountainous river catchment. Journal of Hydrology 398, 246–259. https://doi.org/10.1016/j.jhydrol.2010.12.025

Nearing, M.A., 2000. Evaluating soil erosion models using measured plot data: accounting for variability in the data. Earth Surface Processes and Landforms 25, 1035–1043. https://doi.org/10.1002/1096-9837(200008)25:9<1035::AID-ESP121>3.0.CO;2-B

Nearing, M.A., 1998. Why soil erosion models over-predict small soil losses and under-predict large soil losses. CATENA 32, 15–22. https://doi.org/10.1016/S0341-8162(97)00052-0

Nearing, M.A., Govers, G., Norton, L.D., 1999. Variability in soil erosion data from replicated plots. Soil Science Society of America Journal 63, 1829–1835. https://doi.org/10.2136/sssaj1999.6361829x

Nearing, M.A., Pruski, F.F., O'Neal, M.R., 2004. Expected climate change impacts on soil erosion rates: A review. Journal of Soil and Water Conservation 59, 43–50.

Neitsch, S.L., Arnold, J.G., Kiniry, J.R., Williams, J.R., 2011. Soil and water assessment tool theoretical documentation version 2009. Texas Water Resources Institute.

New, M., Hewitson, B., Stephenson, D.B., Tsiga, A., Kruger, A., Manhique, A., Gomez, B., Coelho, C.A.S., Masisi, D.N., Kululanga, E., Mbambalala, E., Adesina, F., Saleh, H., Kanyanga, J., Adosi, J., Bulane, L., Fortunata, L., Mdoka, M.L., Lajoie, R., 2006. Evidence of trends in daily climate extremes over southern and west Africa. Journal of Geophysical Research 111. https://doi.org/10.1029/2005JD006289

Niang, I., Ruppel, O.C., Abdrabo, M.A., Essel, A., Lennard, C., Padgham, J., Urquhart, P., 2014. Africa, in: Barros, V.R., Field, C.B., Dokken, D.J., Mastrandrea, M.D., Mach, K.J., Bilir, T.E., Chatterjee, M., Ebi, K.L., Estrada, Y.O., Genova, R.C., Girma, B., Kissel, E.S., Levy, A.N., MacCracken, S., Mastrandrea, P.R., White, L.L. (Eds.), Climate Change 2014: Impacts, Adaptation, and Vulnerability. Part B: Regional Aspects. Cambridge University Press, Cambridge, United Kingdom and New York, NY, USA, pp. 1199–1265.

Nikulin, G., Jones, C., Giorgi, F., Asrar, G., Büchner, M., Cerezo-Mota, R., Christensen, O.B., Déqué, M., Fernandez, J., Hänsler, A., van Meijgaard, E., Samuelsson, P., Sylla, M.B., Sushama, L., 2012. Precipitation Climatology in an Ensemble of CORDEX-Africa Regional Climate Simulations. Journal of Climate 25, 6057–6078. https://doi.org/10.1175/JCLI-D-11-00375.1

Nkonya, E., Karsenty, A., Msangi, S., Souza Jr, C., Shah, M., Von Braun, J., Galford, G., Park, S., 2012. Sustainable land use for the 21st century.

Norouzi Banis, Y., Bathurst, J.C., Walling, D.E., 2004. Use of caesium-137 data to evaluate SHETRAN simulated long-term erosion patterns in arable lands. Hydrological Processes 18, 1795–1809. https://doi.org/10.1002/hyp.1447

N'Tcha M'Po, Y., Lawin, A.E., Oyerinde, G.T., Yao, B.K., Afouda, A.A., 2016. Comparison of Daily Precipitation Bias Correction Methods Based on Four Regional Climate Model Outputs in Ouémé Basin, Benin. Hydrology 4, 58. https://doi.org/10.11648/j.hyd.20160406.11

Nunes, J.P., Seixas, J., Keizer, J.J., 2013. Modeling the response of within-storm runoff and erosion dynamics to climate change in two Mediterranean watersheds: A multi-model, multi-scale approach to scenario design and analysis. CATENA 102, 27–39. https://doi.org/10.1016/j.catena.2011.04.001

Obeta, I.N., Adewumi, J.K., 2013. Soil Loss in Samaru Zaria Nigeria: A comparison of WEPP and EUROSEM Models. Nigerian Journal of Technology 32, 197–202.

O'Gorman, P.A., Schneider, T., 2009. The physical basis for increases in precipitation extremes in simulations of 21st-century climate change. Proceedings of the National Academy of Sciences 106, 14773–14777. https://doi.org/10.1073/pnas.0907610106

Oguntunde, P.G., Abiodun, B.J., 2013. The impact of climate change on the Niger River Basin hydroclimatology, West Africa. Climate Dynamics 40, 81–94. https://doi.org/10.1007/s00382-012-1498-6

Okou, F.A.Y., Tente, B., Bachmann, Y., Sinsin, B., 2016. Regional erosion risk mapping for decision support: A case study from West Africa. Land Use Policy 56, 27–37. https://doi.org/10.1016/j.landusepol.2016.04.036

Op de Hipt, F., Diekkrüger, B., Steup, G., Yira, Y., Hoffmann, T., Rode, M., 2017. Applying SHETRAN in a Tropical West African Catchment (Dano, Burkina Faso)—Calibration, Validation, Uncertainty Assessment. Water 9, 101. https://doi.org/10.3390/w9020101

Osman, A.M., Thorne, C.R., 1988. Riverbank stability analysis. I: Theory. Journal of Hydraulic Engineering 114, 134–150. https://doi.org/10.1061/(ASCE)0733-9429(1988)114:2(134)

Oudin, L., Hervieu, F., Michel, C., Perrin, C., Andréassian, V., Anctil, F., Loumagne, C., 2005a. Which potential evapotranspiration input for a lumped rainfall–runoff model?: Part 2—Towards a simple and efficient potential evapotranspiration model for rainfall–runoff modelling. Journal of Hydrology 303, 290–306. https://doi.org/10.1016/j.jhydrol.2004.08.026

Oudin, L., Hervieu, F., Michel, C., Perrin, C., Andréassian, V., Anctil, F., Loumagne, C., 2005b. Which potential evapotranspiration input for a lumped rainfall–runoff model? Journal of Hydrology 303, 290–306. https://doi.org/10.1016/j.jhydrol.2004.08.026

Ouedraogo, I., Tigabu, M., Savadogo, P., Compaoré, H., Odén, P.C., Ouadba, J.M., 2010. Land cover change and its relation with population dynamics in Burkina Faso, West Africa. Land Degradation & Development 21, 453–462. https://doi.org/10.1002/ldr.981

Oyerinde, G., Hountondji, F., Lawin, A., Odofin, A., Afouda, A., Diekkrüger, B., 2017. Improving Hydro-Climatic Projections with Bias-Correction in Sahelian Niger Basin, West Africa. Climate 5, 8. https://doi.org/10.3390/cli5010008

Paeth, H., Hall, N.M.J., Gaertner, M.A., Alonso, M.D., Moumouni, S., Polcher, J., Ruti, P.M., Fink, A.H., Gosset, M., Lebel, T., Gaye, A.T., Rowell, D.P., Moufouma-Okia, W., Jacob, D., Rockel, B., Giorgi, F., Rummukainen, M., 2011. Progress in regional downscaling of west African precipitation. Atmospheric Science Letters 12, 75–82. https://doi.org/10.1002/asl.306

Panagos, P., Borrelli, P., Poesen, J., Meusburger, K., Ballabio, C., Lugato, E., Montanarella, L., Alewell, C., 2016. Reply to the comment on "The new assessment of soil loss by water erosion in Europe" by Fiener & Auerswald. Environmental Science & Policy 57, 143–150. https://doi.org/10.1016/j.envsci.2015.12.011

Pandey, A., Himanshu, S.K., Mishra, S.K., Singh, V.P., 2016. Physically based soil erosion and sediment yield models revisited. CATENA 147, 595–620. https://doi.org/10.1016/j.catena.2016.08.002

Paré, S., Söderberg, U., Sandewall, M., Ouadba, J.M., 2008. Land use analysis from spatial and field data capture in southern Burkina Faso, West Africa. Agriculture, Ecosystems & Environment 127, 277–285. https://doi.org/10.1016/j.agee.2008.04.009

Parkin, G., 1996. A three-dimensional variably-saturated subsurface modelling system for river basins. (Phd thesis). Newcastle University, Newcastle upon Tyne, United Kingdom, Newcastle upon Tyne <https://theses.ncl.ac.uk/dspace/handle/10443/3161>.

Parkin, G., O'donnell, G., Ewen, J., Bathurst, J.C., O'Connell, P.E., Lavabre, J., 1996. Validation of catchment models for predicting land-use and climate change impacts. 2. Case study for a Mediterranean catchment. Journal of Hydrology 175, 595–613. https://doi.org/10.1016/S0022-1694(96)80027-8

Persson, M., 2015. Education and political participation. British Journal of Political Science 45, 689–703. https://doi.org/10.1017/S0007123413000409

Piani, C., Weedon, G.P., Best, M., Gomes, S.M., Viterbo, P., Hagemann, S., Haerter, J.O., 2010. Statistical bias correction of global simulated daily precipitation and temperature for the application of hydrological models. Journal of Hydrology 395, 199–215. https://doi.org/10.1016/j.jhydrol.2010.10.024

Pinson, W.T., Yoder, D.C., Buchanan, J.R., Wright, W.C., Wilkerson, J.B., 2003. Design and evaluation of an improved flow divider for sampling runoff plots, in: 2003 ASAE Annual Meeting. American Society of Agricultural and Biological Engineers, p. 1.

Post, W.M., Emanuel, W.R., Zinke, P.J., Stangenberger, A.G., 1982. Soil carbon pools and world life zones. Nature 298, 156–159. https://doi.org/10.1038/298156a0

Ramankutty, N., 2004. Croplands in West Africa: A Geographically Explicit Dataset for Use in Models. Earth Interactions 8, 1–22. https://doi.org/10.1175/1087-3562(2004)8<1:CIWAAG>2.0.CO;2

Randall, D.A., Wood, R.A., Bony, S., Colman, R., Fichefet, T., Fyfe, J., Kattsov, V., Pitman, A., Shukla, J., Srinivasan, J., 2007. Climate models and their evaluation, in: Climate Change 2007: The Physical Science Basis. Cambridge University Press, pp. 589–662.

Rasmussen, P.P., Gray, J.R., Glysson, G.D., Ziegler, A.C., 2009. Guidelines and procedures for computing time-series suspended-sediment concentrations and loads from in-stream turbidity-sensor and streamflow data. US Geological Survey, Reston, United States.

Rawls, W.J., Brakensiek, D.L., 1985. Prediction of soil water properties for hydrologic modeling, in: Watershed Management in the Eighties. ASCE, pp. 293–299.

Rawls, W.J., Nemes, A., Pachepsky, Y., 2004. Effect of soil organic carbon on soil hydraulic properties, in: Developments in Soil Science. Elsevier, pp. 95–114. https://doi.org/10.1016/S0166-2481(04)30006-1

Rode, M., Suhr, U., 2007. Uncertainties in selected river water quality data. Hydrology and Earth System Sciences 11, 863–874. https://doi.org/hal- 00305056

Rompaey, A.J.J.V., Govers, G., 2002. Data quality and model complexity for regional scale soil erosion prediction. International Journal of Geographical Information Science 16, 663–680. https://doi.org/10.1080/13658810210148561

Roose, E., Kabore, V., Guenat, C., 1999. Zai Practice: A West African Traditional Rehabilitation System for Semiarid Degraded Lands, a Case Study in Burkina Faso. Arid Soil Research and Rehabilitation 13, 343–355. https://doi.org/10.1080/089030699263230

Roose, E., Sarrailh, J.-M., 1989. Erodibilité de quelques sols tropicaux. Vingt années de mesure en parcelles d'érosion sous pluies naturelles. Cahiers Orstom Série Pédologie 25, 7–30 <http://www.documentation.ird.fr/hor/fdi:30456>.

Roose, E.J., 1977. Use of the universal soil loss equation to predict erosion in West Africa. Soil Conservation Society of America, Ankeny, United States.

Roudier, P., Ducharne, A., Feyen, L., 2014. Climate change impacts on runoff in West Africa: a review. Hydrology and Earth System Sciences 18, 2789–2801. https://doi.org/10.5194/hess-18-2789-2014

Ruelland, D., Ardoin-Bardin, S., Collet, L., Roucou, P., 2012. Simulating future trends in hydrological regime of a large Sudano-Sahelian catchment under climate change. Journal of Hydrology 424–425, 207–216. https://doi.org/10.1016/j.jhydrol.2012.01.002

Rutter, A.J., Kershaw, K.A., Robins, P.C., Morton, A.J., 1972. A predictive model of rainfall interception in forests, 1. Derivation of the model from observations in a plantation of Corsican pine. Agricultural Meteorology 9, 367–384. https://doi.org/10.1016/0002-1571(71)90034-3

Rutter, A.J., Morton, A.J., Robins, P.C., 1975. A Predictive Model of Rainfall Interception in Forests. II. Generalization of the Model and Comparison with Observations in Some Coniferous and Hardwood Stands. Journal of Applied Ecology 12, 367–380. https://doi.org/10.2307/2401739

Saxton, K.E., Rawls, W.J., 2006. Soil Water Characteristic Estimates by Texture and Organic Matter for Hydrologic Solutions. Soil Science Society of America Journal 70, 1569. https://doi.org/10.2136/sssaj2005.0117

Saxton, K.E., Rawls, W.J., Romberger, J.S., Papendick, R.I., 1986. Estimating Generalized Soil-water Characteristics from Texture1. Soil Science Society of America Journal 50, 1031. https://doi.org/10.2136/sssaj1986.03615995005000040039x

Schaap, M.G., Leij, F.J., van Genuchten, M.T., 2001. rosetta: a computer program for estimating soil hydraulic parameters with hierarchical pedotransfer functions. Journal of Hydrology 251, 163–176. https://doi.org/10.1016/S0022-1694(01)00466-8

Schmengler, A.C., 2010. Modeling soil erosion and reservoir sedimentation at hillslope and catchment scale in semi-arid Burkina Faso (Phd thesis). Rheinische Friedrich-Wilhelms-Universität Bonn, Bonn, <http://hss.ulb.uni-bonn.de/2011/2483/2483.htm>.

Schmengler, A.C., Vlek, P.L., 2015. Assessment of accumulation rates in small reservoirs by core analysis, 137Cs measurements and bathymetric mapping in Burkina Faso. Earth Surface Processes and Landforms 40, 1951–1963. https://doi.org/10.1002/esp.3772

Scoccimarro, E., Gualdi, S., Bellucci, A., Zampieri, M., Navarra, A., 2013. Heavy Precipitation Events in a Warmer Climate: Results from CMIP5 Models. Journal of Climate 26, 7902–7911. https://doi.org/10.1175/JCLI-D-12-00850.1

Serdeczny, O., Adams, S., Baarsch, F., Coumou, D., Robinson, A., Hare, W., Schaeffer, M., Perrette, M., Reinhardt, J., 2016. Climate change impacts in Sub-Saharan Africa: from physical changes to their social repercussions. Regional Environmental Change. https://doi.org/10.1007/s10113-015-0910-2

Sharma, D., Das Gupta, A., Babel, M.S., 2007. Spatial disaggregation of bias-corrected GCM precipitation for improved hydrologic simulation: Ping River Basin, Thailand. Hydrology and Earth System Sciences 11, 1373–1390. https://doi.org/10.5194/hess-11-1373-2007

Shen, H.W., Julien, P.Y., 1993. Erosion and sediment transport, in: Maidment, D.R. (Ed.), Handbook of Hydrology. McGraw-Hill, New York.

Shields, A., 1936. Anwendung der Aehnlichkeitsmechanik und der Turbulenzforschung auf die Geschiebebewegung. Technische Hochschule Berlin, Berlin.

Shuttleworth, W.J., 1993. Evaporation, in: Maidment, D.R. (Ed.), Handbook of Hydrology. McGraw-Hill, New York.

Sivakumar, M.V.K., Gnoumou, F., 1987. Agroclimatology of West Africa: Burkina Faso, Information Bulletin. International Crops Research Institute for the Semi-Arid Tropics, Patancheru, India.

Slaymaker, O., 2001. Why so much concern about climate change and so little attention to land use change. The Canadian Geographer/Le Géographe canadien 45, 71–78. https://doi.org/10.1111/j.1541-0064.2001.tb01169.x

Smith, P., House, J.I., Bustamante, M., Sobocká, J., Harper, R., Pan, G., West, P.C., Clark, J.M., Adhya, T., Rumpel, C., Paustian, K., Kuikman, P., Cotrufo, M.F., Elliott, J.A., McDowell, R., Griffiths, R.I., Asakawa, S., Bondeau, A., Jain, A.K., Meersmans, J., Pugh, T.A.M., 2016. Global change pressures on soils from land use and management. Global Change Biology 22, 1008–1028. https://doi.org/10.1111/gcb.13068

Stephenne, N., Lambin, E.F., 2001. A dynamic simulation model of land-use changes in Sudano-sahelian countries of Africa (SALU). Agriculture, ecosystems & environment 85, 145–161. https://doi.org/10.1016/S0167-8809(01)00181-5

Sylla, M.B., Elguindi, N., Giorgi, F., Wisser, D., 2016a. Projected robust shift of climate zones over West Africa in response to anthropogenic climate change for the late 21st century. Climatic Change 134, 241–253. https://doi.org/10.1007/s10584-015-1522-z

Sylla, M.B., Nikiema, P.M., Gibba, P., Kebe, I., Klutse, N.A.B., 2016b. Climate Change over West Africa: Recent Trends and Future Projections, in: Yaro, J.A., Hesselberg, J. (Eds.), Adaptation to Climate Change and Variability in Rural West Africa. Springer International Publishing, Cham, pp. 25–40. https://doi.org/10.1007/978-3-319-31499-0_3

Teutschbein, C., Seibert, J., 2012. Bias correction of regional climate model simulations for hydrological climate-change impact studies: Review and evaluation of different methods. Journal of Hydrology 456–457, 12–29. https://doi.org/10.1016/j.jhydrol.2012.05.052

The World Bank, 2017. Burkina Faso | Data [WWW Document]. Burkina Faso. URL http://data.worldbank.org/country/burkina-faso (accessed 2.16.17).

Thiombiano, A., Kampmann, D., 2010. Biodiversity Atlas of West Africa, Volume II: Burkina Faso (No. II). Ouagadougou & Frankfurt/Main.

Toy, T.J., Foster, G.R., Renard, K.G., 2002. Soil erosion: processes, prediction, measurement, and control. John Wiley & Sons, Hoboken, United States.

Tripkovic, V., 2014. Quantifying and upscaling surface and subsurface runoff and nutrient flows under climate variability (Phd thesis). Newcastle University, Newcastle upon Tyne, <https://theses.ncl.ac.uk/dspace/handle/10443/2380>.

UN DESA (United Nations Department of Economic and Social Affairs and Population Division), 2015. World Population Prospects: The 2015 Revision, Key Findings and Advance Tables. Working Paper, No. ESA/P/WP. 241.

UNDP (United Nations Development Programme) (Ed.), 2016. Human development for everyone, Human development report. United Nations Development Programme, New York, NY.

UNEP (United Nations Environmental Programme), 2012. Global Environment Outlook 4 (No. 4). UNEP, Valletta, Malta.

Valentin, C., Rajot, J.-L., Mitja, D., 2004. Responses of soil crusting, runoff and erosion to fallowing in the sub-humid and semi-arid regions of West Africa. Agriculture, Ecosystems & Environment 104, 287–302. https://doi.org/10.1016/j.agee.2004.01.035

Van Genuchten, M.T., 1980. A closed-form equation for predicting the hydraulic conductivity of unsaturated soils. Soil Science Society of America Journal 44, 892–898. https://doi.org/10.2136/sssaj1980.03615995004400050002x

van Reeuwijk, R.P., 2002. Procedures for Soil Analysis, 6th ed, Technical Paper. ISRIC, Wageningen, Netherlands.

Vereecken, H., Maes, J., Feyen, J., 1990. ESTIMATING UNSATURATED HYDRAULIC CONDUCTIVITY FROM EASILY MEASURED SOIL PROPERTIES: Soil Science 149, 1–12. https://doi.org/10.1097/00010694-199001000-00001

Vicente-Serrano, S.M., Beguería, S., López-Moreno, J.I., 2010. A Multiscalar Drought Index Sensitive to Global Warming: The Standardized Precipitation Evapotranspiration Index. Journal of Climate 23, 1696–1718. https://doi.org/10.1175/2009JCLI2909.1

Villani, V., Rianna, G., Mercogliano, P., Zollo, A., Schiano, P., 2014. Statistical approaches versus weather generator to downscale rcm outputs to point scale: a comparison of perfor-

mances. Journal of Urban and Environmental Engineering 8, 142–154. https://doi.org/10.4090/juee.2014.v8n2.142154

Visser, S.M., Sterk, G., Karssenberg, D., 2005. Modelling water erosion in the Sahel: application of a physically based soil erosion model in a gentle sloping environment. Earth Surface Processes and Landforms 30, 1547–1566. https://doi.org/10.1002/esp.1212

Vizy, E.K., Cook, K.H., 2012. Mid-Twenty-First-Century Changes in Extreme Events over Northern and Tropical Africa. Journal of Climate 25, 5748–5767. https://doi.org/10.1175/JCLI-D-11-00693.1

Wagner, P.D., Kumar, S., Schneider, K., 2013. An assessment of land use change impacts on the water resources of the Mula and Mutha Rivers catchment upstream of Pune, India. Hydrology and Earth System Sciences 17, 2233–2246.

Walling, D.E., 2009. The impact of global change on erosion and sediment transport by rivers: current progress and future challenges (No. 3), The United Nations World Water Development Report. UNESCO, Paris, France.

Walling, D.E., Collins, A.L., Sichingabula, H.M., Leeks, G.J.L., 2001. Integrated assessment of catchment suspended sediment budgets: a Zambian example. Land Degradation & Development 12, 387–415. https://doi.org/10.1002/ldr.461

Waongo, M., 2015. Optimizing Planting Dates for Agricultural Decision-Making under Climate Change over Burkina Faso/West Africa (Phd thesis). Universität Augsburg, Augsburg, Germany <https://opus.bibliothek.uni-augsburg.de/opus4/frontdoor/index/index/docId/3280>.

Wendt, R.C., Alberts, E.E., Hjelmfelt, A.T., 1986. Variability of runoff and soil loss from fallow experimental plots. Soil Science Society of America Journal 50, 730–736. https://doi.org/10.2136/sssaj1986.03615995005000030035x

Wicks, J.M., 1988. Physically-based mathematical modelling of catchment sediment yield (Phd thesis). Newcastle University, Newcastle upon Tyne <https://theses.ncl.ac.uk/dspace/handle/10443/152>.

Wicks, J.M., Bathurst, J.C., 1996. SHESED: a physically based, distributed erosion and sediment yield component for the SHE hydrological modelling system. Journal of Hydrology 175, 213–238. https://doi.org/10.1016/S0022-1694(96)80012-6

Wicks, J.M., Bathurst, J.C., Johnson, C.W., Ward, T.J., 1988. Application of two physically-based sediment yield models at plot and field scales, in: Sediment Budgets (Proceedings of the Porto-Alegre Symposium). Presented at the Assembly of the International Association of Hydrological Sciences, Brazil, pp. 583–591.

Wilson, C.O., Weng, Q., 2011. Simulating the impacts of future land use and climate changes on surface water quality in the Des Plaines River watershed, Chicago Metropolitan Statistical Area, Illinois. Science of The Total Environment 409, 4387–4405. https://doi.org/10.1016/j.scitotenv.2011.07.001

Wischmeier, W.H., Mannering, J.V., 1969. Relation of Soil Properties to its Erodibility. Soil Science Society of America Journal 33, 131. https://doi.org/10.2136/sssaj1969.03615995003300010035x

WMO (World Meteorological Organization), 2010. Manual on Stream Gauging Volume 1 - Fieldwork (No. 1044). World Meteorological Organization, Lausanne.

WMO (World Meteorological Organization), 1993. Siting and Exposure of Meteorological Instruments (SEMI) (No. 55), Instruments and Observing Methods. World Meteorological Organization, Lausanne.

Wösten, J.H.M., Pachepsky, Y.A., Rawls, W.J., 2001. Pedotransfer functions: bridging the gap between available basic soil data and missing soil hydraulic characteristics. Journal of Hydrology 251, 123–150. https://doi.org/10.1016/S0022-1694(01)00464-4

WWAP (United Nations World Water Assessment Programme), 2015. World Water Development Report 2015: Water for a Sustainable World. Unesco Paris.

Yahmed, D.B., 2005. Atlas du Burkina Faso, Atlas de l'Afrique. Éditions J.A., Paris, France.

Yalin, M.S., 1963. An expression for bed-load transportation. Journal of the Hydraulics Division 89, 221–250.

Yang, D., Kanae, S., Oki, T., Koike, T., Musiake, K., 2003. Global potential soil erosion with reference to land use and climate changes. Hydrological Processes 17, 2913–2928. https://doi.org/10.1002/hyp.1441

Yira, Y., 2016. Modelling Climate and Land Use Change Impacts on Water Resources in the Dano Catchment (Burkina Faso, West Africa) (Phd thesis). Rheinische Friedrich-Wilhelms-Universität Bonn, Bonn, <http://hss.ulb.uni-bonn.de/2017/4583/4583.htm>.

Yira, Y., Diekkrüger, B., Steup, G., Bossa, A.Y., 2017. Impact of climate change on hydrological conditions in a tropical West African catchment using an ensemble of climate simulations. Hydrology and Earth System Sciences 21, 2143–2161. https://doi.org/10.5194/hess-21-2143-2017

Yira, Y., Diekkrüger, B., Steup, G., Bossa, A.Y., 2016. Modeling land use change impacts on water resources in a tropical West African catchment (Dano, Burkina Faso). Journal of Hydrology 537, 187–199. https://doi.org/10.1016/j.jhydrol.2016.03.052

Young, M.D.B., Gowing, J.W., Hatibu, N., Mahoo, H.M.F., Payton, R.W., 1999. Assessment and development of pedotransfer functions for semi-arid sub-Saharan Africa. Physics and Chemistry of the Earth, Part B: Hydrology, Oceans and Atmosphere 24, 845–849. https://doi.org/10.1016/S1464-1909(99)00091-X

Zhang, H., Huang, G.H., Wang, D., Zhang, X., 2011. Uncertainty assessment of climate change impacts on the hydrology of small prairie wetlands. Journal of Hydrology 396, 94–103. https://doi.org/10.1016/j.jhydrol.2010.10.037

Zhang, R., 2015. Integrated modelling for evaluation of climate change impacts on agricultural dominated basin (Phd thesis). University Evora, Evora <https://dspace.uevora.pt/rdpc/handle/10174/13270>.

Zougmore, R., Mando, A., Ringersma, J., Stroosnijder, L., 2003. Effect of combined water and nutrient management on runoff and sorghum yield in semiarid Burkina Faso. Soil Use Manage. 19, 257–264. https://doi.org/10.1079/SUM2003199

Zoungrana, B.J., Conrad, C., Amekudzi, L.K., Thiel, M., Da, E.D., Forkuor, G., Löw, F., 2015. Multi-temporal landsat images and ancillary data for land use/cover change (LULCC) detection in the southwest of Burkina Faso, West Africa. Remote Sensing 7, 12076–12102. https://doi.org/10.3390/rs70912076

APPENDIX

Appendix A: Soil depth, texture and coarse particle content

		Depth [cm]				Sand [%]				Clay [%]				Silt [%]				Coarse P [%]			
	Horizon N	**1**	**2**	**3**	**4**	**1**	**2**	**3**	**4**	**1**	**2**	**3**	**4**	**1**	**2**	**3**	**4**	**1**	**2**	**3**	**4**
Soil component																					
Endopetric_Plinthosol	n	24	15	9	0	11	16	2	0	11	16	2	0	11	16	2	0	11	16	4	1
	Mean	13.4	36	66.7		35.1	26.6	25.4		19.9	30.3	34.5		45.9	43.7	37.8		51.8	61.7	71.5	90
	Sd.	4.51	2.62	10		8.28	7.26	12.5		9.52	8.36	0.57		9.94	7.95	6.61		19	19.9	14.2	
	Min	8	34	60		21	15.2	16.6		10.2	12.2	34.1		36.7	33.8	33.2		1	12.5	56.5	90
	Max	22	40	80		46.7	40.5	34.2		42	42	34.9		68.9	62.4	42.5		68.6	79.9	90	90
Epipetric_Plinthosol	n	15	3	0	0	16	16	0	0	16	16	0	0	16	16	0	0	16	16	2	0
	Mean	12	45			40.3	29.4			16.5	25.4			43.2	45.4			62.2	65.2	90	
	Sd.	2.54	0			7.94	8.07			3.35	7.12			8.24	8.79			19.8	17.2	0	
	Min	10	45			23.6	15.9			12.2	13.3			30.1	35.4			14	19.9	90	
	Max	15	45			52.5	43.8			22.8	38.5			63.6	63			85	85	90	
Gleyic_Lixisol	n	3	9	9	0	1	3	0	0	1	3	0	0	1	3	0	0	1	3	0	0
	Mean	17	37	74		32.1	14.4			18.2	31.5			47	51.1			40	37.1		
	Sd.	0	0	0		2.16				3.14				0.7				29.4			
	Min	17	37	74		32.1	12.9			18.2	27.9			47	50.5			40	10.6		
	Max	17	37	74		32.1	16.9			18.2	33.4			47	51.9			40	68.7		
Gleyic_Plinthosol	n	3	9	0	0	1	1	1	0	1	1	1	0	1	1	1	0	1	1	1	0
	Mean	40	100			27.3	17.1	15.1		26.2	60.1	60.4		49.8	35	37.9		72.2	72.4	53.6	
	Sd.	0	0																		
	Min	40	100			27.3	17.1	15.1		26.2	60.1	60.4		49.8	35	37.9		72.2	72.4	53.6	
	Max	40	100			27.3	17.1	15.1		26.2	60.1	60.4		49.8	35	37.9		72.2	72.4	53.6	
Haplic_Cambisol	n	41	45	42	9	6	10	1	1	6	10	1	1	6	10	1	1	6	10	1	1
	Mean	13.6	43.8	89.7	100	26.7	31.6	15.7	8.76	31.3	30.6	27.4	20.6	43	38.7	56.6	60.5	36.6	43.4	0	20
	Sd.	6.2	21.7	19.5	0	7.66	13.4			13.3	14.2			6.66	6.94			17.9	23.9		
	Min	5	13	43	100	14.8	16.6	15.7	8.76	10.7	12	27.4	20.6	36.8	29.3	56.6	60.5	13.5	3.09	0	20
	Max	24	70	100	100	34	50.5	15.7	8.76	46.9	50	27.4	20.6	55.3	51.7	56.6	60.5	58.5	76.9	0	20
Haplic_Gleysol	n	66	60	27	0	10	20	3	0	10	20	3		10	20	3	0	10	20	3	0
	Mean	22.5	49.7	77		20.4	14	17.6		29.8	37.1	43.1		53.8	51	49.7		10.5	9.55	24	
	Sd.	9.74	16.9	20.5		10.3	7.42	8.74		11.3	10.7	17.1		11.3	7.3	8.76		15.5	10.5	19.5	
	Min	8	28	51		3.7	2.2	11.5		16.5	22.8	24		34.5	36.9	41.7		0	0	1.79	
	Max	40	77	100		37.4	36.4	27.6		53.2	60.4	57.1		65.4	66	59.1		46.5	38.1	38.9	
Haplic_Lixisol	n	18	18	0	0	2	1	1	0	2	1	1	0	2	1	1		2	1	1	0

		Depth [cm]				Sand [%]				Clay [%]				Silt [%]				Coarse P [%]			
	Horizon N	**1**	**2**	**3**	**4**	**1**	**2**	**3**	**4**	**1**	**2**	**3**	**4**	**1**	**2**	**3**	**4**	**1**	**2**	**3**	**4**
	Mean	26.5	62.5			21.5	14.3	14.6		22.5	38.3	37.4		60.3	55.7	55.5		14	19.9	19.9	
	Sd.	3.6	2.57			2.63				12.7				4.03				0			
	Min	23	60			19.6	14.3	14.6		13.6	38.3	37.4		57.4	55.7	55.5		14	19.9	19.9	
	Max	30	65			23.4	14.3	14.6		31.5	38.3	37.4		63.1	55.7	55.5		14	19.9	19.9	
Haplic_Plinthosol	n	42	57	39	0	25	41	6	0	25	41	6	0	25	41	6	0	25	41	6	0
	Mean	16.7	50.8	98.2		32.9	22.4	24.4		22.4	37.4	37.3		45.6	40.4	40.1		52.3	56	56.2	
	Sd.	5.97	10.5	8.6		11.2	8.08	6.78		10	11.9	10.7		10.2	8.62	8.35		18.7	21.8	17.1	
	Min	7	30	69		10.7	2.83	15.6		7.82	15.6	20.6		24.3	20.7	28.8		2.75	0	33.5	
	Max	23	63	102		51.7	38.1	36.5		45.4	62.9	48		69.9	58.1	51.1		75.3	83.6	82.6	
Haplic_Stagnosol	n	18	18	15	0	1	5	0	0	1	5	0	0	1	5	0	0	1	5	0	0
	Mean	17	31	100		43.9	14.5			20.9	38.3			36.2	46.4			57	26.9		
	Sd.	3.09	11.3			5.83				2.97				3.85				18.3			
	Min	14	20	100		43.9	4.48			20.9	33.2			36.2	42.7			57	10.2		
	Max	20	42	100		43.9	18.6			20.9	40.5			36.2	50.7			57	56.9		
Lixic_Gleysol	n	15	27	15	0	2	3			2	3	0	0	2	3	0	0	2	3	0	0
	Mean	14.8	56.7	86		25.1	16.1			16.7	27.8			58.3	56.4			21.6	22		
	Sd.	6.59	20.9	17.7		0.65	7.25			1.24	8.74			2.05	3.54			6.29	2.56		
	Min	7	28	65		24.7	10.4			15.8	20.2			56.9	52.3			17.2	19.2		
	Max	20	75	100		25.6	24.2			17.6	37.4			59.7	58.6			26.1	24.1		
Lixic_Plinthosol	n	26	30	42	9	8	15	0	0	8	15	0	0	8	15	0	0	8	15	2	0
	Mean	19.1	43.7	95.1	100	37.2	25.7			18.2	31.4			45.9	43.1			54.3	56.7	38.2	
	Sd.	6.62	13.4	15.5	0	11.1	7.91			7.79	9.68			14.3	8.53			17.3	20.3	26	
	Min	12	30	40	100	19.6	11.8			10.7	19.6			21.6	29.6			14	12.3	19.9	
	Max	27	60	101	100	54.4	41			34.3	57.6			65	59.6			71.8	82.6	56.6	
Lixic_Stagnosol	n	9	12	9	0	1	1	1	0	1	1	1	0	1	1	1	0	1	1	1	
	Mean	23	50.3	100		32.1	21.6	28.8		31.7	46.4	39.6		45.5	41.1	40.7		14.1	10.8	35.6	
	Sd.	0	17.6	0																	
	Min	23	21	100		32.1	21.6	28.8		31.7	46.4	39.6		45.5	41.1	40.7		14.1	10.8	35.6	
	Max	23	60	100		32.1	21.6	28.8		31.7	46.4	39.6		45.5	41.1	40.7		14.1	10.8	35.6	
Plinthic_Cambisol	n	9	9	6	0	1	2	0	0	1	2	0	0	1	2	0	0	1	2	0	0
	Mean	10	49	100		26.5	26.5			29	29			39.4	39.4			22	26.1		
	Sd.	0	0	0		3.5				5.44				4.15				21.3			
	Min	10	49	100		26.5	24			29	25.2			39.4	36.4			22	11.1		
	Max	10	49	100		26.5	29			29	32.9			39.4	42.3			22	41.2		
Plinthic_Gleysol	n	16	18	15	0	3	6	0	0	3	6	0	0	3	6	0	0	3	6	0	0
	Mean	14.2	27	50.6		32.6	23.1			17.7	31.1			51.8	44.3			39.1	45.6		
	Sd.	2.56	7.84	12.2		15.6	11.4			2.85	8.74			16.2	5.85			29.5	17.9		

		Depth [cm]				Sand [%]				Clay [%]				Silt [%]				Coarse P [%]			
	Horizon N	**1**	**2**	**3**	**4**	**1**	**2**	**3**	**4**	**1**	**2**	**3**	**4**	**1**	**2**	**3**	**4**	**1**	**2**	**3**	**4**
	Min	12	17	41		15.6	7.9			14.5	20.8			38.8	37.1			12.3	22.3		
	Max	17	34	65		46.1	33.1			19.6	42.3			70	49.8			70.7	66.4		
Plinthic_Lixisol	n	6	0	0	0	2	2	2	0	2	2	2	0	2	2	2	0	2	2	2	0
	Mean	24				20.8	10.7	14.9		22	31.4	34.6		56.3	54.9	46.8		40	37.1	68.7	
	Sd.	0				7.17	4.64	8.84		4.54	3.14	7.27		0.45	1.68	1.44		0	0	0	
	Min	24				15.7	7.39	8.7		18.8	29.2	29.4		56	53.7	45.8		40	37.1	68.7	
	Max	24				25.9	13.9	21.2		25.2	33.6	39.7		56.7	56.1	47.8		40	37.1	68.7	
Plinthic_Stagnosol	n	15	18	15	0	2	4	0	0	2	4	0	0	2	4	0	0	2	4	0	0
	Mean	14.8	33	101		32.9	24.9			18.6	34.1			48.8	40.9			7.34	24.3		
	Sd.	4.06	1.03	0.51		7.71	5.57			6.39	9.49			14.5	10.4			10.4	29.2		
	Min	10	32	100		27.4	18.9			14.1	23.5			38.5	30.2			0	1.09		
	Max	18	34	101		38.4	31.1			23.2	44.9			59	54.4			14.7	67		
Stagnic_Cambisol	n	18	21	9	6	2	6	1	0	2	6	1	0	2	6	1	0	2	6	1	0
	Mean	25	38.6	69	100	26.7	18.6	24.7		28.9	37.5	31.3		53.1	48	63.5		45.3	33.5	12.5	
	Sd.	5.14	3.59	0	0	7.59	5.71			4.41	8.86			14.3	7.8			26.2	19.7		
	Min	20	30	69	100	21.3	10.7	24.7		25.8	29.4	31.3		42.9	40.4	63.5		26.8	7.81	12.5	
	Max	30	40	69	100	32	23.8	24.7		32	51.2	31.3		63.2	62.4	63.5		63.8	62.6	12.5	
Stagnic_Plinthosol	n	18	27	27	18	3	6	1	1	3	6	1	1	3	6	1	1	3	6	1	1
	Mean	12.5	54	83	100	30.5	17.1	15.9	16.5	31.4	45.3	60.3	62.6	46.8	41.5	29.5	33.1	36.8	57.8	81.4	78.4
	Sd.	2.57	17.3	26.9	0	10.3	7.98			8.67	11.8			8.67	9.28			34.1	19.8		
	Min	10	38	60	100	23.7	8.21	15.9	16.5	25.2	31.4	60.3	62.6	40.6	29.3	29.5	33.1	0.88	22.9	81.4	78.4
	Max	15	73	120	100	42.4	27.2	15.9	16.5	41.3	59.8	60.3	62.6	56.7	55	29.5	33.1	68.6	77.7	81.4	78.4
Gleyic cambisol	n	1	3	0	0	1	3	0	0	1	3	0	0	1	3	0	0	1	3	0	0
	Mean	20	26.7			21	21.3			32	32			43	42.9			26.8	43.4		
	Sd.	0	5.86			0	3.49			0	3.44			0	2.59			0	16.6		
	Min	20	20			21	17.3			32	29.4			43	40.4			26.8	33.2		
	Max	20	26.7			21	21.3			32	32			43	42.9			26.8	43.4		
Haplic leptosol	n																				
	Mean	26.5	62.5			21.5	14.3	14.6		22.5	38.3	37.4		60.3	55.7	55.5		14	19.9	19.9	
	Sd.																				
	Min																				
	Max																				
Stagnic lixisol	n	1				1				1				1				1			
	Mean	7				47.2				23.5				30.9				71			
	Sd.																				
	Min																				
	Max																				

Appendix B: Bulk density (BD), soil organic carbon content (SOC), residual water content (θ_s), saturated hydraulic conductivity (K_{sat})

		BD [g/cm³]				SOC [%]				θs [Vol.%]				K_{sat} [cm/day]			
Soil component	**Horizon N**	**1**	**2**	**3**	**4**	**1**	**2**	**3**	**4**	**1**	**2**	**3**	**4**	**1**	**2**	**3**	**4**
Endopetric_Plinthosol	n	11	16	4	1	11	16	2	0	24	15	9	0	24	15	9	0
	Mean	1.49	1.52	1.66	1.9	1.158	0.801	0.968		36.34	36.26	34.42		1669	820.1	909.1	
	Sd.	0.07	0.08	0.17		0.412	0.579	0.135		3.437	2.584	5.737		617.3	328	661.2	
	Min	1.34	1.39	1.5	1.9	0.485	0.28	0.872		31.25	31.71	29.14		303.4	283.6	450.2	
	Max	1.6	1.7	1.9	1.9	1.815	2.258	1.064		40.87	39.3	41.85		2482	1172	1790	
Epipetric_Plinthosol	n	16	16	2	0	16	16	0	0	15	3	0	0	15	3	0	0
	Mean	1.52	1.48	1.9		1.786	0.947			36.7	44.29			1005	1731		
	Sd.	0.09	0.12	0		0.56	0.391			5.021	0			549.6	42.82		
	Min	1.35	1.15	1.9		0.451	0.066			27.48	44.29			0.314	1706		
	Max	1.7	1.68	1.9		2.619	1.522			41.36	44.29			1485	1780		
Gleyic_Lixisol	n					1	3	0	0	3	9	9		3	9	9	0
	Mean	1.4	1.5		0	0.921	0.349			41.25	35.58	33.59		389.3	704.3	1037	
	Sd.	0.26				0.134				0	1.601	1.105		9.917	1032	604.2	
	Min	1.4	1.24			0.921	0.22			41.25	33.5	32.15		377.9	7.252	362.6	
	Max	1.4	1.75			0.921	0.488			41.25	37.03	34.57		395.1	2108	1762	
Gleyic_Plinthosol	n	1	1	1	0	1	1	1	0	3	9	0	0	3	9	0	0
	Mean	1.64	1.61	1.42		1.177	0.634	0.64		42.27	48.21			954.9	0.047		
	Sd.									0	1.614			0	0.002		
	Min	1.64	1.61	1.42		1.177	0.634	0.64		42.27	46.08			954.9	0.044		
	Max	1.64	1.61	1.42		1.177	0.634	0.64		42.27	49.52			954.9	0.048		
Haplic_Cambisol	n	6	10	1	1	6	10	1	1	41	45	42	9	41	45	42	9
	Mean	1.32	1.47	1.41	1.07	1.223	0.657	0.446	0.952	45.85	42.77	41.86	38.8	1172	401.1	318.8	10.95
	Sd.	0.2	0.14			0.345	0.453			4.059	5.232	5.448	0.983	785.3	606.6	497.3	9.555
	Min	1.04	1.31	1.41	1.07	0.895	0	0.446	0.952	36.67	35.02	33.08	37.79	8.815	0.551	0.512	1.133
	Max	1.62	1.77	1.41	1.07	1.884	1.47	0.446	0.952	51.5	51.16	49.95	40.03	2489	2117	1888	24.93
Haplic_Gleysol	n	10	20	3	0	10	20	3	0	66	69	33	0	66	69	33	0
	Mean	1.38	1.49	1.32		1.379	0.614	0.408		43.12	39.84	40.5		229.6	169.2	74	
	Sd.	0.15	0.1	0.23		0.563	0.297	0.126		6.724	5.998	4.069		348	367.8	216.2	
	Min	1.14	1.3	1.06		0.861	0	0.31		28.69	31.11	31.61		0.113	0.143	0.105	
	Max	1.59	1.73	1.46		2.581	1.197	0.55		50.95	49.06	44.5		1265	1632	803.3	
Haplic_Lixisol	n	2	1	1	0	2	1	1	0	18	18	0	0	18	18	0	0
	Mean	1.46	1.15	1.15		1.108	1.123	0.945		37.32	36.62			263.1	165		

		BD [g/cm³]				SOC [%]				θs [Vol.%]				K_{sat} [cm/day]			
	Horizon N	**1**	**2**	**3**	**4**	**1**	**2**	**3**	**4**	**1**	**2**	**3**	**4**	**1**	**2**	**3**	**4**
	Sd.	0.02				0.131				3.435	1.178			392.1	189.8		
	Min	1.45	1.15	1.15		1.015	1.123	0.945		32.51	34.33			23.87	6.267		
	Max	1.47	1.15	1.15		1.201	1.123	0.945		41.41	37.92			1753	477.5		
Haplic_Plinthosol	n	25	41	6	0	25	41	6	0	42	57	39	0	42	57	39	0
	Mean	1.48	1.54	1.59		1.598	0.641	0.49		39.8	42.43	39.27		1098	519	858.3	
	Sd.	0.13	0.13	0.11		0.717	0.305	0.357		7.785	8.743	5.425		786.3	751.3	664.9	
	Min	1.15	1.22	1.46		0.448	0	0.058		28.91	25.37	30.58		55.23	0.628	40.79	
	Max	1.7	1.75	1.76		3.175	1.276	1.122		53.33	54.25	51.42		2220	2251	2176	
Haplic_Stagnosol	n	1	5	0	0	1	5	0	0	18	18	15	0	18	18	15	0
	Mean	1.51	1.46			0.262	0.962			37.59	35.31	39.91		6.757	3.432	33.56	
	Sd.	0.23				0.468				0.654	4.761	2.039		6.412	3.192	64.55	
	Min	1.51	1.19			0.262	0.41			36.7	28.91	36.59		1.395	0.435	0.209	
	Max	1.51	1.66			0.262	1.633			38.43	39.9	42.68		26.11	10.04	160.7	
Lixic_Gleysol	n	2	3	0	0	2	3	0	0	15	27	15	0	15	27	15	0
	Mean	1.48	1.47			0.838	0.482			38.13	40.5	44.52		755.2	119.9	71.74	
	Sd.	0.04	0.16			0.131	0.1			6.117	8.687	8.511		988.1	133.5	145.3	
	Min	1.45	1.28			0.745	0.366			32.44	33.61	33.61		2.929	0.062	0.058	
	Max	1.51	1.57			0.93	0.548			45.83	59.49	51.91		2467	326.4	352.5	
Lixic_Plinthosol	n	8	15	2	0	8	15	0	0	26	30	42	9	26	30	42	9
	Mean	1.52	1.6	1.37		1.591	0.663			35.12	34.47	39.14	34.32	959.6	1085	537.8	127.4
	Sd.	0.09	0.23	0.31		0.564	0.408			4.664	5.391	7.048	1.356	842.8	635.6	725.7	171.5
	Min	1.35	1.15	1.15		0.721	0.141			28.42	29.34	24.37	32.52	52.52	5.828	0.105	13.05
	Max	1.62	1.96	1.59		2.574	1.732			45.92	44.78	48.19	35.37	1981	1918	2149	356
Lixic_Stagnosol	n	1	1	1	0	1	1	1	0	9	12	9	0	9	12	9	0
	Mean	1.4	1.52	1.67		2.003	0.792	1.118		45.45	41.46	36.07		1160	384.4	12.11	
	Sd.									0.786	2.695	0.703		213	658.2	0.259	
	Min	1.4	1.52	1.67		2.003	0.792	1.118		44.82	39.17	35.13		954.9	18.68	11.94	
	Max	1.4	1.52	1.67		2.003	0.792	1.118		46.49	45.84	36.6		1432	1498	12.46	
Plinthic_Cambisol	n	1	2	0	0	1	2	0	0	9	9	6	0	9	9	6	0
	Mean	1.24	1.1			1.596	1.209			54.73	50.07	47.57		1202	403.2	14.15	
	Sd.	0.14				0.022				1.359	1.326	0.756		903.4	264.4	8.93	
	Min	1.24	1			1.596	1.194			53.32	48.71	46.88		293.7	50.77	5.136	
	Max	1.24	1.2			1.596	1.225			56.42	51.73	48.26		2341	639.7	24.12	
Plinthic_Gleysol	n	3	6	0	0	3	6	0	0	16	18	15	0	16	18	15	0
	Mean	1.41	1.61			1.79	0.751			43.4	41.43	34.66		652.4	287.2	343.4	
	Sd.	0.15	0.15			0.366	0.316			2.035	2.323	1.72		613.5	441.3	553.1	
	Min	1.31	1.44			1.37	0.41			40.29	37.43	31.6		42.74	0.101	7.833	

		BD [g/cm³]				SOC [%]				θs [Vol.%]				K_{sat} [cm/day]			
	Horizon N	**1**	**2**	**3**	**4**	**1**	**2**	**3**	**4**	**1**	**2**	**3**	**4**	**1**	**2**	**3**	**4**
	Max	1.59	1.82			2.04	1.224			46.13	44.72	36.54		1697	1166	1432	
Plinthic_Lixisol	n	2	2	2	0	2	2	2	0	6	0	0	0	6	0	0	0
	Mean	1.4	1.5	1.75		0.645	0.515	0.371		29.29				23.98			
	Sd.	0	0	0		0.156	0.045	0.019		0.639				8.147			
	Min	1.4	1.5	1.75		0.535	0.483	0.358		28.7				13.3			
	Max	1.4	1.5	1.75		0.755	0.547	0.384		29.87				33.07			
Plinthic_Stagnosol	n	2	4	0	0	2	4	0	0	15	18	15	0	15	18	15	0
	Mean	1.35	1.6			0.807	0.442			40.89	39.91	37.96		475.3	76.25	9.983	
	Sd.	0.09	0.06			0.152	0.355			3.082	1.414	1.976		457.7	148	7.382	
	Min	1.28	1.56			0.699	0.043			37.27	37.5	34.59		9.964	0.072	1.641	
	Max	1.41	1.68			0.915	0.905			44.31	42.03	40.53		1313	397.2	19.1	
Stagnic_Cambisol	n	2	6	1	0	2	6	0	0	18	21	9	6	18	21	9	6
	Mean	1.28	1.38	1.4		1.119	0.721	0.7		45.87	46.48	50.88	47.53	774	209.5	503.2	977.3
	Sd.	0.13	0.06			1.15	0.454			5.511	4.258	1.111	0.269	633.1	211.4	286.9	1022
	Min	1.19	1.31	1.4		0.306	0.228			39.36	38.68	49.73	47.29	15.5	14.32	125.3	43.2
	Max	1.38	1.46	1.4		1.933	1.383			52.76	51.51	52.26	47.78	1779	549.1	775.2	1910
Stagnic_Plinthosol	n	3	6	1	1	3	6	1	1	18	27	27	18	18	27	27	18
	Mean	1.53	1.66	1.75	1.67	1.467	0.568	0.676	0.119	40.34	35.3	35.52	38.23	66.23	515.7	496.1	231.8
	Sd.	0.18	0.17			0.318	0.342			1.683	3.702	2.132	3.599	113	763.4	669.9	275.7
	Min	1.34	1.44	1.75	1.67	1.168	0.199	0.676	0.119	37.44	30.06	32.28	34.18	5.876	2.266	0.227	0.201
	Max	1.69	1.85	1.75	1.67	1.8	0.999	0.676	0.119	42.46	39.4	38.68	41.95	313.8	2381	2186	747.3
Gleyic cambisol	n	1	3	0	0	1	3	0	0	9	15	0	0	9	15	0	0
	Mean	1.19	1.4			1.93	1.082			50.09	50.43			666.5	669		
	Sd.	0	0.04				0.29			2.586	0.653			14.41	10.9		
	Min	1.19	1.37			1.93	0.803			44.78	49.73			650.7	653.4		
	Max	1.19	1.4			1.93	1.082			52.76	51.51			683.9	686.5		
Haplic leptosol	n																
	Mean	1.46	1.15	1.15		1.108	1.123	0.945		37.32	36.62			263.1	165		
	Sd.																
	Min																
	Max																
Stagnic lixisol	n	1				1											
	Mean	1.24				0.8											
	Sd.																
	Min																
	Max																

Appendix C: Event-wise precipitation, sediment yield, runoff and runoff coefficient.

		Precipitation [mm]		Sediment yield [g/m²]			Runoff [mm]			Runoff coefficient [%]		
Plot n° (repetition)	Event [dd.mm.yyyy]	max 5 min intensity	event sum	Cotton	Sorghum	Fallow	Cotton	Sorghum	Fallow	Cotton	Sorghum	Fallow
1	24.05.2015	4.3	22.85	0.75	0.21		2.50	2.75		10.94	12.04	
1	11.06.2015	5.8	25.8		0.34	1.69		0.85	1.64		3.29	6.37
1	17.06.2015	5	19.5	3.99	1.32	0.36	2.30	1.65	0.25	11.79	8.46	1.28
1	21.06.2015	3.9	25.75		1.08	1.54		1.00	1.64		3.88	6.38
1	07.07.2015	6.6	11.2	1.99	0.90	0.13	3.45	0.50	0.25	30.80	4.46	2.23
1	09.07.2015	5.7	25.7	9.84	0.63		8.40	2.00		32.68	7.78	
1	10.07.2015	4.8	47.25									
1	16.07.2015	6.2	40.9		0.68			5.70			13.94	
1	21.07.2015	3.85	31.7	1.29	0.03		8.40	0.10		26.50	0.32	
1	03.08.2015	3.8	12.7		0.06			0.35			2.76	
1	07.08.2015	1.8	7.5	0.21	0.03		0.25	0.20		3.33	2.67	
1	10.08.2015	3.9	38.65		1.67	0.07		2.35	1.64		6.08	4.25
1	20.08.2015	1.25	7.5	0.08		0.01	0.15	0.25	0.13	2.00	3.33	1.67
1	22.08.2015	6.1	14.65	0.99	0.06	0.01	0.70	0.55	0.25	4.78	3.75	1.71
1	03.09.2015	2.6	25.05	0.36	0.05	0.01	2.00	0.60	0.50	7.98	2.40	2.00
1	07.09.2015	5.4	69.5		0.15	3.98		1.60			2.30	
1	16.09.2015	2.05	11.8	0.23	0.13	0.09	2.25	0.35	1.64	19.07	2.97	13.93
1	19.09.2015	4	22.35	0.64		0.75	5.50		0.50	24.61		2.24
1	21.09.2015	7.6	38.25		0.33	0.35		1.80	6.39		4.71	16.72
1	22.09.2015	2.8	5.75		0.21			0.25			4.35	
1	26.09.2015	8.7	30.35		1.06	0.26		2.00	9.64		6.59	31.78
1	03.10.2015	5.25	17.55	0.43	0.14	0.05	2.25	1.50	1.89	12.82	8.55	10.79
1	19.10.2015	5.45	17.7	0.46	0.27	0.01	2.25	1.00	0.25	12.71	5.65	1.41
1	27.10.2015	2	19.75	0.12	0.01		1.00	0.25		5.06	1.27	
1	29.10.2015	4.5	28	1.39	0.60		7.00	1.50		25.00	5.36	
2	24.05.2015	4.3	22.85	0.73	0.83		3.02	6.28		13.21	27.47	
2	11.06.2015	5.8	25.8		0.36			2.14			8.29	
2	17.06.2015	5	19.5		1.98	0.36		2.49	1.10		12.78	5.64
2	21.06.2015	3.9	25.75	10.48	0.53	0.50	3.89	0.48	1.50	15.12	1.88	5.83
2	07.07.2015	6.6	11.2	3.14	0.65	0.15	5.14	0.36	0.75	45.93	3.26	6.70
2	09.07.2015	5.7	25.7	4.89	2.07		6.39	5.09		24.88	19.82	
2	10.07.2015	4.8	47.25		5.52			6.63			14.03	
2	16.07.2015	6.2	40.9		0.54			4.50			11.01	
2	21.07.2015	3.85	31.7		0.90	0.08		1.31	2.00		4.13	6.31

		Precipitation [mm]		Sediment yield [g/m²]			Runoff [mm]			Runoff coefficient [%]		
Plot n° (repetition)	Event [dd.mm.yyyy]	max 5 min intensity	event sum	Cotton	Sorghum	Fallow	Cotton	Sorghum	Fallow	Cotton	Sorghum	Fallow
2	03.08.2015	3.8	12.7		0.10	0.01		0.19	0.40		1.47	3.15
2	07.08.2015	1.8	7.5	0.36	0.11	0.01	0.20	0.13	0.15	2.67	1.67	2.00
2	10.08.2015	3.9	38.65		1.72	0.26		5.09	5.63		13.18	14.55
2	20.08.2015	1.25	7.5	0.15		0.01	0.15	0.25	0.15	2.00	3.33	2.00
2	22.08.2015	6.1	14.65	1.35	0.02	0.06	1.00	0.25	1.50	6.83	1.71	10.24
2	03.09.2015	2.6	25.05	0.30	0.02	0.01	0.75	0.38	1.00	2.99	1.50	3.99
2	07.09.2015	5.4	69.5	7.11		0.28	67.89		8.00	97.69		11.51
2	16.09.2015	2.05	11.8	0.29	0.01	0.14	2.89	0.08	2.25	24.53	0.67	19.07
2	19.09.2015	4	22.35	0.96	2.04	2.74	6.64	2.85	2.70	29.73	12.74	12.08
2	21.09.2015	7.6	38.25	2.73	0.20		17.89	1.43		46.78	3.74	
2	22.09.2015	2.8	5.75	0.17	0.03		0.75	0.08		13.04	1.37	
2	26.09.2015	8.7	30.35	3.78	1.09		29.89	4.15		98.50	13.67	
2	03.10.2015	5.25	17.55	0.82	0.92	0.15	2.64	3.32	3.00	15.07	18.92	17.09
2	19.10.2015	5.45	17.7	0.52	0.37	0.03	2.89	1.13	0.90	16.35	6.40	5.08
2	27.10.2015	2	19.75	0.81	0.02		1.64	0.36		8.32	1.85	
2	29.10.2015	4.5	28	2.63	0.26		6.64	0.64		23.73	2.27	
3	24.05.2015	4.3	22.85	1.04	1.21		2.89	5.09		12.67	22.29	
3	11.06.2015	5.8	25.8		0.49	2.74		0.72	2.82		2.79	10.93
3	17.06.2015	5	19.5	13.26	1.56	1.22	7.64	1.00	2.39	39.20	5.13	12.28
3	21.06.2015	3.9	25.75									
3	07.07.2015	6.6	11.2	4.32	0.61	0.37	2.64	0.72	1.00	23.61	6.42	8.93
3	09.07.2015	5.7	25.7	6.18	5.52		6.64	4.50		25.85	17.52	
3	10.07.2015	4.8	47.25		19.72			6.14			13.00	
3	16.07.2015	6.2	40.9		0.46	11.89		5.39	17.39		13.19	42.53
3	21.07.2015	3.85	31.7		0.17			0.50			1.58	
3	03.08.2015	3.8	12.7		0.22			0.19			1.47	
3	07.08.2015	1.8	7.5	0.43		0.03	0.25		0.08	3.33		1.00
3	10.08.2015	3.9	38.65		2.53	0.10		5.39	1.64		13.96	4.25
3	20.08.2015	1.25	7.5	0.27	0.06	0.03	0.20	0.15	0.40	2.67	2.00	5.33
3	22.08.2015	6.1	14.65	3.31	0.10	0.30	1.00	0.25	3.89	6.83	1.71	26.58
3	03.09.2015	2.6	25.05	0.16	0.10		0.50	0.50		2.00	2.00	
3	07.09.2015	5.4	69.5		0.71	1.70		4.14	23.89		5.96	34.38
3	16.09.2015	2.05	11.8	0.55	0.12	0.20	6.64	0.50	5.39	56.31	4.24	45.71
3	19.09.2015	4	22.35	6.24		6.19	7.14		4.64	31.96		20.78
3	21.09.2015	7.6	38.25	16.29	0.06	0.42	37.89	0.50	7.89	99.07	1.31	20.64
3	22.09.2015	2.8	5.75		0.10			0.25			4.35	
3	26.09.2015	8.7	30.35		1.41	0.20		4.14	15.54		13.65	51.22

		Precipitation [mm]		Sediment yield [g/m²]			Runoff [mm]			Runoff coefficient [%]		
Plot n° (repetition)	Event [dd.mm.yyyy]	max 5 min intensity	event sum	Cotton	Sorghum	Fallow	Cotton	Sorghum	Fallow	Cotton	Sorghum	Fallow
3	03.10.2015	5.25	17.55	2.00	0.11	0.28	5.64	0.50	5.39	32.16	2.85	30.74
3	19.10.2015	5.45	17.7	1.13	0.15	0.03	6.64	0.75	0.50	37.54	4.24	2.82
3	27.10.2015	2	19.75	0.17	0.01		1.64	0.13		8.32	0.63	
3	29.10.2015	4.5	28	2.72	1.04	0.25	7.89	2.89	6.64	28.19	10.34	23.73